Capacity Design and Fatigue Analysis of Confined Concrete Columns

by

Anindya Dutta and John B. Mander
State University of New York at Buffalo
Department of Civil, Structural and Environmental Engineering
Buffalo, New York 14260

July 14, 1998

NOTICE

Capacity Design and Fatigue Analysis
of Confined Concrete Columns

by

A. Dutta[1] and J.B. Mander[2]

1   Research Assistant, Department of Civil, Structural and Environmental Engineering, State University of New York at Buffalo
2   Associate Professor, Department of Civil, Structural and Environmental Engineering, State University of New York at Buffalo

MULTIDISCIPLINARY CENTER FOR EARTHQUAKE ENGINEERING RESEARCH
State University of New York at Buffalo
Red Jacket Quadrangle, Buffalo, NY 14261

Preface

The Multidisciplinary Center for Earthquake Engineering Research (MCEER) is a national center of excellence in advanced technology applications that is dedicated to the reduction of earthquake losses nationwide. Headquartered at the State University of New York at Buffalo, the Center was originally established by the National Science Foundation in 1986, as the National Center for Earthquake Engineering Research (NCEER).

Comprising a consortium of researchers from numerous disciplines and institutions throughout the United States, the Center's mission is to reduce earthquake losses through research and the application of advanced technologies that improve engineering, pre-earthquake planning and post-earthquake recovery strategies. Toward this end, the Center coordinates a nationwide program of multidisciplinary team research, education and outreach activities.

MCEER's research is conducted under the sponsorship of two major federal agencies, the National Science Foundation (NSF) and the Federal Highway Administration (FHWA), and the State of New York. Significant support is also derived from the Federal Emergency Management Agency (FEMA), other state governments, academic institutions, foreign governments and private industry.

The Center's FHWA-sponsored Highway Project develops retrofit and evaluation methodologies for existing bridges and other highway structures (including tunnels, retaining structures, slopes, culverts, and pavements), and improved seismic design criteria and procedures for bridges and other highway structures. Specifically, tasks are being conducted to:
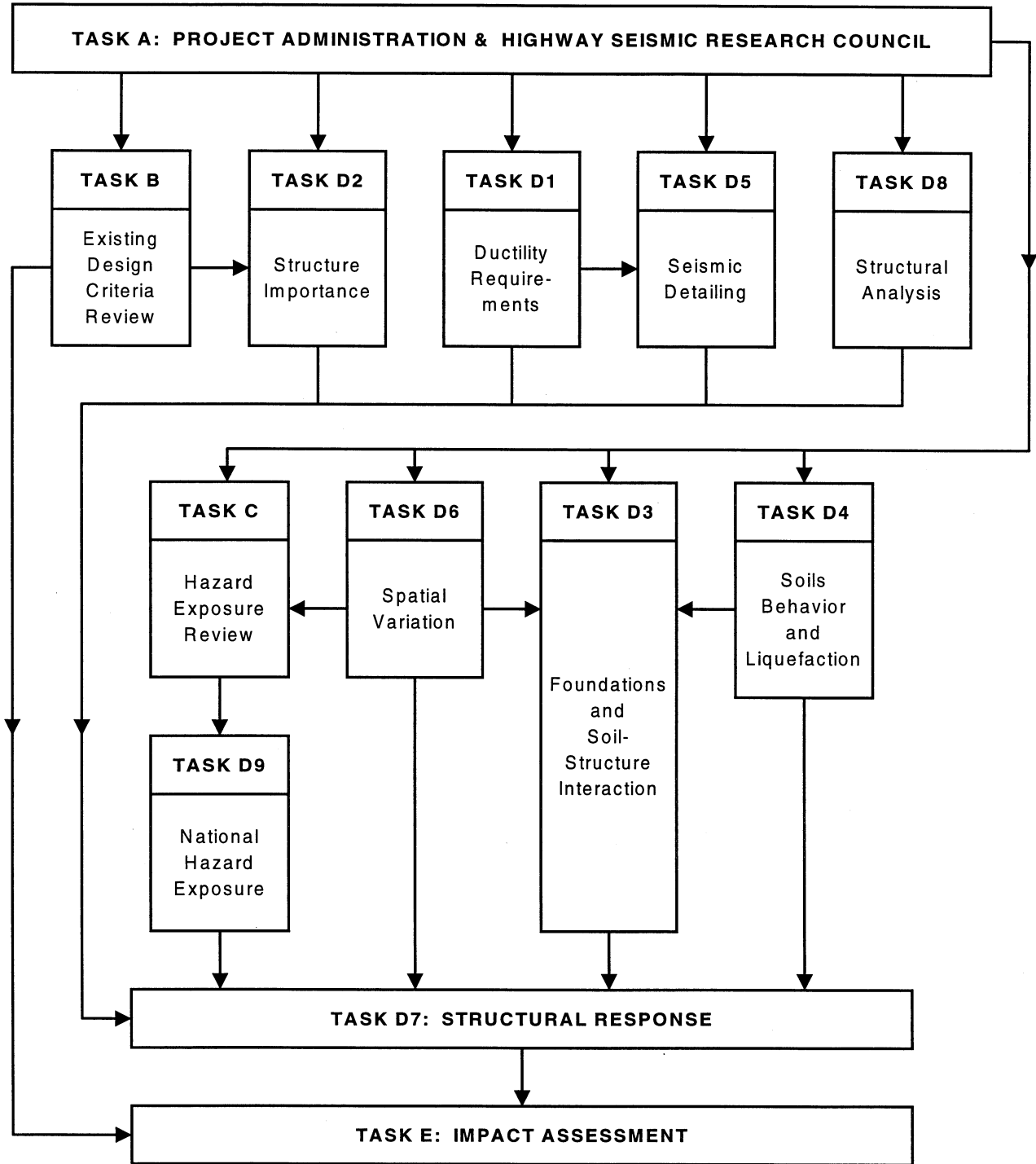* assess the vulnerability of highway systems, structures and components;
* develop concepts for retrofitting vulnerable highway structures and components;
* develop improved design and analysis methodologies for bridges, tunnels, and retaining structures, which include consideration of soil-structure interaction mechanisms and their influence on structural response;
* review and recommend improved seismic design and performance criteria for new highway structures.

Highway Project research focuses on two distinct areas: the development of improved design criteria and philosophies for new or future highway construction, and the development of improved analysis and retrofitting methodologies for existing highway systems and structures. The research discussed in this report is a result of work conducted under the new highway structures project, and was performed within Task 112-D-5.1(a) "Capacity Detailing of Columns, Walls, and Piers for Ductility and Shear" of that project as shown in the flowchart on the following page.

The overall objective of this task was to develop seismic design and capacity detailing recommendations for bridge substructures that have been validated through experimental testing. Three common bridge failure mechanisms are examined: concrete failure due to lack of confinement; buckling of the longitudinal reinforcement; and shear failures both within and outside the plastic hinge zone. Design recommendations are presented as simple equations that require that the

volumetric ratio of transverse reinforcement be determined based on three parameters: longitudinal steel volume, axial load intensity, and the shear span aspect ratio.

SEISMIC VULNERABILITY OF NEW HIGHWAY CONSTRUCTION
FHWA Contract DTFH61-92-C-00112

TASK A: PROJECT ADMINISTRATION & HIGHWAY SEISMIC RESEARCH COUNCIL

TASK B	TASK D2	TASK D1	TASK D5	TASK D8
Existing Design Criteria Review	Structure Importance	Ductility Requirements	Seismic Detailing	Structural Analysis

TASK C	TASK D6	TASK D3	TASK D4
Hazard Exposure Review	Spatial Variation	Foundations and Soil-Structure Interaction	Soils Behavior and Liquefaction

TASK D9

National Hazard Exposure

TASK D7: STRUCTURAL RESPONSE

TASK E: IMPACT ASSESSMENT

ABSTRACT

The capacity design philosophy requires the identification of all potential failure mechanisms. A preferred failure mechanism is chosen and efforts are made, through design detailing, to suppress all other undesirable failure modes. For the seismic design of bridges, the preferred failure mechanism is ductile flexural hinging of the reinforced concrete columns in the substructure. The undesirable failure modes that must be suppressed by design are three: concrete failure due to lack of confinement; buckling of the longitudinal reinforcement; and shear failures both within and outside the plastic hinge zone.

The principal subject of this report is an in-depth examination of these three primary failure modes and establishing a theoretical basis for suppressing their occurrence. First, based on energy balance requirements, the required amount of transverse confinement reinforcement to inhibit hoop fracture resulting from reversed cyclic (low cycle fatigue) loading is derived.

Secondly, the required amount of transverse reinforcement to inhibit buckling of the longitudinal compression reinforcement is considered a new approach to the inelastic buckling problem based on plastic analysis is presented. The theory distinguishes between local buckling (between two levels of hoops) and global buckling (that occurs over several levels of hoops or spirals). This approach to bar stability analysis is validated against experimental results.

The third undesirable failure mode that needs to be suppressed concerns shear resistance. Shear failures can occur both within and without the potential plastic hinge zone. Moreover, the level of shear resistance to be provided must be based on the maximum flexural overstrength demand. Therefore, following a review of present state-of-the-art and state-of-the-practice recommendations, a new rational method of shear resistance is proposed. This method independently considers the three principal components of shear resistance: steel truss action (V_s); concrete arch or strut action (V_p); and concrete tension field action (V_c). The basis of apportioning each component of resistance is through a principal crack angle (θ), which is derived from energy considerations.

Finally, design recommendations are presented in the form of simple equations that require the determination of a volumetric ratio of transverse reinforcement (ρ_o) based on three main parameters: longitudinal steel volume (ρ_t), axial load intensity ($P_e/f_c'A_g$) and the shear span aspect ratio (M/VD).

ACKNOWLEDGEMENTS

TABLE OF CONTENTS

TABLE OF CONTENTS (con't.)

LIST OF ILLUSTRATIONS

LIST OF ILLUSTRATIONS (CONT'D.)

LIST OF ILLUSTRATIONS (CONT'D.)

LIST OF TABLES

SECTION 1
PROLOGUE

1.1 BACKGROUND

The seismic design philosophy currently followed in the United States relies on controlling damage through energy dissipation. Conventional ductile design assumes earthquake loads to be significantly greater than the available strength capacity of the structural element. Thus it is not surprising that inelastic behavior and damage was observed in structural components resisting lateral loads in catastrophic earthquakes like the Mexico City 1985, Loma Prieta 1989, Northridge 1994 and the Great Hanshin (Kobe) 1995.

Conventional seismic design uses loads from the de-amplified elastic spectra along with special ductile detailing. This is usually done with the aid of response reduction (R) factors specified by code committees. The performance criteria set by such committees are, however, rather implicit and are based mainly on limiting drifts and providing adequate strengths to ensure that inelastic displacements do not lead to collapse. This is a major departure from the long cherished strength-based elastic design whose limitations are now well accepted. There is a general consensus in the engineering community today that the philosophy of providing less strength does not always lead to collapse. Provided that the structural strength can be maintained without major degradation as the inelastic displacements developed, the structure can safely ride through any severe ground excitation. With increased awareness that excessive strength is neither essential nor desirable for good performance, the emphasis in seismic design has shifted from resistance of large seismic forces to the evasion of these forces. Inelastic design (or limit based design) long obscured as a hypothesis has become an essential reality and thus was born the concept of "Capacity Design."

The capacity design philosophy, first implemented in New Zealand during the 1970's (Park and Paulay, 1975) was a step in formally changing the course of earthquake engineering. The first step in this design approach lies in identifying the most probable failure modes that might arise in the event of a major ground shaking. Ductility, which is a measure of structure's ability to deform into the inelastic range without significant strength decay is the single most important target of the entire design exercise. Thus, certain modes of inelastic behavior are more desirable than others. This is because undesirable modes may lead to failure while desirable modes may lead to controlled ductile response; an essential attribute of maintaining strength while the structure is subjected to reversals of inelastic deformations under seismic response. These undesirable modes are deliberately averted by amplifying the structure's resistance compared to those which are desirable. Thus, for concrete structures, for example, the required shear strength must exceed the required flexural strength to ensure that inelastic shear deformations, associated with large deterioration of stiffness and strength, do not occur. However, the question that necessarily arises is how much damage should necessarily be allowed? The answer is related to the economy of construction which requires that the accepted level of damage be tied to the expected risk of earthquake exposure. Therefore, for minor earthquakes of relatively frequent occurrence, no damage except possibly that of minor cosmetic nature is acceptable. For earthquakes of moderate strength, and correspondingly larger return intervals, a limited amount of permanent structural damage is generally considered acceptable. But for large earthquakes with a very low probability of occurrence (this is often referred nowadays to as the "maximum capable event" and has a return period in excess of some 2000 to 3000 years) a considerable amount of damage is generally considered acceptable. But in any case the prevention of collapse should be the supreme design objective.

It has become a norm that seismic design should encourage structural forms that possess adequate ductility. Although in reinforced concrete frame design, plastic hinges are normally expected to form in the beams (the so called "strong column weak beam" philosophy), column plastic hinges at the base of the structure are required to complete the plastic deformation mechanism (refer figure 1-1). For bridge structures it is neither feasible nor desirable to locate the plastic hinges in the superstructure. Thus, the columns tend to be the primary source of

2

energy dissipation unless mechanical energy dissipators are incorporated into the design. Since it is a common practice to rely on the ductile inelastic flexural response of the plastic hinges as the primary source of energy dissipation, proper care should be taken in detailing the locations where plastic hinges are expected to occur. Therefore, a proper understanding of the different potential failure modes is necessary in order to correctly design and detail ductile regions and to provide "capacity protection" to the remainder of the structure.

Based on numerous experimental studies, it has been observed that failure in a reinforced concrete beam/column member can arise in the form:

(i)   Shear or flexure-shear failure of the column outside the potential plastic hinge zone.

(ii)   Failure of the connections by either:

     (a)   bond failure of the lap-splice zone at the end of the columns.

     (b)   anchorage-bond failure within the connection.

     (c)   joint shear failure adjacent to the column.

(iii)   Premature concrete failure due to lack of confinement.

(iv)   Failure of the confined core concrete due to compression buckling of the longitudinal reinforcing bars.

(v)   Fracture of the transverse hoop reinforcement (leading to failure modes (i) to (iii))

(vi)   Failure due to low cycle fatigue of the longitudinal reinforcement.

It is now well accepted that the first three failure modes can be averted by providing sufficient amount of transverse reinforcement. Modes (iv) and (v) can also be averted if a sufficient amount of transverse reinforcement is provided leaving mode (vi) as the final, but unavoidable, failure mode. This is schematically illustrated in figure 1-2. Thus a systematic study of these three failure modes (modes iv, v and vi) is considered to be an important step in preventing catastrophic structural failure through premature failure of the plastic hinge regions.
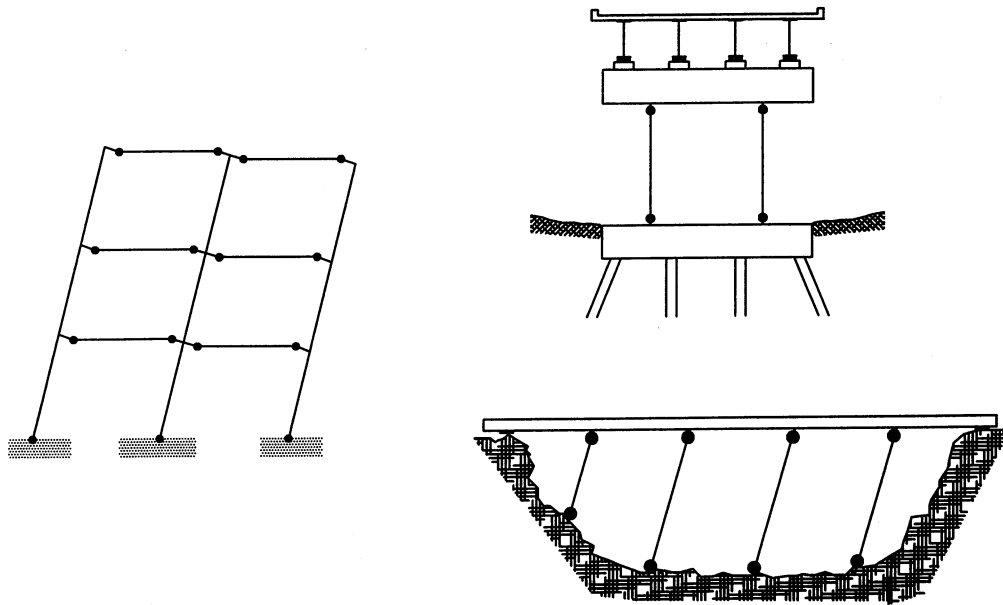
Figure 1-1 Admissible Failure Mechanisms in Reinforced Concrete Sections
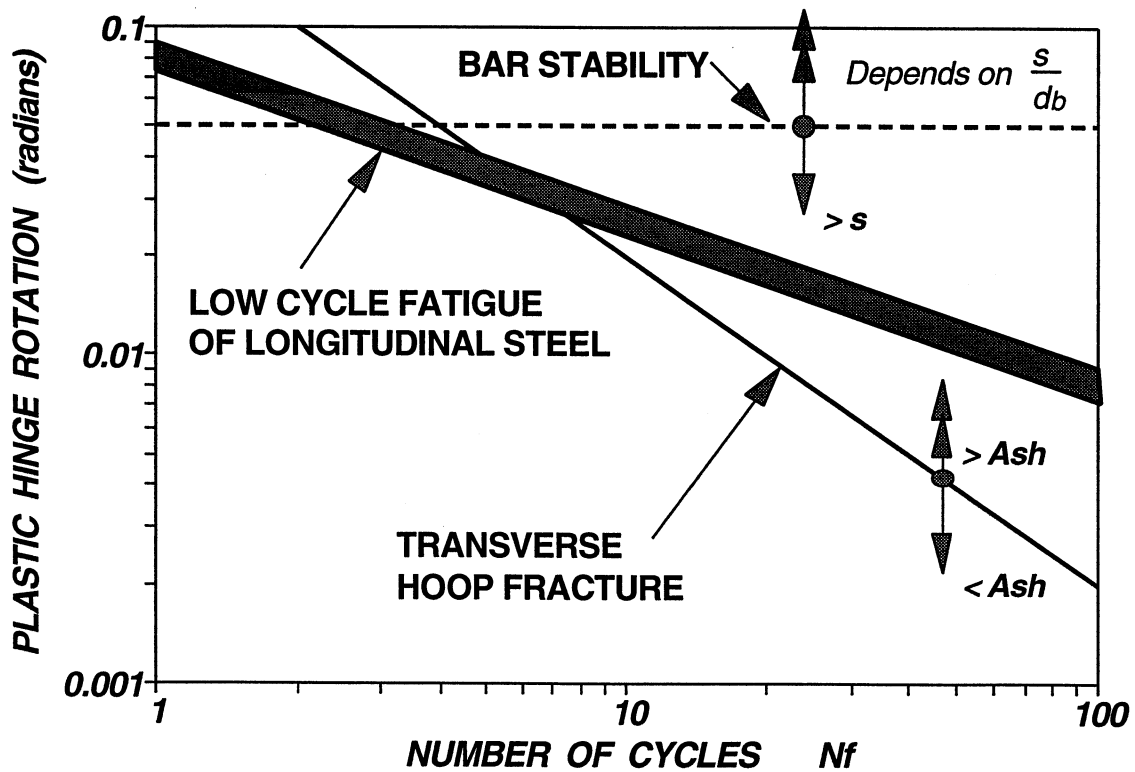
Figure 1-2 General Fatigue Theory for Confined Concrete Sections

1.2 Significance of Current Research

As it is possible to avert failure modes (i) to (iii) by using the principles of capacity design, then it is necessary to provide the appropriate theoretical background for analyzing the three most important failure modes—modes (iv) to (vi) since each are characteristic of column failures. Studies to this end have been performed by Dutta (1995) and Mander and Cheng (1995) who analyzed the fatigue life based on low cycle fatigue of the longitudinal reinforcement. However it is also realized that the necessary condition to ensure that failure occurs through low cycle fatigue is the prevention of non-ductile failure modes like shear failure and buckling of the longitudinal rebars. Since this can be done by the provision of transverse reinforcement, an adequate theoretical model is required for the purpose. This research effort addresses these problems that are detrimental to ductile failure and proposes design solutions that will ensure satisfactory performance in the event of a strong ground shaking.

1.3 Scope of this Study

This study can be conceived to be presented in two parts. In the first part a complete analysis of the problem of transverse hoop fracture is performed based on energy balance considerations. The latter part of this section deals with validation of the theory with experimental results obtained from past research and design implications. It should be mentioned that there is a paucity of experimental results where a distinct <u>flexural</u> failure was observed due to hoop fracture and buckling of longitudinal reinforcement. Every effort has been made to identify such well documented data and utilize herein. Since in the capacity design philosophy the most acceptable form of failure is through low cycle fatigue of the longitudinal reinforcement, it is necessary that there be adequate provision of lateral hoop reinforcement so that other modes do not become overriding. This is more important for shear failure and longitudinal bar buckling both of which are preventable by adequate hoop steel. The second section of this report which is mainly a design section, such design issues are investigated in greater detail. Firstly the problem of longitudinal bar buckling is analyzed from energy considerations and current code provisions examined. Another important problem of shear

design is also examined based on the recent research findings of Kim and Mander (1997). Simple design charts and expressions are proposed that will ensure a proper hierarchy of failure modes in the capacity design ladder. A worked out example is also provided in section 10 to guide the reader through the working procedure of the proposed methodology. Finally an epilogue and references are presented in sections 11 and 12 respectively.

SECTION 2
DEVELOPMENT OF ENERGY BASED FATIGUE THEORY

2.1 INTRODUCTION

Satisfactory seismic performance of reinforced concrete bridge columns require that the behavior be ductile under a severe earthquake excitation. A ductile response is characterized by the structure's ability to undergo large inelastic displacements without significant loss in the load carrying capacity. As it is a common practice to rely on ductile inelastic flexural response of plastic hinges as the primary mode of energy dissipation, proper care should be taken in detailing the locations where hinging is expected to occur. Since the inception of capacity design, ductility has been presumed as the principal criterion for design. However ductility, whether it be explicitly or implicitly incorporated into design requirements, does not account for the duration of ground shaking. The duration effect is important in inelastic design as the cumulative effects of ductility and energy absorption may lead to premature failure even at modest ductility demands. The temptation to overcome this problem is to merely strengthen a structure, but based on recent experience in Japan (Kobe) and elsewhere, it should be realized that "stronger" structures are not the panacea to damage avoidance and enhanced performance.

As an alternative to ductility based design, energy may be used as the basis for developing design paradigms. Energy-based methods are based on the premise that the energy demand during an earthquake (or an ensemble of earthquakes) can be predicted and that the energy supply/capacity of a structural element can be established. The design objective is to balance the energy absorption capacity of members with the hysteretic energy absorption demands imposed on members by the design earthquake ground motion. As the energy absorption accumulates over time, it is possible to address the duration effects in an implicit way. Although the resurgence of energy-based design is very recent, it was apparently first proposed by Housner (1956). He was the first to point out that the ground motion actually feeds

7

a certain amount of energy into the structure — some of which is dissipated through damping and the remainder stored in the structure as kinetic energy (i.e., motion of the mass) and strain energy (deformation of structural members). Based on the idea (in 1956) that a safe and economical seismic resistant design should proceed thorough plastic analysis or limit design, while allowing permanent deformations to occur without failure of a member, it was suggested that the design be tied to the concept of plastic energy, E_p dissipated by the structure and related to the inelastic deformation by

$$E_p = E_t - E_e \tag{2-1}$$

where E_t is the maximum kinetic energy which would be obtained if the structure behaved completely elastically, and E_e is the elastic energy of the structure when it reaches yield point. Although the energy expression was rudimentary, Housner's paper formulated the fundamental concept that at any instant of time the sum of the kinetic energy, strain energy, energy dissipated through damping and permanent deformations must equate to the total energy input. Since then there has been considerable developments on energy concepts (Uang and Bertero, 1990).

Another way of thinking about energy is to utilize the concept of low cycle fatigue. As earthquakes impose cyclic effects on structures, it is possible to express the duration effects of an earthquake in terms of an effective number of cycles of loading which is consistent with the energy absorption demand. In a similar fashion it is possible to consider the number of displacement cycles that lead to failure in a member based on its energy absorption capacity.

It is well known that following the principles of capacity design where a hierarchy of failure mechanisms is chosen by the designer himself, it is possible to suppress all undesirable failure modes such as shear, loss of bond and anchorage and joint failure (Paulay and Priestley, 1992). This leaves low cycle fatigue as the only unavoidable cause of failure (Mander and Cheng, 1995). Therefore, to ensure that plastic hinges do not fail in an undesirable fashion, the fatigue life based on transverse hoop fracture should be higher than that based on the low cycle fatigue of the longitudinal reinforcement. Although a significant research has been done on the fracture of transverse hoop reinforcement, there has been very little effort in merging it with the

8

concept of fatigue. The first significant effort to this end was done by Mander et al. (1984) who proposed an energy balance theory for predicting the hoop fracture in a column subjected to axial compression only. Since earthquakes loads are cyclic in nature, their theory in the present form is not suitable for direct application. This research modifies the theory incorporating cyclic effects so that it can used to give a reliable estimate of the fatigue life using energy concepts. This is reported in the following.

2.2 BASIS OF ENERGY BALANCE THEORY

Ductile members, because of their significant ability to dissipate strain energy before failure, exhibit a prolonged load-deformation characteristic. Additional ductility available from confined concrete sections can be attributed to the strain energy stored in the transverse reinforcement. Mander et al. (1984) proposed an energy balance approach in which the external work done *(EWD)* on the section was equated to the internal energy absorption capacity *(IWD)* of the section. They developed an energy balance equation of the form $EWD = IWD$ such that

$$EWD = U_s + U_{cc} \tag{2-2}$$

$$IWD = U_{sh} + U_{co} \tag{2-3}$$

where U_s = work done by the compression steel, U_{cc} = work done by the concrete in compression, U_{sh} = energy required to cause the first hoop to fracture and U_{co} = energy required to fail an equivalent unconfined concrete column. When the external work done by the concrete and the steel exceeds the amount of strain energy available, then it is assumed that the maximum useful strain has been attained and subsequently the transverse hoops will fracture. Hence the fatigue life is defined. It should be emphasized that the early energy-balance work of Mander et al. (1984) was strictly for columns in pure axial compression. Cyclic flexure was not explicitly accounted for in defining the ultimate axial strain.

9

2.3 Energy Absorption Capacity

The strain energy available from the transverse reinforcement prior to first hoop fracture (U_{sh}) is given by

$$U_{sh} = \rho_s A_{cc} \int_0^{\varepsilon_{sf}} f_s \, d\varepsilon = U_{sf} \rho_s A_{cc} \qquad (2\text{-}4)$$

where the integral $\int_0^{\varepsilon_{sf}} f_s \, d\varepsilon = U_{sf}$ = area beneath the tension stress-strain curve of the transverse reinforcing steel between zero strain and fracture strain (ε_{sf}) shown in table 2-1 for a range of reinforcing steel tested by Mander et al. (1984, 1988a,b); ρ_s = volumetric ratio of the transverse reinforcement and A_{cc} = area of the core concrete.

Table 2-1 Showing strain energy required to fracture reinforcing steel in tension

Diameter (mm)	f_y (MPa)	E_s (GPa)	E_{sh} (MPa)	ε_{sh}	ε_{su}	f_{su} (MPa)	ε_{sf}	U_{sf} (MJ/m³)
16	295	200	3500	0.025	0.19	433	0.25	98
20	286	200	4000	0.023	0.18	446	0.28	111
24	260	195	4500	0.018	0.18	429	0.29	111
16	360	200	6000	0.016	0.15	567	0.24	121

Thus, from the experimental observations of Mander et al. (1984, 1988a,b), it can be concluded that U_{sf} is largely independent of steel grade and typically given by

$$U_{sf} = \int_0^{\varepsilon_{sf}} f_s \, d\varepsilon = 110 \; MJ/m^3 \quad (\pm 10\%) \qquad (2\text{-}5)$$

thus equation (2-4) can be rewritten (in MPa units) as

$$U_{sh} = 110 \, \rho_s A_{cc} \qquad (2\text{-}6)$$

The strain energy of plain unconfined concrete (U_{co}) is given by

10

$$U_{co} = A_g \int_0^{\varepsilon_{cu}} f_c \, d\varepsilon \tag{2-7}$$

where the integral is actually the area beneath the unconfined concrete stress strain curve and A_g = the gross area of the concrete cross section. Note that this the energy required to fail a column in the event there was no lateral confinement (Dutta, 1995). Based on the observation of Mander et al. (1984), it is suggested that the strain energy for column concrete can be approximated to $0.008 f_c'$. These strain energies for steel and concrete are shown in figure 2-1. Equation (2-3) thus can be rewritten as

$$IWD = 0.008 f_c' A_g + \rho_s U_{sf} A_{cc} \tag{2-8}$$

Dividing equation (2-8) by $f_c' A_g$ gives a normalized internal energy absorption capacity

$$u_{in} = \frac{IWD}{f_c' A_g} = 0.008 + \rho_s \frac{U_{sf}}{f_c'} \frac{A_{cc}}{A_g} \tag{2-9}$$

2.4 APPLIED ENERGY DEMAND

It is assumed that the available internal strain energy capacity given by equation (2-9) is progressively consumed due to the external work done by the plastic straining of the confined core concrete and the longitudinal steel in compression. This plastic work done by the steel and the concrete in compression can be obtained directly from the cyclic stress-strain curves of steel and concrete.

Accordingly the total work done by the steel in compression is given by

$$U_s = 2 N_c \sum_{i=1}^{n} A_{st_i} \omega_{p_i} \tag{2-10}$$

where $2N_c$ = total number of reversals to the fracture of the hoop steel, n = number of steel layers in compression, A_{st_i} = steel area in the i-th compression layer, and ω_{p_i} = plastic work done by the compression steel (refer figure 2-2).

11
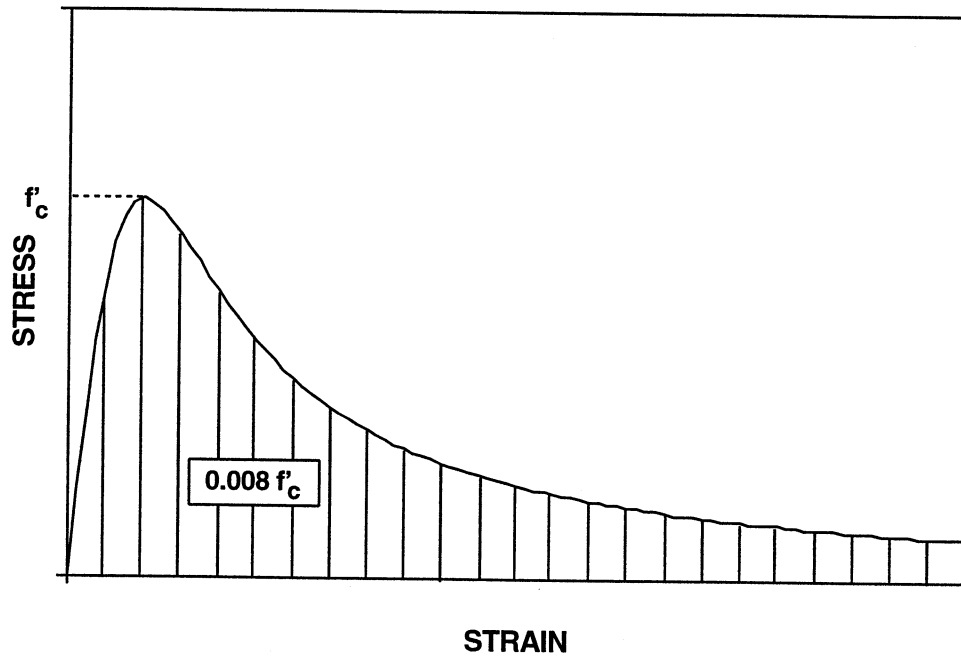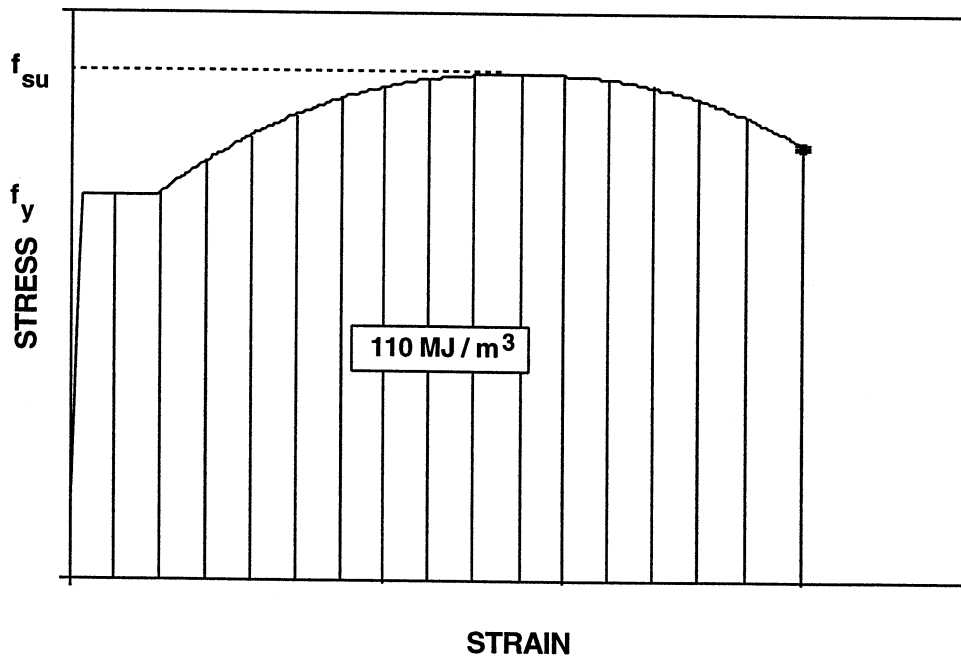
(a) Concrete

(a) Steel

Figure 2-1 Showing Strain Energy of Concrete and Steel

Conservatively ω_{p_i} can be expressed as

$$\omega_{p_i} = f_y(\varepsilon_{sp_i}) \tag{2-11}$$

where f_y = yield stress of the longitudinal reinforcement and ε_{sp_i} = plastic strain amplitude as shown in figure 2-2. Note that it is assumed that the energy transfer between the longitudinal steel and the transverse steel occurs only when the strain in the vertical reinforcement is purely compression. Physically it can be argued that only under such a scenario is the full potential of the hoop steel utilized as it tries to prevent the steel from buckling and thus occurs the transfer of energy as the vertical steel bears against the lateral reinforcement.

The work done by the concrete in compression can be expressed as the product of the area under the concrete stress strain curve at each reversal and the actual area under compression. However, as can be seen from figure 2-3, the confined concrete does not strictly follow the skeleton curve after the first reversal. In reality it follows a curve where the area beneath it is somewhat less. This is due to the progressive softening of the concrete as it is loaded cyclically. Thus it is worthwhile at this point to define a cyclic loading efficiency factor for concrete (η_c) which is the ratio of the area under the curve <u>after</u> the first reversal to the area under the curve <u>at</u> the first reversal. The work done, being equal to the area under the concrete stress strain curve at each reversal, can be expressed as

$$\begin{aligned} Work &= A_c \times \int_0^{\varepsilon_{cp}} f_c \, d\varepsilon_p \\ &= C_c(\varepsilon_{cp}') \end{aligned} \tag{2-12}$$

where A_c = area under compression, the integral denotes the area under the plastic stress strain curve for concrete, C_c = concrete compression force and ε_{cp}' the plastic strain at the location through which the concrete compression force C_c acts.

Thus the externally applied energy that damages the confined reinforced concrete section can now be written in accordance with the equation (2-2) as

13
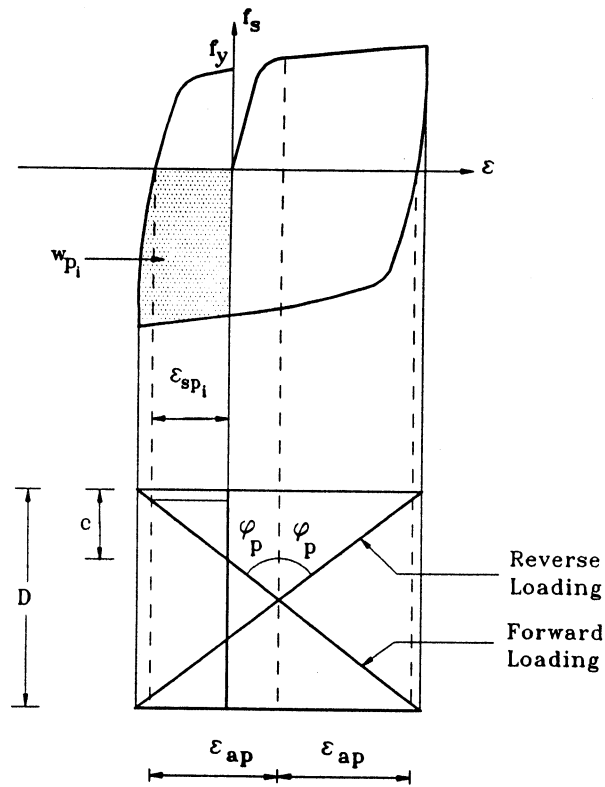
Figure 2-2 Showing Plastic Work done by the Compression Steel.

$$\eta = \frac{\text{Area abcdea}}{\text{Area afgea}}$$
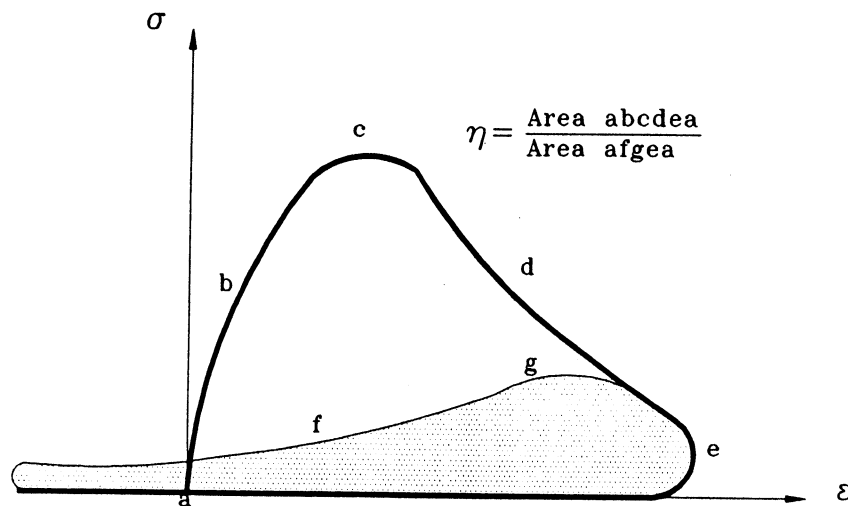
Figure 2-3 Decay in Concrete Stress Strain Behavior due to Repeated Cycling.

14

$$EWD = 2N_c \sum_{i=1}^{n} A_{st_i} f_y \, \varepsilon_{sp_i} + [2 + 2(N_c - 1) \, \eta_c] C_c \, \varepsilon'_{cp} \qquad (2\text{-}13)$$

where it has been shown that the efficiency factor (η_c) becomes effective after the first reversal.

Assuming that the concrete compression force C_c acts at a depth ξc (refer figure 2-4) from the top compression fiber, where c is the depth of the neutral axis, the plastic strain amplitude (ε'_{cp}) at the location of the concrete compression force is given by

$$\varepsilon'_{cp} = (\phi_p D)\left(\frac{c}{D}\right)(1 - \xi) \qquad (2\text{-}14)$$

In the same way, the plastic strain amplitude for the i-th compression steel layer (ε_{sp_i}) can be written as

$$\varepsilon_{sp_i} = \phi_p (c - y_i) = \phi_p D \left[\frac{c}{D} - \frac{y_i}{D}\right] \qquad (2\text{-}15)$$

where ϕ_p = plastic curvature, D = overall depth of the section (the product ($\phi_p D$) being the dimensionless plastic curvature), c = depth of the neutral axis from the extreme compression fiber and y_i = distance of the i-th steel layer from the extreme compression fiber.

Combining equations (2-13), (2-14) and (2-15) the external work done (EWD) can be expressed as:

$$EWD = 2N_c \sum_{i=1}^{n} A_{st_i} f_y \left(\frac{c}{D} - \frac{y_i}{D}\right)(\phi_p D) + [2 + 2(N_c - 1)\eta_c] C_c \left(\frac{c}{D}\right)(1 - \xi)(\phi_p D) \qquad (2\text{-}16)$$

where $2N_c$ = numbers of reversals to failure.

Dividing equation (2-16) by $f'_c A_g$ gives a normalized energy consumption capacity.

$$u_{ex} = 2N_c \sum_{i=1}^{n} \left(\frac{A_{st_i}}{A_g}\right)\left(\frac{f_y}{f'_c}\right)\left(\frac{c}{D} - \frac{y_i}{D}\right)(\phi_p D) + [2 + 2(N_c - 1)\eta_c]\left(\frac{C_c}{f'_c A_g}\right)\left(\frac{c}{D}\right)(1 - \xi)(\phi_p D) \qquad (2\text{-}17)$$

or in other words

15
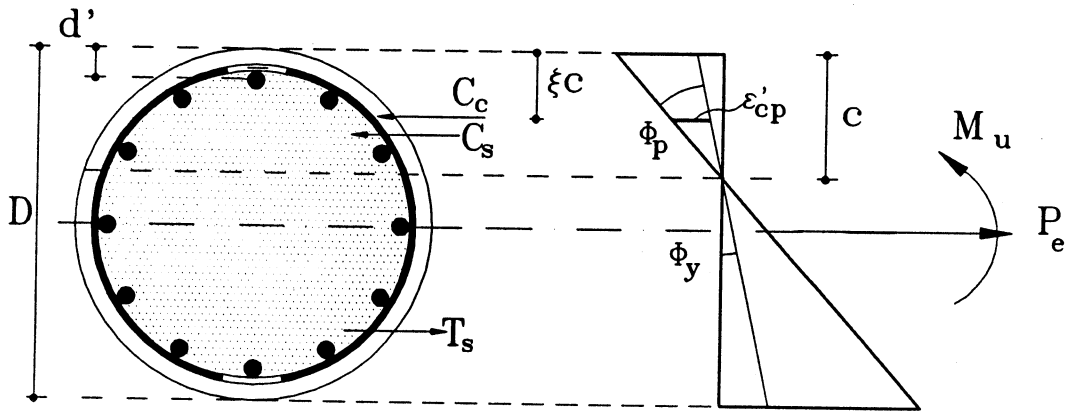
Figure 2-4 Force Equilibrium in a Concrete Section subjected to Flexure and Axial Compression.

16

$$u_{ex} = 2 N_c \overline{u}_{ex,s} + \left[2 + 2(N_c - 1)\eta_c)\right]\overline{u}_{ex,c} \qquad (2\text{-}18)$$

where the notations are easily identifiable.

2.5 DEVELOPMENT OF FATIGUE RELATIONS

Using the principles of virtual work in which the internal energy absorption capacity is equaled to the energy consumption capacity, it is possible to write

$$u_{in} = u_{ex} \qquad (2\text{-}19)$$

from which the dimensionless plastic curvature can be obtained as

$$\phi_p D = \frac{0.008 + \rho_s \dfrac{U_{sf}}{f_c'} \dfrac{A_{cc}}{A_g}}{\displaystyle\sum_{i=1}^{n} \dfrac{A_{st_i}}{A_g}\left(\dfrac{f_y}{f_c'}\right)\left(\dfrac{c-y_i}{D}\right) + \left(\eta_c + \dfrac{1-\eta_c}{N_c}\right)\left(\dfrac{C_c}{f_c' A_g}\right)\left(\dfrac{c}{D}\right)(1-\xi)} \; (2N_c)^{-1} \qquad (2\text{-}20)$$

It will be noted that equation (2-20) can be written in a familiar low cycle (plastic) fatigue – life format which may take the general form

$$\phi_p D = \Theta_{hoop}^{*} \, (2N_c)^{-1} \qquad (2\text{-}21)$$

where

$$\Theta_{hoop}^{*} = \frac{0.008 + \rho_s \dfrac{U_{sf}}{f_c'} \dfrac{A_{cc}}{A_g}}{\dfrac{f_y}{f_c'} \displaystyle\sum_{i=1}^{n} \dfrac{A_{st_i}}{A_g} \dfrac{c-y_i}{D} + \left(\eta_c + \dfrac{1-\eta_c}{N_c}\right)\left(\dfrac{C_c}{f_c' A_g}\right)\left(\dfrac{c}{D}\right)(1-\xi)} \qquad (2\text{-}22)$$

Alternatively, it is possible to convert the above cyclic life equations into a form that gives the cumulative plastic drift, as follows:

$$\Sigma \, \theta_p \, = \, (2N_c)(\phi_p D)\left(\frac{L_p}{D}\right) \, = \, \left(\frac{L_p}{D}\right)(\Theta^*_{hoop}) \qquad\qquad \text{(2-23)}$$

where the plastic hinge length is given by Paulay and Priestley (1992) as

$$L_p \, = \, 0.08\,L \, + \, 4400\,\varepsilon_y d_b \qquad\qquad \text{(2-24)}$$

where $L =$ length of the column to the point of contraflexure, ε_y and d_b are the yield strain and diameter of the longitudinal reinforcing bar.

Equation (2-20) can be used to give an estimate of the plastic curvature obtainable from a section corresponding to the number of cycles (N_c). However, the inherent problem in using equation (2-20) lies in the evaluation of the neutral axis depth c and the concrete compression force ratio ($C_c / f'_c A_g$). As a result, it was decided to form two parallel analysis procedures. In the first one, the neutral axis depth ratio (c/D) is formulated based on force equilibrium considerations and strain hardening of the longitudinal reinforcement. This is referred to as "Exact Computational Solution". In the second method, referred to as the "Simplified Direct Approach", the neutral axis depth is computed based on some rational arguments. These methods are discussed in what follows.

2.6 CONCLUSIONS

In this section a fatigue life theory of confined concrete based on the fracture of transverse hoop is derived from first principles. It is observed that the expression for fatigue life can be evaluated using both a rigorous computational approach, as well as a simplistic approach based on some rational assumptions. Both of these approaches are examined in greater detail in the following sections.

18

SECTION 3
EXACT COMPUTATIONAL SOLUTION

3.1 INTRODUCTION

This section explores a rigorous computational moment curvature approach to solve for the concrete component of the external work done $\bar{u}_{ex,c}$. Numerical integration across the section using a fiber element approach is commonly used to solve this problem (Mander, 1984; Chang and Mander, 1994a). Alternatively, a stress block approach can be adopted such as that used recently for rectangular sections by Goel (1995). However, in order to maintain generality without sacrificing accuracy, a numerical integration strategy that employs Gauss Quadrature is investigated. This method is general and is applicable to section of any arbitrary shape. The most important advantage of this solution scheme is that it is simple and lends itself easily to spreadsheet type computer programming.

3.2 MOMENT-CURVATURE ANALYSIS OF A CONFINED CONCRETE COLUMN

For a given cross sectional strain profile, the moment capacity (M) of a section can be determined by using two equilibrium equations in conjunction with strain compatibility. For a given concrete strain in the geometric centroid of the section ε_0 and section curvature ϕ, the strain at any location can be found from

$$\varepsilon_{si} = \varepsilon_0 + \phi y \tag{3-1}$$

where y denotes the location of the point from the geometric centroid of the section with the convention positive downward. The steel strains ε_{s1}, ε_{s2}, ε_{s3} ... can be determined using the same equation and the stresses f_{s1}, f_{s2}, f_{s3} ... corresponding to strains evaluated from stress-strain curve of steel. Steel forces may then be determined from the steel stresses and areas of steel. For the bar i, the force equation is

$$F_{si} = f_{si} A_{si} \qquad (3\text{-}2)$$

Force equilibrium requires

$$C_c + \sum_{i=1}^{n} A_{si} f_{si} = P_u \qquad (3\text{-}3)$$

Normalizing

$$\frac{C_c}{f_c' A_g} = \frac{P_u}{f_c' A_g} - \sum_{i=1}^{n} \frac{A_{si} f_{si}}{f_c' A_g} \qquad (3\text{-}4)$$

where C_c is the sum of concrete forces from confined core concrete and unconfined cover concrete obtained by integrating the respective concrete stresses over the cross sectional area in compression as

$$\iint f_c \, dx \, dy \qquad (3\text{-}5)$$

The moment-curvature relationship for a given axial load level is determined by incrementing the curvature ϕ. For each value of ϕ, the centroidal strain ε_0 is found by adjusting it until the force equilibrium equation (3-4) is satisfied. The internal forces and centroidal strain so determined are then used to calculate the moment M

$$M = \iint f_c \, y \, dx \, dy + \sum_{i=1}^{n} A_{si} f_{si} y_i \qquad (3\text{-}6)$$

In order to evaluate the integrals in equation (3-5) and (3-6) and to maintain generality without sacrificing accuracy, a numerical integration strategy that employs Gauss Quadrature is investigated. This method is discussed in the following.

3.2.1 Gauss Quadrature Technique

Gauss quadrature is a very powerful method of numerical integration which employs unequally spaced intervals. The numerical integration of $\int_a^b f(x) \, dx$ is given by

$$\bar{I} = \Omega\,[\,w_1 f(x_1) + w_2 f(x_2) + \cdots\cdots + w_n f(x_n)\,]\tag{3-7}$$

where x_k are the n equally spaced points determined by the type and degree of orthogonal polynomial used, and the w_k are the weight factors associated with each integration point. The quantity Ω is a constant determined by the limits of the integral and expressed as

$$\Omega = b - a\tag{3-8}$$

Thus by using Gauss Quadrature, it is possible to break down any difficult integral into a summation of discrete products with an associated weight factor. Although this form of numerical integration is widely applied to finite element analysis, the use of this technique in moment-curvature analysis is new and appealing due to its simplicity. The weight factors to be used for integration are however dependant on the degree of polynomial used and can be obtained from any textbook on mathematical functions (e.g. Chapra and Canale, 1985). The weight factors and integration points for 4, 5 and 6 Gauss points with limits from 0 to 1 are shown in Table 3-1.

Table 3-1 Integration points and weights for Gauss-Legendre quadrature

Order	Integration Points	Weight Factors	Truncation Error
4	0.069432 0.330009 0.669991 0.930568	0.173928 0.326072 0.326072 0.173928	$\dfrac{1}{3.473 \times 10^6} f^{(8)}(\xi)$
5	0.046910 0.230765 0.500000 0.769235 0.953089	0.118463 0.239312 0.284450 0.239312 0.118463	$\dfrac{1}{1.238 \times 10^9} f^{(10)}(\xi)$
6	0.033765 0.169395 0.380690 0.619310 0.830605 0.966235	0.085617 0.180381 0.233957 0.233957 0.180381 0.085617	$\dfrac{1}{1.426 \times 10^{15}} f^{(8)}(\xi)$

Although it is obvious that the level of numerical accuracy improves with the higher number of Gauss points, it was observed through a number of test runs that an optimum level of accuracy is achieved by the use of fourth and sixth order polynomials for rectangular and circular sections respectively. The use of a higher order polynomial for circular sections was necessitated by the added non-linearity involved due to the shape of the section. A typical example of a comparison of an "exact" analysis and the Gauss quadrature method is shown in figure 3-1. Here the results of a rigorous fiber element analysis of a circular section is compared with a six point Gaussian integration scheme using the parameters listed in table 3-1.

3.2.2 Moment Curvature Analysis using Gauss Quadrature Technique

For a confined concrete column, the moment capacity of eccentric compressive concrete stress block consists of the following:

$$M_u = M_s + M_c + M_{cc} \qquad (3\text{-}9)$$

where M_u = the ultimate moment capacity of the section for a given curvature (ϕ) that also has an associated centroidal strain ε_0 and neutral axis depth c (figure 2-4), M_s = moment generated by the longitudinal reinforcement, and M_c, M_{cc} = moment generated by the cover and core concrete respectively.

Following the numerical integration scheme, the axial load contribution from the concrete (both cover and core) can be calculated as

$$C_c = c \sum_{k=1}^{6} w_k \left(b_o f_{co} + b_c f_{cc} \right)_k \qquad (3\text{-}10)$$

where w_k = weight factor, b_o, b_c = breadth of the cover and confined core concrete, f_{co}, f_{cc} = cover and core concrete stress at the k-th Gauss point and c = depth of the neutral axis. The moment capacity of the reinforcing steel can be calculated taking moment of all the steel forces about the middle of the section. Hence,

22
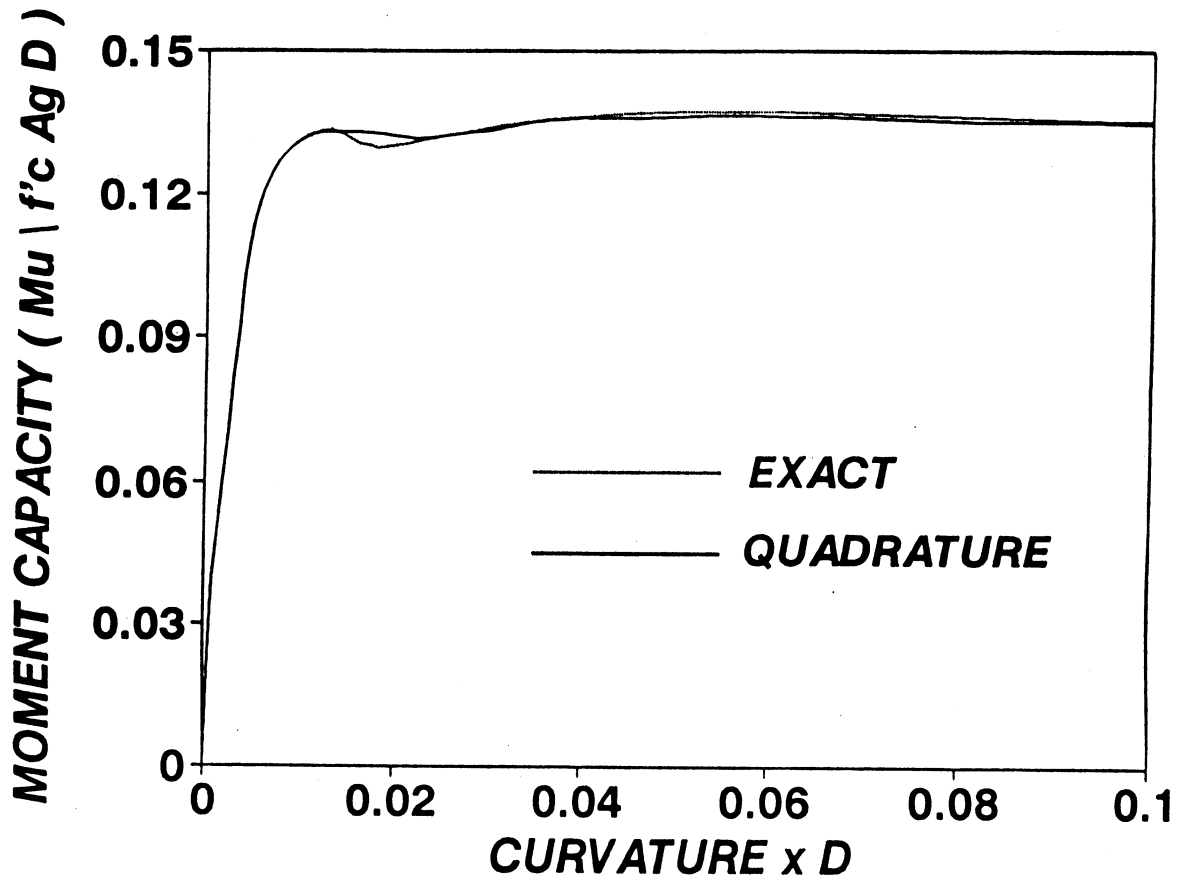
Figure 3-1 Comparison of Exact and Gauss Quadrature based Moment Curvature Analysis.

$$M_s = \sum_i A_{si} f_{si} y_i \qquad \text{(3-11)}$$

in which i = index to refer to the ith layer of steel, A_{si} = = area of steel in the ith layer, f_{si} = the steel stress corresponding to calculated steel strain, and y_i = the distance from the mid-depth reference axis to the center of the ith longitudinal reinforcement. Using the same integration scheme, the concrete contribution to the moment can be calculated as

$$M_c + M_{cc} = c \sum_{k=1}^{6} w_k \, y_k \left(b_o f_{co} + b_c f_{cc} \right)_k \qquad \text{(3-12)}$$

where the symbols are as explained previously. The term y_k in equation (3-12) refers to the distance of the k-th Gauss point from the middle of the section.

If the centroidal strain ε_0 and curvature ϕ are known, the axial force (P_u) and the moment (M_u) can be easily calculated. But normally the inverse problem in which ε_0 and ϕ are to be determined from known values of P_u and M_u, or a mixed problem, is encountered. In this case, some degree of iteration is required to find a solution. The Newton-Raphson algorithm can be utilized for the purpose. Considering the first terms only in the Taylors series expansion

$$\left\{ \begin{matrix} \varepsilon_{0_{i+1}} \\ \phi_{i+1} \end{matrix} \right\} = \left\{ \begin{matrix} \varepsilon_{0_i} \\ \phi_i \end{matrix} \right\} + \left\{ \begin{matrix} \Delta \varepsilon_{0_i} \\ \Delta \phi_i \end{matrix} \right\} \qquad \text{(3-13)}$$

where the incremental strain $\Delta \varepsilon_{0_i}$ and curvature $\Delta \phi_i$ are determined from

$$\left\{ \begin{matrix} \Delta P_{u_i} \\ \Delta M_{u_i} \end{matrix} \right\} = \begin{bmatrix} \dfrac{\partial P_u}{\partial \varepsilon_0} & \dfrac{\partial P_u}{\partial \phi} \\ \dfrac{\partial M_u}{\partial \varepsilon_0} & \dfrac{\partial M_u}{\partial \phi} \end{bmatrix} \left\{ \begin{matrix} \Delta \varepsilon_{0_i} \\ \Delta \phi_i \end{matrix} \right\} \qquad \text{(3-14)}$$

Using the first row of equation (3-14), $\Delta \varepsilon_{0_i}$ can be solved as

24

$$\Delta \varepsilon_{0_i} = \frac{\Delta P_{u_i} - \dfrac{\partial P_u}{\partial \phi} \Delta \phi_i}{\dfrac{\partial P_u}{\partial \varepsilon_0}}$$

where the partial differentials are evaluated using a numerical differentiation technique.

3.2.3 Stress-Strain Relations for Concrete and Steel

Appropriate stress strain models for confined and unconfined concrete need to be used for the evaluation of the concrete component of the moment. Although significant research has been performed on formulating appropriate stress-strain models (eg. Popovics (1973), Kent and Park (1971)), most of them are unable to accurately control the descending branch of concrete for both confined and unconfined cases. However, Tsai's (1988) equation capable of describing the behavior of both confined and unconfined concrete fairly satisfactorily, was chosen for describing the stress-strain behavior of concrete. The parameters to be used in the equation are based on the recommendations made by Chang and Mander (1994). These were calibrated against experiments to improve the quality of analytical predictions. The stress-strain model (refer figure 3-2) together with the parameters necessary for determining the confined concrete behavior are described in Appendix A.

Reinforcing Steel Stress-Strain Relations: Reinforcing steel forms an important component of structural concrete. Hence accurate modeling of its behavior is important. For nominal strength calculations an elasto-perfectly-plastic stress-strain model is customarily assumed. However, for a rigorous moment-curvature analysis capturing the effects of the strain-hardening branch is important since large moment capacity of the section may be obtained at very large strains.

In this study, the stress-strain behavior of reinforcing steel considering the strain hardening branch can be accurately represented by the single relationship suggested by Chang and Mander (1994) which is given by

25
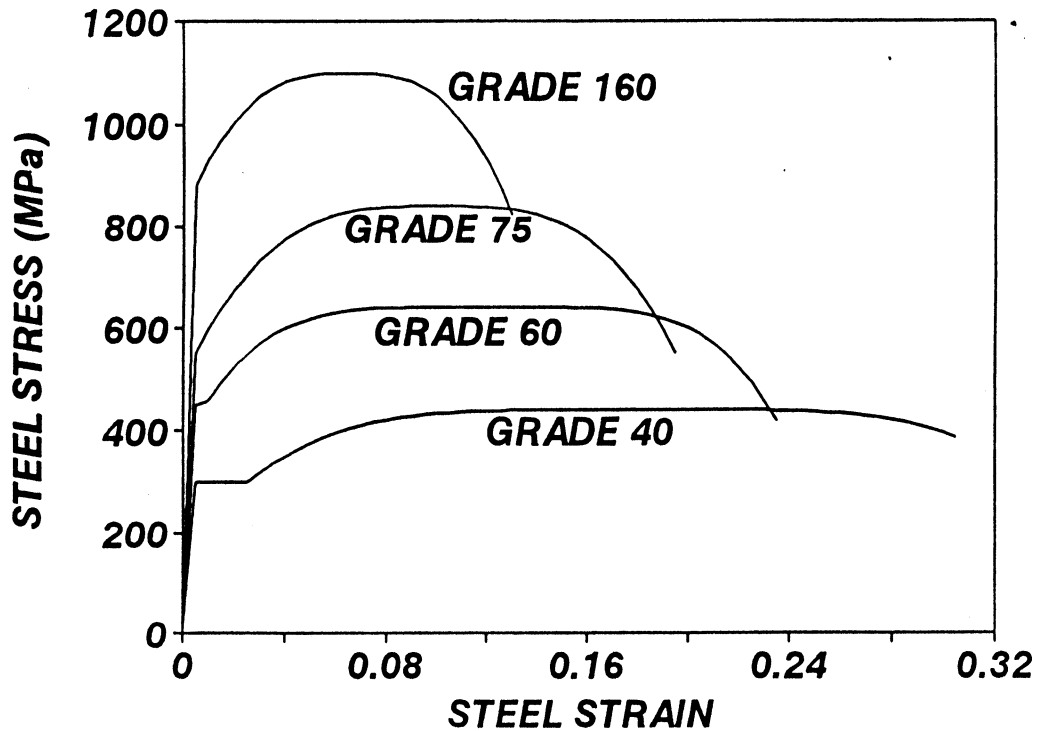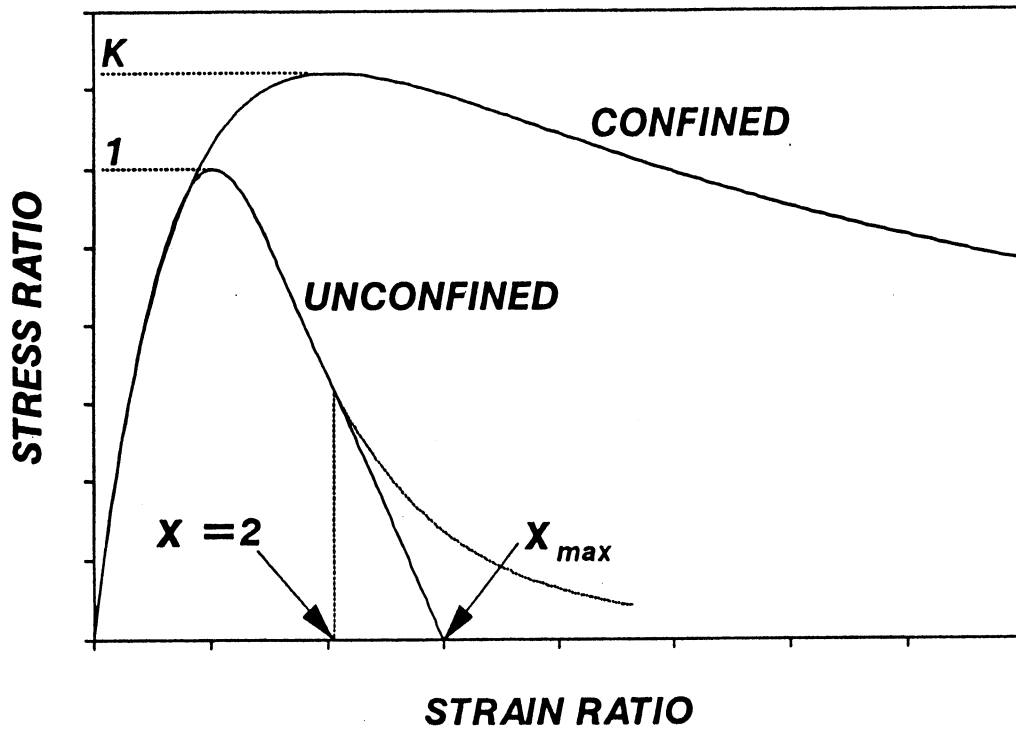
Figure 3-2   Constitutive Relations for Unconfined and Confined Concrete and Reinforcing Steel

$$f_s = \frac{E_s \varepsilon_s}{\left\{ 1 + \left| \frac{E_s \varepsilon_s}{f_y} \right|^{20} \right\}^{0.05}} + \left(\frac{1 + sign(\varepsilon_s - \varepsilon_{sh})}{2} \right)(f_{su} - f_y)\left[1 - \left| \frac{\varepsilon_{su} - \varepsilon_s}{\varepsilon_{su} - \varepsilon_{sh}} \right|^p \right] \qquad (3\text{-}16)$$

in which, ε_{su} = strain hardening strain, f_{su} = ultimate stress, E_{sh} = strain hardening modulus, ε_{su} = ultimate strain of reinforcement and the power p is given by

$$p = E_{sh} \frac{\varepsilon_{su} - \varepsilon_{sh}}{f_{su} - f_y} \qquad (3\text{-}17)$$

Based on the Chang and Mander model (1994), the stress-strain curves for typical grades of steel reinforcement are plotted in figure 3-2.

3.3 COMPUTATION OF THE NUMBER OF CYCLES TO FAILURE

Before the number of cycles to failure (N_c) can be obtained, it is necessary to evaluate the concrete component of the normalized plastic work $\bar{u}_{ex,c}$ in equation (2-18). Assuming that at any step of the moment curvature analysis the curvature (ϕ_i), neutral axis depth (c), and centroidal strain ε_{0_i} are known the plastic curvature can be obtained as

$$\phi_{p_i} = \phi_i - \phi_y \qquad (3\text{-}18)$$

where ϕ_y denotes the lowest of the curvatures to produce either an extreme fiber compression strain of 0.002 or yielding of the furthest tension steel. Thus using Gauss Quadrature

$$\bar{u}_{ex,c} = c \sum_{k=1}^{6} w_k \left[\frac{f_{cc} b_{cc} + f_{co} b_{co}}{f_c' A_g} \right]_k \left(\frac{c}{D} - \frac{y_{c_k}}{D} \right)(\phi_p D) \qquad (3\text{-}19)$$

where f_{cc} = confined core concrete stress, b_{cc} = width of the core concrete, f_{co} = unconfined cover concrete stress, b_{co} = width of the unconfined cover concrete (all at k-th Gauss point), and y_{c_k} = distance of the k-th Gauss point from the extreme compression fiber. A slight modification is also required to the steel term $\bar{u}_{ex,s}$. Assuming that the i-th steel layer has yielded, the plastic work is given by

$$\bar{u}_{ex,s} = \sum_{i=1}^{n} \left(\frac{A_{st_i}}{A_g}\right)\left(\frac{f_y}{f_c'}\right)(\varepsilon_{s_i} - \varepsilon_y) \tag{3-20}$$

where ε_{s_i} = total strain in the i-th steel layer obtained by equation (3-3) with $y_0 = 0$ for symmetric sections and ε_y = yield strain of steel. Thus equation (2-18) can be rewritten as

$$u_{ex} = 2N_c \bar{u}_{ex,s} W_s + (2 + 2(N_c - 1)\eta_c) \bar{u}_{ex,c} W_c \tag{a}$$

$$= \left[\bar{u}_{ex,s} W_s + \left(\eta_c + \frac{1 - \eta_c}{N_c}\right)\bar{u}_{ex,c} W_{cc}\right] \tag{b}$$

(3-21)

where W_s and W_{cc} are the weighing factors which accounts for the fact that the critical cross tie which is first to fracture, only absorbs a proportion of the total work done by the steel and core concrete. Mander et al. (1984, 1988a,b) who considered the concentric axial compression case, introduced these weighing factors (W_s and W_{cc}) which allow the work done on the critical cross tie to be calculated. The weighing factor for the longitudinal steel is evaluated as

$$W_s = \frac{Number\ of\ bars\ restrained\ by\ the\ critical\ cross\ tie}{Total\ number\ of\ longitudinal\ bars} \tag{3-22}$$

Similarly for the concrete,

$$W_{cc} = \frac{Length\ of\ the\ critical\ tie}{Total\ length\ of\ bar\ in\ one\ hoop\ set} \tag{3-23}$$

For a detailed summary refer to Appendix B. It is also to be noted that the weighing factors for concrete needs to be incorporated in the expression for internal energy absorption as well. Thus equation (2-9) can be rewritten as

$$u_{in} = 0.008\ W_{cc} + \rho_s \frac{U_{sf}}{f_c'} \frac{A_{cc}}{A_g} W_{cc} \tag{3-24}$$

Thus using equations (3-21) and (3-24), the number of cycles to failure can be evaluated as

28

$$N_c = \frac{u_{in} - 2(1 - \eta_c)u_{ex,c}}{2 u_{ex,c} \dfrac{W_s}{W_{cc}} + 2\eta_c u_{ex,c}}$$

(3-25)

If needed, the cumulative plastic drift can be assessed by

$$\Sigma\theta_p = 2N_c (\phi_p D)\left(\frac{L_p}{D}\right)$$

(3-26)

where L_p = length of the plastic hinge. Thus a complete fatigue history based on transverse hoop fracture can be obtained.

3.4 CONCLUSIONS

In this section the fatigue expressions for confined concrete based on the fracture of transverse hoops is evaluated using a detailed computational approach. This method uses a Gauss Quadrature integration scheme which is particularly appealing due to it's simplicity and ability to be suited to spreadsheet based computer programming. Fatigue expressions so evaluated are presented in the form of number of cycles versus dimensionless plastic curvature from which it is possible to have an idea of the plastic curvature obtainable from a section before failure occurs through the fracture of transverse hoops.

SECTION 4
SIMPLIFIED DIRECT APPROACH

4.1 INTRODUCTION

In the previous section a detailed computational approach to formulate the fatigue life based on transverse hoop fracture was investigated. Although the method is very accurate, it is lengthy and apparently not simple enough for quick evaluation. As a result it was decided to formulate a parallel analysis procedure which though not as involved as the previous one is able to give fairly accurate results. This method henceforth to be referred as the simplified direct approach will be discussed next.

Before proceeding any further it is important to lay down the assumptions on which this method is based. They are as follows:

(i)   At high levels of axial load the cover concrete is expected to fall off and the behavior of concrete can be entirely attributed to the core concrete.

(ii)   Neutral axis depth (c) is less than half the overall dimension of the section.

(iii) Under large curvatures, all the tension and compression steel yields and the behavior can be assumed to be elasto-plastic.

(iv)   Stress block depth factor (β) is assumed to be equal to 1.0.

(v)   Concrete stress strain decay parameter η_c is assumed to be equal to 0.33.

Following the above assumptions it is possible to greatly simplify the expressions for energy consumption capacity and applied energy demand.

31

4.2 ENERGY ABSORPTION CAPACITY

It was shown previously in equation (2-8), that the total energy absorption capacity is the sum of the strain energy of an equivalent unconfined concrete column and the energy required to fracture the lateral hoop. Following assumption (i) where the effect of the cover concrete is neglected, it is possible to replace the gross cross sectional area in the same by the area of the confined core concrete. Also incorporating the weighing factors for concrete mentioned earlier, the normalized energy absorption capacity can be written as

$$u_{in} = \frac{IWD}{f_c' A_g} = 0.008 \frac{A_{cc}}{A_g} W_{cc} + \rho_s \frac{U_{sf}}{f_c'} \frac{A_{cc}}{A_g} W_{cc} \qquad (4\text{-}1)$$

where the unconfined concrete column is presumed to have the same dimensions as the confined core.

4.3 APPLIED ENERGY DEMAND

It was proposed that the available energy capacity denoted by the above expression is progressively consumed by the concrete and the longitudinal steel doing work in compression. Following some of the simplifying assumptions made earlier it is possible to formulate explicit expression for the energy consumption capacity. Such expressions are greatly dependant on the shape of the section. Thus it was decided to study two very basic sectional shapes, viz rectangular and circular. The case of a rectangular section is examined first.

4.3.1 Analysis for Rectangular Section

It is well known that depending on the relative proportion of the sides of a rectangular section, the longitudinal steel can be arranged in various possible ways. Thus at this point a new factor termed as the reinforcing steel configuration factor for rectangular sections (γ_r) is introduced which denotes the proportion of the total reinforcing steel area that exists in each of the two sides of the member. Specific cases are as follows:

- *square sections* with reinforcing steel placed symmetrically around the perimeter $\gamma_r = 0.5$

- *rectangular sections* (beams) with the steel lumped at the outer faces (top and bottom reinforcement in case of beams) $\gamma_r = 0.0$

- *wall sections* with two layers of steel running parallel to the long sides; when bending is about the strong axis, $\gamma_r = 1.0$ and when bending is about the weak axis $\gamma_r = 0.0$.

Accordingly it can be stated the area of steel which is in the compressive portion of the section (above the neutral axis according to the adopted convention) is given by

$$(A_{st})_{compression} = \left[0.5(1-\gamma_r) + \gamma_r\left(\frac{c''}{D''}\right)\right]A_{st} \qquad (4\text{-}2)$$

where c''/D'' denotes the neutral axis depth ratio for the section neglecting the cover concrete, $\gamma_r =$ reinforcing steel configuration factor for rectangular sections as shown in figure 4-1, and $A_{st} =$ total area of the longitudinal steel. Note that the first term in square brackets has a factor of 0.5 because only half of $(1 - \gamma_r)A_{st}$ amount of steel located above the neutral axis does work in compression along with $\gamma_r A_{st}(c''/D'')$ quantity.

Making a simplifying assumption that the centroid of the compression steel is located half way from the extreme compression fiber to the neutral axis, the work done by the compression steel is given by

$$\bar{u}_{ex,s} = \frac{A_{st}}{A_g}\left[0.5(1-\gamma_r) + \gamma_r\left(\frac{c''}{D''}\right)\right]\frac{f_y}{f_c'}\frac{c''}{2D''}\frac{D''}{D}(\phi_p D) \qquad (4\text{-}3)$$

Replacing A_{st}/A_g by the percentage of longitudinal steel (ρ_t), the above expression can be simplified to

$$\bar{u}_{ex,s} = 0.25\frac{\rho_t f_y}{f_c'}\left[(1-\gamma_r) + 2\gamma_r\left(\frac{c''}{D''}\right)\right]\frac{c''}{D''}\frac{D''}{D}(\phi_p D) \qquad (4\text{-}4)$$

33
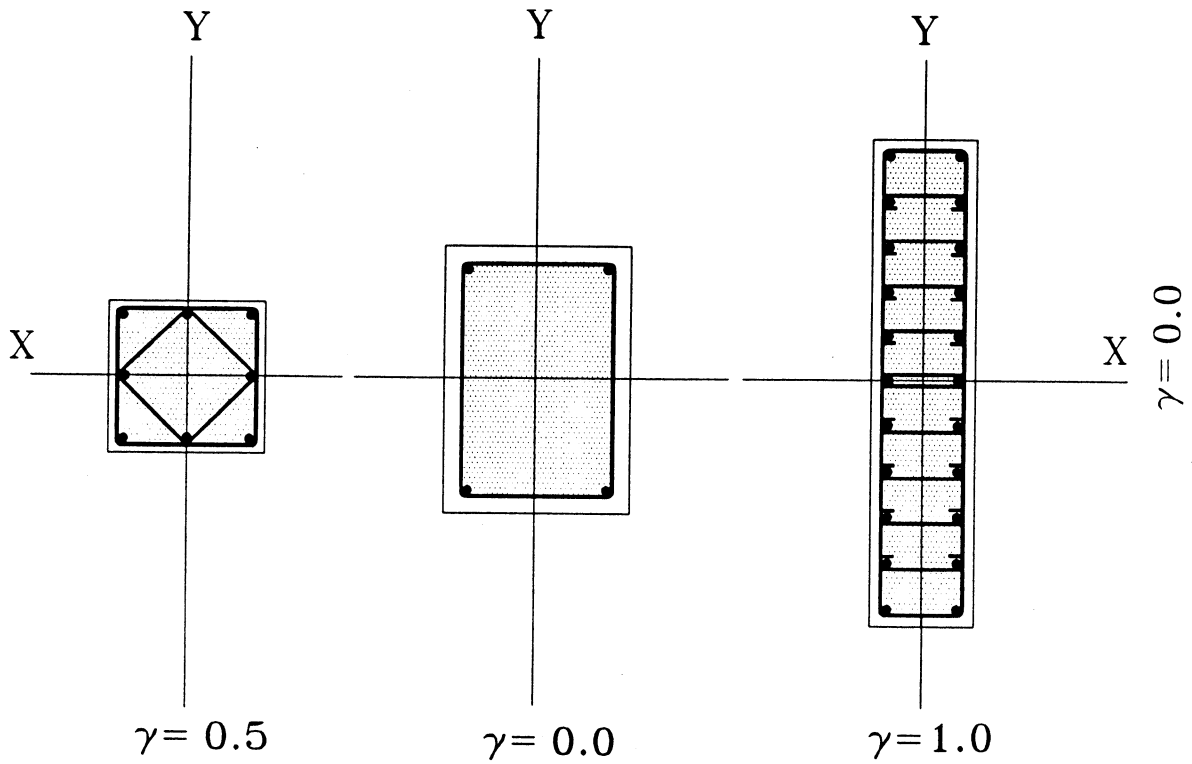
Figure 4-1 Reinforcing Steel Configuration Factor for Rectangular Column Sections.
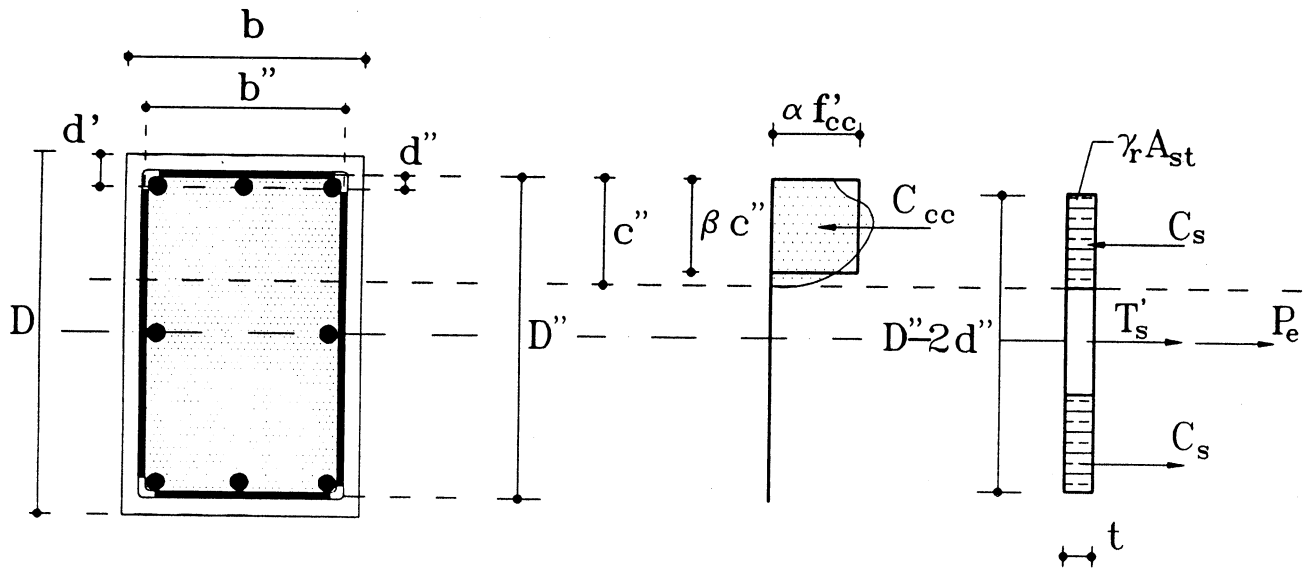
Figure 4-2 Evaluation of Neutral Axis Depth for Rectangular Sections.

The compressive force in the core concrete for a rectangular section can be written as

$$C_{cc} = (\alpha_c f'_{cc})(\beta_c c'') b'' \qquad (4\text{-}5)$$

where $\alpha_c \beta_c$ are the equivalent core concrete stress block parameters, f'_{cc} = compressive strength of the core concrete = $K f'_c$ (K being a factor representing the magnification of f'_c due to confinement), and b'', c'' are as shown in figure 4-3. Normalizing equation (4-5) by $f'_c A_g$, one obtains

$$\frac{C_{cc}}{f'_c A_g} = (\alpha_c \beta_c) K \frac{(b'' c'')}{A_g} = (\alpha_c \beta_c) K \left(\frac{c''}{D''}\right)\left(\frac{A_{cc}}{A_g}\right) \qquad (4\text{-}6)$$

where $A_{cc} = b'' D''$ denotes the area of core concrete. Assuming that the concrete compression force acts at a depth $0.5\,\beta_c$ from the extreme compression fiber the work done by the concrete in compression is given by

$$\overline{u}_{ex,c} = \frac{C_{cc}}{f'_c A_g} \left[(1-0.5\beta_c) \frac{c''}{D''} \frac{D''}{D} (\phi_p D)\right] \qquad (4\text{-}7)$$

where the part in square brackets denotes the effective plastic strain at the point of application of the concrete compressive force. Combining equations (4-4), (4-6) and (4-7) the normalized external work done can be expressed as

$$u_{ex} = 2N_c \frac{0.25\rho_s f_y}{f'_c}\left[(1-\gamma_r)+2\gamma_r \frac{c''}{D''}\right] \frac{c''}{D''}\frac{D''}{D}(\phi_p D) + 2N_c\left[\eta_c + \frac{1-\eta_c}{N_c}\right](0.5\alpha_c) K \frac{A_{cc}}{A_g}\left(\frac{c''}{D''}\right)^2 \frac{D''}{D}(\phi_p D) \qquad (4\text{-}8)$$

in which β_c was taken as 1.0. To reduce some of the non-linearities of the above equation, η_c can be taken as 0.33 and N_c associated with it as 4.0. This is based on a statistical observation of specimens that have failed due to fracture of transverse hoops. A mean N_c of 4.0 was observed for most. Thus equation (4-8) can be simplified as

35
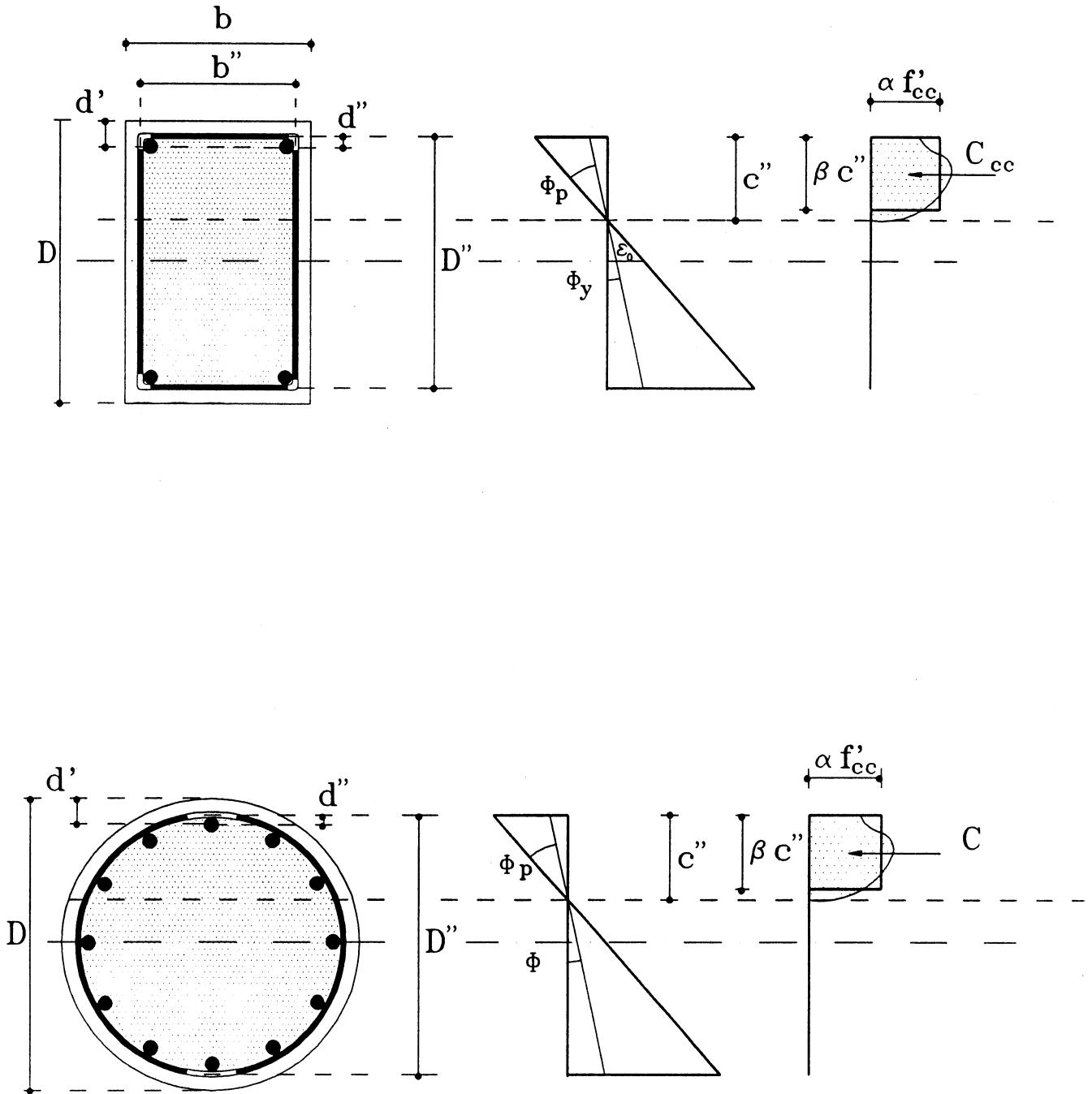
Figure 4-3 Core Concrete Parameters for Rectangular and Circular Column Sections.

36

$$u_{ex} = 2N_c\frac{0.25\rho_s f_y}{f_c'}\left[(1-\gamma_r)+2\gamma_r\frac{c''}{D''}\right]\frac{c''}{D''}\frac{D''}{D}(\phi_p D)+2N_c(0.25\alpha_c)K\frac{A_{cc}}{A_g}\left(\frac{c''}{D''}\right)^2\frac{D''}{D}(\phi_p D) \qquad (4\text{-}9)$$

Incorporating the weighing factors for concrete and steel mentioned previously, and equating this to equation (4-1), it is possible to solve for the dimensionless plastic curvature as

$$(\phi_p D) = \frac{4\left(0.008 + \rho_s \dfrac{U_{sf}}{f_c'}\right)}{\dfrac{\rho_t f_y}{f_c'}\left[(1-\gamma_r)+2\gamma_r\left(\dfrac{c''}{D''}\right)\right]\dfrac{c''}{D''}\dfrac{D''}{D}\dfrac{A_g}{A_{cc}}\dfrac{W_s}{W_{cc}}+\alpha_c K\left(\dfrac{c''}{D''}\right)^2\left(\dfrac{D''}{D}\right)}(2N_c)^{-1} \qquad (4\text{-}10)$$

and the cumulative plastic drift as

$$\Sigma\theta_p = \frac{4\left(0.008 + \rho_s \dfrac{U_{sf}}{f_c'}\right)\left(\dfrac{L_p}{D}\right)}{\dfrac{\rho_t f_y}{f_c'}\left[(1-\gamma_r)+2\gamma_r\left(\dfrac{c''}{D''}\right)\right]\dfrac{c''}{D''}\dfrac{D''}{D}\dfrac{A_g}{A_{cc}}\dfrac{W_s}{W_{cc}}+\alpha_c K\left(\dfrac{c''}{D''}\right)^2\left(\dfrac{D''}{D}\right)} \qquad (4\text{-}11)$$

The neutral axis depth (c''/D'') in equations (4-10) and (4-11) can be found from force equilibrium on the column section which requires

$$P_e = C_{cc} + C_s - T_s \qquad (4\text{-}12)$$

where P_e = applied axial load and C_s and T_s are the forces provided by the longitudinal compression and tension reinforcement, respectively.

Consider the column section shown in figure 4-2. Let γ_r denote the proportion of the longitudinal steel arranged on both sides. Thus $(1 - \gamma_r)$ denotes the proportion of the longitudinal steel arranged at the top and at the bottom of the section, respectively. Assuming that under large curvatures all the steel yields, from figure 4-2 it can be seen that the tension and compression forces due to $0.5(1 - \gamma_r)A_{st}$ on the top an bottom layer equilibrate each other and hence the remaining steel $(\gamma_r A_{st})$ distributed along the sides over a depth $(D'' - 2d'')$ of the section

with a total thickness t given by

$$t = \frac{\gamma_r A_{st}}{(D'' - 2d'')}$$

(4-13)

where the sectional parameters are easily identified from figure 4-3. Out of this $\gamma_r A_{st}$ a part will be in tension and the remaining in compression. Assuming that the compressive force in a steel strip of thickness t and depths $c'' - d''$ equal to a tensile force in a strip of same dimension below the neutral axis, the net tensile force in steel can be assumed to be concentrated in a strip of thickness and depth $(D'' - 2c'')$ arranged symmetrically about the neutral axis. Thus equation (4-12) can be revised as:

$$P_e = C_{cc} - T_s'$$

(4-14)

where T_s' is the tensile force in the strip of depth $(D'' - 2c'')$. Thus

$$T_s' = t(D'' - 2c'')f_y = \gamma_r \rho_t f_y A_g \frac{(1 - 2c''/D'')}{(1 - 2d''/D'')}$$

(4-15)

Putting the values of C_{cc} and T_s' in equation (4-14)

$$\frac{P_e}{f_c' A_g} = (\alpha_c \beta_c)(K)\left(\frac{c''}{D''}\right)\left(\frac{A_{cc}}{A_g}\right) - \gamma_r \rho_t \left(\frac{f_y}{f_c'}\right) \frac{(1 - 2c''/D'')}{(1 - 2d''/D'')}$$

(4-16)

with $\beta_c = 1.0$, it is possible to solve for c''/D'' as

$$\frac{c''}{D''} = \frac{\left(\frac{P_e}{f_c' A_g}\right) + \left(\frac{\gamma_r \rho_t f_y/f_c'}{1 - 2d''/D''}\right)}{\left(\alpha_c K \frac{A_{cc}}{A_g} + \frac{2\gamma_r \rho_t f_y/f_c'}{1 - 2d''/D''}\right)}$$

(4-17)

However, one point is to be borne in mind that the confined core concrete parameter α_c and the confinement coefficient K also depends on ρ_s and the ratio f_{yh}/f_c' where f_{yh} denotes the yield

38

stress of the hoop steel. A regression analysis yielded a simplified expression relating α_c and K with the rest as

$$\alpha_c = 0.625 \left(1 + \rho_s \frac{f_{yh}}{f_c'} \right) \tag{4-18}$$

$$K = 1 + 2.1 \rho_s \frac{f_{yh}}{f_c'} \tag{4-19}$$

These equations are plotted in figure 4-4(a) and 4-5(a) and the theoretical basis is given in Appendix A.

4.3.2 Analysis for Circular Section

Analysis for circular sections can be performed in the same line as the rectangular sections done previously. A reinforcing steel configuration factor for circular sections (γ_c) is defined which conceptually denotes the proportion of the longitudinal steel arranged in the top and bottom quarter of the section. Thus for a circular section with 10 numbers of longitudinal bars, $\gamma_c = 0.3$ and for a circular section with 20 or more numbers of longitudinal bars $\gamma_c = 0.5$. A linear interpolation is allowed for the intermediate range.

It should be noted that the concrete compression force for a circular section is more difficult to derive. To determine the core concrete compression force (C_{cc}), consider a circle of diameter D'' having a chord bisected by a diameter as shown in figure 4-6. The ratio of the area in compression (A_c) to the core concrete area (A_{cc}) can be written as

$$\left(\frac{A_c}{A_{cc}} \right) = \frac{1}{2\psi} (\psi - \sin \psi) \tag{4-20}$$

where ψ = angle subtended at the center by the chord $= 2\cos^{-1}\left(1 - 2\frac{c''}{D''} \right)$. Using a regression analysis, Kim (1996) showed that equation (4-20) can be approximated to

39
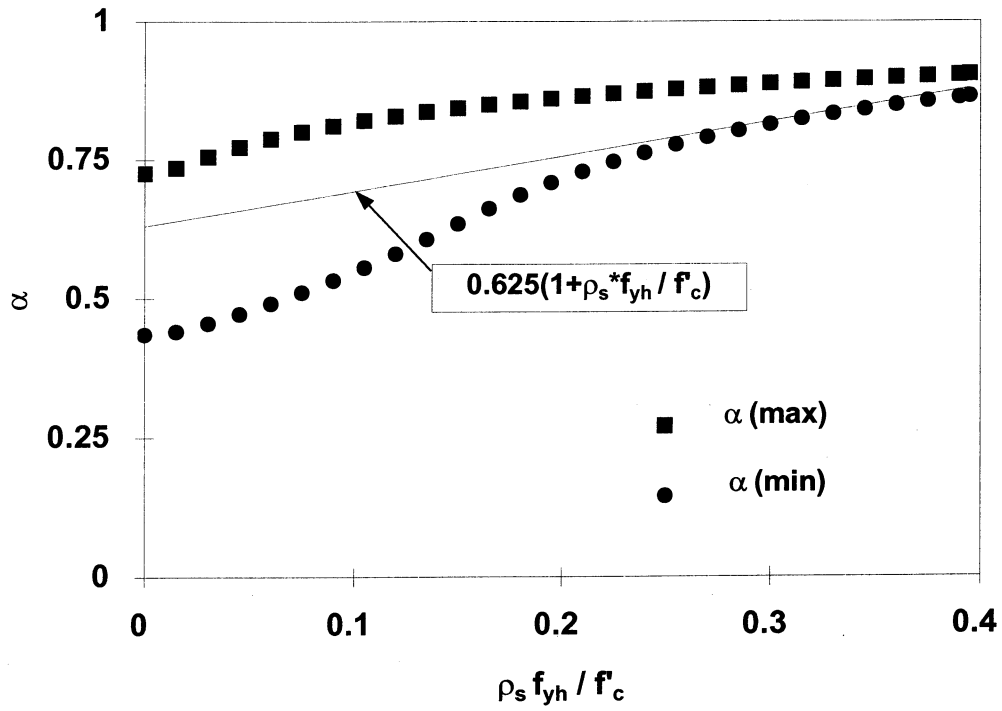
(a) Rectangular Section
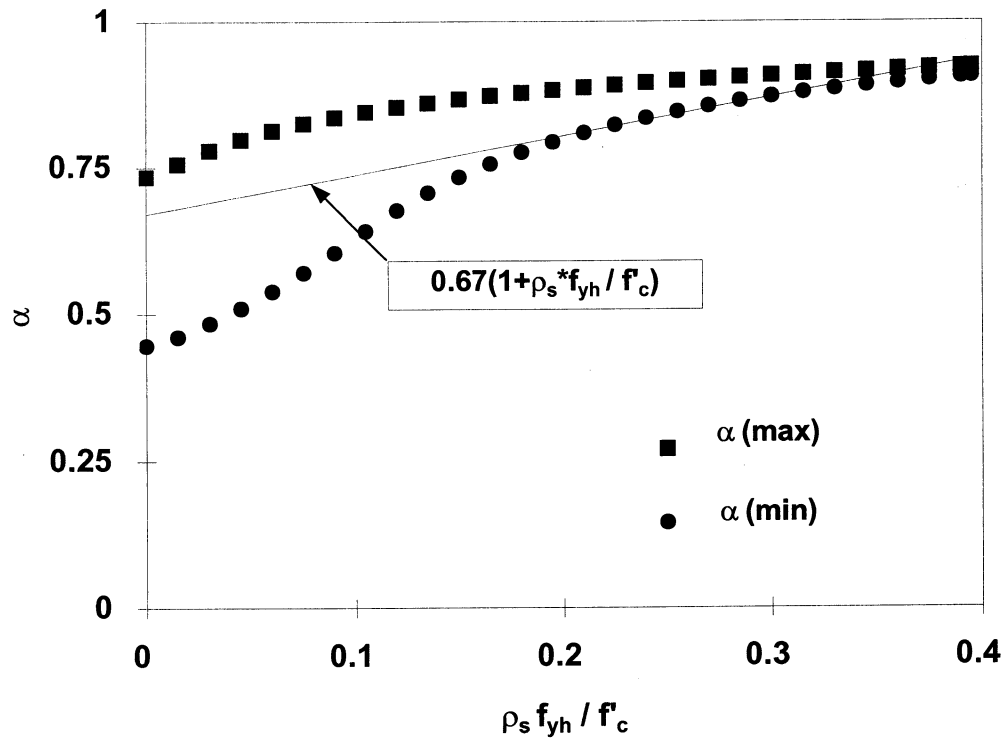
(b) Circular Section

Figure 4-4 Simplified Stress Block Parameters
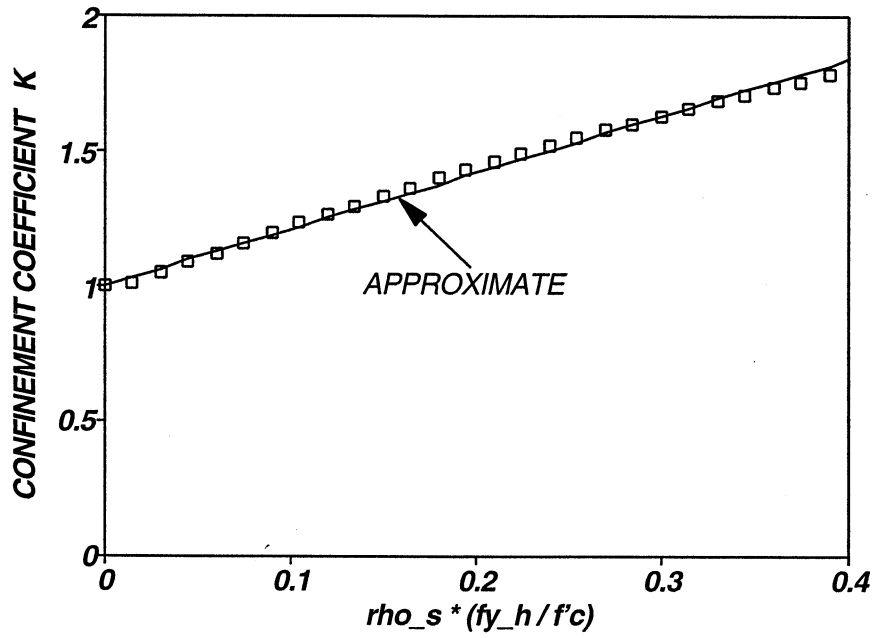
(a) Rectangular Section
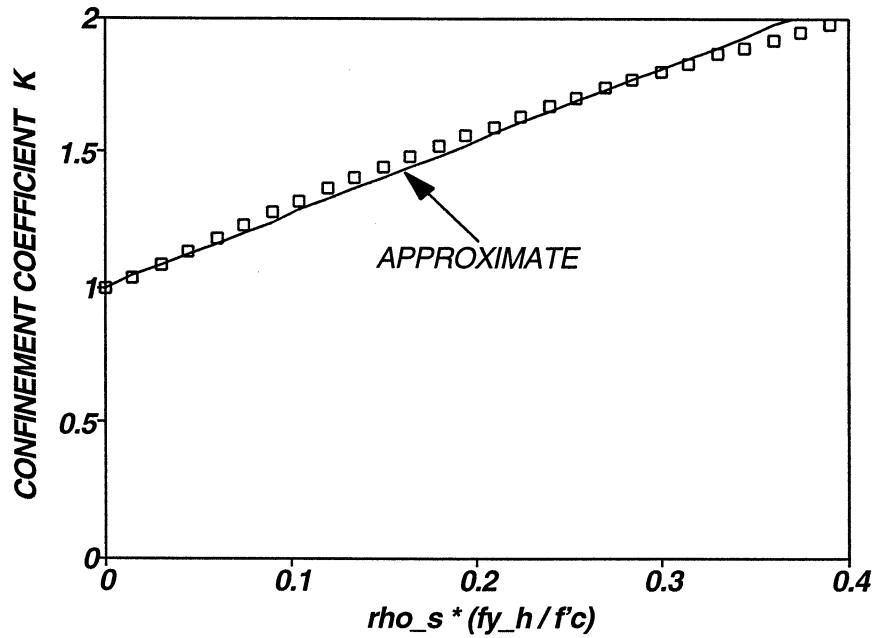
(b) Circular Section

Figure 4-5 Comparison of Exact and Approximate Confinement Coefficient.

41

$$\left(\frac{A_c}{A_{cc}}\right) = 1.32\left(\beta_{cc}\frac{c''}{D''}\right)^{1.38} \qquad (4\text{-}21)$$

which is demonstrated by figure 4-7.

Although the use of stress block analysis should technically be limited to rectangular sections only, it was determined in this study that the error in using the same stress block parameters for a circular section was negligible. This is particularly true for circular bridge columns which possess low levels of axial load and are not significantly influenced by the concrete compression force.

Thus the compression force in the core concrete can be approximated as

$$C_{cc} = 1.32\,\alpha_{cc}\left(\beta_{cc}\frac{c''}{D''}\right)^{1.38} f'_{cc}A_{cc} \qquad (4\text{-}22)$$

where α_{cc}, β_{cc} = core concrete block parameters for circular sections (see later), f'_{cc} = compressive strength of the core concrete, and c'', D'', A_{cc} as were defined earlier. Normalizing equation (4-22) by $f'_c A_g$ and substituting $\beta_c = 1.0$

$$\frac{C_{cc}}{f'_c A_g} = 1.32\,\alpha_{cc}\left(\frac{c''}{D''}\right)^{1.38} K\frac{A_{cc}}{A_g} \qquad (4\text{-}23)$$

where $K = f'_{cc}/f'_c$.

It is possible to derive an expression for the neutral axis depth ratio (c''/D'') for a circular section in the same way as was done for a rectangular section. Assuming that under large curvatures all the steel yields, it can be reasoned that the tension and compression forces due to $0.5(1 - \gamma_c)A_{st}$ on the top an bottom layer equilibrate each other and hence the remaining steel $(\gamma_c A_{st})$ can be thought to be distributed along the sides over a depth $(D'' - 2d'')$ of the section with a total thickness t given by

42
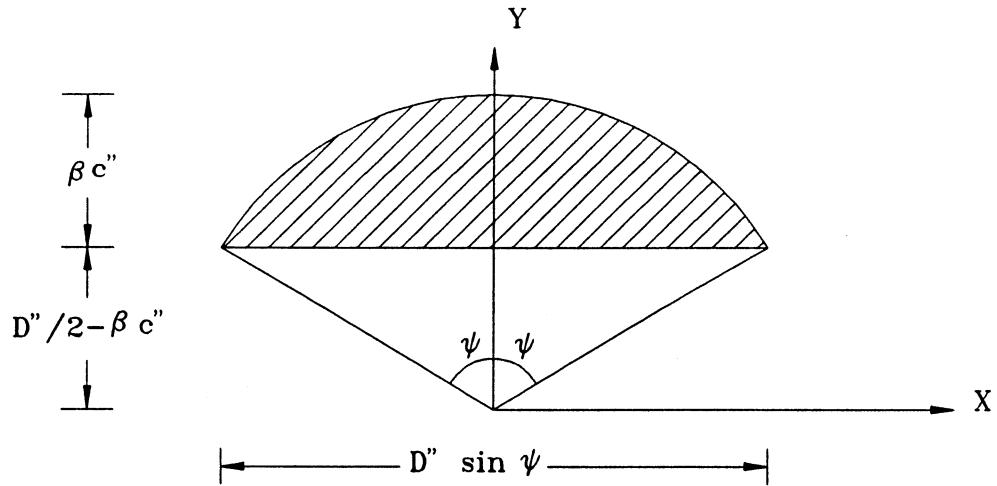
Figure 4-6 Showing Area in Compression in a Circular Column Section.
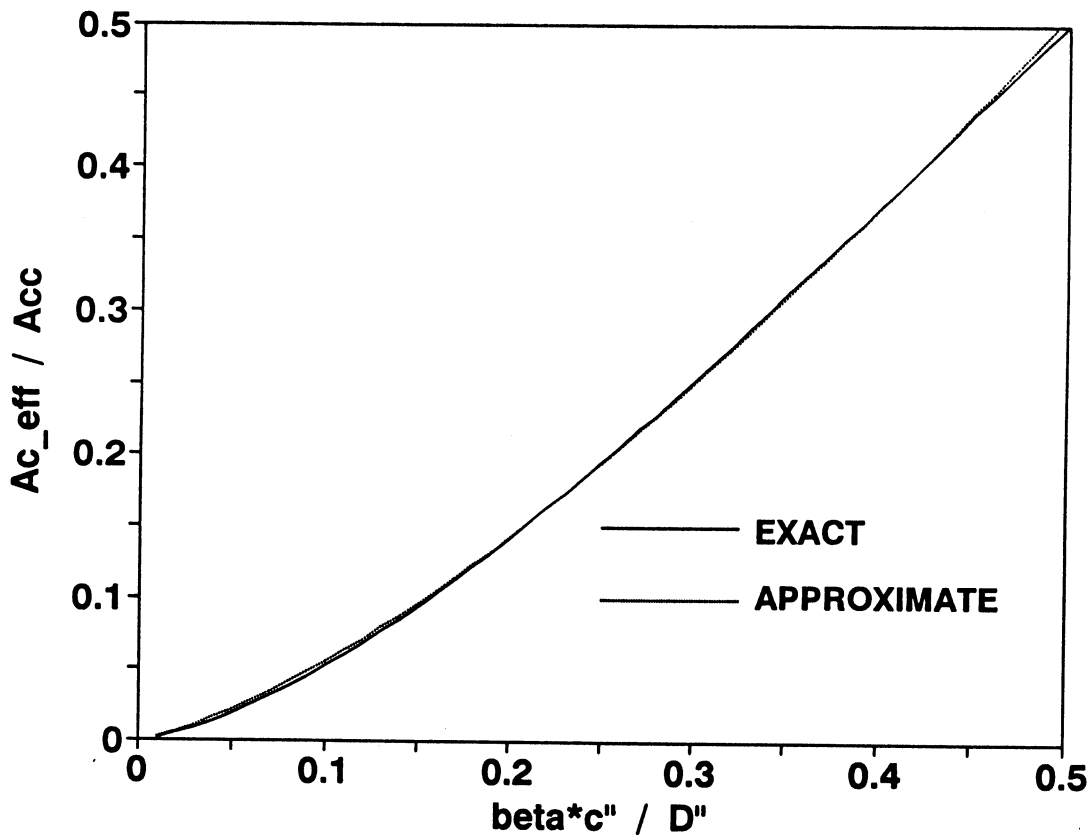
Figure 4-7 Approximate Solution for Evaluating Area in Compression.

43

$$t = \frac{\gamma_c A_{st}}{(D'' - 2d'')} \qquad (4\text{-}24)$$

where the sectional parameters are easily identified from figure 4-3. Thus an expression analogous to equation (4-14) can be written for circular sections with

$$T_s' = t(D'' - 2c'')f_y = \gamma_c \, p_t f_y A_g \frac{(1 - 2c''/D'')}{(1 - 2d''/D'')} \qquad (4\text{-}25)$$

Thus

$$P_e = C_{cc} - \gamma_c A_{st} f_y \left[\frac{1 - 2c''/D''}{1 - 2d''/D''} \right] \qquad (4\text{-}26)$$

where P_e = applied axial load and d'' = depth from the center of the hoop steel to the centroid of the nearest rebar. The concrete compression force ratio $(C_{cc}/f_c'A_g)$ in the above expression is given by equation (4-22) from which

$$\frac{c''}{D''} = \left[\frac{\dfrac{P_e}{f_c'A_g} + \gamma_c \dfrac{p_t f_y}{f_c'} \left(\dfrac{1 - 2c''/D''}{1 - 2d''/D''} \right)}{1.32 \, \alpha_{cc} \, K \, \dfrac{A_{cc}}{A_g}} \right]^{0.725} \qquad (4\text{-}27)$$

Noting that for circular sections the weight factors for steel and concrete are both equal to 1.0 and the concrete compression force acts at a depth $0.6\beta_c$ from the extreme compression fiber, the normalized external work done can be written as

$$u_{ex} = 2N_c \frac{0.25 p f_y}{f_c'} \left[(1 - \gamma_c) + 2\gamma_c \frac{c''}{D''} \right] \frac{c''}{D''} \frac{D''}{D} (\phi_p D) + 2N_c \left[\eta_c + \frac{1 - \eta_c}{N_c} \right] (1.32 \alpha_c) K \frac{A_{cc}}{A_g} \left(\frac{c''}{D''} \right)^{2.38} (1 - 0.6\beta_c) \frac{D''}{D} (\phi_p D) \qquad (4\text{-}28)$$

As before assuming η_c to be 0.33, N_c associated with it as 4.0 and $\beta_c = 1.0$, the above expression can be equated to equation (4-1) to solve for the dimensionless plastic curvature as and the cumulative plastic drift as

44

$$(\phi_p D) = \frac{4\left(0.008 + \rho_s \dfrac{U_{sf}}{f'_c}\right)}{\dfrac{\rho_t f_y}{f'_c}\left[(1-\gamma_c)+2\gamma_c\left(\dfrac{c''}{D''}\right)\right]\dfrac{c''}{D''}\dfrac{D}{D''}+\alpha_c K\left(\dfrac{c''}{D''}\right)^{2.38}\left(\dfrac{D''}{D}\right)}(2N_c)^{-1} \qquad (4\text{-}29)$$

$$\Sigma\theta_p = \frac{4\left(0.008 + \rho_s \dfrac{U_{sf}}{f'_c}\right)\left(\dfrac{L_p}{D}\right)}{\dfrac{\rho_t f_y}{f'_c}\left[(1-\gamma_c)+2\gamma_c\left(\dfrac{c''}{D''}\right)\right]\dfrac{c''}{D''}\dfrac{D}{D''}+\alpha_c K\left(\dfrac{c''}{D''}\right)^{2.38}\left(\dfrac{D''}{D}\right)} \qquad (4\text{-}30)$$

However, it is important to note that the confined core concrete parameter α_{cc} and the confinement coefficient K depends on ρ_s and the ratio of f_{yh}/f'_c where f_{yh} = yield stress of the hoop steel and f'_c = unconfined compression strength of concrete. A regression analysis can be performed similar to a rectangular section yielding

$$\alpha_c = 0.667\left(1 + \rho_s \frac{f_{yh}}{f'_c}\right) \qquad (4\text{-}31)$$

$$K = 1 + 2.7\,\rho_s \frac{f_{yh}}{f'_c} \qquad (4\text{-}32)$$

The details are given in Appendix A. It is to be noted that for routine evaluation purposes γ_c can be assumed to be equal to 0.5.

4.4 CONCLUSIONS

In this section an alternative approach to solving the fatigue expressions is proposed. This method is based on some rational assumptions and gives a reliable estimate of the available plastic curvature from a confined concrete section before failure occurs through the fracture of transverse hoops.

SECTION 5
VALIDATION OF THEORETICAL FATIGUE-LIFE CAPACITY
WITH EXPERIMENTAL RESULTS

5.1 INTRODUCTION

In the preceding section, at attempt was made to look into the failure of columns through transverse hoop fracture. A fatigue theory was developed that can be tailored to serve two purposes — that is a quick estimation of the ultimate curvature using a direct simplified method of analysis, or a more thorough approach to give an accurate assessment of fatigue capacity.

However, to validate a theory, one needs to compare theoretical prediction against experimental observations. This section examines observed results obtained by previous experimental investigators for the purpose of validating the present fatigue theory.

5.2 INTERPRETATION OF EXPERIMENTAL PLASTIC CURVATURE

Experimental values of plastic curvature ($\phi_p D$) can be obtained either directly from experimental results (if measured), otherwise inferred values must be computed as follows. The experimental displacement ductility factor μ_Δ is given by

$$\mu_\Delta = \frac{\Delta_u}{\Delta_y} \qquad (5\text{-}1)$$

where Δ_u = ultimate displacement and Δ_y = yield displacement. Now the ultimate displacement is the sum of plastic and yield displacements where the plastic displacement (Δ_p) is given by

$$\Delta_p = \Delta_u - \Delta_y = \phi_p L_p (L - 0.5 L_p) \qquad (5\text{-}2)$$

where L = length of the column and L_p = plastic hinge length given by equation (2-24). Combining equation (5-1) and (5-2) one obtains

$$\mu_\Delta = \frac{\Delta_p + \Delta_y}{\Delta_y} = \left(\frac{\Delta_p}{\Delta_y}\right) + 1 \tag{5-3}$$

that is:

$$\mu_\Delta = \frac{\phi_p L_p (L - 0.5 L_p)}{\Delta_y} + 1 \tag{5-4}$$

from which the non-dimensional plastic curvature $\phi_p D$ can be expressed as

$$(\phi_p D) = \frac{2(\Delta_u - \Delta_y)}{\left(\dfrac{L_p}{D}\right)^2 \left[\left(\dfrac{2L}{L_p/D}\right) - D\right]} \tag{5-5}$$

The experimental cumulative plastic drift can be obtained by summing up all the positive and negative plastic drift amplitudes to a given stage of loading. For example, if a specimen with a yield drift of 0.25% (0.0025 radians) is cycled five times to a drift of ±3% then the cumulative plastic drift is $|5 \times 2 \times (0.03 - 0.0025) = 0.275$ *radians*.

5.3 DETERMINATION OF EFFECTIVE NUMBER CYCLES TO FAILURE

5.3.1 Background

Since most experiments are conducted on specimens with different displacement amplitudes, it is necessary to adopt an appropriate method of cycle counting. Furthermore, this is also necessary for determining the effective number of cycles of loading in an earthquake time-history. The former and latter cases requiring cycle counting are needed for determining cyclic demand and cyclic capacity respectively.

5.3.2 Miner's Linear Accumulation Rule

The effective number of cycles (N_{eff}) to failure can be obtained using Miner's linear damage accumulation rule which states that the damage accumulated up to the i-th loading cycle is given by

$$D_t = \Sigma D_i \tag{5-6}$$

where D_T is total damage and D_i = damage fraction for the i-th cycle of loading given by

$$D_i = \frac{n_i}{(N_f)_i} \tag{5-7}$$

where n_i = total number of cycles at the current rotational amplitude θ_{ji} and $(N_f)_i$ = fatigue life at the rotational amplitude θ_{ji}.

5.3.3 Effective Number of Cycles

By employing Miner's rule on effective (or equivalent) number of cycles can be derived for a variable cycle history. The linear log-log relationship of plastic rotation to number of cycles of reversals $(2N_f)$ was first obtained by Coffin (1954) and Manson (1953). Later Koh and Stephens (1991) suggested that even total rotation can be used instead of plastic rotation as follows:

$$N_f = Q\,\theta_j^{1/q} \tag{5-8}$$

where Q = fatigue ductility coefficient and q = fatigue ductility exponent. Thus combining equations (5-6), (5-7) and (5-8) the <u>total</u> damage due to a random loading history can be obtained as

$$D_{random} = \sum \left(\frac{n_i}{Q\,\theta_{ji}^{1/q}} \right) = \sum \frac{n_i}{Q} (\theta_{ji})^{-1/q} \tag{5-9}$$

Damage at incipient failure for N_{eff} cycles at an effective rotational amplitude $\theta_{j\,eff}$ is given by

$$D_{constant} = \frac{N_{eff}}{Q\,\theta_{j\,eff}^{1/q}} = \frac{N_{eff}}{Q}\,(\theta_{j\,eff}^{-1/q}) = 1 \qquad\qquad (5\text{-}10)$$

The effective number of cycles (N_{eff}) can be determined by equating the total damage due to random loading and that due to constant equivalent amplitude (equation (5-10)). Hence,

$$\frac{D_{random}}{D_{constant}} = \frac{\sum n_i(\theta_{ji})^{-1/q}}{\sum N_{eff}(\theta_{j\,eff})^{-1/q}} = 1 \qquad\qquad (5\text{-}11)$$

from which

$$N_{eff} = \sum n_i \left(\frac{\theta_{ji}}{\theta_{j\,eff}}\right)^{-1/q} \qquad\qquad (5\text{-}12)$$

Mander et al. (1994) showed that for concrete fatigue the coefficient q has a value of -0.5.

An explanatory example of the damage accumulation analysis is given using a typical laboratory deformation history. To illustrative this concept, consider the accumulated damage that results from the small amplitude cycles in a typical laboratory test. For example, the testing protocol used in much of the current NCEER experimental research uses _two_ completely reversed cycles of lateral loading at increasing drift amplitudes of θ = $\pm 0.25\%$, $\pm 0.5\%$, $\pm 1\%$, $\pm 2\%$, $\pm 3\%$, $\pm 4\%$ +... until failure occurs or when the actuator runs out of stroke capacity. Now suppose if the aforementioned cyclic loading protocol is used, and a specimen fails on the second cycle when the maximum experimental drift is θ_{max} = $\pm 5\%$, then the effective number of cycles _prior_ to the $\pm 5\%$ drift amplitude is:

$$N_{eff}^c = \sum \left(\frac{\theta_i}{\theta_{max}}\right)^2 = \frac{2}{5^2}\,(0.25^2 + 0.5^2 + 1^2 + 2^2 + 3^2 + 4^2) = 2.27 \qquad (5\text{-}13)$$

Note that this result implies that the damage done prior to the two cycles of loading at the $\pm 5\%$ drift amplitude is 2.27 cycles. Then the total number of cycles at the 5% drift amplitude is 2.27 + 2 = 4.27 cycles. This means that, instead of using the variable amplitude test protocol, had constant amplitude testing been done, failure would have occurred after the completion of

cycle 4 at the ±5% drift amplitude.

The major problem in choosing experimental specimens from the myriad of records that exist is the availability of specimens where the failure mode was clearly defined to be due to hoop fracture. However, test results of Yok Lung Wong (1990), Watson et al. (1986), Zahn et al. (1986) show that a few specimens clearly failed due to hoop fracture. As a result they were chosen for validating the theory. A short description of those chosen specimens is given in the following.

5.4 DESCRIPTION OF TEST SPECIMENS

Square Columns Tested by Watson et al. Watson (1986) tested four square columns (400 mm square) as part of her Master's study at the University of Canterbury, New Zealand. Column Unit 3 which failed by hoop fracture was reinforced with twelve HDIG bars (f_y = 446 MPa) arranged uniformly all around the periphery. The transverse reinforcement consisted of 7 mm diameter octagonal hoops (f_{yh} = 346 MPa) with a total transverse reinforcement ratio ρ_s = 0.0072. The concrete used had an unconfined compression strength of f'_c = 44 MPa. The loading on the column consisted of two completely reversed cycles of displacement ductility factors of 2, 4, and 6 before failing at about 40% of the third cycle to μ_Δ = 6. A constant axial load of P = 0.3$f'_c A_g$ was applied throughout testing. Yield displacement was recorded at 7.65 mm.

Circular Columns Tested by Yok Lung Wong. Yok Lung Wong (1990) carried out an experimental investigation of seismic shear behavior of spirally reinforced concrete circular columns as part of his doctoral dissertation at the University of Canterbury, New Zealand. Sixteen cantilever column specimens, with an aspect ratio of 2, were tested under quasi-static multi-directional lateral loading conditions. The main variables studied were the amount of spiral steel content, axial compression load intensity, and displacement history.
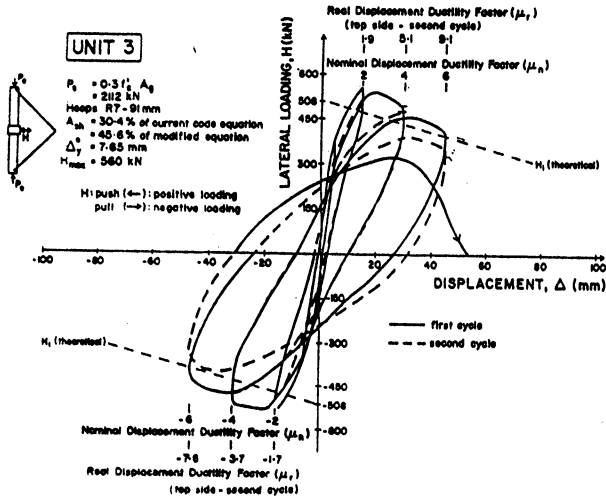
(a) Force Displacement Hysteretic Curve.
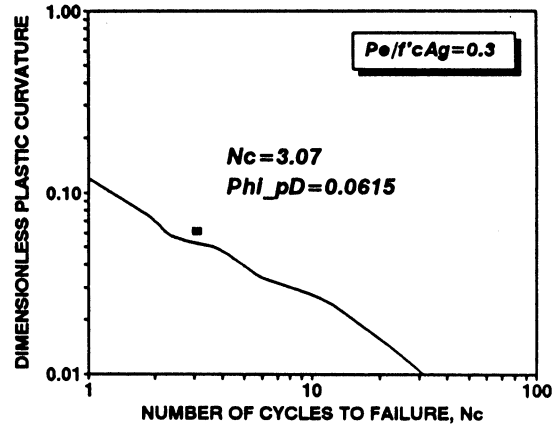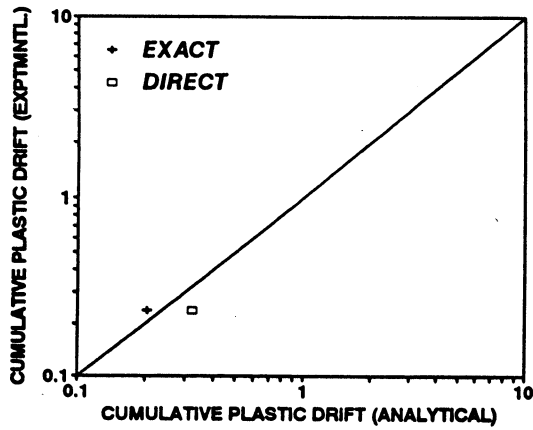
(b) Exact Computational Method.

(c) Experimental vs. Analytical Cumulative Plastic Drift.
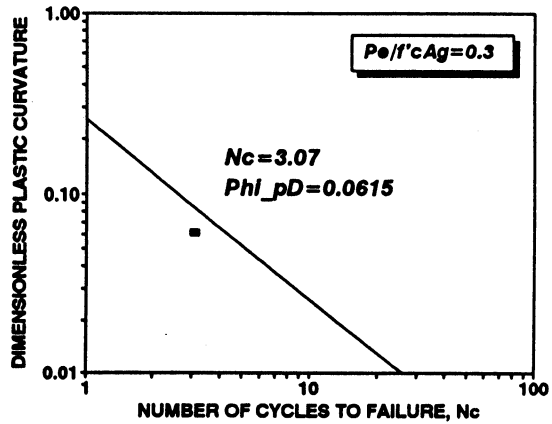
(d) Simplified Direct Method.

Figure 5-1 Comparison of Experimental and Analytical Results for Unit 3 of Watson et al.

The diameter of all test columns was 400 mm and were reinforced with twenty 16 mm diameter Grade 380 deformed steel bars giving a longitudinal reinforcement content of ρ_t = 3.2%. Transverse reinforcement consisted of either 6 mm or 10 mm diameter Grade 275 mild steel round bars, but in the form of spirals. The thickness of concrete cover the spiral was 15 mm, except in Unit 15 where it was 11 mm. Reinforcement details of relevant column specimens are provided in Table 1. The column units relevant to this section were mainly subjected to two different types of loading patterns. The unidirectional 'u' type displacement pattern was cyclic along the East-West principal axis. The loading history consisted of five complete displacement cycles to a ductility factor μ of 1.5, 2, 4, 6 and possibly 8. In the bi-directional 'b' type displacement pattern one loading cycle consisted of the completion of one displacement path along both the North-South and East-West principal axes, respectively. Eventually the columns were subjected to two load cycles to displacement ductility factor of μ = 1.25, 2, 3, 4, 5 and possibly 6.

Table 5-1 Reinforcement Details and Material Properties of Column Units

| Unit Number | $\dfrac{P}{f_c' A_g}$ | Spiral Reinforcement | | | | Longitudinal Reinforcement | Concrete |
		d_b (mm)	s (mm)	ρ_s (%)	f_{yh} (MPa)	f_y (MPa)	f_c' (MPa)
1	0.19	10	60	1.450	300	423	38
6	0.0	6	30	1.032	340	475	42
8	0.19	6	30	1.032	340	475	39
9	0.39	6	40	0.774	340	475	27
10	0.39	10	65	1.340	300	475	37

Unit 1, which was subjected to unidirectional loading pattern, performed reasonably well until μ = 6. On the second cycle at μ = 8, core concrete became loose and finally, when the column was displaced to μ = -7.3 (in the reversed direction), fracture of the spiral took place which led to abandonment of the test. Unit 2 subjected to biaxial loading sustained the loading

(a) Force Displacement Hysteretic Curve.
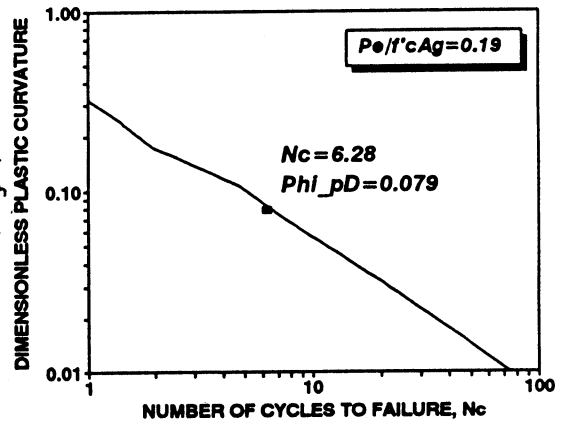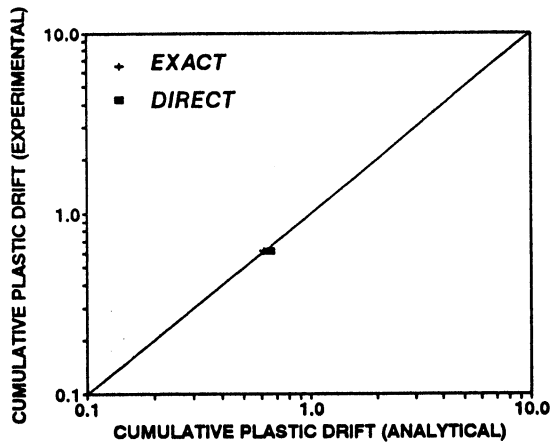
(b) Exact Computational Method.

(c) Experimental vs. Analytical Cumulative Plastic Drift.

(d) Simplified Direct Method.

Figure 5-2 Comparison of Experimental and Analytical Results for Unit 1 of Wong et al.

(a) Force Displacement Hysteretic Curve.

(b) Exact Computational Method.

(c) Force Displacement Hysteretic Curve.

(d) Simplified Direct Method.

(e) Experimental vs. Analytical Cumulative Plastic Drift.

Figure 5-3 **Comparison of Experimental and Analytical Results for Unit 6 of Wong et al.**

55

(a) *Force Displacement Hysteretic Curve.*

(b) *Exact Computational Method.*

(c) *Force Displacement Hysteretic Curve.*

(d) *Simplified Direct Method.*

(e) *Experimental vs. Analytical Cumulative Plastic Drift.*

Figure 5-4 Comparison of Experimental and Analytical Results for Unit 8 of Wong et al.
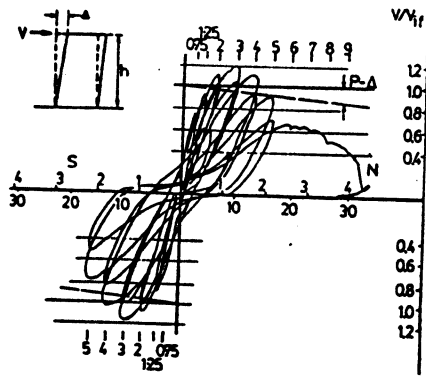
56

(a) *Force Displacement Hysteretic Curve.*

(b) *Exact Computational Method.*

(c) *Force Displacement Hysteretic Curve.*

(d) *Simplified Direct Method.*

(e) *Experimental vs. Analytical Cumulative Plastic Drift.*

Figure 5-5 Comparison of Experimental and Analytical Results for Unit 9 of Wong et al.

57

(a) **Force Displacement Hysteretic Curve.**
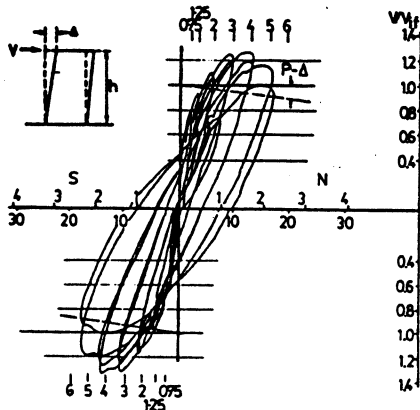
First displacement path

(b) **Exact Computational Method.**
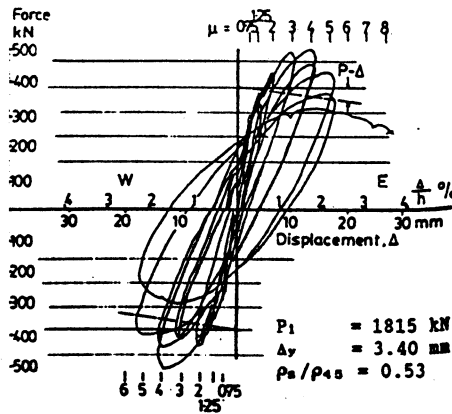
Second displacement path

(c) **Force Displacement Hysteretic Curve.**
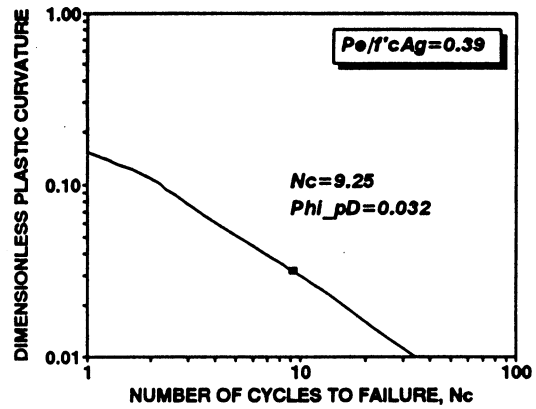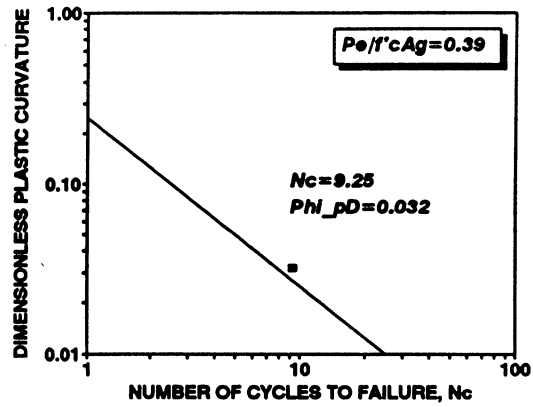
(d) **Simplified Direct Method.**
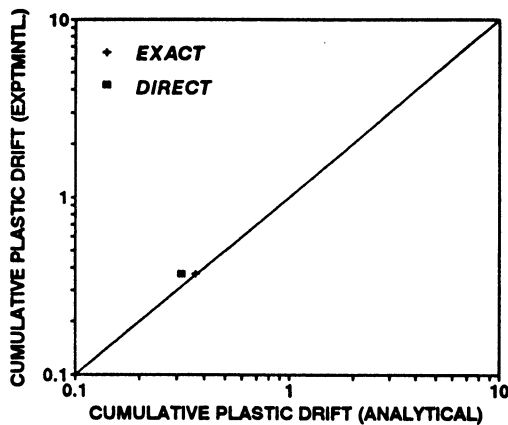
(e) **Experimental vs. Analytical Cumulative Plastic Drift.**

Figure 5-6 Comparison of Experimental and Analytical Results for Unit 10 of Wong et al.

with minor cracking before failing due to fracture of spiral at the first cycle to $\mu = 8$. Units 8 and 10 sustained the second and first cycles, respectively, to $\mu = 8$ before failing due to spiral fracture and consequent buckling of longitudinal bars. Unit 9 performed exceptionally well until $\mu = 8$. However, at $\mu = 9$, the column lost its axial and lateral load resistance at the occurrence of spiral fracture and consequent buckling of the longitudinal bars.

Circular Columns Tested by Ang, Priestley and Paulay (1990). The seismic shear strength of bridge columns was investigated by Ang et al. who tested twenty five circular columns with various aspect ratios and axial load levels. Unit 8 (having an aspect ratio of 2) which failed by hoop fracture was circular in section with a diameter of 400 mm and a clear cover of 15 mm. It was reinforced with 20-HD16 bars with a nominal yield strength of 448 MPa. The hoop reinforcement consisted of 6 mm bars with a yield strength of 372 MPa and a spiral pitch of 30 mm. Concrete used had an unconfined compression strength of 28.7 MPa while the axial load ratio on the column was 0.2. The column was subjected to five completely reversed cycles at displacement ductility factors of 2, 3 and 4 before it failed at a displacement ductility factor of 6 after 3.25 cycles. The yield displacement of the specimen was recorded at 6.8 mm.

Octagonal Column Tested by Zahn, Park and Priestley (1986). While investigating the strength and ductility of bridge columns Zahn et al. (1986) tested two octagonal columns. Test Unit 6 which failed by hoop fracture had a maximum outer dimension of 400 mm and a clear cover of 13 mm. The specimen was reinforced with 16-DH16 bars with a nominal yield strength of 337 MPa. The hoop reinforcement consisted of 6 mm bars with a yield strength of 446 MPa and a spiral pitch of 75 mm. The concrete used had an unconfined compression strength of $\rho_t = 30$ MPa. The axial load applied to the column throughout testing was $P_e = 0.58 f_c' A_g$. The column was subjected to two completely reversed cycles at displacement ductility factors of $\mu = 2$ and 4 before it failed after 2.25 cycles at a the displacement ductility factor of $\mu = 6$. The yield displacement of the specimen was recorded as $\Delta_y = 10.23$ mm.
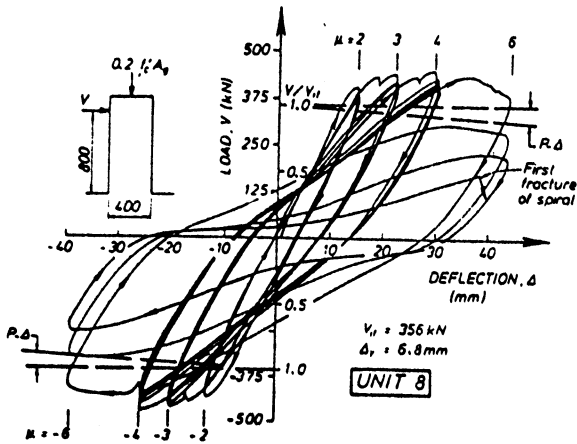
(a) Force Displacement Hysteretic Curve.
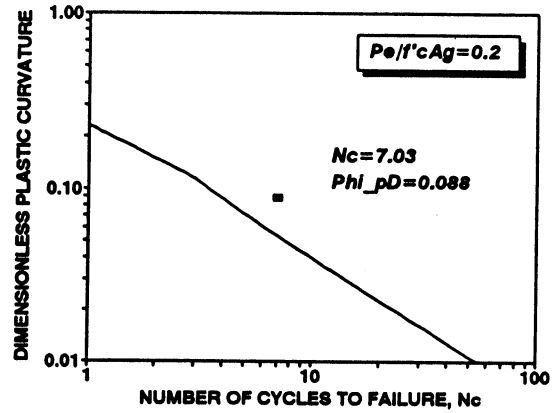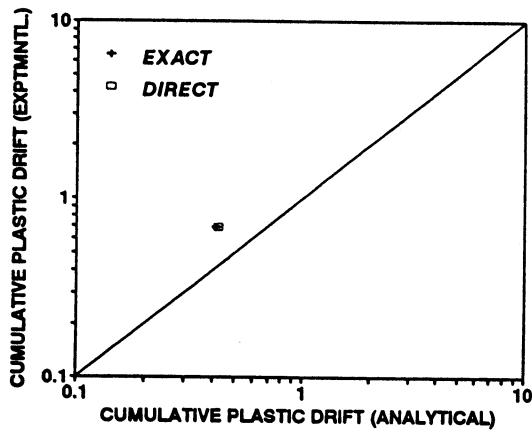
(b) Exact Computational Method.

(c) Experimental vs. Analytical Cumulative Plastic Drift.
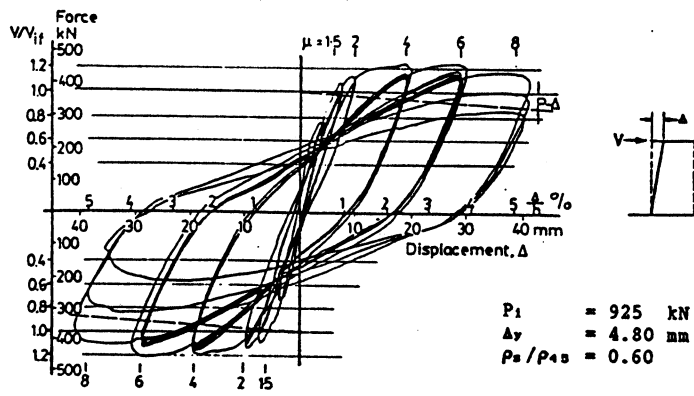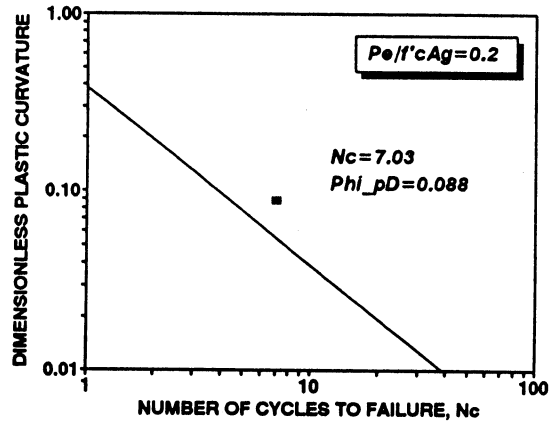
(d) Simplified Direct Method.

Figure 5-7 Comparison of Experimental and Analytical Results for Unit 8 of Ang et al.
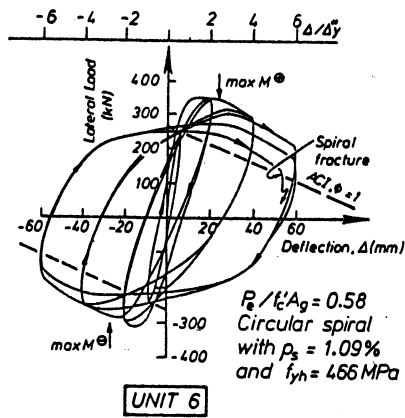
(a) Force Displacement Hysteretic Curve.
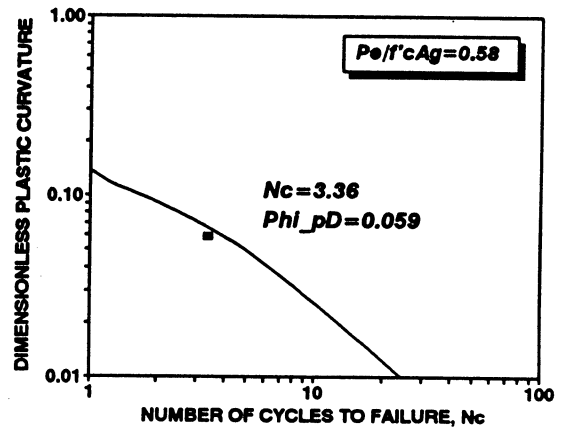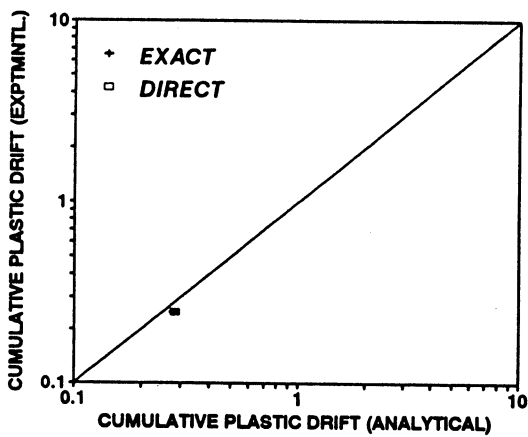
(b) Exact Computational Method.

(c) Experimental vs. Analytical Cumulative Plastic Drift.

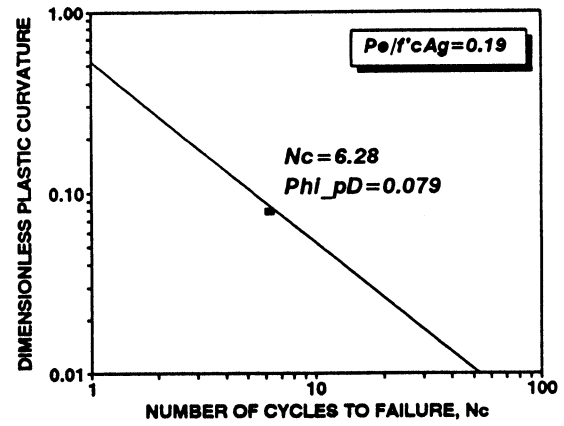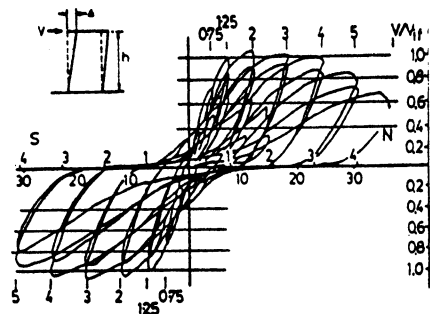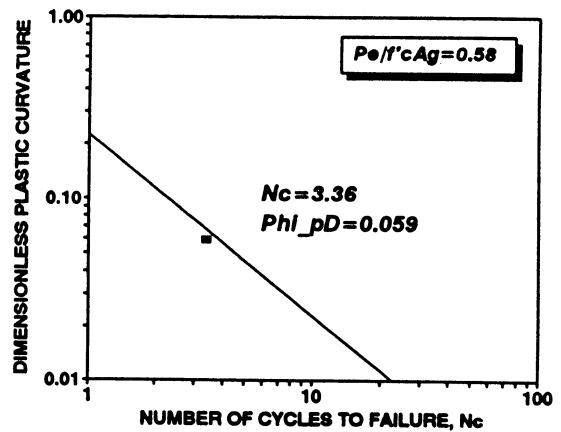(d) Simplified Direct Method.

Figure 5-8 Comparison of Experimental and Analytical Results for Unit 6 of Zahn et al.

61

5.5 Comments On Analytical Predictions

The two analytical methods to predict the fatigue life discussed previously are compared with the test results in figures 5-1 to 5-8, respectively. The experimental and analytically predicted values of cumulative plastic drift are also shown in the same figures. It will be noted that a reasonable degree of conservatism is found in the theoretical predictions. Possible reasons for this could be the way in which the effective number of cycles is calculated. The analytically obtained values of number of cycles to failure are designated as heavy dots on the fatigue-life plots. As is observed the analytical predictions are very much justified.

SECTION 6
THEORETICAL FATIGUE LIFE DEMAND

6.1 INTRODUCTION

Deterministic methods of analysis are necessary to access the energy demand imposed or reinforced concrete structures by earthquakes. Since the energy demand depends on both the duration and magnitude of the response, unlike ductility demand which depends on the maximum inelastic seismic displacement, it is important that a reliable analytical model be developed which will simulate the inelastic behavior of a reinforced concrete structural element. Significant contributions to this end have been done by Chang and Mander (1994b) who devised a macro model for the determination of hysteretic DEMAND on bridge columns. Their model, which was calibrated against the actual behavior of concrete columns via the fiber element analysis as well as experiments on near full size model structures, was used to represent the single degree of freedom idealization (figure 6-1) of the structure system. By utilizing this well calibrated model, that is representative of overall behavior of a structure system, it is possible to obtain a reliable prediction of seismic energy demand on a structure.

6.2 ANALYSIS OF ENERGY DEMAND

To facilitate the design of structures subjected to severe seismic excitation, it is desirable to develop energy spectrum which indicates how the peak energy responses of a SDOF structure vary with the characteristics of the structures for a particular excitation. The influence of different ground motions and structural characteristics on the input seismic energy have recently been studied by Uang and Bertero (1990). Their suggested energy balance equation is given by equation

$$E_i = E_k + E_s + E_d + E_h \tag{6-1}$$

where E_i = input energy, E_k = kinetic energy, E_s = strain energy, E_d = damping energy and E_h =
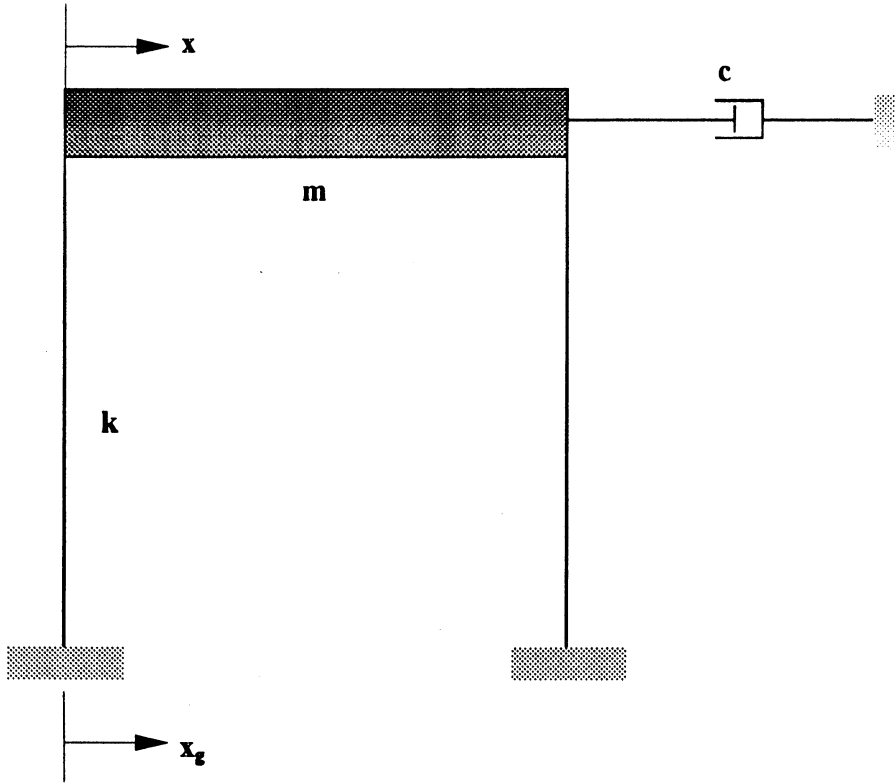
Figure 6-1 Equivalent SDOF System Used in Analysis.
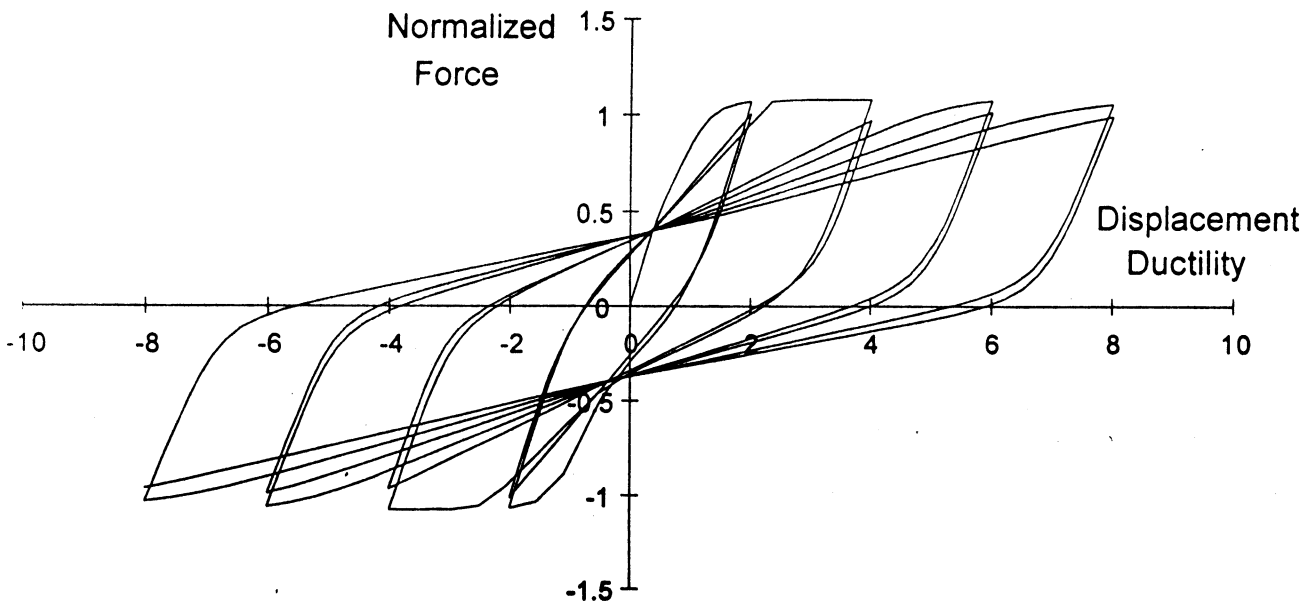
Figure 6-2 Smooth Hysteretic Model.

hysteretic energy. In this particular expression, the various components are easily computed. For example, the hysteretic energy E_h absorbed by the structure can be found by numerically integrating the non-linear force-displacement history over the duration of the event, thus

$$E_h = \int_0^t F\,dx = \sum_{i=1}^n \frac{1}{2}(F_i + F_{i-1})(x_i + x_{i-1}) - \frac{1}{2}\frac{F_n^2}{K_e} \qquad (6\text{-}2)$$

where F_i, x_i = force and displacement at i th time-step, F_{i-1}, x_{i-1} are the same at the $i-1$ th timestep and F_n = the residual force that remains in the structure at the end of the earthquake or at the last (n-th) timestep of a non-linear analysis. The absolute kinetic energy is given by:

$$E_k = \frac{1}{2}m(\dot{x} + \dot{x}_g)^2 \qquad (6\text{-}3)$$

where $\dot{x}$ = relative velocity of the structure with respect to the ground and $\dot{x}_g$ = velocity of the moving ground. The damping energy is a positive increasing quantity given by

$$E_d = \int C\dot{x}\,dx = C\sum \frac{1}{2}(\dot{x}_i + \dot{x}_{i-1})(x_i - x_{i-1}) \qquad (6\text{-}4)$$

As is noticeable from the energy expression, the relative magnitude of the energy terms are strongly dependent on the magnitude of the hysteretic energy E_h. The amount of hysteretic energy dissipated will depend on the extent of inelastic actions the structure is subjected to. This in turn depends on the natural period of vibration and the strength reduction factor R_μ which is defined as:

$$R_\mu = \frac{(S_a/g)}{(F_y/W)} = \frac{C_d}{C_c} \qquad (6\text{-}5)$$

where S_a = period dependant spectral acceleration, g = gravitational acceleration, F_y = structural yield strength and W = weight of the structure. Thus, $C_d = S_a/g$ = seismic base shear demand, and $C_c = F_y/W$ = base shear capacity.

Energy absorption demand, normalized with respect to the weight of the structure (E_h/W), can be plotted in spectral form for selected R_μ factors and natural periods, T. The
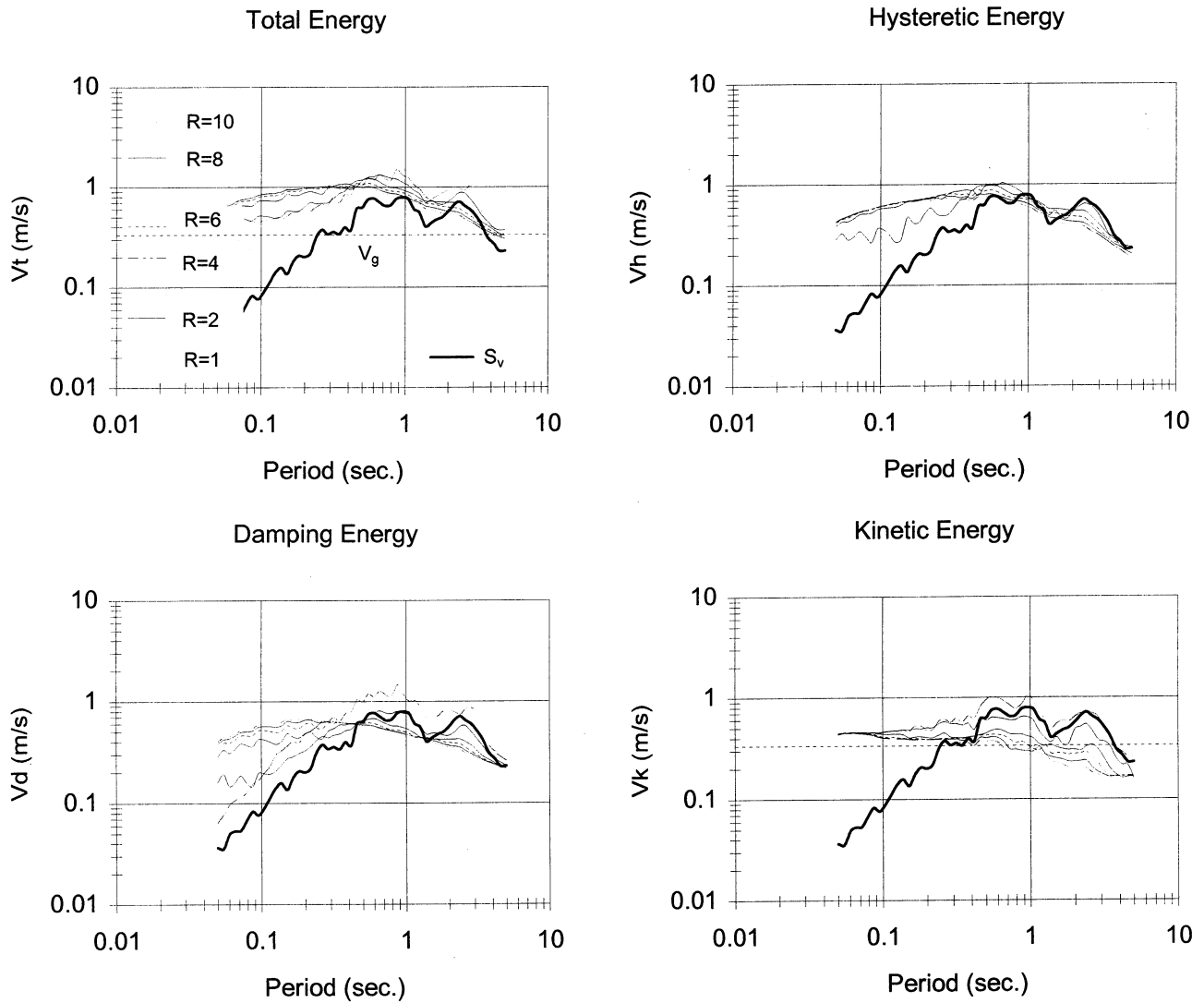
Figure 6-3 Total, Hysteretic, Damping and Kinetic Energy Spectra for El-Centro (1940).

results of such an analysis for the El Centro (1940) N-S motion are shown in figure 6-3. This is compared with total input energy, kinetic energy and the energy consumed by viscous damping. It is evident that for moderate R_μ factors ($R_\mu > 4$) hysteretic energy consumes most of the input energy thus reducing the response. Although these energy spectra may be insightful from a comparative sense, as they stand, they are not very useful for design purposes.

6.3 DEMAND BASED ON THE EQUIVALENT NUMBER OF CYCLES

A more convenient way to express hysteretic energy absorption demand is to determine the equivalent number of equi-amplitude displacement cycles. To overcome the fact that materials and elements may degrade in strength on cycling, in this study the average energy absorption per cycle over <u>four</u> constant amplitude cycles was chosen to define the energy absorbed by one cycle, E_{loop}. Thus the effective number of cycles is defined as the ratio of the total energy absorbed in the variable amplitude seismic response to the energy absorbed by one cycle at an effective displacement amplitude (X_{eff}), thus

$$N_c = \frac{E_h}{E_{loop}} \qquad (6\text{-}6)$$

The previous equation (6-6) relating cyclic loading history to displacements can be restated as

$$N_c = \sum_i \left(\frac{x_i}{X_{eff}} \right)^2 \qquad (6\text{-}7)$$

It is important to note that this formulation assumes a symmetric (equal positive and negative amplitude) loading history. Real earthquake time histories are not necessarily symmetric, thus in order to obtain an effective displacement amplitude (X_{eff}) an approach suggested by Chang and Mander (1994b) is proposed. For a general displacement response history, the standard deviation of the inelastic response history can readily be computed from which the effective amplitude can be defined as:

67

$$X_{eff} = \sqrt{3}\, x_{STD} + x_y \qquad\qquad (6\text{-}8)$$

where x_y = yield displacement, and x_{STD} = the standard deviation of the plastic displacements.

An effective ductility amplitude can also be defined as

$$\mu_{eff} = \frac{X_{eff}}{x_y} \qquad\qquad (6\text{-}9)$$

It is at this ductility amplitude that E_{loop} is defined and thus the number of loading cycles, N_c. Figure 6-4 and plots the Northridge (Sylmar hospital — 360°) spectra for:

(a)   spectral acceleration (S_a / g).

(b)   effective deformation (X_{eff}).

(c)   normalized hysteretic energy (E_h / W).

(d)   effective ductility, $\mu_{eff} = R_\mu X_{eff} / S_d$.

(e)   effective number of cycles (N_c).

(f)   factor of symmetry (R_{eff}) which is normally used to express the degree of asymmetry in the deformation history and is defined as

$$R_{eff} = \frac{\mu_{min}}{\mu_{max}} \qquad\qquad (6\text{-}10)$$

in which μ_{max} = the maximum positive ductility, and μ_{min} = the minimum ductility having a normal range from -1 for equi-amplitude to about 0.4 for predominantly one-sided response.

(g)   normalized total energy (E_t / W).

(h)   maximum deformation (x_{max}).

(i)   normalized damping energy (E_d / W).

(j)   maximum ductility (μ_{max}).

(k)   normalized kinetic energy (E_k / W).

(l)   inelastic magnification factor   ($X_{max} / S_d = D_{inelastic} / D_{elastic}$).

(a) Spectral Acceleration

(b) Effective Deformation

(c) Hysteretic Energy

(d) Effective Ductility

(e) Effective Number of Cycles

(f) Factor of Symmetry
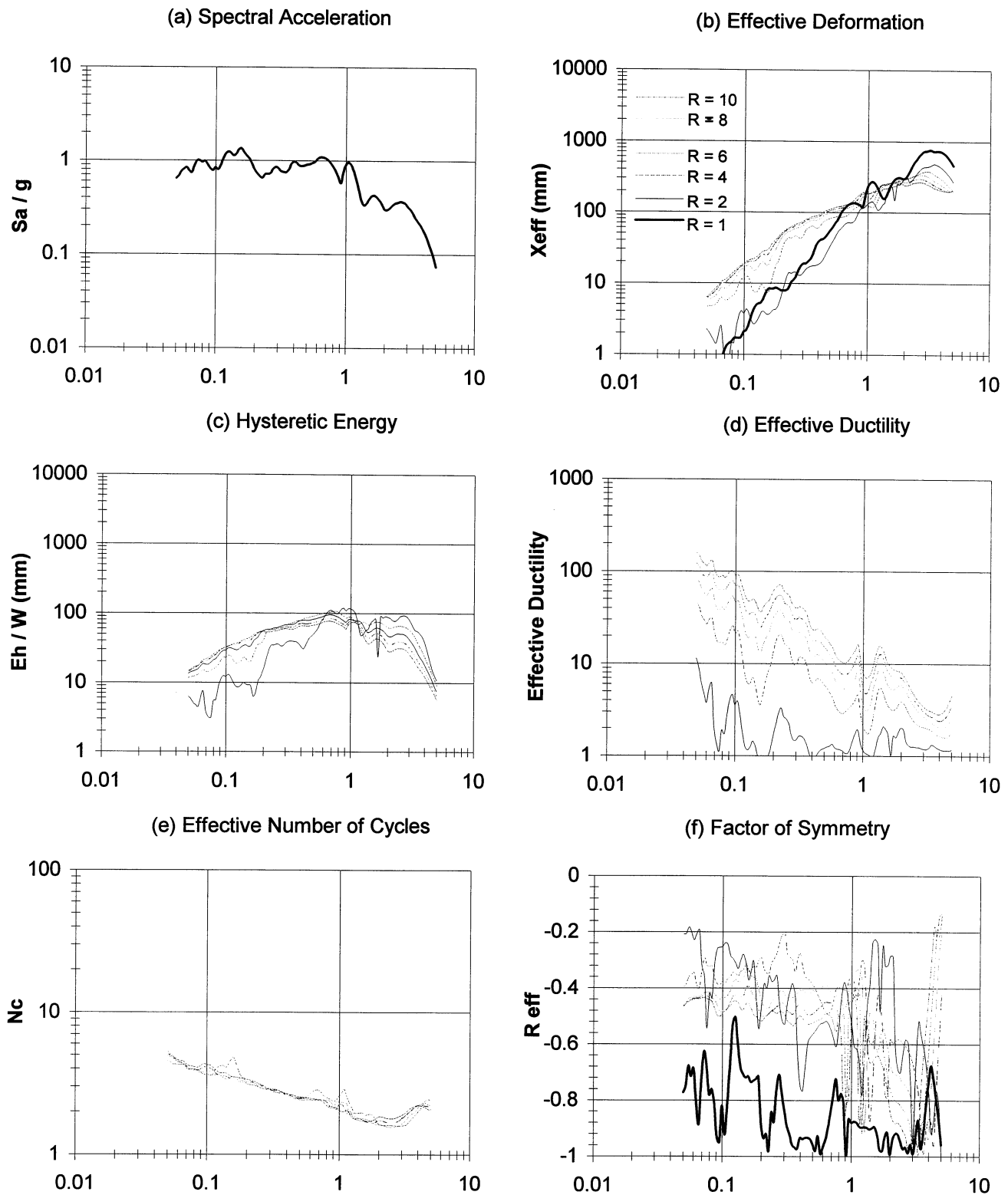
Figure 6-4 Energy, Ductility and Low-cycle Fatigue Demand Spectra for Northridge (Sylmar Hospital-360 deg.) with 5 % Viscous Damping Ratio.

(g) Total Energy Spectra
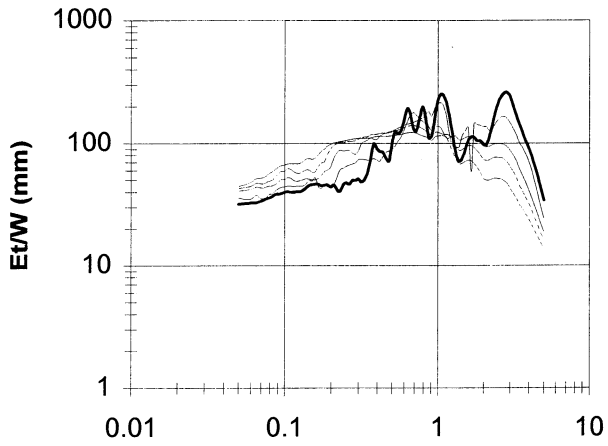
(h) Maximum Deformation
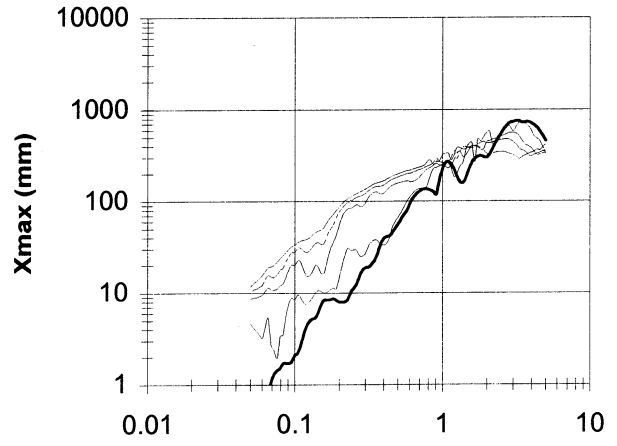
(i) Damping Energy
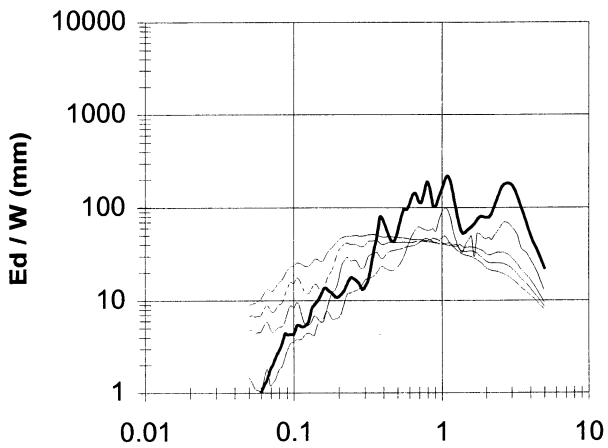
(j) Maximum Ductility
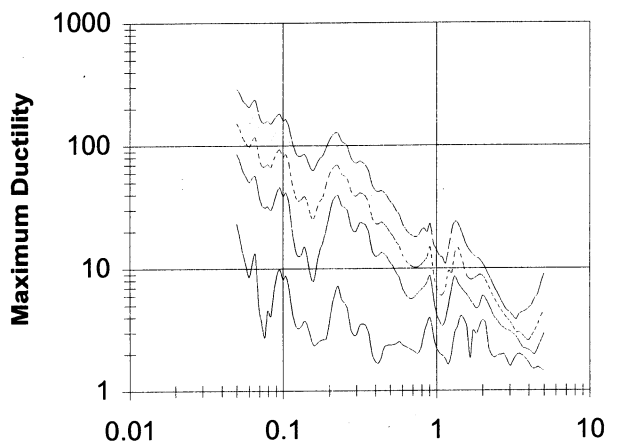
(k) Maximum Kinetic Energy
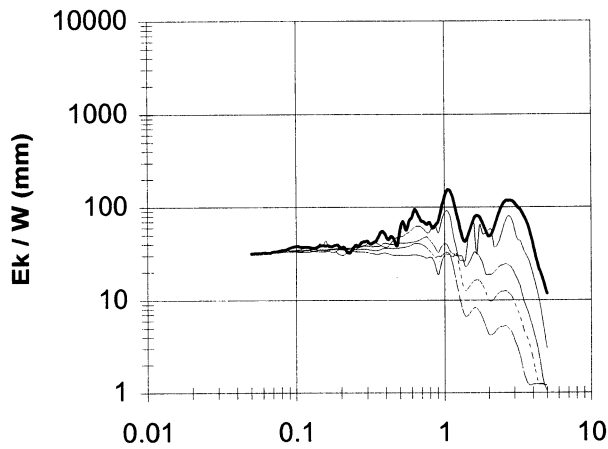
(l) Inelastic Magnification Factor
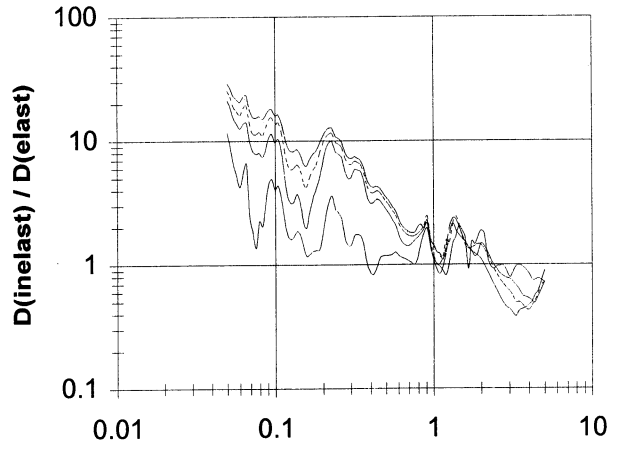
Figure 6-4 Continued.

70

Such spectra can be plotted for any given earthquake motion. Of particular interest to this study are the energy and cyclic loading spectra. It is to be noted that the peak energy occurs at the location of the maximum pseudo-velocity T_{PV}, and for most motions $T_{PV} = 0.7$ sec. This period divides the "short" and the "long" period motions. It is also of interest to compare cyclic loading spectra for several earthquake motions. Figure 6-5 shows such a comparison plot for a force reduction factor of $R_\mu = 6$. It is evident that the range of cycles follows a trend between earthquakes that is quite consistent, demand is largely independent of R_μ. For design purposes it is proposed that an envelope spectra be adopted as follows:

$$N_c = 7\,T^{-1/3} \tag{6-11}$$

but
$$4 \le N_c \le 20$$

This equation thus defines *seismic fatigue demand*.

By balancing this seismic fatigue demand against the aforementioned fatigue capacity it is possible to define certain design limit states. This is discussed in the next section.

6.4 CONCLUSIONS

In this section the energy demand imposed on a structure due to a strong ground shaking is analyzed using a sophisticated hysteretic rule that is representative of the true behavior of a reinforced concrete bridge column. Although it is well known that earthquake loads are reversive in nature, there is no generalized approach of counting the effective number of cycles based on energy criterion. Using an approach suggested by Chang and Mander (1994b), a simple approach of evaluating the effective number of completely reversed cycles is studied in detail. It is found that this quantity is linked to the effective period of the structure through a simple expression which represents a logical upper bound for an ensemble of earthquakes.
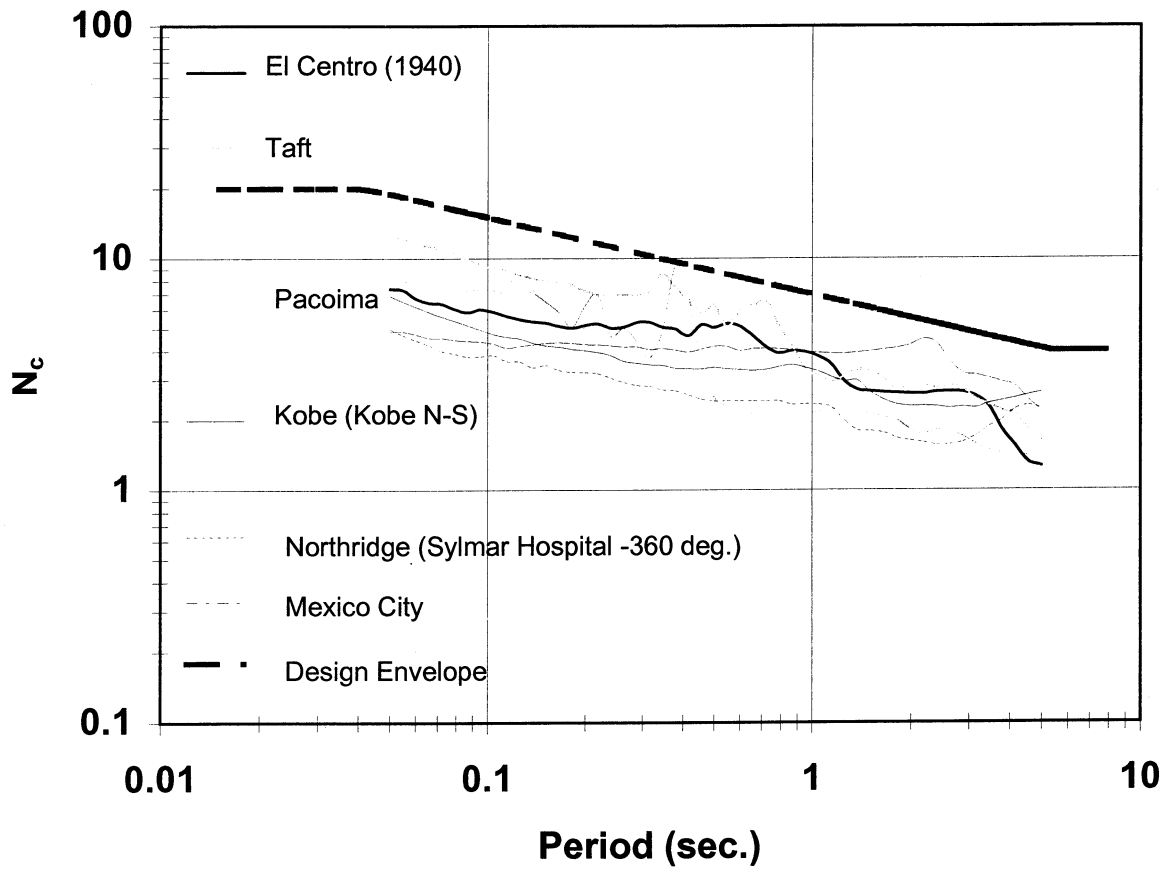
Figure 6-5 Effective Number of Inelastic Cycles.

SECTION 7
DESIGN EQUATIONS FOR CONFINEMENT

7.1 INTRODUCTION

This section addresses one of the most important issues regarding seismic design of reinforced concrete structures. It is well known that adequate ductility can be achieved from a reinforced concrete section if it is properly confined especially in the plastic hinge zones where most of the inelastic actions are expected to occur. Moreover in the capacity design process where undesirable failure (modes like shear failure, confinement failure, failure due to hoop fracture etc.) need to be prevented, it is of paramount importance that an adequate quantity of lateral hoop reinforcement be provided if structure is to be capacity protected.

In the preceding sections an energy based fatigue theory was developed from first principles. However, the fatigue expressions developed so far can only be used for evaluation of a particular section with a known volumetric ratio of transverse steel. In an inverse form they can be used as design equations if the plastic curvature demand is known. Following the capacity design principles, the only unavoidable mode of failure is failure due to low cycle fatigue of the longitudinal reinforcement. If the capacity of the section is set to the ultimate capacity obtainable before a longitudinal bar fracture occurs, the same fatigue equations can be used to give a value of the volumetric ratio of the transverse steel. In other words, it would ensure that the capacity of the section based on hoop fracture will be higher than that based on low cycle fatigue of the longitudinal reinforcement.

7.2 FATIGUE FAILURE THEORY OF STEEL REINFORCEMENT

In a recent study on the low cycle fatigue behavior of reinforcing steel, Mander et al. (1994) showed that the plastic strain amplitude (ε_{ap}) given in terms of the fatigue life (N_f cycles

73

to failure) by the relation

$$\varepsilon_{ap} = 0.08 \, (2 \, N_f)^{-0.5}$$ (7-1)

and a re-plot of the results given by Mander et al. (1994) in terms of total strain amplitude gives a simple relation of the form

$$\varepsilon_a = 0.08 \, (2 \, N_f)^{-0.333}$$ (7-2)

where $2 \, N_f =$ number of reversals to the appearance of the first fatigue crack, $\varepsilon_a =$ total strain and $\varepsilon_{ap} =$ plastic strain at the level of the reinforcing bar. This result is plotted with experimental results from low cycle fatigue tests on two types of reinforcing steel in figure 7-1.

It is possible to transform the low cycle fatigue behavior of individual rebars into familiar fatigue expressions for concrete columns. Consider the strain diagram shown in figure 7-2. Through geometry an equation can be derived which relates the total plastic strain range $(2 \, \varepsilon_{ap})$ with the dimensionless plastic curvature of the section $(\phi_p D)$:

$$2 \, \varepsilon_{ap} = \phi_p D \left(1 - \frac{2d'}{D} \right)$$ (7-3)

where $D =$ overall depth (diameter) of the section and $d' =$ distance from the top of the section to the centroid of the nearest longitudinal reinforcing steel.

Equating equations (7-1) and (7-3) one obtains an expression relating the dimensionless plastic curvature $(\phi_p D)$ with the number of cycles to failure (N_f)

$$\phi_p D = \frac{0.113}{1 - 2d'/D} N_f^{-0.5}$$ (7-4)

This equation defines the plastic curvature <u>demand</u>
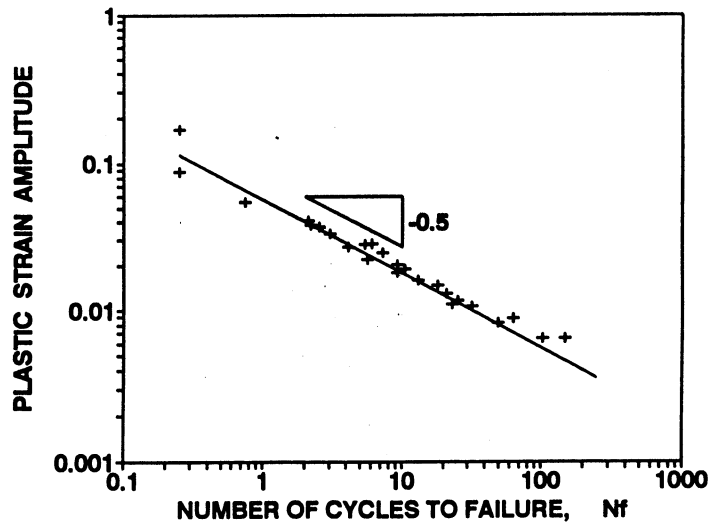
(a) Coffin-Manson Plastic Strain-Life Model
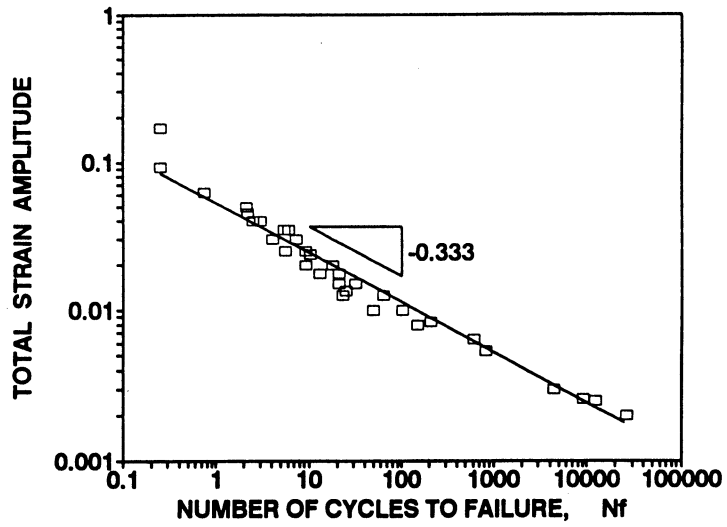
(b) Koh-Stephens Total Strain-Life Model

Figure 7-1 Fatigue Life of Reinforcing Steel based on the Test Results of Mander et al. (1994).

75
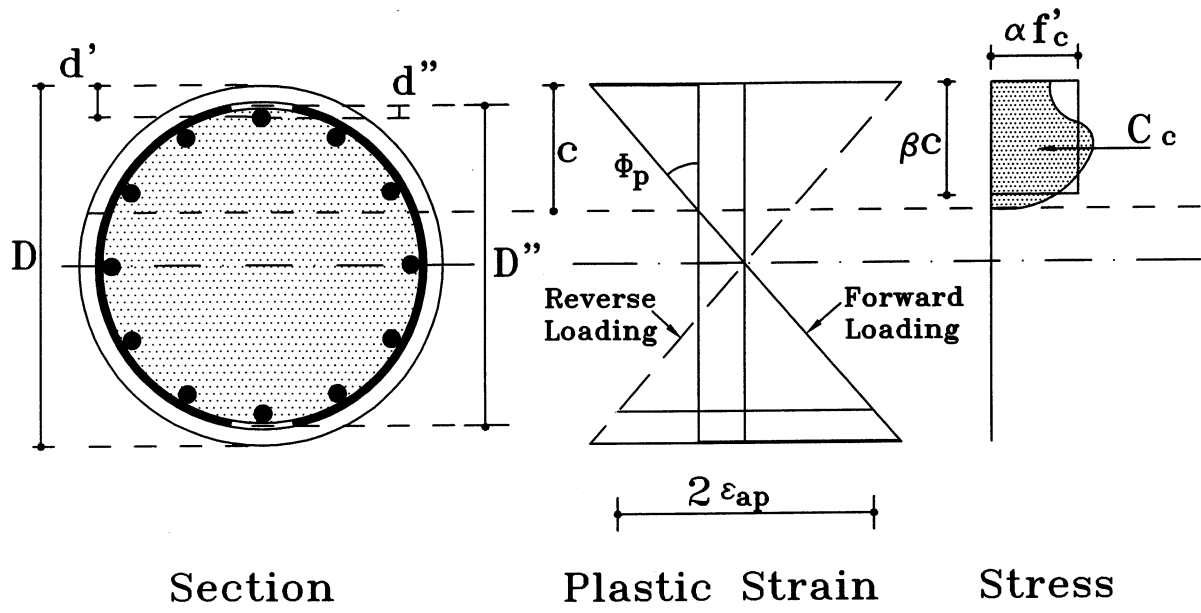
Figure 7-2 Showing the Plastic Strain Amplitude

7.3 DESIGN EQUATIONS USING THE EXACT COMPUTATIONAL METHOD

The exact computational method discussed earlier can be used for evaluating the volumetric ratio of transverse steel as well. One important thing to be remembered at this point is that the design equations should implicitly have the information about the period of the structure they are to be used for. In a design problem, where the structure is yet to be constructed, an estimation of the fundamental period can only be based on rational predictions.

According to Chang and Mander (1994b), the analytical fatigue demand expression is as given by equation (6-11). Note that this equation has a limit such that $4 \leq N_c \leq 20$. Thus for very short period structures, $N_c = 20$ and for long period structures $N_c = 4$. Hence if design curves are formulated corresponding to $N_c = 4$, 10 and 20, a whole range of structures from very low periods to very long periods can be covered.

Turning the attention to equation (2-9) and (3-25), it can be seen that by rearranging terms the volumetric ratio of transverse steel can be solved as

$$\rho_s = \left[2 N_c \bar{u}_{ex,s} \frac{W_s}{W_{cc}} + 2N_c \left(\eta_c + \frac{1 - \eta_c}{N_c} \right) \bar{u}_{ex,c} - 0.008 \right] \frac{f_c'}{U_{sf}} \frac{A_g}{A_{cc}} \tag{7-5}$$

in which the terms $\bar{u}_{ex,s}$ and $\bar{u}_{ex,c}$ needs to be evaluated corresponding to the dimensionless plastic curvature given by equation (7-4) and a particular value of the axial load ratio. Given the sectional dimensions the algorithm is as follows.

Step I   For a particular value of N_c, evaluate the dimensionless plastic curvature given by equation (7-4).

Step II   Assume a value of the yield curvature and hence find the total curvature

$$\phi = \phi_p + \phi_y \tag{7-6}$$

Step III   Assume a value of the neutral axis depth (c).

Step IV   Assume a concrete confinement ratio ($K = f'_{cc}/f'_c$).

Step V   Using Gauss Quadrature evaluate the axial load on the section as per equation (3-3).

Step VI   Evaluate $\bar{u}_{ex,s}$ and $\bar{u}_{ex,c}$ and solve for ρ_s in equation (7-5).

Step VII   Find the confinement ratio (K) for this ρ_s according to Mander et al. (1984).

Step VIII   If the confinement ratio K obtained from step VII is not within tolerable limits of the confinement coefficient initially assumed in step IV, start in step III with a new value of the neutral axis depth.

The whole process can be performed with different longitudinal steel percentages (ρ_t). Figure 7-3 shows design charts for both circular and rectangular sections corresponding to $\rho_t = 1$, 1.5 and 2 % respectively.

7.4 SIMPLIFIED DESIGN EQUATIONS FOR CONFINEMENT

In the previous subsection a detailed method for deriving design equations for confinement was discussed. It was based on an iterative approach that considered the effect of confinement (K) from the actual (provided) volumetric ratio of lateral reinforcement. This is an *implicit* approach which will yield an "exact" solution. However, it lacks appeal due to the repetitive nature of the calculations involved. For typical bridge columns axial loads are generally low ($P < 0.2f'_c A_g$) and confinement of concrete is seldom an issue. Therefore, protracted design for confinement should ideally be avoided. This necessitates the development of a simplified more easy-to-use explicit formulation that can still capture the essence of the problem without being unduly complex.

By simplifying the foregoing analysis, and assuming the cyclic demand (N_c) is in the range of 10 to 20 cycles, the following form of an explicit design equation is proposed:
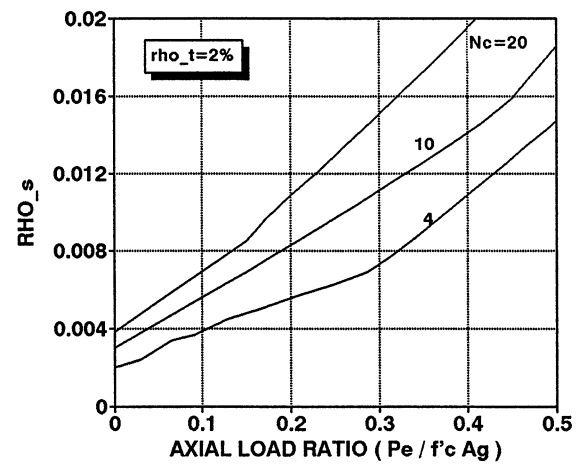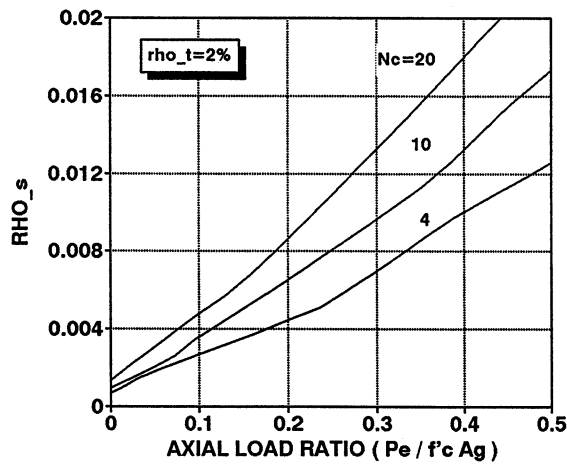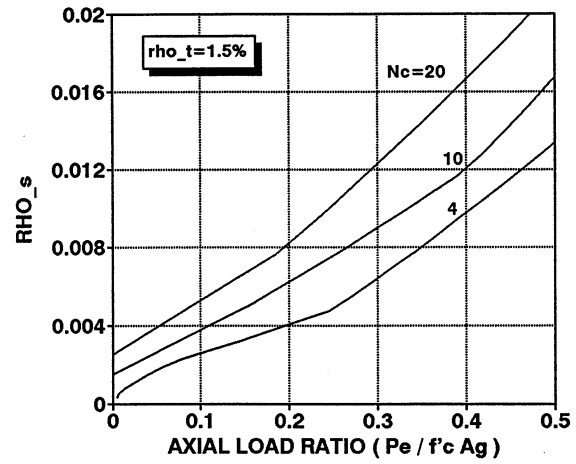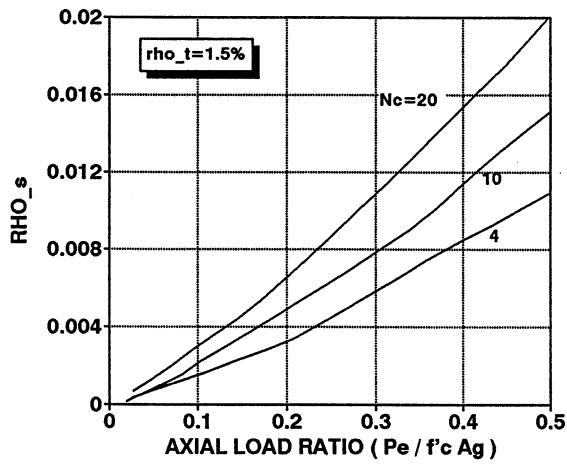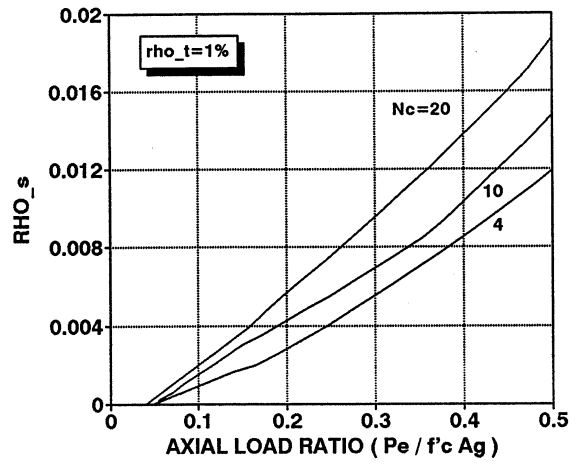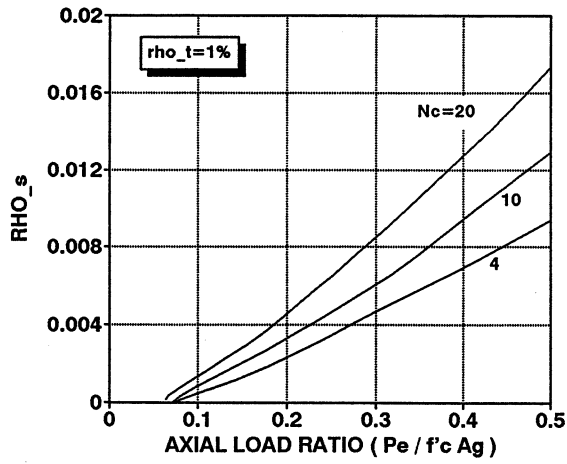
Design Charts for Circular Sections.   *Design Charts for Rectangular Sections.*

Figure 7-3 Design Charts for Column Sections using the Exact Approach

$$\rho_s = 0.008 \frac{f'_c}{U_{sf}} \left[\Psi \left(\frac{P_e}{f'_c A_g} + \rho_t \frac{f_y}{f'_c} \right)^2 \left(\frac{A_g}{A_{cc}} \right)^2 - 1 \right] \qquad (7\text{-}7)$$

where $\Psi = 12$ for circular sections and $\Psi = 15$ for rectangular sections.

The proposed simplified explicit design formula is compared with the theoretically "exact" implicit formulation in figure 7-4. Satisfactory agreement is evident; the simplified approach tends to become conservative for high axial load levels and/or high volumes of longitudinal reinforcement.

For low levels of axial load, the design of the transverse reinforcement is invariably governed by either bar stability (antibuckling requirements) or shear. These two design issues are analyzed in the following two sections.

7.5 COMPARISON OF PROPOSED FORMULATION WITH EXISTING DESIGN EQUATIONS

This section compares the proposed design equations for concrete confinement with the existing code provisions and recommendations.

7.5.1 The Evolution of US Design Practice

The importance of concrete confinement for achieving high ductility has been understood by the code committees for a long period of time. Design equations that stipulate the provision of lateral reinforcement in the form of spirals has been in the ACI code as

$$\rho_s \geq 0.45 \left(\frac{A_g}{A_c} - 1 \right) \frac{f'_c}{f_y} \qquad (7\text{-}8)$$

where $A_g =$ gross column area, $A_c =$ area of core of spirally reinforced concrete member measured to outside diameter of spiral, $f'_c =$ unconfined compression strength of concrete and
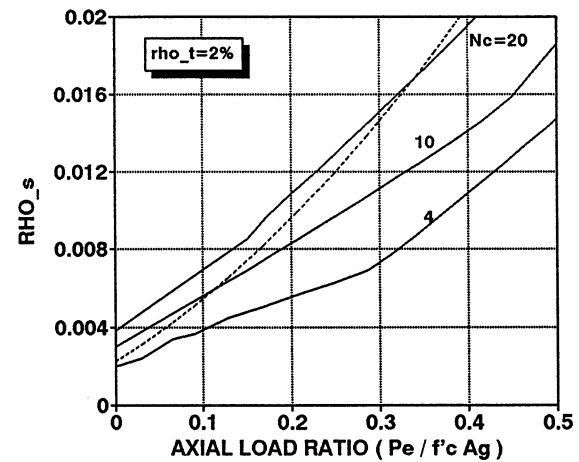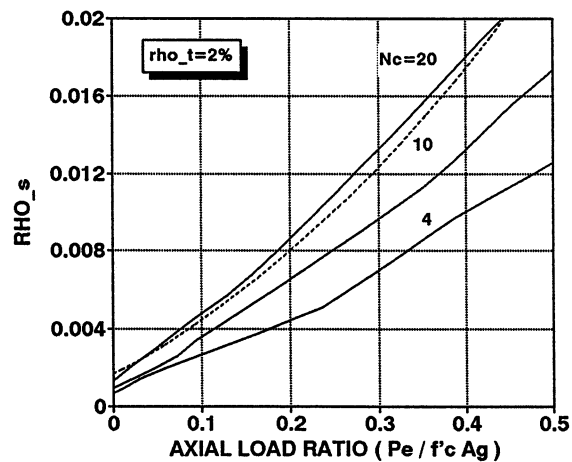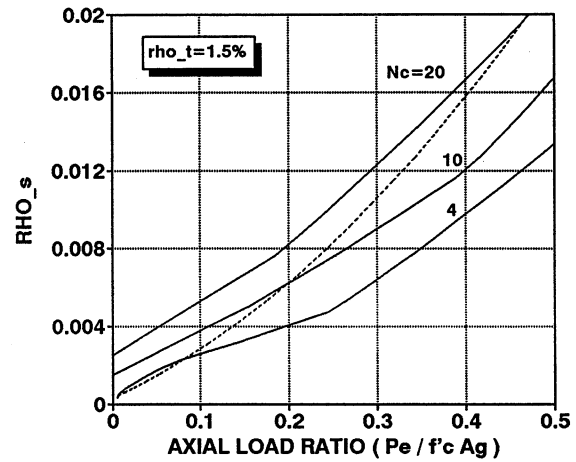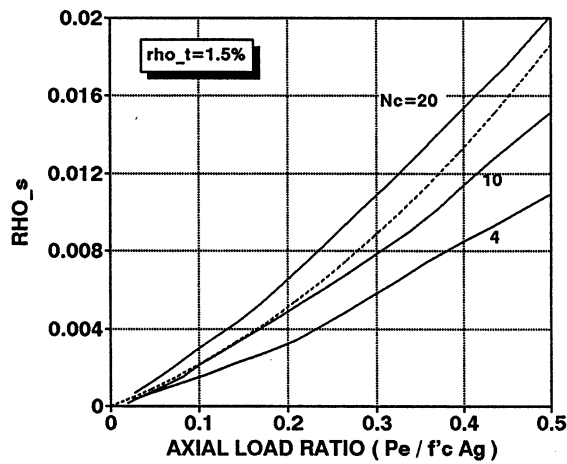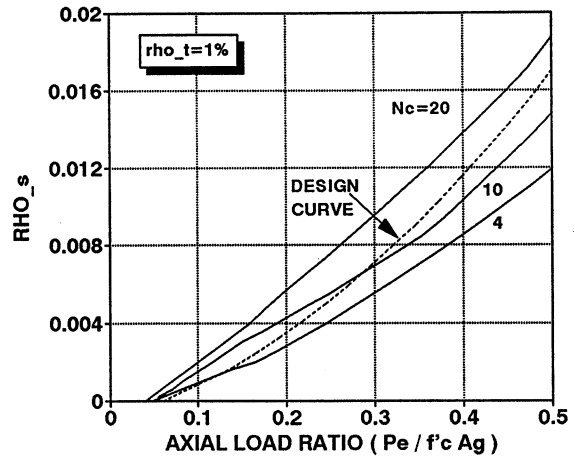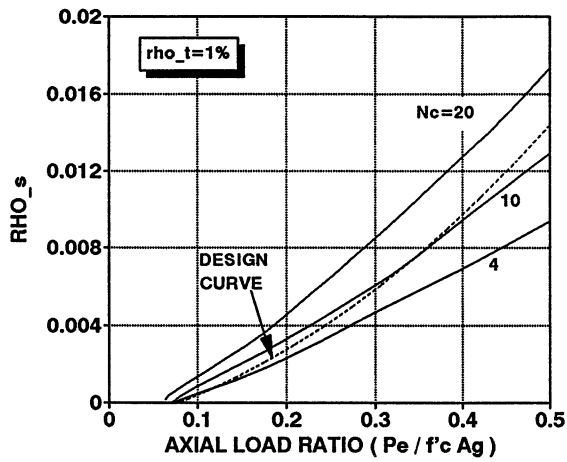
Design Charts for Circular Sections.   *Design Charts for Rectangular Sections.*

Figure 7-4 Comparison of the Proposed Design Form with "Exact" Solution.

81

f_y = specified yield strength of spiral reinforcement $\not>$ 60 ksi.

Special provisions for structures in seismically active areas also require that the volumetric ratio of spiral or circular hoop reinforcement ρ_s shall not be less than

$$\rho_s \geq 0.12 \frac{f_c'}{f_{yh}} \tag{7-9}$$

Bridge piers typically possess columns with large diameters, thus the cover dimension is relatively small and the core area (A_c) is only marginally less than the gross area (A_g), therefore for bridge columns equation (7-9) always tends to govern.

For rectangular sections the ACI code requires that the total area of rectangular hoop reinforcement be not less than either of

$$A_v \geq 0.3 (s\, h_c\, f_c'/f_{yh})\left[A_g/A_{ch} - 1\right] \tag{7-10}$$

$$\text{or,} \quad A_v = 0.09\, s\, h_c\, f_c'/f_{yh} \tag{7-11}$$

where f_{yh} = specified yield strength of transverse reinforcement, h_c = cross sectional dimension of column core measured center-to-center of confining reinforcement and A_{ch} = cross sectional area of the structural member measured out-to-out of transverse reinforcement. ACI 318-95 also requires that such reinforcement be provided when the axial load ratio $(P/f_c'A_g)$ exceeds 0.1.

The proposed design equations along with ACI and other currently used equations for concrete confinement are plotted in figure 7-5. Significant differences between these approaches will be noted. An explanation for these differences follow.

The ACI confinement equation have their roots in the early work on confinement by Richart et al. (1928) who showed that the confined strength of concrete is given by
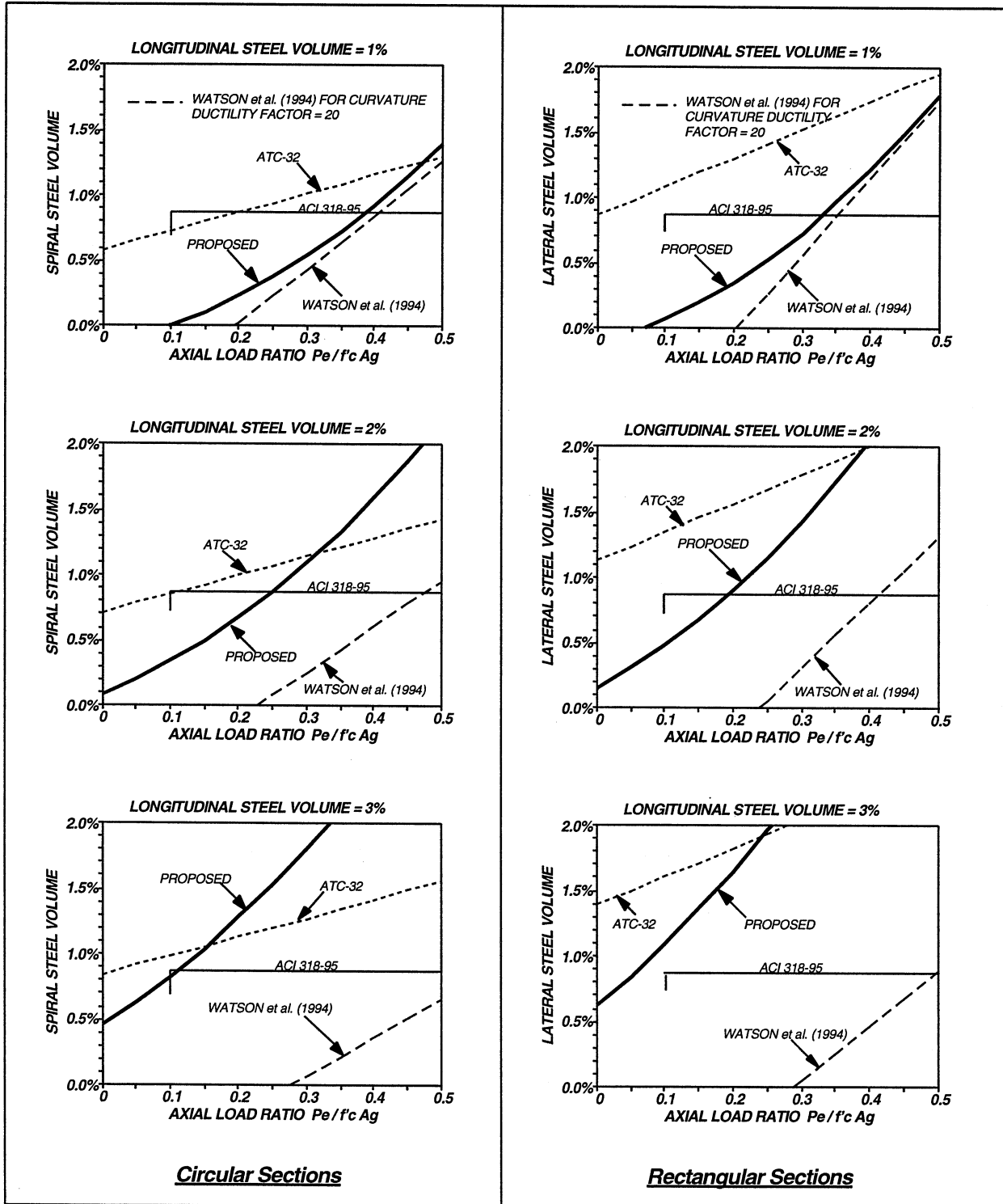
Figure 7-5 Comparison of Proposed Energy-Based Confinement Design Formulation with Existing Code Provisions and Other Recommendations.

$$f'_{cc} = f'_c + 4.1f'_l \tag{7-12}$$

where f'_l = confining pressure exerted by the transverse reinforcement. Using this as a starting point code writers subsequently derived equation (7-8) with the objective of preserving axial load capacity of a column before and after the concrete cover spalls. Details of this derivation may be found in Park and Paulay (1975). This formulation has long been criticized for being unrealistic, especially at low axial loads where the preservation of axial load is not really a concern, but rather the preservation of flexural strength and ductility capacity.

As a result of numerous moment-curvature analyses (see Park and Paulay, 1975 for details) as well as tests on circular and square columns by Priestley et al. (1981) and Park et al. (1982) the New Zealand Concrete Code (NZS 3101) adopted modified forms of equations (7-8) through (7-11). The ACI equations (7-8) through (7-11) were multiplied by $(0.5 + 1.25 P_e / f'_c A_g)$. This had the effect of reducing the transverse steel requirements for columns where $P_e < 0.4 f'_c A_g$ and increasing the requirements for $P_e > 0.4 f'_c A_g$. CALTRANS also adopted the modified design equations, but did not permit the decrease in steel volume for $P_e < 0.4 f'_c A_g$. Given that practically all bridge columns fell into that category there was really no departure from the ACI/AASHTO requirements.

Equations (7-8) through (7-11) have recently been further modified in the ATC-32 bridge design recommendations for CALTRANS. The principal design equation for flexural confinement in circular columns reinforced with circular hoops or spirals is given by

$$\rho_s \geq 016 \frac{f'_{ce}}{f_{ye}} \left[0.5 + 1.25 \frac{P_e}{f'_{ce} A_g} \right] + 0.13 (\rho_l - 0.01) \tag{7-13}$$

For rectangular sections the total area A_v of tie reinforcement in the direction perpendicular to core dimension h_c is given by

$$A_v \geq 012\, s_t h_c \frac{f'_{ce}}{f_{ye}} \left[0.5 + 1.25 \frac{P_e}{f'_{ce} A_g} \right] + 0.13\, s_t h_c (\rho_l - 0.01) \tag{7-14}$$

where f'_{ce} = unconfined compression strength of concrete, f_{ye} = yield strength of the transverse reinforcement, ρ_l = longitudinal reinforcement ratio, s_t = spacing of the transverse reinforcement and the remaining symbols are as explained previously.

From these equations it is evident that if extra longitudinal reinforcement is placed in a column above the minimum $\rho_l = 0.01$, then additional transverse reinforcement is also required, presumably to resist the additional flexural overstrength demands on the hinge zone.

It should be stressed, however, that these design equations have their roots in axial load preservation. It is considered to be a nonsense to use this as a basis for preserving flexural strength and ductility.

7.5.2 The Evolution of Confinement Requirements for New Zealand Bridge Design

Prior to the advent the New Zealand Concrete Design Code (NZS 3101, 1982), New Zealand did not use its own code. Instead, ACI 318-71 was used for buildings (i.e. equations 7-8 through 7-11, above were used), the AREA specifications were used by the New Zealand Railways (this also used the ACI equations), and two CDP publications were used by the Ministry of Works and Development (MWD) for highway bridge design (see MWD, 1975 and MWD, 1978).

The MWD recognized the irrationality of the ACI formula, and thus required the designers to use a more fundamental approach. Moment curvature analyses were required to ensure the monotonic flexural strength capacity of members was maintained to high curvature ductility factors, the latter being determined from a plastic mechanism analysis. Subsequent experimental research by Priestley et al. (1981) and Park et al. (1982) demonstrated that the approach was excessively conservative. This was due to the use of the Kent-Park (1971) stress

strain relations that do not adequately describe the enhanced strength of confined concrete. The fundamental moment-curvature approach was temporarily abandoned in favor of the recommendations by Park et al. (1982) to use the modifier $(0.5 + 1.25 P_e / f'_c A_g)$ with ACI equations. These equations found their way into the new code NZS 3101 and were subsequently used for buildings as well as bridges.

Because of the recognized shortcomings of the modified ACI equations, the Road Research Unit and the New Zealand Railways sponsored considerable research efforts on the fundamentals of confined concrete design for flexure and axial load. Early work on that program by Mander et al. (1984) resulted in advanced cyclic moment-curvature analysis techniques and the well known stress-strain relations for confined concrete (Mander et al. 1988a,b).

In a follow up to Mander's work Zahn et al. (1986) proposed a design approach that was based on moment-curvature analyses. The basis of Zahn's approach was in the definition of the ultimate curvature ductility. The ultimate curvature was defined in two ways:
(a) When hoop fracture occurred at the completion of <u>four</u> fully reversed cycles of loading; and
(b) After four fully reversed cycles if the flexural strength dropped to 80% of the nominal flexural capacity.

These criteria appear to be based on (a) cyclic demand imposed by typical earthquakes and (b) post-earthquake serviceability and/or collapse prevention. Although these are sound reasons for both of these criteria, the basis for the chosen values is purely arbitrary. Consequently on doing his numerous moment-curvature analyses, Zahn found that it is criteria (b) above that generally governs.

Additional experimental work was conducted by Watson and Park (1994) to validate the approach proposed by Zahn et al. (1986). The emphasis of this work was on investigating the performance of columns with limited transverse reinforcement. Consequently, Watson, Zahn and Park (1994) proposed the following design equations for transverse reinforcement:

86

For rectangular sections:

$$\rho_v = \frac{A_{sh}}{s\,b_c} = \frac{A_g}{A_c} \frac{\left(\dfrac{\phi_u}{\phi_y} - 33\rho_t m + 22\right)}{111} \frac{f_c'}{f_{yh}} \frac{P}{\phi f_c' A_g} - 0.006 \qquad \text{(7-15)}$$

and for circular sections:

$$\rho_s = \frac{4A_{bh}}{s\,D''} = 1.4 \frac{A_g}{A_c} \frac{\left(\dfrac{\phi_u}{\phi_y} - 33\rho_t m + 22\right)}{111} \frac{f_c'}{f_{yh}} \frac{P}{\phi f_c' A_g} - 0.008 \qquad \text{(7-16)}$$

where b_c = core width of the section measured perpendicular to direction of transverse bars under consideration in the center of peripheral hoop, ϕ_u = ultimate curvature, ϕ_y = yield curvature, $m = f_y / 0.85 f_c'$ with f_y = yield strength of longitudinal reinforcement, ϕ = strength reduction factor and the remaining symbols are as explained previously. It is of interest to note that the design formulations of Watson et al. (1994) suggest that ductility can be improved by increasing the longitudinal reinforcement. This is contrary to earlier findings of Mander et al. (1984, 1988a,b) and subsequent recommendations of ATC-32. Mander et al. (1984, 1988a,b) showed that additional longitudinal reinforcement places additional internal energy demands on the core concrete, this must be restrained by hoop steel with greater energy absorption capacity.

7.5.3 Comparison for Typical Bridge Columns

A comparison of the confinement requirements previously proposed by ACI (1995), NZS 3101 (1995), ATC-32 (1996) and Watson and Park (1994) with the energy based approach proposed herein is given in figure 7-5. It is evident that for low axial loads, and low longitudinal steel volumes the contemporary methods are in reasonable agreement—the existing ACI/AASHTO provisions being unnecessarily conservative. Conversely, for axial loads and high steel volumes where there are considerable energy demands on the confined core concrete the proposed formulation requires considerably more reinforcement than the existing ACI/AASHTO provisions. This is necessary if flexural ductility is to be maintained rather the

axial load capacity. As mentioned previously, the Watson, Zahn and Park (1994) recommendations do not agree with any other design method for high longitudinal steel contents. The use of this method is not recommended as the underlying assumptions defining failure are considered to be fundamentally flawed.

7.6 CONCLUSIONS

In this section the design equations for confinement of reinforced concrete beam-columns are derived. This is done by equating the capacity of a confined concrete section to the demand imposed on it by the ground shaking. As it has been observed that if capacity design procedure is followed, the only unavoidable mode is the low cycle fatigue of the longitudinal reinforcement, demands are calculated on the premise that the final failure will be through fracture of the tension reinforcement. Note that the quantity of lateral reinforcement so evaluated might not be critical if shear and buckling aspects are considered. This are important issues which are addressed in the following two sections.

SECTION 8
COMPRESSION BUCKLING FAILURE OF LONGITUDINAL REINFORCEMENT

8.1 INTRODUCTION

Buckling of longitudinal reinforcement is a commonly reported mode of failure. If the spacing of the transverse hoops is too large, then the compression steel may buckle inelastically under high compressive strains. The longitudinal reinforcement then becomes ineffective and unable to sustain axial compressive forces. This in turn places higher load demands on the core concrete. The additional load demand in both the longitudinal compression steel and the confined core concrete leads to a more rapid deterioration of moment capacity under cyclic loading.

Buckling of longitudinal reinforcement in a reinforced concrete column may be manifest in one of two ways: local buckling; or global buckling. Both of these types of buckling are shown in figure 8-1.

Local buckling occurs when the longitudinal reinforcement buckles in double curvature between two adjacent levels of transverse hoop reinforcement. Therefore, from a design point of view, the maximum spacing (s) between successive levels of transverse hoops that will ensure an adequate level of axial force transfer needs to be known. This section will first review theories on elastic and inelastic buckling and draw conclusions on specifying maximum hoopset spacing to ensure good inelastic performance of the longitudinal reinforcement. A new theory on inelastic buckling is then advanced based on energy considerations. This theory is useful for not only identifying the required hoop spacing, buckling strains and stresses, but also as a principal method of analysis for assessing global buckling mechanisms.

Global buckling occurs when the transverse reinforcement provides insufficient restraining force to inhibit buckling locally. Buckling may take place over one or more levels

89
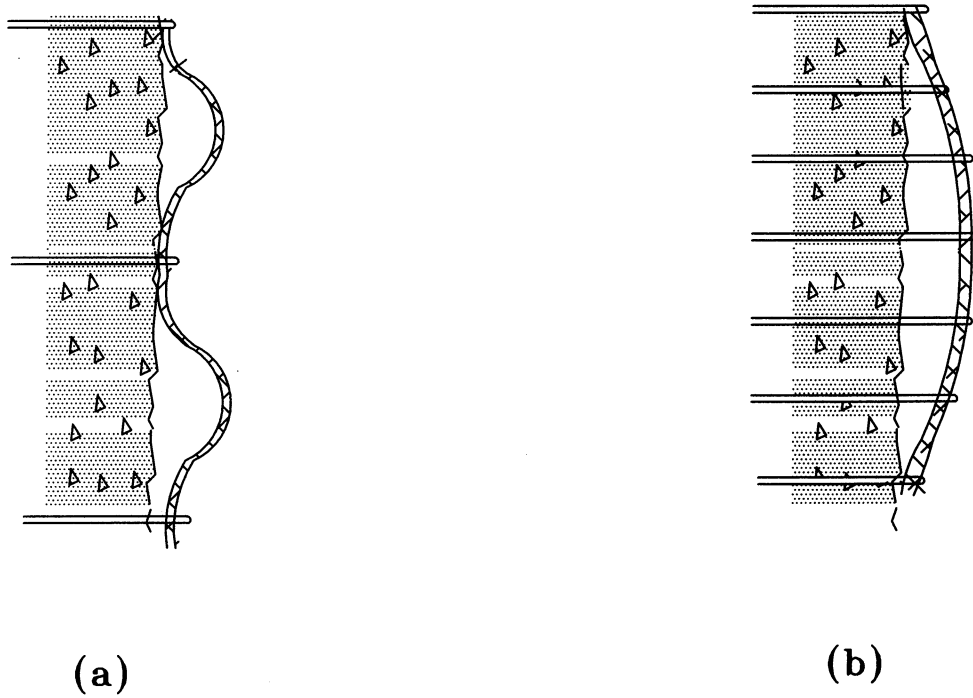
Figure 8-1   Possible Buckling Modes in a Reinforced Concrete Column: (a) Local Buckling and (b) Global Buckling

of transverse reinforcement as shown in figure 8-1(b). Previous attempts at solving the global buckling problem have invariably modeled the transverse reinforcement as a spring with an elastic modulus E. When the transverse reinforcement yields, however, the modulus of that steel is near zero and any elasticity based theories will strictly be invalid. This research uses an equilibrium plasticity theory, derived from energy considerations, to determine the global buckling limit states of stress (from which the ultimate compression strain can be inferred) together with the number of transverse hoops over which buckling will occur. In an inverse form this global buckling theory can be used to assess the amount of transverse reinforcement necessary to provide a required level of axial strain (or stress) to ensure good seismic performance under reversed cyclic loading.

8.2 LOCAL BUCKLING

Consider a longitudinal reinforcing bar buckling over a length s (the center-to-center hoopset spacing) under double curvature. For convenience, consider a one-quarter portion of this buckled bar such that the length of the cantilever column is $L = s/4$. Assume that the cantilever column is axially loaded as shown in figure 8-2(b). If the axial load is increased from zero to its maximum at which inelastic buckling occurs, then the axial and transverse load-deformation paths are shown in figures 8-2(c) and (d). As the axial load is increased, initially there will be no transverse displacement as the load is less than the elastic Euler buckling capacity. However, when the yield stress is attained, the elastic modulus of the column vanishes, incipient buckling is inevitable. Provided the column is short enough, lateral buckling will cause certain fibers of the cross section to unload with an elastic modulus (E_s) while others will continue to load and strain-harden with a tangent modulus E_t. As P increases, however, a particular value of thrust will be reached beyond which further increases are impossible, the member continues to deflect, and at least two equilibrium positions are found for the same value of the axial load. Such a situation also describes a condition of general structural instability-not one of buckling, but rather one where *large displacements* lead to *geometric non-linearity*.

91
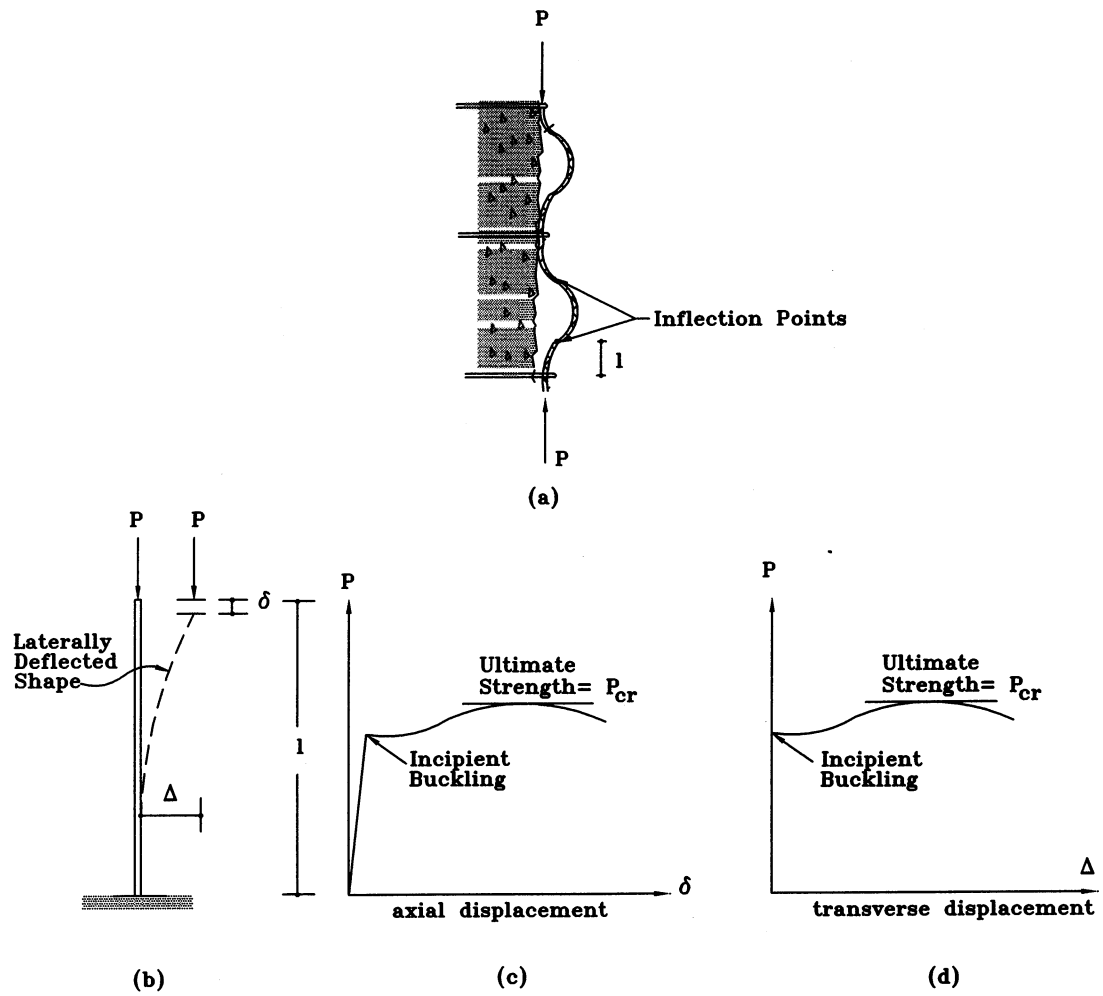
Figure 8-2 Analysis of Local Buckling in a Reinforced Concrete Column

8.2.1 Elastic and Pseudo-Elastic Buckling Analysis

This subsection first examines the classical stability problem formulated from the theory of elasticity and then goes on to show how this has been modified over the years to accommodate inelastic buckling. An alternative approach is then developed based on plastic equilibrium.

The theoretical solution to the critical buckling load was formulated by Euler (1759) who studied the behavior of a pin-pinned column and suggested that the critical buckling load for such class of columns be expressed by the well-known Euler buckling formula

$$P_{cr} = \frac{\pi^2 E I}{l^2} \tag{8-1}$$

where E = modulus of elasticity, I = moment of inertia and l = length between the pin ends of the column. For a column with fixed-fixed ends assuming that the point of contraflexure occurs at the quarter points adjacent to the fixed ends where $s = 2l$, the critical buckling load is modified as follows:

$$P_{cr} = \frac{4 \pi^2 E I}{s^2} \tag{8-2}$$

where $l = s/4$ = center-to-center spacing between individual hoop sets (or spiral pitch). Expanding equation (8-2) to solve for the critical buckling stress f_{cr}, one obtains

$$f_{cr} = \frac{P_{cr}}{A} = \frac{4 \pi^2 E}{s^2} \frac{I}{A} = \frac{4 \pi^2 E}{s^2} r^2 \tag{8-3}$$

in which A = cross sectional area, I = second moment of area and $I/A = r^2$, r being the radius of gyration. For a circular section, the radius of gyration r is related to the diameter d by the relation

$$r = \sqrt{\frac{I}{A}} = \sqrt{\frac{\pi / 64 \, d^4}{\pi / 4 \, d^2}} = \frac{d}{4} \qquad \text{(8-4)}$$

However, for an actual reinforcing bar taking into account the rolled deformations, Mander et al. (1984) showed that

$$r = 0.955 \left(\frac{d_b}{4} \right) \qquad \text{(8-5)}$$

where d_b = nominal diameter of the deformed reinforcing bar. Substituting this in equation (8-3) and rearranging one obtains

$$\frac{s}{d_b} = 1.5 \sqrt{\frac{E_{eff}}{f_{cr}}} \qquad \text{(8-6)}$$

where E_{eff} = effective modulus of elasticity which is averaged in some way across the section to account for the fact that when buckling commences the modulus of elasticity amongst the different fibers in the section varies. The determination of the effective modulus has been the source of much debate over many years. Some of this debate, germane to the present problem of inelastic buckling of reinforcing steel, is chronicled below.

a) *Elastic Buckling*. The maximum spacing of the hoops needed to prevent elastic buckling can be found by taking $E_{eff} = E_s$ and $f_{cr} = f_y$ as shown in figure 8-3a. For example, considering Grade 60 reinforcing bars with an upper bound yield stress of $f_y = 500 \, MPa$ and $E_s = 200 \, GPa$, the maximum spacing to ensure that the buckling stress just equals the yield stress given by equation (8-6) $s = 30 \, d_b$. A larger spacing would lead to elastic buckling wherein the corresponding stress will be less than the yield stress.

b) *Inelastic Buckling Using the Tangent Modulus Theory*. First attempts at assessing the inelastic buckling capacity of columns used the tangent modulus E_t (Engesser, 1898). For reinforcing steel it is assumed that $E_{eff} = E_t = E_{sh}$ = strain hardening modulus. If the spacing of the hoops are sufficiently close to prevent elastic bucking, lateral displacement commences when

94
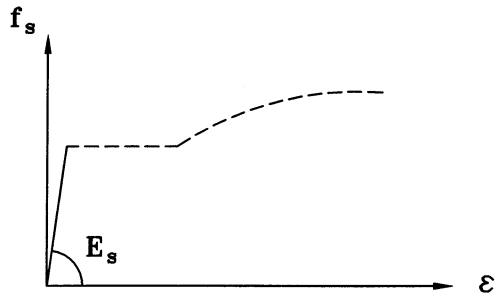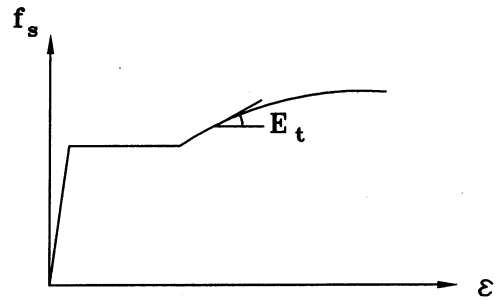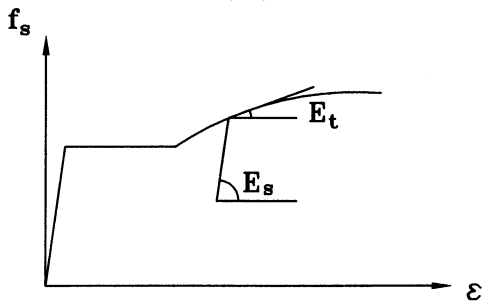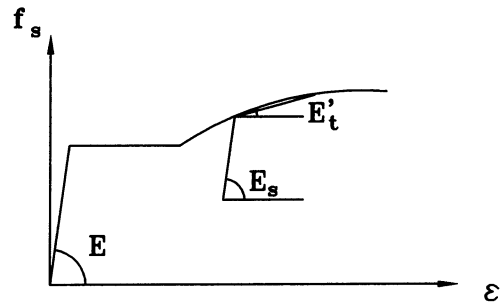
Figure 8-3 Showing the Various Modulii of Elasticity

95

the tangent modulus (figure 8-3b) is exceeded. However, experimental results have shown higher stresses can be sustained by the reinforcing bars at spacings greater than those given by tangent modulus theory, although significant buckling may have already started. The small curvatures that result from bending beyond the tangent modulus stress require some stress reversal to obtain section equilibrium. As a result, stiffening occurs and if the tangent modulus is used in equation (8-6), a lower bound solution to the buckling stress will be given.

c) *Inelastic Buckling Using Double Modulus Theory*. The non-reversible nature of the stress-strain relation directly leads to a double modulus solution. As the column bends at the tangent modulus load, the compressive strain follows the loading branch of the stress-strain curve thereby adhering to the tangent modulus (E_t), whereas the reversal strain will unload along the elastic modulus (E_s). In order to maintain both force and moment equilibrium, an equivalent double modulus or reduced modulus (E_r) results. A solution for a <u>rectangular</u> section was formulated by von Karman (1910) as

$$E_r = \frac{4 E_s E_t}{\left(\sqrt{E_s} + \sqrt{E_t}\right)^2} \tag{8-7}$$

For reasons that will become clearer below, the above equation for <u>rectangular</u> section can be restated as

$$\frac{E_s}{E_r} = \left[0.5 \left(\frac{E_s}{E_t}\right)^{\frac{1}{2}} + 0.5\right]^2 \tag{8-8}$$

Osgood (1935) used an numerical solution to derive the interrelationship between E_r, E_s and E_t for a number of different cross-sectional shapes. His result was re-derived in this study for a circular cross section. From this numerical solution it has been found that an empirical relationship between E_r, E_s and E_t can be formed for a circular section reinforcing bar with typical steel properties:

$$\frac{E_s}{E_r} = \left[0.5 \left(\frac{E_s}{E_t'} \right)^{\frac{1}{2.3}} + 0.5 \right]^{2.3} \qquad (8\text{-}9)$$

The development of this relationship is presented in Appendix C.

d) *Secant Modification to Double Modulus Theory*   The so-called column paradox was discussed by Shanley (1947). He argued that if the stress-strain relationship was governed only by the tangent modulus, equilibrium of the section would not be possible during stress reversal. So the double modulus theory will give the correct inelastic buckling load for an initially loaded perfectly straight column which is never the case in actual practice. Thus, the double modulus theory may be regarded as an upper bound solution. But because a real column is neither perfectly straight to begin with, nor is the material stress-strain relationship perfectly bi-linear (it is continuously non-linear after yielding) the real ultimate stress lies somewhere between the tangent modulus (lower bound) and double modulus (upper bound) theoretical solutions. Since the double modulus uses the instantaneous tangent modulus, a sudden buckling occurs on reaching the double modulus stress together with very small curvatures. Again, because buckling commences at yield, when the lower bound theoretical tangent modulus solution is exceeded, a strain gradient across the section will have minimum strain variation from at least ε_y^- to ε_{sh}^-. Figure 8-3d shows a secant modulus of elasticity (E_t') calculated between two stress-strain coordinates separated by a probable strain variation of, say, ε_{sh}. Thus if E_t' is used instead of the tangent modulus E_t to obtain the reduced modulus (E_r), a more realistic value of the hoop spacing will be obtained that can prevent longitudinal bar buckling at a particular ultimate compression steel strain. This secant modification to the double modulus theory was first suggested by Mander et al. (1984) with the results reproduced in figure 8-4. Reasonably good agreement between that theory and experimental results was observed.

As an alternative to the above-mentioned secant modified double modulus theory which has its roots in classical Euler buckling, a force (and moment) equilibrium solution of the buckled shape will now be derived based on energy considerations similar to the one followed

97
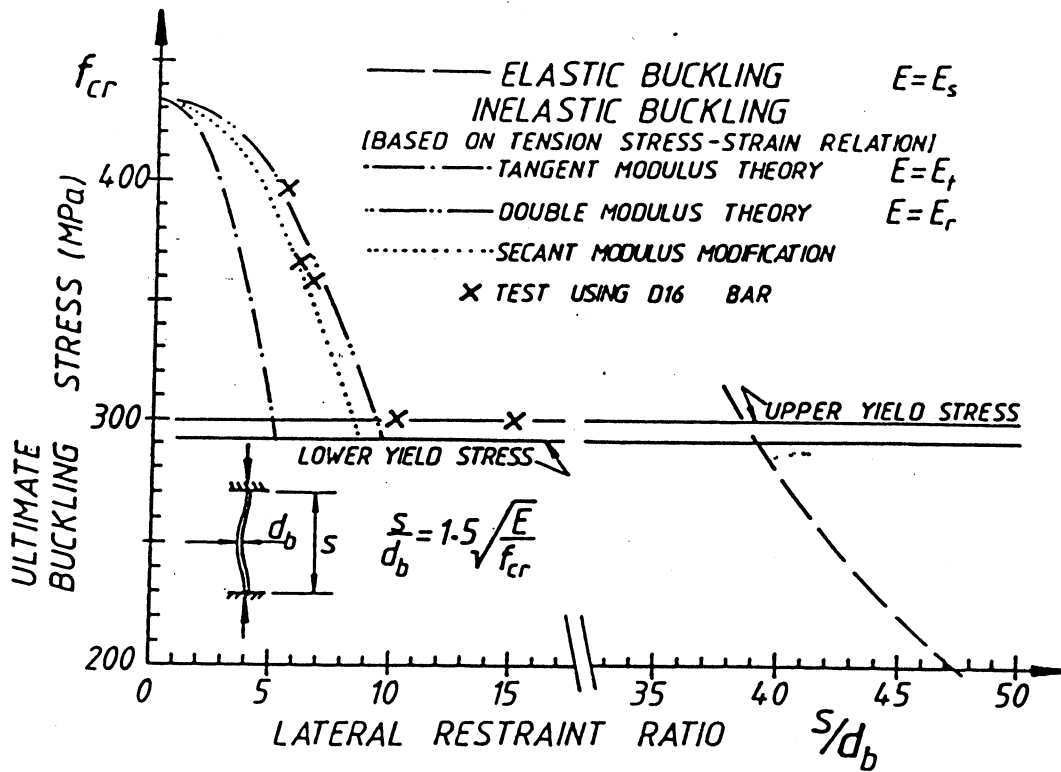
Figure 8-4 Showing the Comparison of Experimental and Analytical Predictions of Mander et al. (1984)

by Gomes and Appleton (1997).

8.2.2 Plastic Analysis Approach for solving the Local Buckling Problem

Consider a flexural reinforcement bar as shown in figure 8-5 fixed at the two ends. End reactions may consist of a moment, a horizontal shear force, and the applied axial load. However, shear force aids the buckling and hence the critical buckling condition is attained when $V = 0$. Focussing on the equilibrium of the quarter-length of the buckled bar, it can be stated that the lateral plastic displacement Δ_p will increase up to a point when the full plastic moment capacity will be mobilized at the base of the buckled bar. At this instant, the plastic moment capacity M_p corresponding to the critical <u>ultimate</u> load P_{cr} will equal the P-Δ moment at the base of the buckled bar which is distributed as shown in figure 8-5b. The plastic moment M_p has an associated plastic curvature Φ_p which is conceivably distributed in the form of a n-th degree parabolic curve as shown in figure 8-5c. Details of the derivation of the curvature shape is given in Appendix C. Postulating a rigid plastic mechanism whereby it is assumed that the resistance to the vertical load is entirely provided by the plastic moments that develop at the extremities a virtual work equation can be written as

$$EWD = IWD \qquad (8\text{-}10)$$

$$P_{cr} \cdot 2\,\delta_p = 4\,M_p\,\theta_p \qquad (8\text{-}11)$$

$2\,\delta_p$ being the total downward movement of the axial load due to buckling and θ_p, M_p are the plastic rotations and the plastic moments as shown in figure 8-5d. From geometry however,

$$\frac{\delta_p}{\Delta_p} = \tan\left(\frac{\theta_p}{2}\right) \approx \frac{\theta_p}{2} \quad (\textit{for small } \theta_p\,) \qquad (8\text{-}12)$$

and

$$\frac{\Delta_p}{s/2} = \sin(\theta_p) \approx \theta_p \qquad (8\text{-}13)$$

Combining equations (8-12) and (8-13)

(a) Local Buckling (b) Moment (c) Curvature

(d) Mechanism
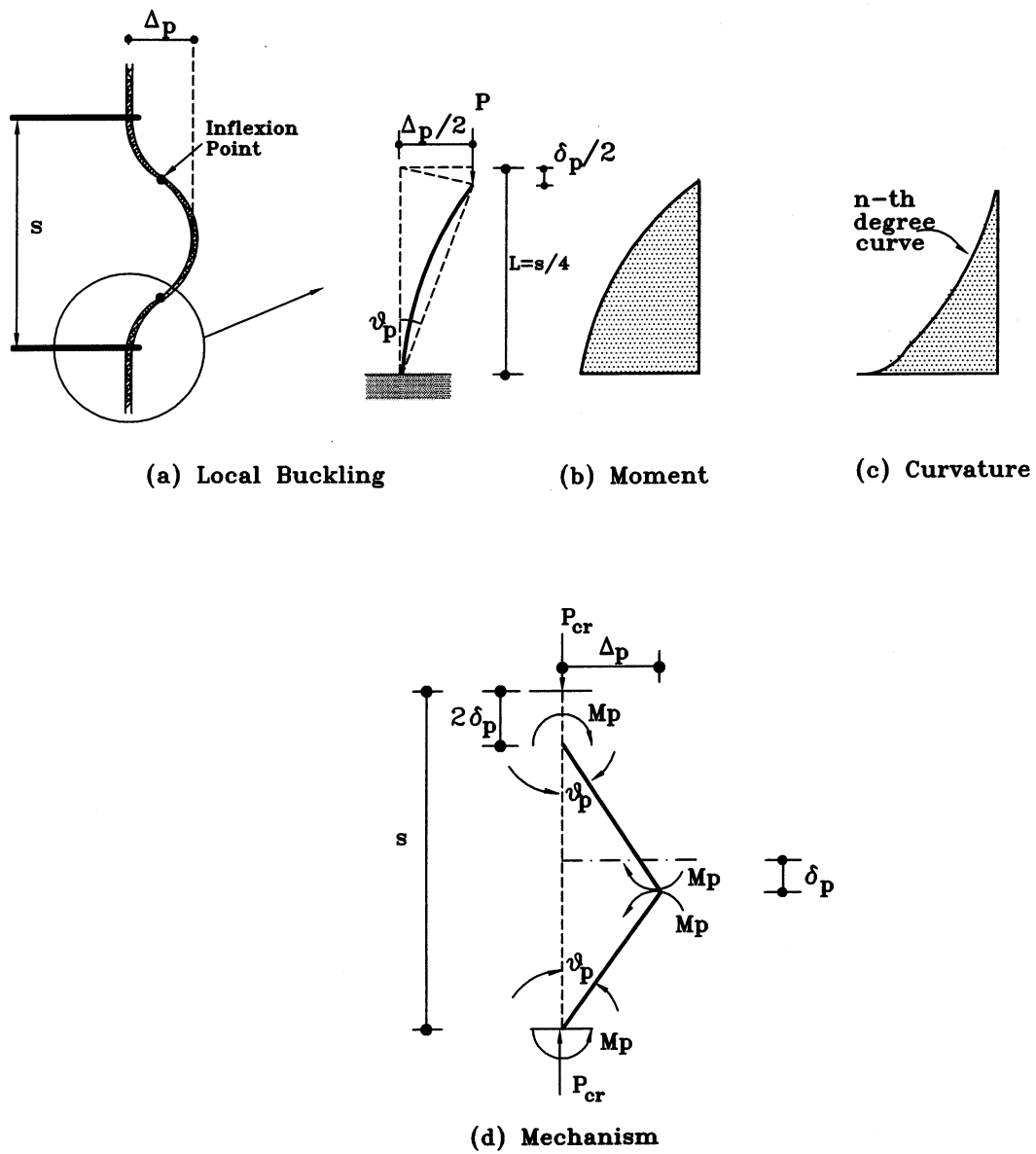
Figure 8-5 Plastic Analysis of Local Buckling of Longitudinal Reinforcement

100

$$\delta_p = \frac{s}{4} \theta_p^2 \qquad \text{(8-14)}$$

Substituting the expression for δ_p in equation (8-11) and on subsequent simplification

$$P_{cr} = \frac{8 M_p}{s \theta_p} \qquad \text{(8-15)}$$

Dividing both sides of the above equation by the area of cross section, the same equation can be written in terms of stresses as

$$f_{cr} = \frac{32}{\pi} \frac{M_p}{d_b^2 s \theta_p} \qquad \text{(8-16)}$$

The plastic rotation θ_p can be obtained by integrating the plastic curvature diagram using the well-known moment curvature theorem. For an assumed polynomial shape function, this is usually expressible in the form

$$\theta_p = \Upsilon \Phi_p \frac{s}{4} \qquad \text{(8-17)}$$

where the coefficient Υ depends on the shape of the moment curvature diagram (refer Appendix C) and Φ_p is the plastic curvature corresponding to the plastic moment M_p.

The plastic curvature Φ_p corresponding to any plastic moment M_p can be obtained from moment curvature analysis. However, in the absence of such rigorous analysis, it was observed that satisfactory results can be obtained for Grade 60 reinforcement if the moment-curvature relationship for a particular axial load is approximated by a cubic curve as

$$\Phi_p = \Phi_{pp} \left[1 - \left(1 - \frac{M_p}{M_{pp}} \right)^{\frac{1}{3}} \right] \qquad \text{(8-18)}$$

where Φ_{pp} is the plastic curvature corresponding to the peak plastic moment M_{pp}. These parameters are plotted in figure 8-6b.
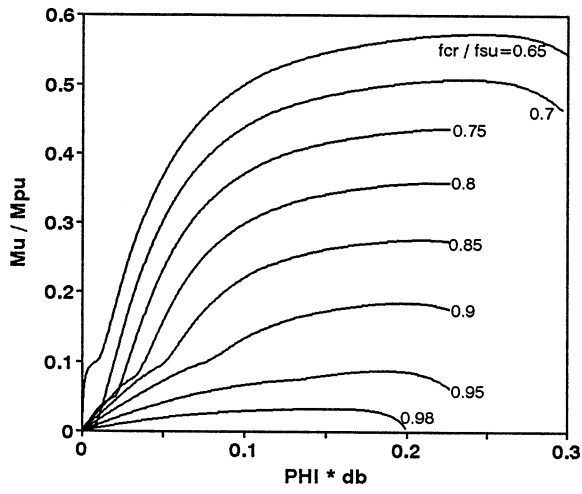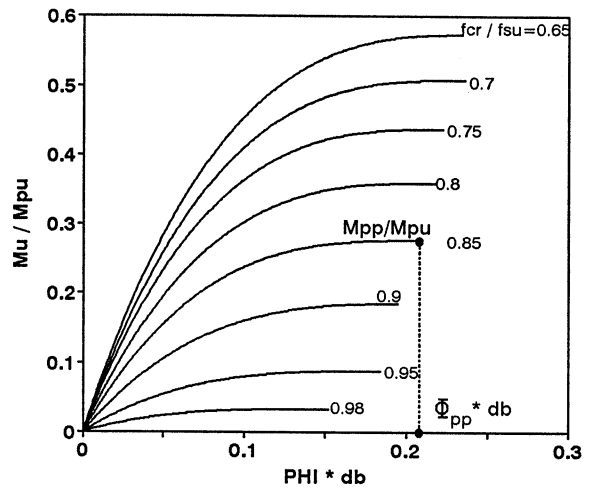
101

(a) Moment-Curvature

(b) Approximate Moment-Curvature
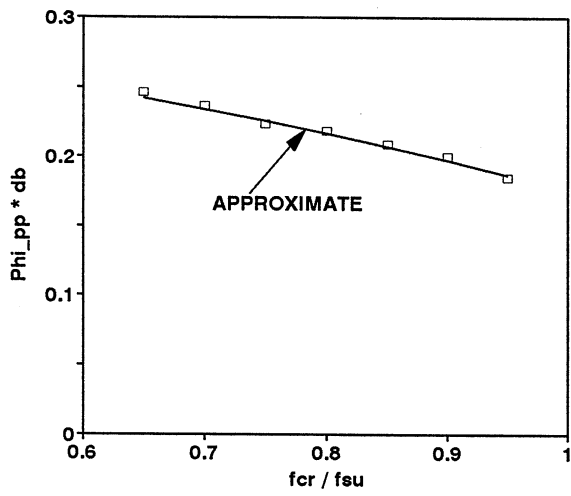
(c) Curvature and Critical Stress
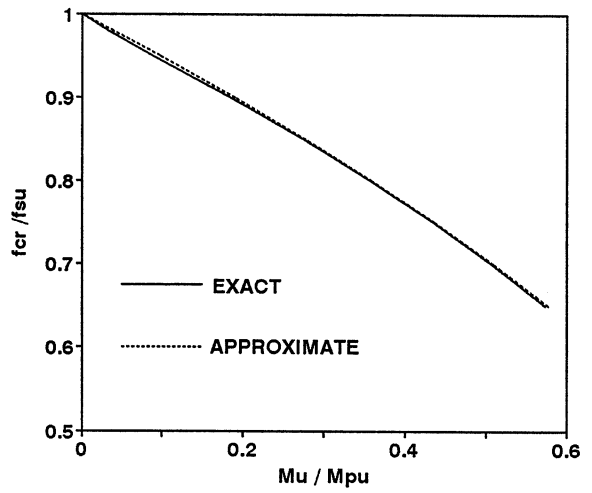
(d) Interaction Diagram

Figure 8-6 Moment/Curvature-Axial Load Interaction for Grade 60 Reinforcement.

The maximum plastic moment M_{pp} depends upon the magnitude of the axial compression. For a particular critical ultimate load P_{cr}, the associated peak plastic moment can be obtained from the interaction diagram via a complete moment curvature analysis that considers the strain-hardening effect of the steel. For nominal Grade 60 reinforcing steel it can be shown that the plastic moment is related to the critical stress by a simple expression

$$M_{pp} = M_{pu}\left[1 - \left(\frac{f_{cr}}{f_{su}}\right)^2\right] \tag{8-19}$$

where $M_{pu} = f_{su}d_b^3/6 =$ fully plastic ultimate moment for a circular section without any axial load and $f_{su} =$ ultimate stress in the longitudinal reinforcement. This expression gives an almost perfect match for Grade 60 reinforcement; some slight error is introduced when applying the formula to Grade 40 reinforcing steel and prestressing threadbars, but this error is minimal.

The dimensionless plastic curvature $\Phi_{pp}d_b$ at peak plastic moment can also be related to the maximum plastic moment ratio according to a linear relation given by

$$\Phi_{pp}d_b = \varsigma + \lambda\left[\frac{M_{pp}}{M_{pu}}\right] = (\varsigma + \lambda) - \lambda\left[\frac{f_{cr}}{f_{su}}\right]^2 \tag{8-20}$$

The parameters ς and λ are strongly dependant on the grade of steel. For nominal Grade 60 reinforcing bars ς and λ have values of 0.175 and 0.115, respectively. This is plotted in figure 8-6 for Grade 60 reinforcing. Similar analysis can be performed on any variety of steel and expressions similar to the above may be found.

Substituting equations (8-17) through (8-20) into equation (8-16) and simplifying one obtains

$$f_{cr} = \frac{128}{\pi d_b^2 s \Upsilon \Phi_{pp}} \cdot \left[\frac{M_p}{1 - \left(1 - \frac{M_p}{M_{pp}}\right)^{1/3}}\right] \tag{8-21}$$

For the minimum buckling load, the second term in square brackets should be minimized. It

103

can be easily inferred that this term is minimum when $M_p = M_{pp}$. Hence substituting equations (8-19) and (8-20) into the above equation and simplifying further

$$\frac{s}{d_b} = \frac{2.61}{\sqrt{\Upsilon}} \sqrt{\frac{f_{su}}{f_{cr}} \left[\frac{1 - \left| \frac{f_{cr}}{f_{su}} \right|^2}{(\varsigma + \lambda) - \lambda \left| \frac{f_{cr}}{f_{su}} \right|^2} \right]} \qquad (8\text{-}22)$$

Assuming a parabolic distribution of the curvature (details in Appendix C) for which $\Upsilon = 0.233$, and using $\varsigma = 0.175$ and $\lambda = 0.115$, the above equation for Grade 60 reinforcement can be reduced to

$$\frac{s}{d_b} = 10 \sqrt{\frac{f_{su}}{f_{cr}} \left[\frac{1 - \left| \frac{f_{cr}}{f_{su}} \right|^2}{1 - 0.4 \left| \frac{f_{cr}}{f_{su}} \right|^2} \right]} \qquad (8\text{-}23)$$

which can easily be solved by fixed point iteration. It is also of interest to note that this buckling equation does not explicitly require the evaluation of an effective secant modulus.

8.2.3 Comparison with Experimental Results

To validate the foregoing theory, a comparison will now be made with the results of previous experimental investigations. Although experimental results for pure axial compression on reinforcing bars do not abound, every attempt has been made to collect available data and compare it with equation (8-23). In spite of the fact that the above equation is calibrated for nominal Grade 60 reinforcing bars which is the most widely used reinforcement variety in the U.S. today, it is of interest to compare the predictions of this formula for other grades of steel as well. What follows is a brief summary of the test specimens and a comparison with the analytical predictions.

104

<u>Specimens Tested by Mander et al. (1995)</u>: Mander et al.(1995) while investigating the constant amplitude low cycle fatigue behavior of reinforcing bars tested two varieties of reinforcement in axial compression. The first type of material used was ASTM A722 type II hot-rolled and proof-stressed alloy-steel thread bar ("Specification" 1987) having a specified minimum ultimate stress tensile strength of 1083 MPa. The second type of material used was ASTM A615 Grade 40 deformed billet-steel reinforcing bar ("Specification" 1987) having a minimum specified yield strength of 276 MPa. The tension and compression stress-strain properties along with other relevant information is provided in table 8-1.

Table 8-1   Showing Relevant Information for Reinforcing Bars Tested by Mander et al. (1995)

Speci-men	d_b (mm)	s/d_b	f_y (MPa)	E_s (GPa)	E_{sh} (MPa)	ε_{sh}	f_{su} (MPa)	ε_{su}	ε_{sf}
P1	15.88	6	869	221.3	11030	0.0039	1130	0.063	0.092
P5	15.88	6	-917	220.6	12130	-0.0041	-1076	-0.028	-
P8	15.88	8	-915	219	4380	-0.0042	-936	-0.012	-
P15	15.88	9	-908	234	1170	-0.0039	-914	-0.007	-
R13		9.6	331	215.1	8274	0.0091	565	0.144	0.17
R2		6	-338	213.7	8619	-0.008	-531	-0.045	-

<u>Specimens Tested by Monti et al.(1993)</u> While investigating the cyclic behavior of FeB44 steel rebars of the Italian production Monti et al.(1993), carried out axial compression tests on specimens of three different spacings. The s/d_b ratios studied were 5, 8 and 11 respectively. These reinforcing bars had a nominal yield strength of 440 MPa and were of diameters 16, 20 and 24 mm respectively. These test results are compared in figure 8-7.
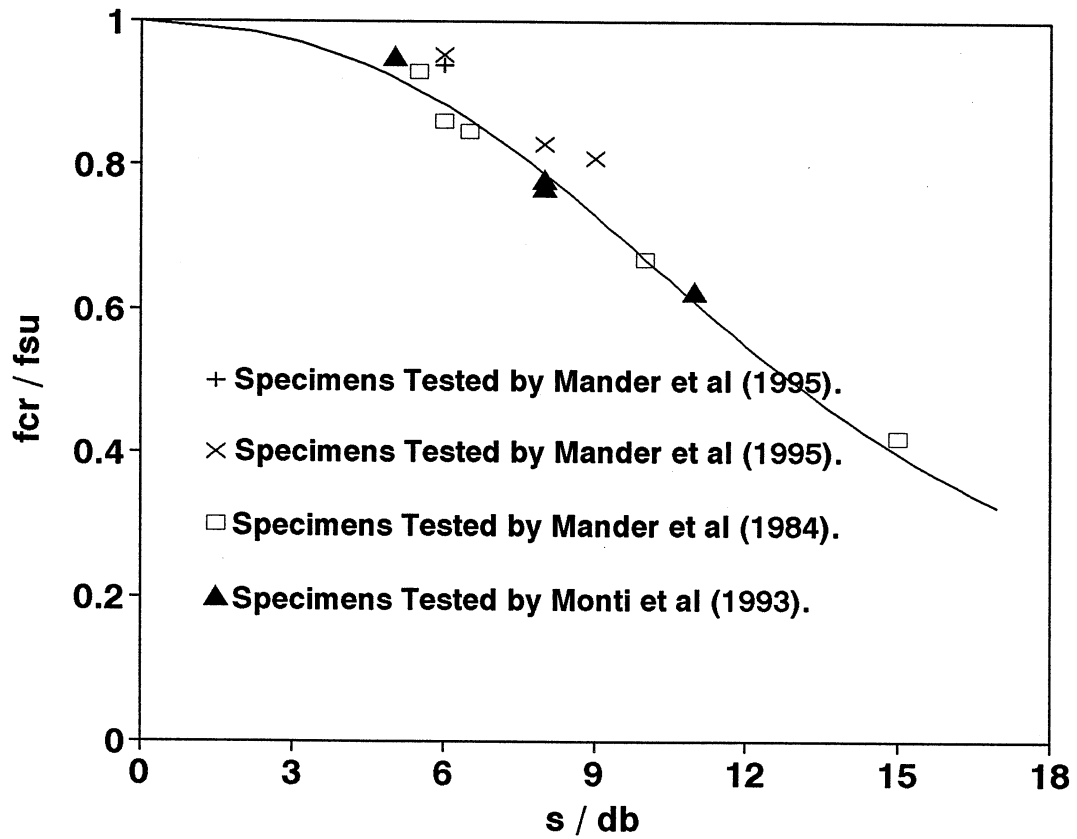
Figure 8-7 Comparison of Experimental Results with Analytical Expression for Local Buckling.

Specimens Tested by Mander et al.(1984): Mander et al. (1984) as part of his doctoral studies at the University of Canterbury studied the inelastic compression buckling failure of reinforcing bars. The reinforcing bars were 16 mm. in diameter with a nominal yield strength of 295 MPa. The ultimate strength was measured at 433 MPa. These test results are also plotted in figure 8-7.

From figure 8-7 it can be seen that equation (8-20) give a reliable prediction of the critical ultimate strength corresponding to any s/d_b ratio. Although some scatter is evident in the analytical prediction for different varieties of steel, this is to be expected since equation (8-23) was calibrated for Grade 60 reinforcement alone. Nevertheless, the procedure outlined can be adapted for any variety of steel. Keeping this in mind the analytical predictions may be regarded as satisfactory.

8.3 GLOBAL BUCKLING

It has been often observed in laboratory experiments on near full-sized reinforced concrete columns that the buckling of the longitudinal reinforcement is not necessarily confined between two adjacent levels of hoop reinforcement. In many instances the longitudinal reinforcement actually buckles over one or more layers of lateral reinforcing. Although current codes dictate a maximum spacing of six times the longitudinal bar diameter ($s = 6d_b$) based on simple compression tests (such as those described in Section 8.2) longitudinal reinforcement may continue to buckle if insufficient transverse reinforcement is provided. This results in poor overall column performance and rapid decay in moment capacity after the onset of buckling. This inadequate performance is due to lack of recognition by codes of the distinction between local and global buckling, and the fixation on concrete confinement requirements. It is generally not recognized that the longitudinal steel also needs to be "confined" against global buckling. Only recently has work commenced on the effect of global buckling of longitudinal reinforcement.

Bresler and Gilbert (1961) first investigated the global buckling behavior of reinforcing steel over two hoop spacings. Using an assumed deflected shape for the buckled bar they used Ritz method to express the equivalent lateral stiffness of the hoop reinforcement in terms of it's effective modulus. Scribner (1986) also looked at the global buckling problem from an analytical perspective and concluded that the tie diameter be at least one-half the longitudinal bar diameter to prevent global buckling. He used an energy minimization approach similar to Bresler and Gilbert (1961) with elastic tie forces to predict the buckling length for a global buckling failure of longitudinal reinforcement. Papia et al. (1986) analyzed the global buckling problem representing the longitudinal rebar-hoop steel system as an inverted beam on elastic foundation with the tie stiffness depending on the geometrical and mechanical characteristics. Buckling was identified by the non-positive definiteness of the system matrix (i.e. when the determinant became zero). Priestley et al. (1996) extending the local buckling results of Mander et al. (1984), also studied the global buckling behavior of reinforcing steel based on an assumed deflected shape and <u>elastic</u> restraining forces in the tie. It is of interest to note that all of these researchers assumed some form of elastic or pseudo elastic tie forces in their formulations. However, any elasticity-based formulation constitutes a major departure from the real situation where in the plastic hinge zones of columns, the hoops invariably yield, drastically losing stiffness.

In this study an approach based on energy principles is advanced to predict the buckled length for rebars failing in global buckling. A virtual work approach as used previously is followed to solve the issue of global buckling. Following this a comparison with test specimens with observed cases of global buckling is performed. Finally some design issues are addressed and detailing strategies presented that will result in improved performance.

8.3.1 Plastic Analysis Approach for solving the Global Buckling Problem

Consider a segment of a longitudinal reinforcement shown in figure 8-8 that has buckled between N_h lateral hoops. Assuming the lateral hoop spacing is s, the total (global) buckled length is given by

(a) Global Buckling   (b) Mechanism
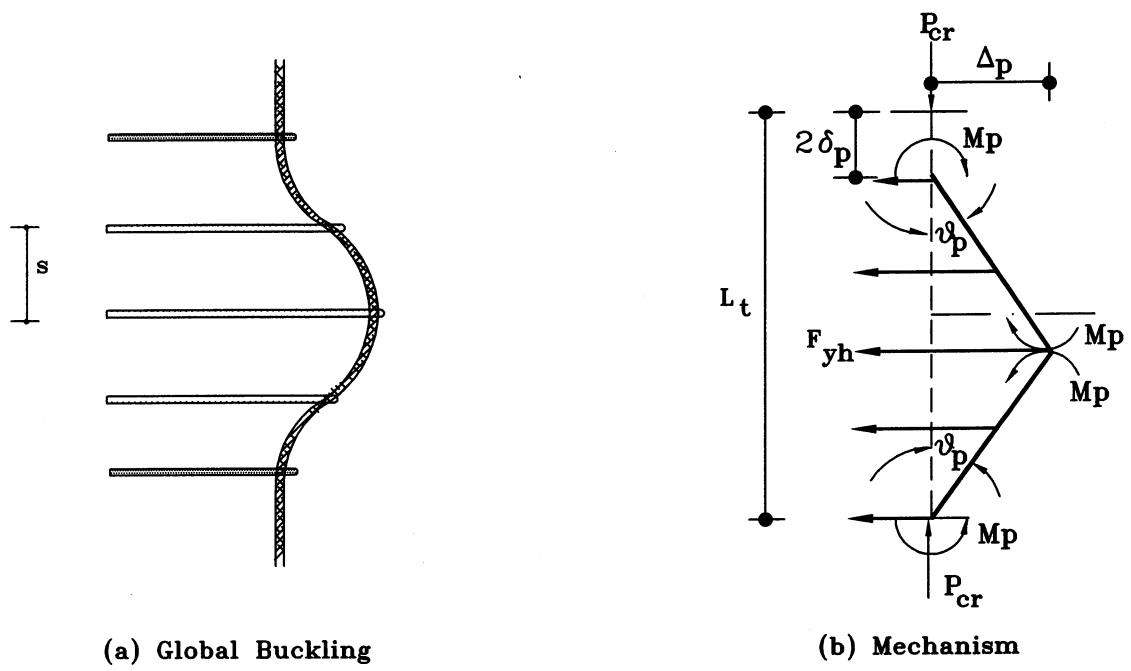
Figure 8-8 Plastic Analysis of Global Buckling of Longitudinal Reinforcement

$$L_b = (N_h + 1)s \qquad (8\text{-}24)$$

Now assuming that lateral hoops over which the longitudinal steel buckles have all yielded, then the total restraining force is given by

$$R_h = \sum^{N_h} F_{yh} \qquad (8\text{-}25)$$

where $F_{yh} =$ restraining force exerted by <u>one</u> layer (or spiral) of hoop reinforcement. If the total vertical plastic displacement of the segment is $2\delta_p$ and the plastic rotation as shown in figure 8-8 is θ_p, a virtual work equation can be written as follows

$$EWD = IWD \qquad (8\text{-}26)$$

$$P_{cr} \cdot 2\delta_p = 4 M_p \theta_p + N_h F_{yh} \frac{\Delta_p}{2} \qquad (8\text{-}27)$$

in which $\Delta_p =$ mid-span lateral plastic movement of the segment due to buckling and $M_p =$ plastic moment as shown in figure 8-8. Note that in the above equation it is assumed that the external work done by the axial load is entirely resisted by the plastic moments and the lateral hoop forces that do an average plastic work given by the product of the force and average plastic lateral displacement.

From geometrical considerations the following relationships can be found:

$$\frac{\delta_p}{\Delta_p} = \tan\left(\frac{\theta_p}{2}\right) \approx \frac{\theta_p}{2} \quad (\textit{for small } \theta_p) \qquad (8\text{-}28)$$

and

$$\frac{\Delta_p}{(N_h + 1)s/2} = \sin(\theta_p) \approx \theta_p \qquad (8\text{-}29)$$

Combining equations (8-28) and (8-29)

$$\delta_p = (N_h + 1)\frac{s}{4}\theta_p^2 = \frac{L_b\theta_p^2}{4} \qquad (8\text{-}30)$$

Substituting the expression for δ_p into the work equation (8-27) and making some further simplification gives

$$P_{cr}\cdot(N_h + 1)s\theta_p = 8M_p + N_h(N_h + 1)F_{yh}\frac{s}{2} \qquad (8\text{-}31)$$

Assuming the plastic curvature is distributed in the form of a n-th degree parabola (as was also assumed previously for the local buckling), the plastic rotation θ_p can be obtained by integrating the plastic curvature diagram utilizing the well-known moment area theorem. For the assumed n-th degree curve this is given by

$$\theta_p = \Upsilon\frac{s(N_h + 1)}{4}\Phi_p = \Upsilon\frac{L_b}{4}\Phi_p \qquad (8\text{-}32)$$

As stated previously, the minimum buckling load occurs corresponding to the maximum plastic moment M_{pp} which depends upon the magnitude of the axial compression. For a particular critical ultimate load P_{cr}, the associated plastic moment can be obtained from the moment axial load interaction diagram for reinforcing bars. In lieu of such a rigorous analysis, for normal Grade 60 reinforcement the plastic moment can be related to the critical stress by equation (8-19). Also noting that the dimensionless plastic curvature at peak plastic moment is related to the same through equation (8-20), equations (8-19), (8-20) and (8-32) can be substituted into (8-31) and simplified to yield

$$P_{cr}(N_h + 1)^2 s^2 = \frac{32M_{pu}\left[1 - \left|\frac{f_{cr}}{f_{su}}\right|^2\right]d_b}{\Upsilon\left[(\varsigma + \lambda) - \lambda\left|\frac{f_{cr}}{f_{su}}\right|^2\right]} + \frac{2N_h(N_h + 1)F_{yh}sd_b}{\Upsilon\left[(\varsigma + \lambda) - \lambda\left|\frac{f_{cr}}{f_{su}}\right|^2\right]} \qquad (8\text{-}33)$$

Noting that $M_{pu} = f_{su}d_b^3/6$, the above equation can be expressed in terms of the critical ultimate stress by dividing both sides by the area of cross section as

111

$$f_{cr}(N_h+1)^2 s^2 = \frac{6.8 f_{su}\left[1 - \left|\frac{f_{cr}}{f_{su}}\right|^2\right] d_b^2}{\Upsilon\left[(\varsigma + \lambda) - \lambda \left|\frac{f_{cr}}{f_{su}}\right|^2\right]} + \frac{2.55 N_h F_{yh}}{\Upsilon\left[(\varsigma + \lambda) - \lambda \left|\frac{f_{cr}}{f_{su}}\right|^2\right]} \cdot (N_h + 1)\frac{s}{d_b} \qquad (8\text{-}34)$$

The above expression has the lateral yield force term F_{yh} which deserves some special attention at this point. For rectangular sections this is simply given by

$$F_{yh}^{rect} = \frac{\pi}{4}\frac{d_{bh}^2\, f_{yh}}{\kappa} = \frac{A_{bh} f_{yh}}{\kappa} \qquad (8\text{-}35)$$

where A_{bh}, d_{bh}, f_{yh} respectively equal the areas, diameter and the yield stress of the horizontal reinforcement, and $\kappa =$ coefficient which depends on the restraint type as shown in figure 8-9. Thus,

$\kappa = 1.0 =$ for rectangular and square sections;

$\kappa = \dfrac{N}{2\pi} =$ for circular hoops or spirals where $N =$ number of longitudinal bars.

The latter case for circular columns is derived in terms of the radial component of force exerted onto the longitudinal bar

$$F_{yh}^{circ} = \frac{2\pi}{N} f_{yh}\left(\frac{\pi}{4} d_{bh}^2\right) \qquad (8\text{-}36)$$

which means $\kappa = N/2\pi$.

Thus equation (8-34) can be rephrased as

$$f_{cr}(N_h+1)^2 s^2 = \frac{6.8 f_{su}\left[1 - \left|\frac{f_{cr}}{f_{su}}\right|^2\right] d_b^2}{\Upsilon\left[(\varsigma + \lambda) - \lambda \left|\frac{f_{cr}}{f_{su}}\right|^2\right]} + \frac{2}{\kappa}\frac{N_h f_{yh} d_{bh}^2}{\Upsilon\left[(\varsigma + \lambda) - \lambda \left|\frac{f_{cr}}{f_{su}}\right|^2\right]} \cdot (N_h + 1)\frac{s}{d_b} \qquad (8\text{-}37)$$

Using a parabolic approximation for the curvature distribution for Grade 60 reinforcement along with $\varsigma = 0.175$ and $\lambda = 0.115$ respectively, the globally buckled length for rectangular and circular sections similar to the local buckling solution can be solved as

112

(a) $\kappa = 1.0$
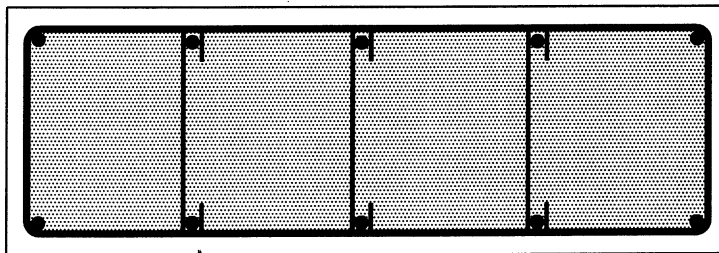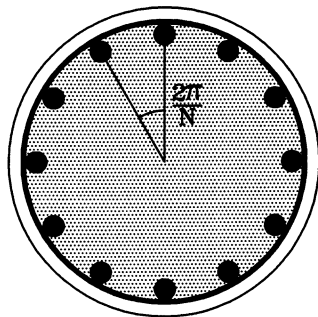
(b) $\kappa = N/2\pi$

Figure 8-9 Restrain Coefficient for Rectangular and Circular Column Sections

113

$$\frac{L_b}{d_b} = (N_h + 1)\left(\frac{s}{d_b}\right) = 10\sqrt{\frac{f_{su}}{f_{cr}}\frac{\left(1 - \left|\frac{f_{cr}}{f_{su}}\right|^2\right)}{\left(1 - 0.4\left|\frac{f_{cr}}{f_{su}}\right|^2\right)}\left[1 + \frac{0.3}{\left[1 - \left|\frac{f_{cr}}{f_{su}}\right|^2\right]}\frac{N_h}{\kappa}\left(\frac{f_{yh}}{f_{su}}\right)\left(\frac{d_{bh}}{d_b}\right)^2 \cdot \frac{L_b}{d_b}\right]} \tag{8-38}$$

Note that in equation (8-38)

$$\frac{f_{yh}}{f_{su}}\left(\frac{d_{bh}}{d_b}\right)^2 = \frac{F_{yh}}{F_{su}} \tag{8-39}$$

which is the ratio of the transverse reinforcement bar force at yield (F_{yh}) to the ultimate strength of one longitudinal reinforcing bar. Solving this ratio for design purposes gives

$$\frac{F_{yh}}{F_{su}} = \kappa\left[0.033\left(\frac{s}{d_b}\right)\left(1 + \frac{1}{N_h}\right)\left(\frac{f_{cr}}{f_{su}} - 0.4\left|\frac{f_{cr}}{f_{su}}\right|^3\right) - \frac{3.33\left[1 - |f_{cr}/f_{su}|^2\right]}{N_h(N_h + 1)(s/d_b)}\right] \tag{8-40}$$

or in other words

$$\frac{F_{yh}}{F_y} = \kappa\frac{f_{cr}}{f_y}\left[0.033\left(\frac{s}{d_b}\right)\left(1 + \frac{1}{N_h}\right)\left(1 - 0.4\left|\frac{f_{cr}}{f_{su}}\right|^2\right) - \frac{3.33\left[|f_{su}/f_{cr}| - |f_{cr}/f_{su}|\right]}{N_h(N_h + 1)(s/d_b)}\right] \tag{8-41}$$

8.3.2 Comparison with Experimental Results

As for the case of local buckling, the analytical expressions for global buckling can be verified by comparing them with actual test results. Although there is ample evidence of global buckling in the literature, most experiments do not give an explicit count of the number of lateral bars over which such buckling may have occurred. Thus only those specimens where there is a good photographic record can be used for comparative purposes. It should be emphasized that buckling (be it local or global) does not always indicate that the reinforcement was stressed beyond its buckling limit state. In many cases global buckling occurs because of premature transverse hoop fracture that leads to early global buckling. Since the theoretical model does

114

not incorporate such fringe effects, it is essential that only those specimens where true global buckling occurred be identified. As a result great caution was exercised in choosing the correct specimens where the failure was purely due to reinforcement buckling. The principal factor for comparison is the buckled length L_b or the term N_h which gives a count of the number of hoops over which the global buckling has occurred. Hence it is necessary to estimate the stress level (f_{cr}/f_{su}) if equation (8-38) is to be used. In experimental documentation such information can usually be inferred from the curvature or strain records at the location of buckling in conjunction with some knowledge about the stress-strain characteristics of the reinforcement. In the absence of such extensive experimental records it will be assumed that global buckling occurred at yield stress level of the longitudinal reinforcement. This assumption appears to be valid for the plastic hinge location. The following gives a brief description of the specimens which were used for comparison purposes.

(i) Bridge Knee Joints tested by Ingham et al.(1997): As part of his doctoral studies Ingham et al.(1997) tested four large scale structural concrete bridge cap beam-column joints. These units represented an as-built joint as well as a repair, a retrofit, and a redesign of the as-built joint. The specimens incorporated differing detailing including haunching, prestressing, and variations in the quantity of spirally-placed joint reinforcement. The specimen of interest is the redesigned unit that had overlapping spiral reinforcement 6.35 mm(#2) in diameter and restrained 19-19.35 mm(#6) longitudinal bars. The overlapping spirals had a pitch of 30 mm and a yield strength of $f_{yh} = 337\,MPa$. The longitudinal reinforcement had a yield strength of $f_y = 431\,MPa$. Since the longitudinal reinforcement was grade 60, the ultimate stress was estimated to be $f_{su} = 640\,MPa$. The test specimen is shown in figure 8-10 and the comparison is summarized in table 8-3.

(ii) Circular Column tested by Cheng (1997) : While investigating the seismic performance of replaceable hinge columns, Cheng (1997)tested an as-built circular column that was reinforced with 12-D13 reinforcing bars with a nominal yield strength of $f_y = 439\,MPa$ and ultimate strength of $f_{su} = 686\,MPa$. The lateral reinforcement consisted of W2 soft wire hoops (4 mm) in diameter with a yield strength of $f_{yh} = 275\,MPa$. The tested specimen is shown in figure 8-11 and the
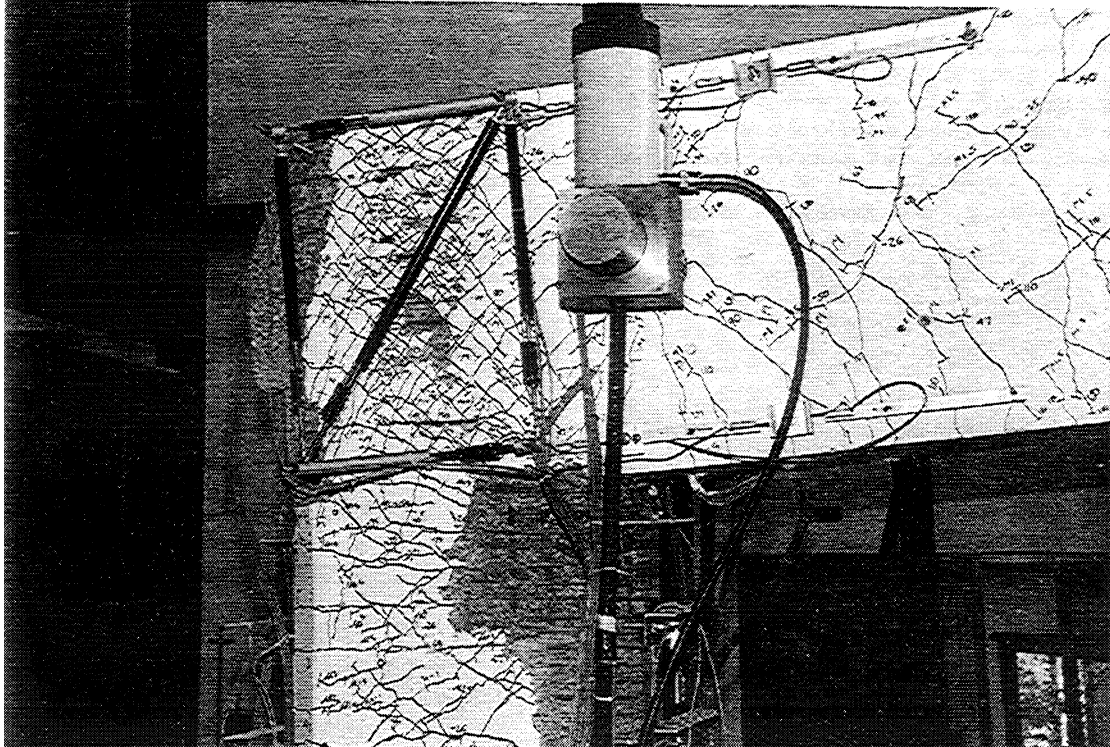
Figure 8-10 Experimental Results of Ingham et al. (1997)

116
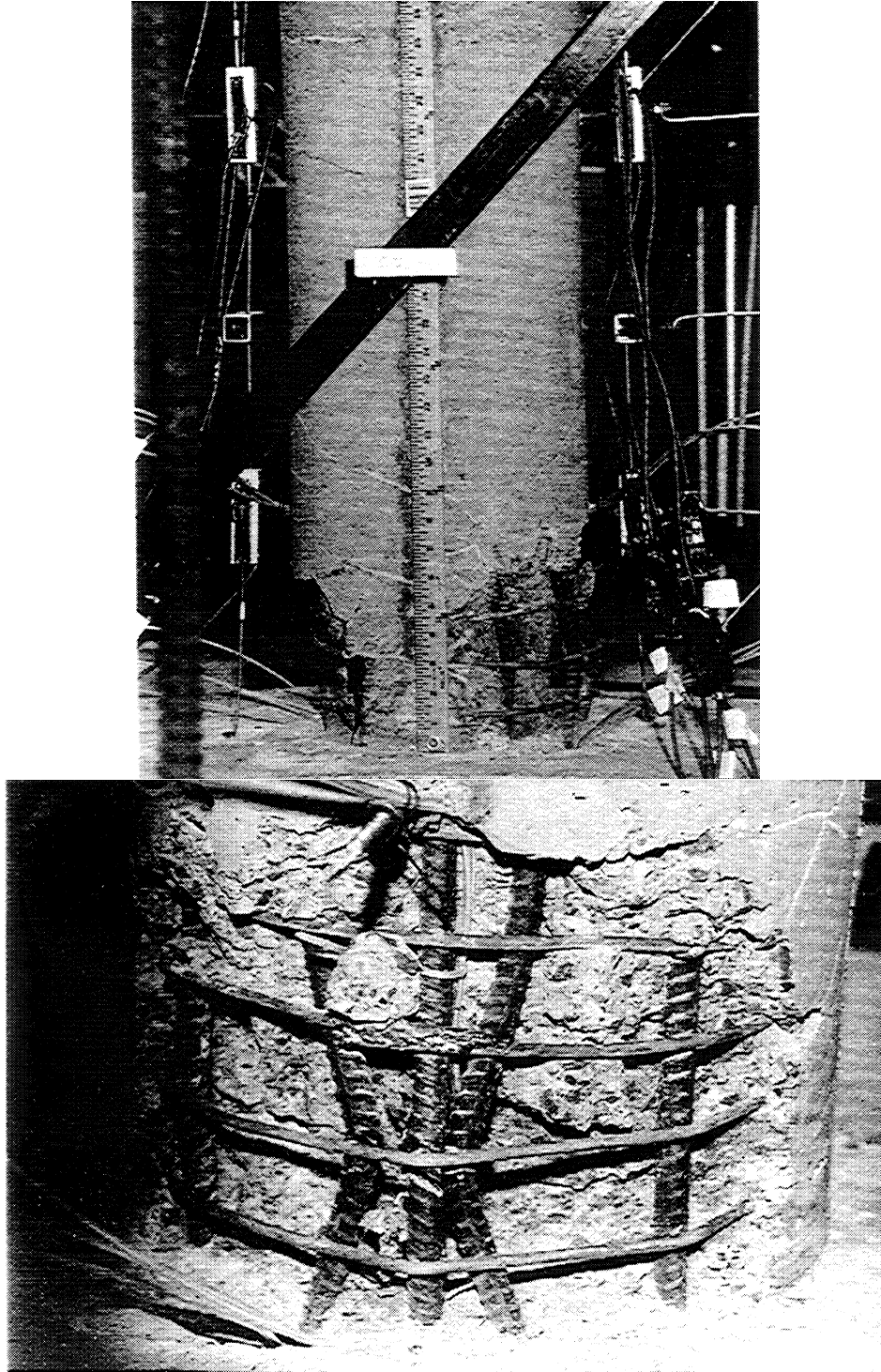
Figure 8-11 Experimental Results of Cheng (1997).

117

comparison is tabulated in table 8-3.

(iii) <u>Square Columns tested by Watson et al.(1986)</u> : Four 400 mm square columns reinforced with 12-HD16 (16 mm diameter) reinforcing bars having a nominal yield strength of f_y = 446 MPa were tested by Watson et al.(1986). Units 2,3 and 4, which suffered longitudinal bar buckling are, shown in figure 8-12. Each lateral reinforcement hoopset consisted of a perimeter hoop and an overlapping octagonal hoop. Relevant lateral reinforcement details are given in table 8-2. The longitudinal bars had a measured ultimate strength of f_{su} = 702 MPa.

Table 8-2 Details of the Lateral Reinforcement for Columns tested by Watson et al.(1986)

Unit	Diameter (mm)	Spacing (mm)	f_{yh} (MPa)
2	8	78	360
3	7	91	364
4	6	94	255

Table 8-3 Comparison of Experimental Observation and Analytical Predictions

Specimens	Visual Count	Analytical Prediction
1. Ingham et al.(1997)	11	11[a]
2. Specimen CO of Cheng et al.(1997)	3	3[a]
3. Unit 2 of Watson et al. (1986)	1	1[a]
4. Unit 3 of Watson et al. (1986)	3	3[a]
5. Unit 4 of Watson et al. (1986)	2	2[a]

a Yield strength was used for calculation
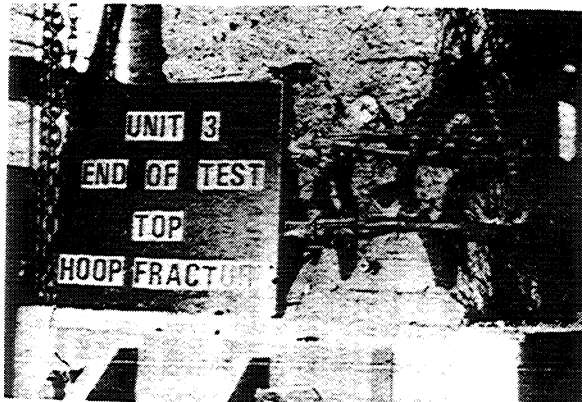
Figure 8-12 Experimental Results of Watson et al. (1986)

8.3.3 Comments on Analytical Comparison

As is evident from table 8-3, the predictions of the analytical expression is consistent with the observed experimental results. Therefore, it appears to be justified to use the same equations in an inverse form for design purposes. This is discussed in the following subsection.

8.4 DESIGN RECOMMENDATIONS

From the foregoing discussion it becomes clear that either premature local or global buckling of the longitudinal reinforcement in a concrete column can lead to poor performance. Thus it is important that transverse reinforcement be designed in such a way that buckling is inhibited in order to maintain satisfactory performance under cyclic loading. In this section an attempt will be made to use equation (8-41) in an inverse form for design. Necessary recommendations will be made for rectangular and circular sections to ensure proper restraint of the longitudinal reinforcement. This is discussed in the following.

8.4.1 Required Ratio of Lateral Reinforcement

Good detailing of reinforced concrete members should ensure that the longitudinal steel is properly confined and is able to sustain longitudinal stresses even under extreme situations. Thus a suitable arrangement of the lateral hoop reinforcement should be provided so that even in the event of buckling a certain level of load bearing capacity is always maintained.

From equation (8-41) it can also be seen that the maximum horizontal bar force is achieved (optimum restraining force) when $N_h = 1.0$. Thus equation (8-41) can be rewritten as

$$\frac{F_{yh}}{F_y} = \kappa \frac{f_{cr}}{f_y} \left[0.066 \left(\frac{s}{d_b}\right)\left(1 - 0.4 \left|\frac{f_{cr}}{f_{su}}\right|^2\right) - \frac{1.667\left[|f_{su}/f_{cr}| - |f_{cr}/f_{su}|^2\right]}{(s/d_b)} \right] \qquad (8\text{-}42)$$

and further simplified to

$$\frac{F_{yh}}{F_y} = \kappa \left(\frac{s}{d_b}\right) \frac{f_{cr}}{f_y} C \qquad (8\text{-}43)$$

where

$$C = 0.066 \left(1 - 0.4 \left|\frac{f_{cr}}{f_{su}}\right|^2\right) - \frac{1.667}{(s/d_b)^2} \left(\left|\frac{f_{su}}{f_{cr}}\right| - \left|\frac{f_{cr}}{f_{su}}\right|\right) \qquad (8\text{-}44)$$

By setting a design objective of $f_{cr} \geq 0.85 f_{su}$, and $s \leq 6 d_b$, it can be shown that $C = 0.032$. Thus a general design equation can be stated as

$$\frac{F_{yh}}{F_y} = \frac{\kappa}{31.25} \left(\frac{s}{d_b}\right) \frac{f_{cr}}{f_y} \qquad (8\text{-}45)$$

More specificity can be given to this equation for rectangular and circular sections as described below.

Rectangular Sections with Cross-ties and/or Rectilinear hoops

For rectangular sections, assume $\kappa = 1.0$, $s = 6 d_b$, $f_{cr} = 1.25 f_y$ and carrying out some rounding gives

$$\frac{A_{bh} f_{yh}}{A_b f_y} = \frac{F_{yh}}{F_y} \geq \frac{1}{4} \qquad (8\text{-}46)$$

which means that the force in the transverse reinforcement need to be at least one fourth the yield force in the longitudinal reinforcement.

Circular Sections with Spirals (or circular hoops)

Since the lateral reinforcement percentage in a circular section is usually expressed as it will be useful if buckling restraint requirements are also linked to this factor. Note that in the above equation $D'' =$ core concrete diameter and the other symbols are as explained previously.

121

$$\rho_s = \frac{4 A_{bh}}{s D''} = \frac{\pi d_{bh}^2}{s D''} \qquad (8\text{-}47)$$

Thus using $\kappa = N / 2\pi$ in equation (8-45)

$$\frac{F_{yh}}{F_y} = \frac{A_{bh} f_{yh}}{A_b f_y} = \frac{N}{2\pi \times 31.25} \left(\frac{s}{d_b} \right) \frac{f_{cr}}{f_y} \qquad (8\text{-}48)$$

Substituting for A_{bh} from equation (8-47) into equation (8-48) and on subsequent simplification

$$\frac{4 A_{bh}}{s D''} = \rho_s = \frac{1}{62.5} \left(\frac{N A_b}{\pi/4 \cdot D^2} \right) \frac{D}{D''} \frac{D}{d_b} \frac{f_{cr}}{f_{yh}} = \frac{N}{15.6\,\pi} \frac{\left(\pi/4 \cdot d_b^2 \right)}{D'' d_b} \frac{f_{cr}}{f_{yh}} \qquad (8\text{-}49)$$

Therefore,

$$\rho_s f_{yh} = \frac{\rho_t f_{cr}}{62.5} \frac{D}{D''} \frac{D}{d_b} = \frac{N}{62.5} \frac{d_b}{D''} f_{cr} \qquad (8\text{-}50)$$

For a design objective of $f_{cr} = 1.25 f_y$ and assuming $D'' = 0.8\,D$, equation (8-49) further simplifies to following two possibilities

$$\rho_s f_{yh} = 0.025 \frac{D}{s} \frac{s}{d_b} \rho_t f_y$$

$$\text{or,} \qquad \rho_s = \frac{f_y}{f_{yh}} \frac{d_b}{D''} \frac{N}{50} \qquad (8\text{-}51)$$

8.4.2 Comments on Design Equations

Before proceeding on to a more detailed discussion of the ramifications of the design equations, it is worthwhile to review the state of the art in anti-buckling reinforcement. Presently, most reinforced concrete and bridge design codes only have one requirement that relates to maintaining bar stability, that is

$$s \leq 6 d_b \tag{8-52}$$

where s = spiral pitch or hoopset spacing and d_b = diameter of the longitudinal reinforcement. From figure 8-7 it is evident that this is sufficient to maintain at least yield strength in a longitudinal bar. Note that this is a local buckling requirement.

It appears that only the New Zealand Concrete Code (NZS 3101) has provisions related to global buckling. That code requires

$$A_{bh} f_{yh} \geq \frac{1}{16} A_b f_y \tag{8-53}$$

This requirement appears to have been selected in an arbitrary fashion by the code writing committee.

The recently published CALTRANS design recommendations contained in ATC 32 make some recommendations for minimum transverse reinforcement to avoid global buckling. These requirements are based on guidelines given by Priestley et al. (1996) who studied the equilibrium of a longitudinal bar under the $P - \Delta$ effects of an assumed deflected shape and the elastic restraining forces in the hoop and claimed that adequate protection can be achieved against buckling if the volumetric ratio of lateral reinforcement is given by

$$\rho_s \geq 0.00013 \, N \tag{8-54}$$

where N = number of longitudinal bars in the column. The above equation was adopted by the ATC 32 (1996) who adopted a slightly more conservative version of the above equation given by

$$\rho_s \geq 0.0002 \, N \tag{8-55}$$

However, the underlying assumption in the above equation is that the tie forces are elastic which is clearly not valid in plastic hinge zones.

123

The inadequacy of the code expressions is also portrayed in figure 8-13a where an alternative form of equation (8-38) is plotted in the form

$$\frac{f_{cr}}{f_{su}} = \frac{0.3\,(N_h+1)(s/d_b)}{\left(|f_{su}/f_{cr}|^2-1\right)} \left[0.033\,(N_h+1)\left(\frac{s}{d_b}\right)\left(1-0.4\left|\frac{f_{cr}}{f_{su}}\right|^2\right) - \frac{N_h}{\kappa}\frac{f_{su}}{f_{cr}}\frac{F_{yh}}{F_{su}}\right] \qquad (8\text{-}56)$$

for various F_{yh}/F_y ratios and N_h. Note that the standard $s/d_b = 6$ has been assumed. The plot clearly shows that the requirement of NZS 3101 does not provide the necessary anti-buckling restraint for rectilinear hoops and global buckling should be expected over some 6 levels of hoopsets. It is interesting to note that with a 45% increase in hoop force at least yield strength of the longitudinal bars can be maintained. However, in order to minimize global buckling at least double the amount of steel given by NZS 3101 code is required.

The design equation for circular sections can be plotted in the usual way as shown in figure 8-13b. Note that equation (8-56) has been plotted for a typical California type bridge column of gross diameter 1200 mm and consisting of 20-32 mm grade 60 reinforcement. Also note that the hoop to longitudinal bar force ratio has been substituted by

$$\frac{1}{\kappa}\frac{F_{yh}}{F_y} = \frac{2f_{yh}}{f_y}\frac{\rho_s}{\rho_t}\frac{s}{D}\frac{D''}{D} \qquad (8\text{-}57)$$

which is obtained from equation (8-46). It can be seen that if lateral reinforcement is provided based on the recommendations of ATC 32, adequate restraint is not provided. From figure 8-13b it is evident that at least two and a half times the ATC-32 quantity is required to maintain adequate performance — that is to keep the bar stress above yield. However, if global buckling is to be minimized, results show that $\rho_s > 0.0006\,N$.

8.5 SEISMIC PERFORMANCE-BASED ANALYSIS

Contemporary seismic design is a two-phase process. In the initial phase, member sizes are adopted design loads determined, flexural reinforcement chosen, and detailing provided in accordance with the tenets of the capacity design philosophy. In the second phase, a seismic

124
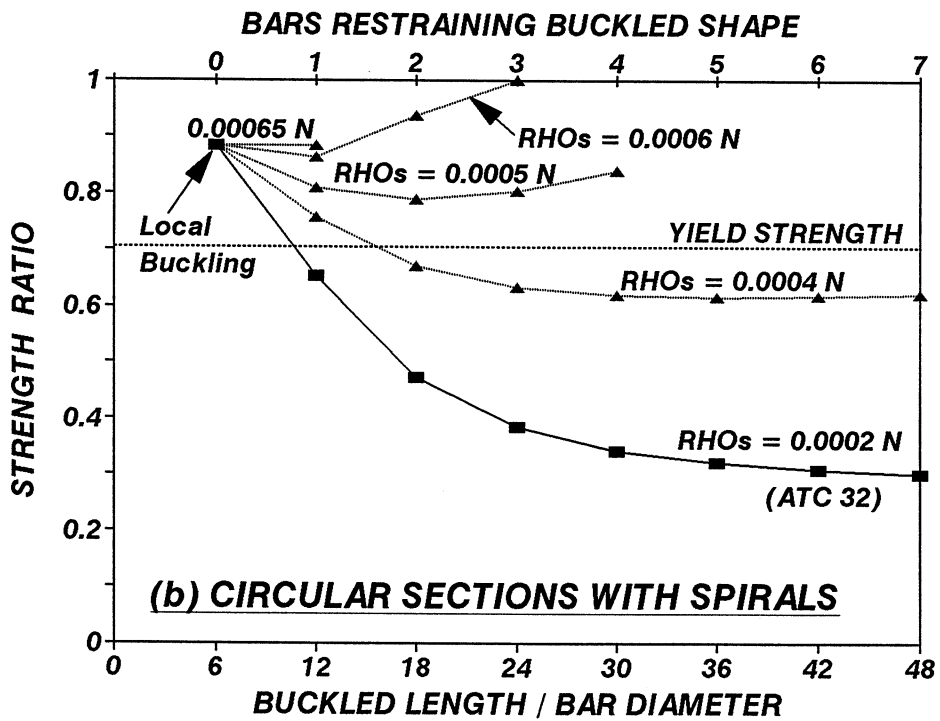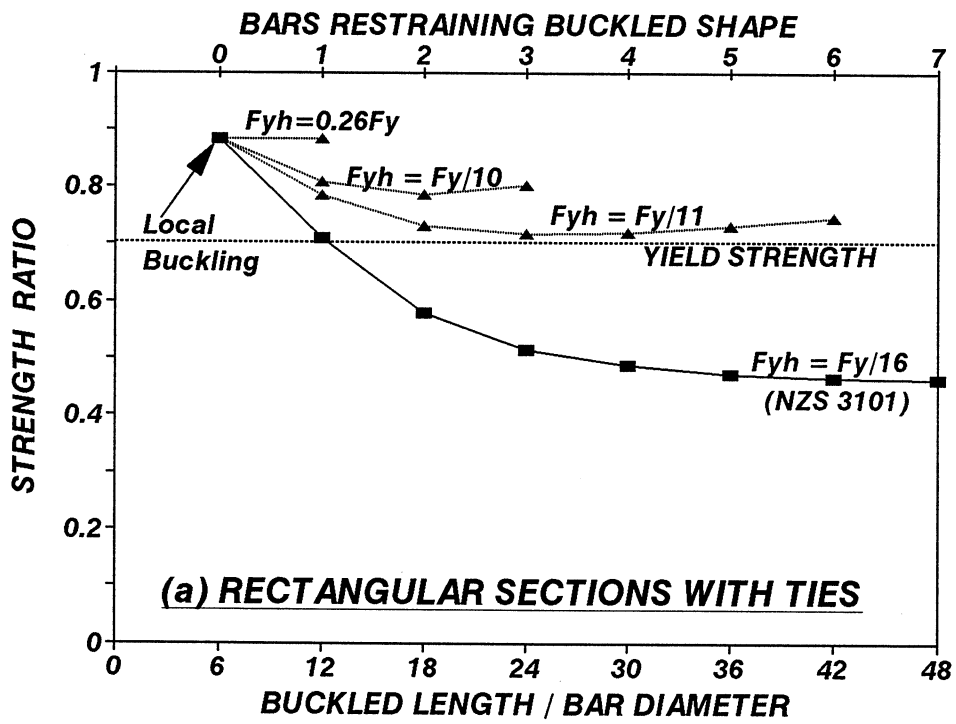
Figure 8-13 Effect of Transverse Reinforcement on Global Buckling Capacity.

performance-based analysis of the design is conducted with the purpose of identifying expected damage patterns for a scenario event. This performance based seismic evaluation requires that a pushover analysis be conducted to identify lateral displacement limit states. In order to conduct such an evaluation, it is necessary to perform a moment-curvature analysis of the critical sections in the structure. Ultimate curvatures are governed by a limiting strain profile which depends on the magnitude of axial load on the member, as well as the ultimate compression strain in the longitudinal reinforcement.

From the foregoing design formulation it is possible to assess the critical (ultimate compression) buckling capacity of the longitudinal reinforcement (f_{cr}/f_{su} from equations (8-23) and (8-56)). However, no information is available regarding strains, nor is the compressive stress-strain relationship known.

Chang and Mander (1989a) have proposed the following stress-strain relationship for reinforcing steel.

$$f_s = \frac{E_s \varepsilon_s}{\left\{1 + \left|\frac{E_s \varepsilon_s}{f_y}\right|^{20}\right\}^{0.05}} + \left(\frac{1 + sign(\varepsilon_s - \varepsilon_{sh})}{2}\right)(f_{su} - f_y)\left[1 - \left|\frac{\varepsilon_{su} - \varepsilon_s}{\varepsilon_{su} - \varepsilon_{sh}}\right|^p\right] \qquad (8\text{-}58)$$

in which ε_{su} = strain hardening strain, f_{su} = ultimate stress, E_{sh} = strain hardening modulus, ε_{su} = ultimate strain of reinforcement and the power p is given by

$$p = E_{sh}\frac{\varepsilon_{su} - \varepsilon_{sh}}{f_{su} - f_y} \qquad (8\text{-}59)$$

The first part of this equation gives the elasto-perfectly plastic (pre-strain-hardened) performance of the material, whereas the second part provides the enhanced strength due to strain-hardening. Mander et al. (1988 and 1994) have noted from experiments that the maximum compressive stress-strain point (f_{su}^-, ε_{su}^-) is generally located on or very near the tensile stress-strain curve. Therefore it is an inverse form of this latter portion that can be used to assess the ultimate compression strain as follows:

$$\varepsilon_{su}^- = \varepsilon_{su}^+ + \left(\varepsilon_{su}^+ - \varepsilon_{sh}^+\right) \left[\frac{1 - \left|f_{cr}^-/f_{su}^+\right|}{1 - f_y^+/f_{su}^+}\right]^{1/p} \tag{8-60}$$

where the + and - superscripts denote tension and compression, respectively. Note that $f_{su}^- = -\left|f_{cr}\right|$.

Experiments by Mander et al. (1984, 1994) and others have also shown that the onset of strain-hardening in compression is about midway along the yield plateau of a companion tensile stress-strain curve. Therefore, the following relationship can be used to define the compressive strain at the onset of strain-hardening

$$\varepsilon_{sh}^- = \frac{f_y^-}{E_s} - \frac{1}{2}\left(\varepsilon_{sh}^+ - \frac{f_y^+}{E_s}\right) \tag{8-61}$$

Once the ultimate compression strain is identified, it is possible, based on section equilibrium to determine the ultimate curvature and hence plastic hinge rotation of the member. Consider a critical strain diagram at ultimate. The plastic curvature can be obtained as follows:

$$\phi_p = \frac{\varepsilon_y^- - \varepsilon_{su}^-}{c'' - d''} \tag{8-62}$$

where ε_y^- = compression yield strain of the longitudinal reinforcement (f_y^-/E_s), c = depth of the confined concrete compression stress block, and d'' = distance from the center of the perimeter confining hoop steel to the center of the longitudinal compression reinforcement.

Normalizing the above equation gives:

$$\phi_p D = \frac{\left(\varepsilon_y^- - \varepsilon_{su}^-\right)}{\left(c''/D'' - d''/D''\right)} \frac{D}{D''} \tag{8-63}$$

where for <u>rectangular</u> sections, the confined stress block depth ratio is given by equation (4-17): and for <u>circular</u> sections by equation (4-27) as:

$$\frac{c''}{D''} = \frac{\left(\dfrac{P_e}{f_c' A_g}\right) + \left(\dfrac{\gamma_r \rho_t f_y / f_c'}{1 - 2d''/D''}\right)}{\left(0.625(1 + \rho_s f_{yh}/f_c')(1 + 2.1\,\rho_s f_{yh}/f_c')\dfrac{A_{cc}}{A_g} + \dfrac{2\gamma_r \rho_t f_y / f_c'}{1 - 2d''/D''}\right)} \tag{8-64}$$

$$\frac{c''}{D''} = \left[\frac{\dfrac{P_e}{f_c' A_g} + 0.5\,\rho_t \dfrac{f_y}{f_c'}\left(\dfrac{1 - 2c''/D''}{1 - 2d''/D''}\right)}{0.9(1 + \rho_s f_{yh}/f_c')(1 + 2.7\,\rho_s f_{yh}/f_c')\dfrac{A_{cc}}{A_g}}\right]^{0.725} \tag{8-65}$$

with the symbols as previously defined.

8.6 SUMMARY AND CONCLUSIONS

Buckling of longitudinal reinforcement in a reinforced concrete column is a common cause of failure in simulated seismic tests. Traditionally the bar stability/buckling problem has been countered by using the well known $s/d_b \le 6$ criteria based on simple compression tests on longitudinal reinforcement. However there is a considerable departure in behavior of a reinforcement in a compression test rig and in a plastic hinge zone. The most important is end restraint which is substantially reduced in the real case due to yielding of hoops. This increases the effective slenderness ratio of the longitudinal bar which, under the circumstances, releases the energy through buckling.

In this research project a new approach based on the plastic analysis of a global buckling mechanism is advanced to tackle the problem of longitudinal bar buckling. Simple expressions are derived for both local and global buckling that correlate well with actual test results. Since it is presumed that transverse steel in an actual plastic hinge zone will always yield, a design criterion allowing for limited global buckling is advanced. This lateral reinforcement if used in new design will result in adequate anti-buckling performance.

128

Finally, the local and global bar stability (anti-buckling) requirements are reiterated below

$$s \leq 6 d_b \qquad (8\text{-}66)$$

For rectangular hoops and ties

where global buckling is not permitted

$$A_{bh} = \frac{A_b}{4} \frac{f_y}{f_{yh}} \qquad (8\text{-}67)$$

where limited global buckling is permitted

$$A_{bh} = \frac{A_b}{10} \frac{f_y}{f_{yh}} \qquad (8\text{-}68)$$

For circular hoops and spirals

where global buckling is not permitted

$$\rho_s > 0.025 \frac{D}{s} \frac{s}{d_b} \frac{f_y}{f_{yh}} \rho_t \qquad (8\text{-}69)$$

where limited global buckling is permitted

$$\rho_s > 0.02 \frac{D}{s} \frac{s}{d_b} \frac{f_y}{f_{yh}} \rho_t \qquad (8\text{-}70)$$

It may also be mentioned here that the less rigorous constraint on the transverse antibuckling reinforcement may be applicable to bridges in low to moderate seismic zones (SPC B and C). For bridges in high seismic zones (SPC D) and critical bridges, the more stringent requirement shall be applicable.

SECTION 9
DESIGN OF TRANSVERSE REINFORCEMENT FOR SHEAR

9.1 HISTORICAL BACKGROUND

Transverse reinforcement is required in seismic resistant reinforced concrete columns for three reasons: (i) to confine the core concrete in potential plastic hinge regions so that large plastic hinge rotations can be attained in the event of an earthquake; (ii) to provide bar stability for the longitudinal reinforcement (this is especially important when the cover concrete has spalled and the longitudinal reinforcement is under a state of high compression strain) and (iii) to provide shear resistance in both plastic hinge regions and regions outside the plastic hinge that behave in an inelastic fashion.

Although the role of transverse reinforcement seems to be well understood, it is the codified design methodologies that are not only unclear, but confusing. This confusion arises from the proliferation of different shear design methodologies that have evolved over this century. The earliest shear design concepts for reinforced concrete were developed some 100 years ago based on simple truss analogies. Shear forces were assumed to be resisted by 45 degree diagonal compressive concrete struts connected by transverse tensile steel ties. From this truss analogy, the well-known relationship may be derived

$$V_s = A_v \frac{d}{s} f_{yh} \tag{9-1}$$

where A_v = area of transverse reinforcement, d = effective depth of the member, f_{yh} = yield stress of the transverse reinforcement, and s = center-to-center spacing of the transverse reinforcement (hoopsets or spirals).

This truss-based shear design methodology gives a lower bound solution to the shear capacity of a member as it does not account for the beneficial effect of the mechanisms of

concrete shear resistance such as diagonal tension, aggregate interlock or arching action. To this end, much research was conducted in the United States during the early part of this century on the shear resistance of beams without transverse reinforcement. Based on numerous tests, it was concluded that a semi-empirical equation taking the following form could conservatively assess the diagonal tension-based effective shear stress capacity of reinforced concrete beam members

$$v_c = \frac{V_c}{b_w d} = 1.9\sqrt{f_c'} + 2500 \, \rho_w \, \frac{V_u d}{M_u} \leq 3.5\sqrt{f_c'} \qquad (9\text{-}2)$$

where all quantities are in pound and inch units (for SI units the coefficients 1.9 and 3.5 should be divided by 12 and the constant 2500 be taken as 17.2) and $V_u d \leq M_u$ at any section. In this equation, the following terms are defined: b_w = effective web width of beam, d = effective beam depth; v_c = shear stress carried by concrete at diagonal tension failure; V_c = the corresponding sectional shear force; ρ_w = longitudinal tensile steel ratio M_u and V_u are the ultimate moment and shear at the section under consideration and f_c' = compression strength of the concrete.

In practice, this equation is difficult to use. Therefore as an alternative, satisfactory conservative designs are possible if one assumes

$$v_c = 0.167\sqrt{f_c' \; MPa} = 2\sqrt{f_c' \; psi} \qquad (9\text{-}3)$$

It should be emphasized, however, that the above equations for the shear resistance carried by the concrete mechanism can only occur if the diagonal cracks are small. Under high moment and shear, such as in a plastic hinge zone of a beam or a column, or for narrow-webbed prestressed concrete beams, the shear resistance carried by any concrete mechanism tends to vanish, especially when coupled with reversed cyclic loading and/or large principal tension strains (ε_1). To more accurately account for such behavior, the Modified Compression Field Theory (MCFT) has been developed by Collins and his coworkers (see Vecchio and Collins (1986), and Collins and Mitchell (1991)). This is a continuum truss approach that accounts for both steel and concrete contributions, the latter being related to the extent of cracking via the principal tension strain.

132

Designers also generally have difficulty designing deep beam members for shear. This is because the plane sections hypothesis for flexure does not hold, therefore the concept of an equivalent shear stress across the section is problematic. Experiments on deep beams, coupling beams and the like have demonstrated this difficulty. To this end, strut and tie models have been proposed. Strut and tie (SAT) models have their roots in the early truss model. They are appealing because truss members can be intuitively apportioned as the designer sees fit. However, neither the extent to which such models can be used nor the inherent conservatism in them, is well understood.

A considerable amount of research on the seismic shear resistance of reinforced concrete columns has recently been conducted. This work, heavily sponsored by CALTRANS, commenced in the 1990's following the 1989 Loma Prieta earthquake, and continued through the mid 1990's. The basic aim of that work was to develop improved shear design provisions for new bridge columns, as well as more reliable assessments of the shear strength of existing non-ductile bridge piers. This work was principally conducted by Priestley, Moehle and their coworkers at the University of California. Both investigators used different approaches for assigning the shear resisting mechanisms leading to different design formulations. This research has culminated in new design recommendations for CALTRANS, recently published in ATC-32. Unfortunately, the approach adopted is steeped in the semi-empirical formulations of the past; it appears that no attempt has been made to unify column shear design provisions with other contemporary approaches (MCFT or SAT) in the LRFD-AASHTO code.

Matters pertaining to shear design continue to remain confusing for structural designers. This is because in recent years, there has been a proliferation of methods amongst the different design codes. Moreover, single codes such as the new LRFD-AASHTO code, permit use of all the shear design methods: MCFT for prestressed concrete beams, SAT models for deep members, as well as the traditional semi-empirical design equations based on equation (9-1) and (9-2), the latter equation being modified for column design.

133

More recently Kim and Mander (1997), based on their FHWA sponsored research, have sought to unify key elements of these apparently divergent shear theories. Although their work focused on a fundamental method of analysis for shear in reinforced concrete, principally for analysis of existing shear-critical members, it can easily be adapted for the design of new reinforced concrete bridge columns and their connections (beam-column joints).

This section first surveys the state-of-the-practice (design codes) and state-of-the-art (recent research). Then, based on the recent work of Kim and Mander (1997), goes on to present a shear design theory for reinforced concrete bridge columns.

9.2 STATE-OF-PRACTICE FOR SHEAR DESIGN OF CONCRETE STRUCTURES

This section provides a survey of current design methodologies used by various design codes in the United States.

9.2.1 AASHTO-ACI Design Approach

AASHTO standard specification for highway bridges (1996), lays down the design criteria for transverse reinforcement to be based on

$$V_u \leq \phi V_n \tag{9-4}$$

where V_u = factored shear force at the section considered, ϕ = undercapacity factor for shear and normally equals 0.85 and V_n = nominal shear strength to be computed by

$$V_n = V_c + V_s \tag{9-5}$$

where V_c = nominal shear strength provided by the concrete which (for members subjected to an axial compressive load N_u), is computed by

$$V_c = 2\left(1 + \frac{N_u}{2000 A_g}\right)\sqrt{f_c'(psi)}\; b_w d = \left(1 + \frac{N_u}{14 A_g}\right)\left(\frac{\sqrt{f_c'\,(MPa)}}{6}\right) b_w d \qquad (9\text{-}6)$$

or

$$V_c = 2\sqrt{f_c'(psi)}\; b_w d = 0.167\sqrt{f_c'\,(MPa)}\; b_w d \qquad (9\text{-}7)$$

where f_c' = unconfined compression strength of concrete, b_w = width of the web and d = distance from the extreme compression fiber to the centroid of the longitudinal tension reinforcement. For a circular section b_w = diameter and d = the distance from the extreme compression fiber to the centroid of the farthest tension steel. Note also that in the above expression, the quantity N_u / A_g is to be expressed in psi (or MPa) units with A_g = gross area of the concrete section.

For members subjected to axial tension, shear carried by concrete is given by

$$V_c = 2\left(1 + \frac{N_u}{500 A_g}\right)\sqrt{f_c'(psi)}\; b_w d = \left(1 + \frac{0.3 N_u}{A_g}\right)\frac{\sqrt{f_c'\,(MPa)}}{6} b_w d \qquad (9\text{-}8)$$

where N_u is negative for tension.

The nominal shear resistance provided by the lateral reinforcement is given by

$$V_s = \frac{A_v f_{yh} d}{s} \le 8\sqrt{f_c'(psi)}\; b_w d \le 0.664\sqrt{f_c'(MPa)}\; b_w d \qquad (9\text{-}9)$$

where A_v = area of shear reinforcement within a distance s and f_{yh} = yield strength of the horizontal reinforcement.

It is generally accepted that design equations incorporated in any code will be conservative in nature. This means that the strength predictions from such equations in most cases will be less than the true material strength. However, since the behavior of concrete in shear is a highly non-linear phenomena, code expressions generally turn out to be overly conservative. It was pointed out by Ang et al. (1989) (also plotted in figure 9-1), that the AASHTO-ACI expressions are no exceptions. As can be seen from the figure, the margin of

conservatism can range anywhere from 2 to as high as 3.5. This large "margin of safety" now appears entirely unwarranted. A lack of rationale behind the expressions adopted by AASHTO and ACI code writers is apparent. Perhaps the major impediment against changing these provisions is because designers are comfortable with them and the approach is easy to use — why make it more difficult and perhaps less safe?

9.2.2 Modified Compression Field Theory in AASHTO

For the design of prestressed and non-prestressed beams, AASHTO LRFD (1994), permits the use of modified compression field theory. According to this theory the nominal shear resistance is given by

$$V_n = V_c + V_s + V_{ps} \tag{9-10}$$

where V_{ps} = component of the prestressing force in the direction of the applied shear and the remaining symbols are as explained previously. The shear carried by the concrete is given by

$$V_c = \frac{\beta}{12} \sqrt{f_c'(MPa)} \; b_v d_v \tag{9-11}$$

where b_v = effective web width taken as the minimum web width within the depth d_v modified for the presence of ducts wherever applicable with d_v being the effective shear depth taken as the distance measured perpendicular to the neutral axis between the resultants of the tensile and compressive forces due to flexure and β = factor indicating the ability of the diagonally cracked concrete to transmit tension and can be obtained from various figures and tables in the AASHTO-LRFD code (1994) [see for example figure 5.8.3.4.2-1 (or table 5.8.3.4.2-1) or figure 5.8.3.4.2-2 (or table 5.8.3.4.2-2) of the AASHTO LRFD (1994) for sections with or without web reinforcement respectively]. In these figures (or tables) β values are given as a function of the shear stress on the concrete given by

$$v = \frac{V_u - \phi V_{ps}}{\phi b_v d_v} \qquad (9\text{-}12)$$

and strain in the reinforcement in the flexural tension side of the member given by

$$\varepsilon_x = \frac{M_u/d_v + 0.5 N_u + 0.5 V_u \cot\theta - A_{ps} f_{po}}{E_s A_s + E_p A_{ps}} \qquad (9\text{-}13)$$

where M_u = factored moment, N_u = factored axial force taken positive if compressive, V_u = factored shear force, A_{ps} = area of prestressing steel on the flexural tension side of the member, f_{po} = stress in prestressing steel when the stress in the surrounding concrete is zero, E_s, A_s = respectively the modulus of elasticity and area of non-prestressing reinforcement on the flexural tension side of the member and E_p = modulus of elasticity of the prestressing reinforcement. Note that θ is the crack angle which can be obtained from various figures and tables in the AASHTO-LRFD code (1994) [see for example figure 5.8.3.4.2-1 (or table 5.8.3.4.2-1) or figure 5.8.3.4.2-2 (or table 5.8.3.4.2-2) of the AASHTO LRFD (1994) for sections with or without web reinforcement respectively]. Such a table for sections with web reinforcement is illustrated in table 9-1.

The required stirrup spacing is also given by

$$s = \frac{A_v f_{yh} d_v (\cot\theta + \cot\alpha)\sin\alpha}{V_s} \qquad (9\text{-}14)$$

where A_v = area of shear reinforcement within a distance s, f_{yh} = yield strength and α = angle of inclination of the transverse reinforcement to the longitudinal axis (in degrees) and remaining symbols are as explained previously.

It is clear from the brief discussion that the MCFT is indeed a mechanics-based approach and eliminates a lot of ambiguities inherent in most other empirical design forms. However, the greatest disadvantage of the MCFT is the lack of simplicity. It has been pointed out by design engineers that MCFT is extremely convoluted in approach and lacks the appeal of the simplistic design equations of AASHTO Standard Specifications. Although MCFT started out as a

Table 9-1 Values of θ and β for members with web reinforcement.

Shear Stress v/f_c'		Longitudinal Strains $\varepsilon_x \times 1000$
		-0.2	-0.15	-0.1	0	0.125	0.25	0.5	0.75	1	1.5	2
≤0.05	θ	27.0	27.0	27.0	27.0	27.0	28.5	29.0	33.0	36.0	41.0	43.0
	β	6.78	6.17	5.63	4.88	3.99	3.49	2.51	2.47	2.23	1.95	1.72
0.075	θ	27.0	27.0	27.0	27.0	27.0	27.5	30.0	33.5	36.0	40.0	42.0
	β	6.78	6.17	5.63	4.88	3.65	3.01	2.47	2.33	2.16	1.90	1.65
0.100	θ	23.5	23.5	23.5	23.5	24.0	26.5	30.5	34.0	36.0	38.0	39.0
	β	6.50	5.87	3.26	3.26	2.61	2.54	2.41	2.28	2.09	1.72	1.45
0.125	θ	20.0	21.0	22.0	23.5	26.0	28.0	31.5	34.0	36.0	37.0	38.0
	β	2.71	2.71	2.71	2.60	2.57	2.50	2.37	2.18	2.01	1.60	1.35
0.150	θ	22.0	22.5	23.5	25.0	27.0	29.0	32.0	34.0	36.0	36.5	37.0
	β	2.66	2.61	2.61	2.55	2.50	2.45	2.28	2.06	1.93	1.50	1.24
0.175	θ	23.5	24.0	25.0	26.5	28.0	30.0	32.5	34.0	35.0	35.5	36.0
	β	2.59	2.58	2.54	2.50	2.41	2.39	2.20	1.95	1.74	1.35	1.11
0.200	θ	25.0	25.5	26.5	27.5	29.0	31.0	33.0	34.0	34.5	35.0	36.0
	β	2.55	2.49	2.48	2.45	2.37	2.33	2.10	1.82	1.58	1.21	1.00
0.225	θ	26.5	27.0	27.5	29.0	30.5	32.0	33.0	34.0	34.5	36.5	39.0
	β	2.45	2.38	2.43	2.37	2.33	2.27	1.92	1.67	1.43	1.18	1.14
0.250	θ	28.0	28.5	29.0	30.0	31.0	32.0	33.0	34.0	35.5	38.5	41.5
	β	2.36	2.36	2.32	2.30	2.28	2.01	1.64	1.52	1.40	1.30	1.25

research tool aimed specifically at evaluation rather than be used for design in an inverse sense, it was recently shown by deV Batchelor (1996), that the MCFT as adopted by the AASHTO is definitely less convenient in predicting the shear strength when compared with the traditional AASHTO-ACI approach. Subsequent discussions to deV Batchelor's paper by Collins (1997) and Kulicki et al. (1997) show that for a given member under a given loading, the MCFT is very vulnerable to misinterpretation. This work poses a serious question regarding the rating of existing structures and failure analysis using MCFT. In the same publication conflicting results obtained by Collins and Kulicki et al. (1997)—persons heavily involved in the development of the shear provisions of the LRFD code, underlines the fact that MCFT needs to be simplified if confusion is to be avoided in future.

9.2.3 Strut and Tie Design Approach in AASHTO

The AASHTO LRFD (1994) code recommends the use of strut and tie (SAT) modeling for the design of deep beams and disturbed regions of reinforced concrete members. This is because in such situations, the conventional methods of strength of materials approach based on Bernoulli's hypothesis are not applicable due to non-linear strain distribution. Under such circumstances the structure or components thereof are to be modeled as an assembly of steel tension ties and concrete compression struts interconnected at nodes to form a truss (refer figure 9-2) capable of carrying all the applied loads to the supports. The AASHTO LRFD (1994) code gives the factored resistance P_r of struts and ties as that of an axially loaded member as

$$P_r = \phi P_n \qquad (9\text{-}15)$$

where P_n = nominal resistance of strut or tie (N) given by

$$P_n = f_{cu} A_{cs} \qquad (9\text{-}16)$$

where f_{cu} = limiting compressive stress in the strut ($< 0.85 f_c'$) and A_{cs} = effective cross sectional area of strut with the under capacity factor ϕ being 0.9 for compression in strut and tie models. If the compression strut contains reinforcement which is parallel to the strut and has been detailed to develop its yield stress (f_y) in compression, the nominal resistance of the strut can

139
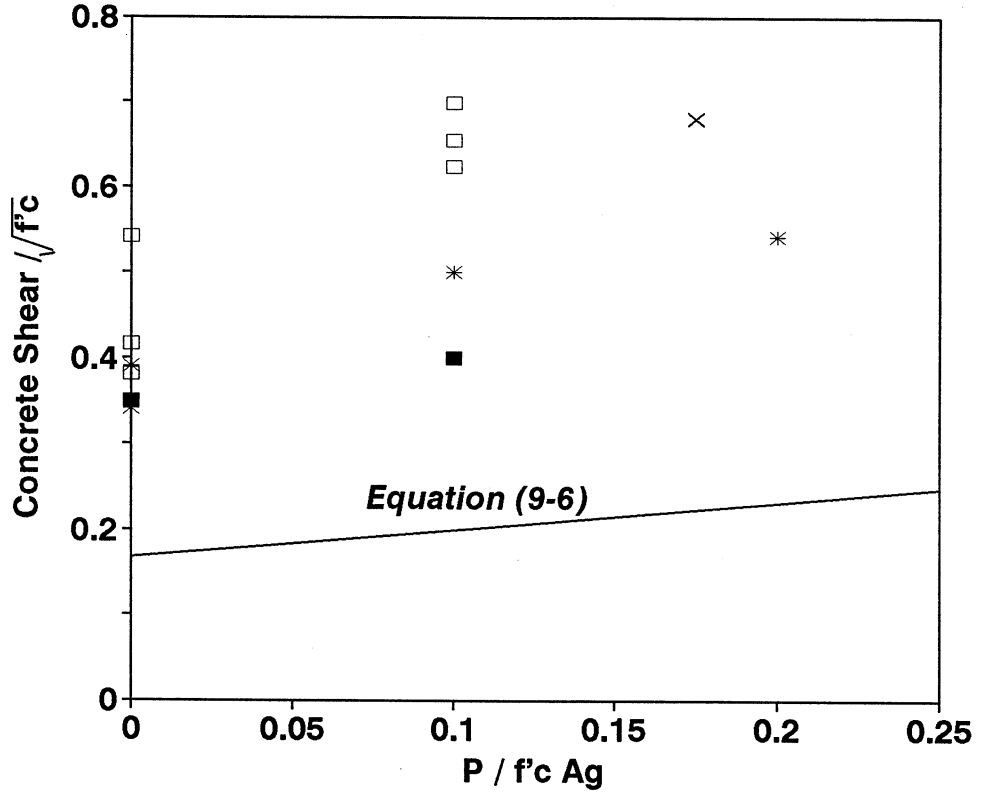
Figure 9-1   Comparison of AASHTO-ACI Expression with Specimens Tested by Ang et al. (1989).
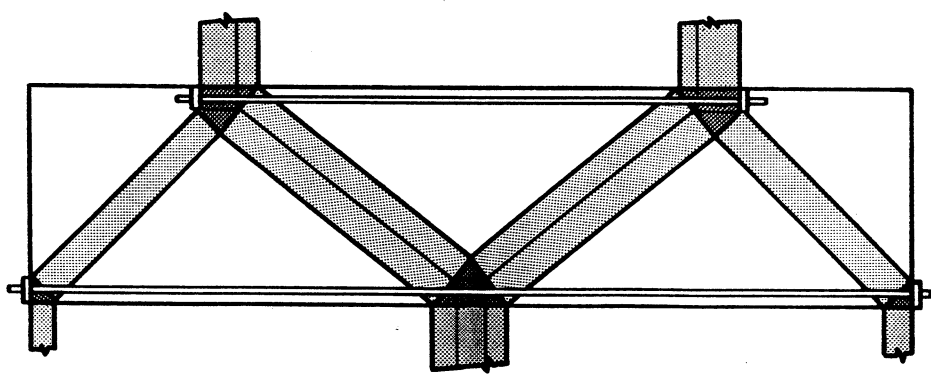
Figure 9-2 Strut and Tie Model.

140

be added to give

$$P_n = f_{cu} A_{cs} + f_y A_{ss} \tag{9-17}$$

where A_{ss} = area of reinforcement in the strut.

The nominal resistance of the tension tie which needs to be anchored to the nodal zones by specified embedment lengths, hooks or mechanical devices is also laid down by the AASHTO LRFD (1994) code as

$$P_n = f_y A_{st} + A_{ps} \left[f_{pe} + f_y \right] \tag{9-18}$$

where A_{st} = total area of mild steel reinforcement in the tie, A_{ps} = area of prestressing steel, f_y = area of mild steel longitudinal reinforcement and f_{ps} = stress in prestressing steel due to prestress after losses.

It is apparent from the above discussion that in the strut and tie model the concrete struts are proportioned to carry the principal compression only. However, the mere notion of principal compression signifies that there should be a principal tension (refer Kim and Mander (1998)) normal to the strut which resists crack opening. Although neglecting the diagonal tension contribution is conservative from a design standpoint, there has not been enough studies to quantify the degree of conservation. From an evaluation point of view, this will definitely lead to error which is hard to circumvent.

9.2.4 Shear Design in ATC-32

The shear provisions in the recently published recommendations for the design of new bridge structures for CALTRANS were developed by the Priestley/Moehle team. Footnotes in that document state that the proposed method was not included in the final version of ATC 32, ostensibly due to lack of rigorous peer review. Therefore the method proposed is essentially the same as the aforementioned AASHTO-ACI approach, but slightly modified to reflect the deterioration of concrete strength and a shape modifier for the shear carried by steel in a circular

141

column (see the factor $\pi/2$ below).

The nominal shear resistance as per ATC-32 is given by the sum of concrete and steel components as

$$V_n = V_c + V_s \qquad (9\text{-}19)$$

where the nominal shear resistance of the concrete V_c in end regions of ductile concrete members subjected to flexure and axial compression is given by

$$V_c = 2\left(k + \frac{P_e}{2000 A_g}\right)\sqrt{f_c'\,(psi)}\, A_e = \left(k + \frac{P_e}{14 A_g}\right)\frac{\sqrt{f_c'\,(MPa)}}{6}\, A_c \qquad (9\text{-}20)$$

where the factor k is 0.5 for end regions and 1 for regions other than end regions, $P_e =$ compressive axial load, $A_g =$ gross area of concrete section, $f_c' =$ unconfined compression strength of concrete and $A_e =$ effective cross sectional area, taken equal to $0.8 A_g$. The shear resistance of the horizontal steel is given by

$$V_s = \frac{\pi}{2}\frac{A_{bh}\,f_{yh}\,D''}{s} \qquad \textit{(for circular sections)} \qquad (9\text{-}21)$$

and by

$$V_s = \frac{A_v\,f_{yh}\,d}{s} \qquad \textit{(for rectangular sections)} \qquad (9\text{-}22)$$

where $A_{bh} =$ cross sectional area of the hoop or the spiral steel, $A_v =$ area of rectangular hoop steel over a spacing s in the direction of applied shear and $d =$ effective depth measured parallel to applied shear taken equal to 0.8 times the sectional dimension parallel to the direction of applied shear. Note that in the above equation D'' denotes the distance between the centerline of the peripheral hoop or spiral.

The equation proposed in ATC 32 is basically of the same form as proposed in the AASHTO Standard Specifications whose shortcomings were discussed already. Moreover the first term inside the parenthesis can be 0.5 in the end regions this may lead to <u>unconservative</u>

seismic designs as it is well known that V_c may vanish in potential plastic hinge zones under large inelastic reversed cyclic loadings

9.3 STATE-OF-THE ART SHEAR THEORIES

This section reviews the state-of-the-art in shear theories. Although these have not been adopted by any codes, certainly they are an advancement over most of the currently practiced methods.

9.3.1 Shear Analysis Methodology suggested by Aschheim and Moehle (1992)

Aschheim and Moehle (1992) and their associates at U.C. at Berkeley suggested a shear analysis methodology similar to the one suggested by the present AASHTO-ACI provisions. According to them the nominal shear resistance is given by the resistance offered by the concrete and steel respectively as

$$V_n = V_c + V_s \qquad\qquad (9\text{-}23)$$

where $V_c =$ shear carried by the concrete and given by

$$V_c = 3.5\left(k + \frac{P}{2000 A_g}\right)\sqrt{f_c'}\,(psi)\,A_e = 0.3\left(k + \frac{P}{14 A_g}\right)\sqrt{f_c'}\,(MPa)\,A_c \qquad (9\text{-}24)$$

where k degrades with increasing member displacement ductility as shown in figure 9-3. Note that in the above equation $P =$ compressive axial load, $A_g =$ gross cross sectional area of column, $f_c' =$ unconfined compression strength of concrete and $A_e =$ effective cross sectional area, taken equal to $0.8 A_g$. The shear carried by the steel is given by
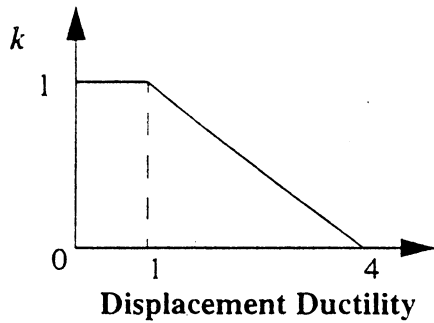
(a) Model
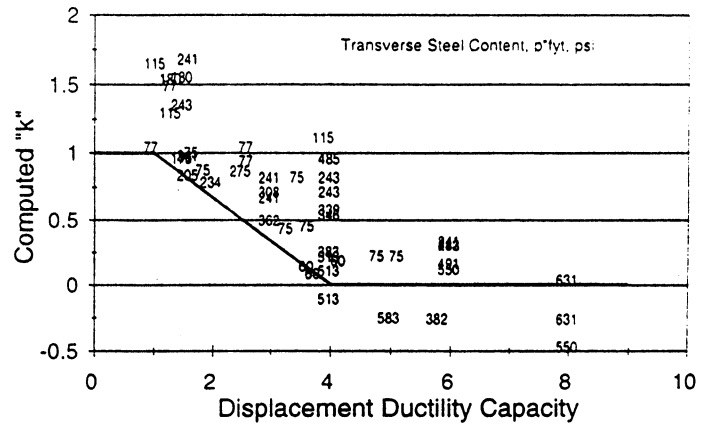
(b) Test Data for θ= 30 degrees

Figure 9-3 Relation between Ductility and Concrete Shear Resisting Mechanism as proposed by Ascheim and Moehle (1992).

$$V_s = \frac{\pi}{2} \frac{A_{bh} f_{yh} d}{s} \cot \theta \qquad (\textit{for circular sections})$$

$$V_s = \frac{A_v f_{yh} d}{s} \cot \theta \qquad (\textit{for rectangular sections})$$

(9-25)

where A_v = <u>total</u> area of transverse reinforcement in the direction of applied shear, A_{bh} = area one leg of the transverse hoop, d = effective depth of the member to be taken as 0.8 times the gross sectional dimension parallel to the direction of applied shear, f_{yh} = yield stress of the transverse reinforcement, and s = center-to-center spacing of the transverse reinforcement (hoopsets or spirals). Based on experimental results they suggested that the crack angle be taken between 30° and 45°.

The expression for V_c adopted by Aschheim and Moehle (1992) is very similar to the AASHTO expression although it is slightly less conservative than the former. However the plot of k versus the displacement ductility factor (figure 9-3) shows that the expression adopted is really a lower bound to all experimental results. Although these equations may be appropriately conservative for design purposes, they are not suitable for evaluation purposes as they will invariably lead to lower strengths potentially leading to a false impression of how a structure is expected to perform. Conversely, when used for seismic design, they will underestimate the concrete shear strength contribution and will lead to a higher volume of transverse reinforcement.

9.3.2 Approach of Priestley et al. for Columns

Priestley et al. (1996) proposed an expression of the type

$$V_n = V_c + V_s + V_p$$

(9-26)

where V_c = nominal shear resistance of concrete defined by

$$V_c = k \sqrt{f_c' (MPa)} \, A_e \qquad (9\text{-}27)$$

$A_e = 0.8A_{gross}$ and $k =$ a coefficient depending on the level of ductility plotted in figure 9-4. The truss mechanism strength for circular column is given by

$$V_s = \frac{\pi}{2} \frac{A_{bh} f_{yh} D''}{s} \cot \theta \qquad (9\text{-}28)$$

where A_{bh} = area of <u>single</u> leg of transverse reinforcement, θ = crack angle and remaining symbols are as explained previously.

For rectangular sections

$$V_s = \frac{A_v f_{yh} D''}{s} \cot \theta \qquad (9\text{-}29)$$

where A_v = total area of transverse reinforcement in a layer in the direction of shear force. The shear strength enhancement resulting from arch action in axial compression is given by

$$V_p = 0.85 \, P \tan \alpha \qquad (9\text{-}30)$$

where P = axial compressive load and $\tan \alpha = jd/L$ = aspect ratio for the column with L = height of the column.

In their recent textbook on bridge design Priestley et al. (1996) have shown that these equations give a greatly improved estimation of shear strength. In spite of this, the approach appears to be fundamentally flawed in that it lacks a rational means of assigning the crack angle, θ. This is arbitrarily set for design and analysis as $35°$ and $30°$, respectively.

9.3.3 Shear Analysis Methodology suggested by Kim and Mander (1998)

Kim and Mander (1998) while studying the seismic behavior of shear critical beam column elements, explored the interaction between flexure and shear through a series of truss

146
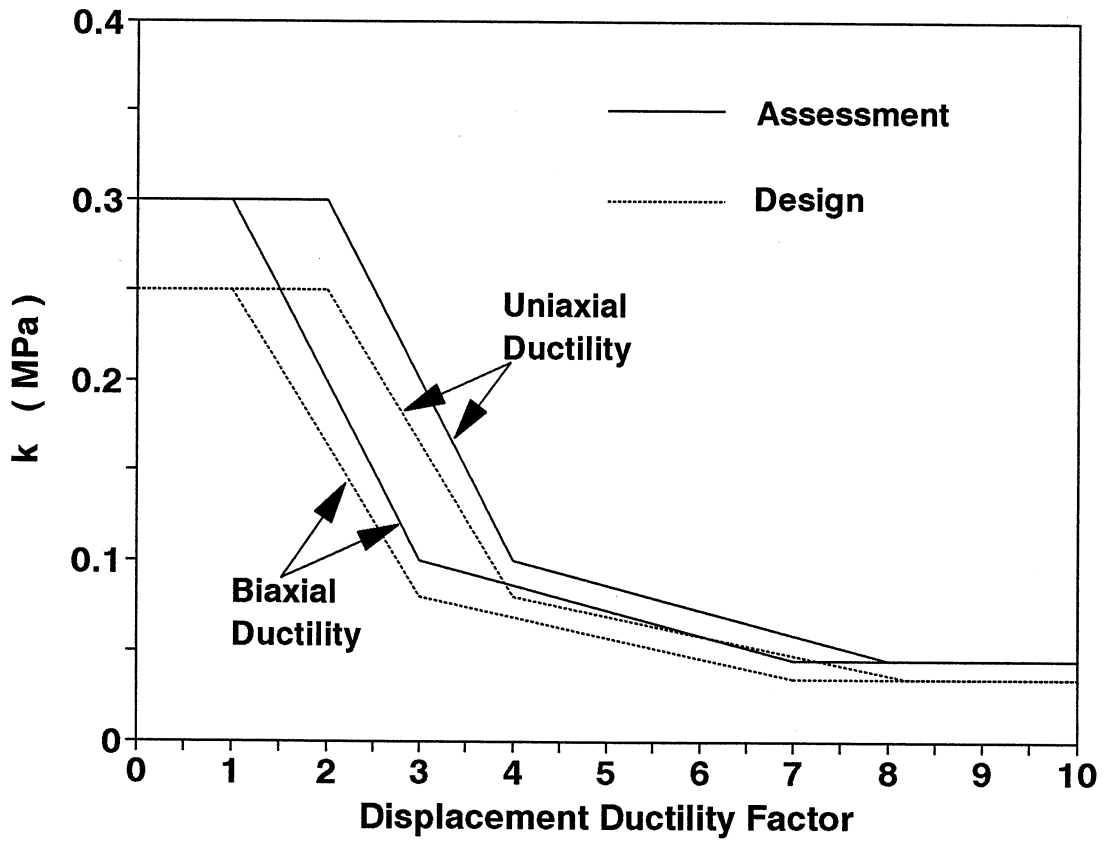
Figure 9-4 Relation between Ductility and Concrete Shear Resisting Mechanism after Priestley et al. (1996).

models. Since a reinforced concrete element is assumed to possess a series of potential crack planes, it can be considered as a truss consisting of finite number of differential truss elements as shown in figure 9-5. Using this truss analogy, they represented the longitudinal reinforcement of a cracked beam-column as the longitudinal chords of a truss and the lateral hoop steel as the transverse tension ties. The differential truss element was further simplified using various numerical integration schemes and valuable information regarding the cracked elastic stiffness in both shear and flexure was obtained.

Using an energy minimization on the virtual work done by shear and flexure components, they also proposed an equation to calculate the crack angle as

$$\theta = \tan^{-1}\left(\frac{\rho_v n + \zeta \dfrac{\rho_v}{\rho_t} \dfrac{A_v}{A_g}}{1 + \rho_v n}\right)^{\frac{1}{4}} > \alpha \tag{9-31}$$

where ρ_v = volumetric ratio of transverse steel given by

$$\rho_v = \frac{A_v}{b_w s} \qquad (\textit{for rectangular column}) \tag{9-32}$$

with A_v = total area of transverse shear reinforcement at spacing s, b_w = breadth of the web and

$$\rho_v = \frac{\rho_s}{2} = \frac{2 A_{bh}}{s D''} \qquad (\textit{for circular column}) \tag{9-33}$$

where A_{bh} = cross sectional area of a single leg of transverse hoop and D'' = diameter of the core concrete. Note also that in equation (9-31), $n = E_s / E_c$ = ratio of modulii of elasticity of steel to concrete, ρ_t = ratio of total area of longitudinal steel to the gross area, A_v / A_g = ratio of column shear area to gross area (in lieu of a more precise analysis, it may be assumed $A_v = 0.8 A_g$) and ζ = constant having values of 0.5704 and 1.5704 for fixed-fixed and fixed-pinned end conditions, respectively.

148
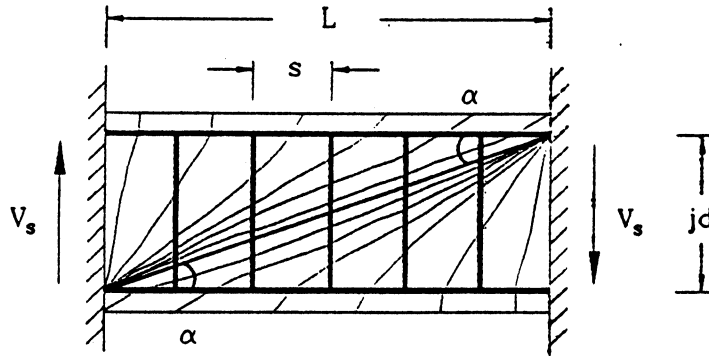
(a) Variable angle crack pattern of a "squat" beam-column
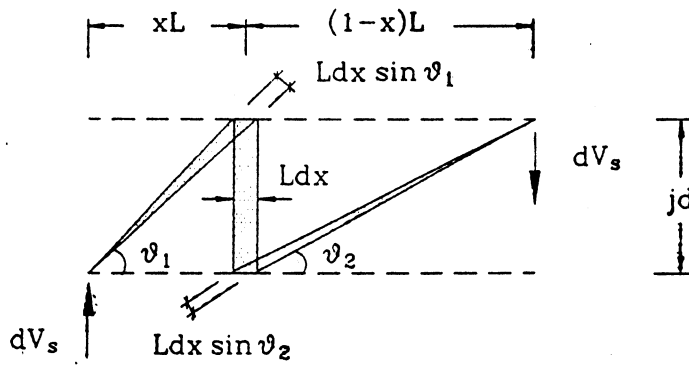
(b) A differential element of a variable angle truss
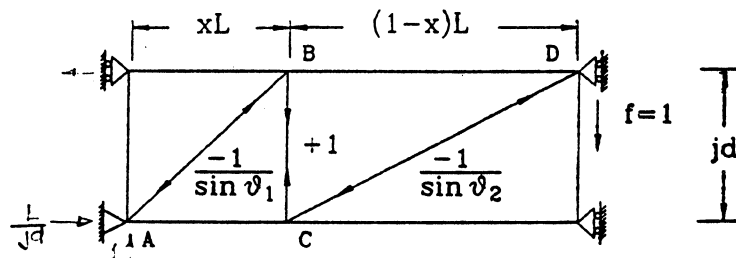
(c) Member forces for a unit load

Figure 9-5 Differential Truss Analogy used by Kim and Mander (1998).

149

In equation (9-31) $\theta \geq \alpha$. The angle α is the corner-to-corner crack angle given by the relationship

$$\alpha = \tan^{-1}\left(\frac{D'}{L}\right) \tag{9-34}$$

where D', L are respectively the pitch circle diameter and length of the beam column element. Equation (9-31) was verified with a large number of experimental results with noticeable crack angles. This is summarized in figure 9-6.

Similar to the shear analysis of Priestley et al. (1996), Kim and Mander (1998) postulate, that the total shear strength of a reinforced concrete beam column arises from three sources:

(a)   truss action that incorporates the transverse hoop steel,

(b)   truss action that incorporates the concrete tensile strength normal to the principal diagonal crack plane, and

(c)   arch action that incorporates the axial load transferring mechanisms.

However, they also observed that when the longitudinal steel yields, the initial bond strength is destroyed along that portion of the rebar as shown in figure 9-7. As the longitudinal rebars are the main source of anchorage of concrete tension ties in a series of differential trusses for the concrete mechanism, it is assumed that the concrete shear transfer mechanism ceases to function whenever those bars have yielded. From figure 9-7 it is evident that such longitudinal rebar yielding is a primary source of reducing the concrete contribution V_c. (It is thus not surprising that certain codes such as NZS 3101 assume that $V_c = 0$ in potential plastic hinge zones). At that instant, shear resistance is entirely due to (a) and (c). This was an important finding that formed the basis of the proposed shear design methodology discussed in the following subsection.

150
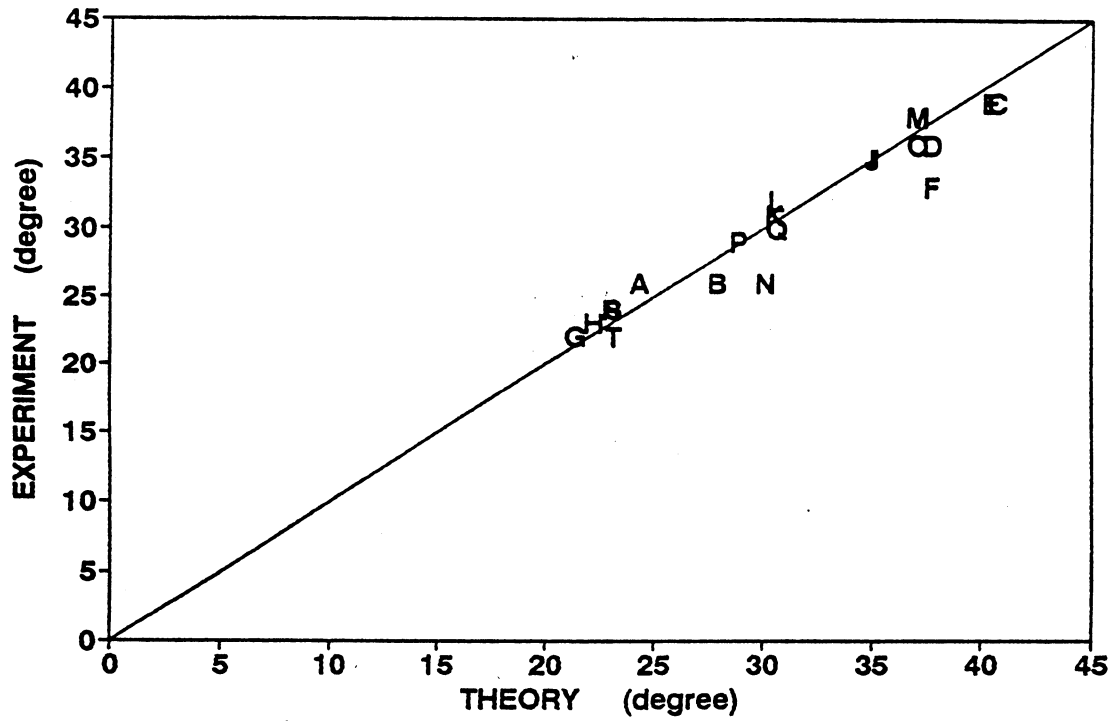
Figure 9-6 Crack Angle comparison between experiment and theory proposed by Kim and Mander (1998).

9.4 PROPOSED SHEAR DESIGN METHODOLOGY

9.4.1 The Basis and Approach

The shear design methodology, that is proposed in what follows, seeks to unify the elements in the previously adopted models so that the empirical elements are removed and substituted with approaches that are defendable from a fundamentals of mechanics point of view.

The proposed shear model is strongly linked to flexural behavior; that is elastic-range behavior in flexure that affects crack patterns, as well as post-elastic deterioration of the concrete mechanism. The capacity design basis is shown in figure 9-8. Note that the shear capacity must always exceed the flexural strength; the principal objective is that in the limit at flexural overstrength (M_{po}) the shear resistance will be provided by the contributions of arch and truss mechanisms—that is V_p and V_s, respectively.

Assume that the total shear strength for a given shear demand arising from flexure is given by

$$V_u = V_s + V_p + \lambda V_c(\varepsilon_1) \tag{9-35}$$

in which V_s = resistance from the steel truss action, V_p = resistance from the corner-to-corner arch action, $V_c(\varepsilon_1)$ = resistance provided by a full diagonal tension field whose strength is a function of the principal tensile strain ε_1, and λ = a reduction factor to denote a loss of concrete tension based truss which can be computed from geometry and strength demand ratios:
For a fixed-free (cantilever) column

$$\lambda_f = \frac{M_y}{M_{po}} - \frac{1}{2}\tan\alpha\tan\theta \tag{9-36}$$

For a fixed-fixed column

152
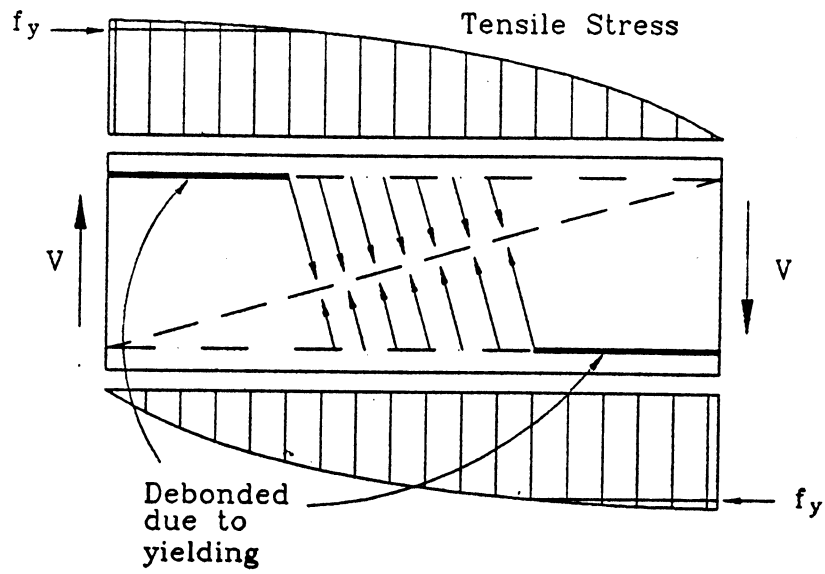
Figure 9-7 Decay in the Concrete Shear Resistance due to Longitudinal Rebar Yielding.
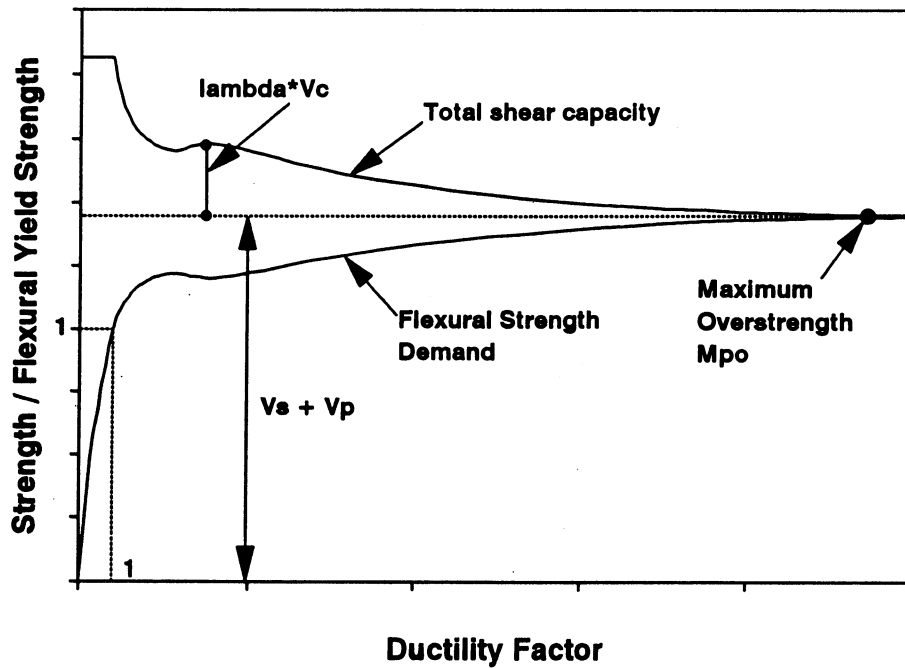
Figure 9-8 Idealized Design Model showing the Effect of Flexural Strength Demand on the required Shear Capacity.

153

$$\lambda_f = \frac{M_y}{M_{po}} - \tan\alpha \tan\theta \qquad (9\text{-}37)$$

These are shown in figure 9-9.

As the displacement is increased in the inelastic regime, the diagonal shear cracks widen and reduce the diagonal shear carrying capacity of the concrete V_c. At the same time while the strength increases well beyond yield, the ability of the concrete mechanism to transfer V_c also reduces (i.e. $\lambda << 1$). Thus the total concrete contribution may be assumed to vanish by the time the flexural overstrength moment capacity M_{po} is reached (figure 9-8). Thus the shear resisting mechanism may be assumed to be described as follows:

as $M \rightarrow M_{po}$, $\lambda V_c \rightarrow 0$, thus

$$V_u = V_s + V_p \qquad (9\text{-}38)$$

From the above equation it is evident that what remains at the ultimate flexural limit state is a shear resistance mechanism composed of only two components: a steel truss and a concrete arch.

It is further argued that at the ultimate flexural limit state the flexural overstrength capacity is also composed of two components: a steel truss (provided by the longitudinal reinforcement) M_s, and an eccentric concrete stress-block arising from the corner-to-corner diagonal concrete arch, M_c. It thus follows that an equation analogous to (9-38) can be written:

$$M_{po} = M_{ps} + M_{pc} \qquad (9\text{-}39)$$

where there is a mapping between the respective shear mechanisms of concrete and steel such that

$$V_u = \frac{M_{po}}{L} = \frac{M_{ps}}{L} + \frac{M_{pc}}{L} \qquad (9\text{-}40)$$

where $V_s = M_{ps}/L$ and $V_p = M_{pc}/L$. The contributions between the components of truss and arch action in flexure are shown in terms of the classical moment axial load interaction diagram in

154
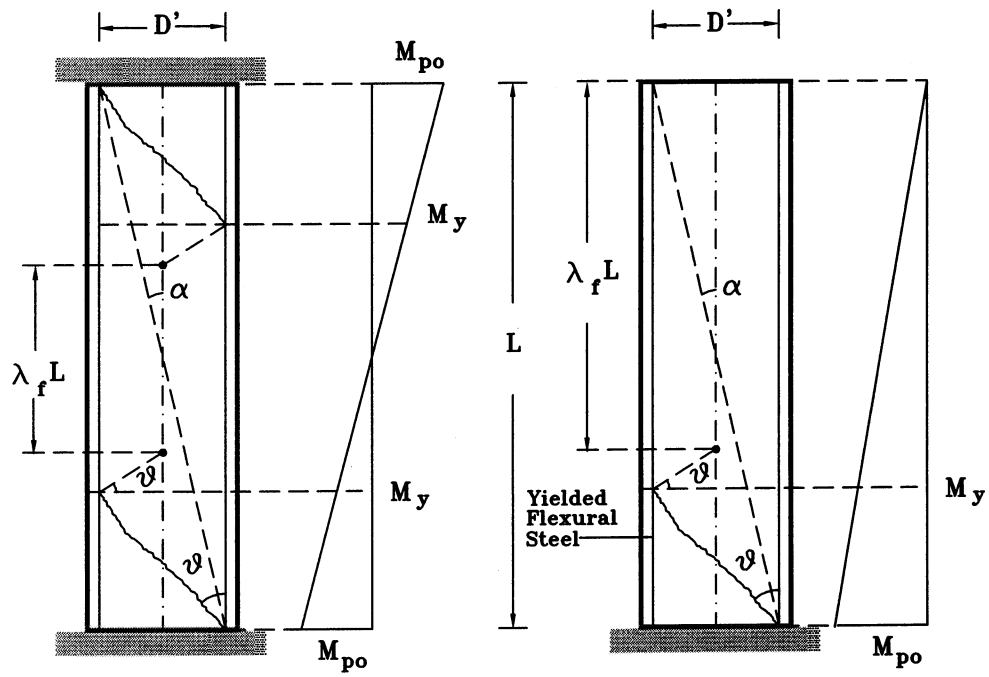
(a) Fixed–Fixed End   (b) Fixed–Free End

Figure 9-9 Undisturbed Zone in Columns Governed by Flexural Failure

figure 9-10.

The remainder of this section presents simplified ways of computing moment overstrength capacity and the constituent components of shear resistance. From this, the inverse problem is formulated, that is the design of transverse reinforcement for shear resistance.

9.4.2 Shear Demand at Flexural Overstrength

Following the approach suggested by Mander, Dutta and Goel (1998), the overstrength capacity of structural concrete elements can be determined in terms of the plastic capacity at balanced failure, that is when the neutral axis passes through the center of the concrete section defined by (P_{bo}, M_{bo}) as shown in figure 9-10.

For bridge columns it may be assumed that the actual axial load demand P_e is always less than the axial load P_{bo} at the overstrength balance point (i.e. $P_e < P_{bo}$). Therefore, assuming a parabolic interaction surface between axial load and moment it follows from figure 9-10 that all moments can be computed from

$$M_{po} = M_{bo}\left(1 - \left(\frac{P_e - P_{bo}}{P_{to} - P_{bo}}\right)^2\right) \tag{9-41}$$

where P_{to}, P_{bo} and M_{bo} are defined below.

The overstrength tension axial load capacity (sign convention here is compression forces are positive) is determined as

$$P_{to} = -1.2A_{st}f_{su} = -1.2\rho_t f_{su}A_g \tag{9-42}$$

where $A_{st} =$ the area of longitudinal reinforcement, $f_{su} =$ ultimate tensile strength of the longitudinal reinforcement, $\rho_t =$ volumetric ratio of longitudinal reinforcement such that $\rho_t = A_{st}/A_g$ where $A_g =$ gross area of the concrete section. The factor 1.2 accounts for the

156

randonmness in ultimate strength and corresponds to 95% confidence limit (5% probability of being exceeded).

The axial load at balance is given by the eccentric concrete stress block covering one-half of the section

$$P_{bo} = \frac{1}{2} \alpha_c \beta_c K (1.3 f_c') A_{cc} \qquad (9\text{-}43)$$

where α_c and β_c are stress block factors for confined concrete, K = confinement ratio and A_{cc} = area of the core concrete. Note that for all practical purposes $\beta_c \approx 1.0$, while α_c and K are given by equations (4-18) and (4-19) for rectangular sections and by equations (4-31) and (4-32) for circular sections, respectively. The factor 1.3 accounts for randomness in concrete strength and corresponds to a 95% confidence limit (5% probability of being exceeded).

When the neutral axis passes through the middle of the section at balanced overstrength capacity the plastic moment contribution from the steel will be given by

$$M_{bso} = 1.2 Z_p f_{su} \qquad (9\text{-}44)$$

where f_{su} = ultimate tensile strength of steel and Z_p = plastic section modulus of the longitudinal reinforcement. Assuming for a column, the longitudinal reinforcement is uniformly distributed around the perimeter so that it can be idealized as a thin tube with a pitch circle diameter D' for circular sections or distance D' between outer layers in a rectangular section, then

$$Z_p^{circ} = \frac{\rho_t}{\pi} D' A_g \qquad (9\text{-}45)$$

and

$$Z_p^{square} = \frac{3}{8} \rho_t D' A_g \qquad (9\text{-}46)$$

Again assuming a parabolic interaction surface between P_e and M_{ps}, it follows:

157

$$M_{ps} = M_{bso} \left(1 - \left(\frac{P_e - P_{bo}}{P_{to} - P_{bo}} \right)^2 \right)$$ (9-47)

Or, in terms of normal sectional dimensions:

$$M_{ps} = 1.2 \, k_{shape} \, \rho_t \, D' A_g \, f_{su} \left(1 - \left(\frac{0.65 - P_e / f_c' A_g}{0.65 + 1.2 \, \rho_t f_{su} / f_c'} \right)^2 \right)$$ (9-48)

where for

- circular sections $\qquad k_{shape} = \dfrac{1}{\pi}$

- for square sections with 25% of the longitudinal reinforcement placed around each face $\qquad k_{shape} = 3/8$

- for wall sections with the longitudinal reinforcement is equally distributed and placed parallel to the two long sides,

$$k_{shape} = \frac{1}{4} \quad \text{for strong axes bending}$$

$$k_{shape} = \frac{1}{2} \quad \text{for weak axes bending}$$

- for rectangular sections where the reinforcement is evenly distributed around the perimeter (equal spacing between bars)

$$k_{shape} = \left[\frac{B'/D' + 0.5}{2(B'/D' + 1)} \right]$$

where B = breadth of section measured along the axis of bending, D = depth of section measured perpendicular to the axis of bending, $B' = B - 2d'$; $D' = D - 2d'$ where d' = distance from the extreme compression fiber to the centroid of the nearest reinforcing steel. Note that in the above formulation, it has been assumed that the normalized balance load

$$\frac{P_{bo}}{f_c' A_g} \approx 0.65 \qquad\qquad (9\text{-}49)$$

based on a large sample of overstrength moment-curvature analysis.

9.4.3 Shear Resistance Provided by Truss Action

The contribution of the transverse reinforcement to shear resistance is given by

$$V_s = A_v f_{yh} \frac{D''}{s} \cot\theta \qquad\qquad (9\text{-}50)$$

where $\theta =$ diagonal crack angle taken as greater of α or

$$\theta = \tan^{-1}\left(\frac{\rho_v n + \zeta \dfrac{\rho_v}{\rho_t} \dfrac{A_v}{A_g}}{1 + \rho_v n} \right)^{\frac{1}{4}} > \alpha \qquad\qquad (9\text{-}51)$$

where the symbols are as explained previously.

In equation (9-51), $A_v =$ average area of transverse reinforcement traversing the principal crack. For rectangular sections this is the combined bar area in one hoopset. However, for circular sections the number of bars in a spiral traversing the crack will affect this average calculation. Kim and Mander (1998) have shown this to be:

$$A_v = 2\left(\frac{s}{D''} \tan\theta \right) \frac{\sin\left(\dfrac{\pi/2}{1 + \dfrac{s}{D''}\tan\theta} \right)}{\sin\left(\dfrac{\pi/2}{1 + \dfrac{D''}{s}\cot\theta} \right)} A_{bh} \qquad\qquad (9\text{-}52)$$

where $A_{bh} =$ area of a single leg of hoop or spiral reinforcement. In the absence of knowing, s and/or θ take $A_v = \frac{\pi}{2} A_{bh}$ as suggested by Priestley (1996) and Aschheim et al. (1992).

159

9.4.4 Shear Resistance Provided by Arch Action

In the shear resistance model proposed herein, it transpires that the arch action is balanced between the concrete moment demand and the shear resistance of the diagonal strut as shown in figure 9-11. Therefore, arch action does not affect the steel truss demand or capacity. The proof of this statement follows.

The concrete moment demand is given by the eccentric concrete stress block

$$M_c = C_c e \tag{9-53}$$

where C_c = eccentric concrete compression force, e = eccentricity from the centroid to the center of the concrete compression stress block.

The shear demand arising from this moment is given by

$$V_d = \frac{2 M_c}{L} = \frac{2 C_c e}{L} \tag{9-54}$$

Also the shear capacity of the diagonal strut is given from geometry (refer figure 9-11) by

$$V_p = C_c \tan \alpha \tag{9-55}$$

where $\tan \alpha = 2e/L$, thus

$$V_d = \frac{2 M_c}{L} = 2 C_c \frac{e}{L} = V_p = C_c \tan \alpha = C_c \frac{2e}{L} \tag{9-56}$$

9.4.5 Design of Transverse Reinforcement

The design criteria for transverse reinforcement is based on

$$\phi V_s \geq \frac{\Lambda M_s}{L} \tag{9-57}$$

160
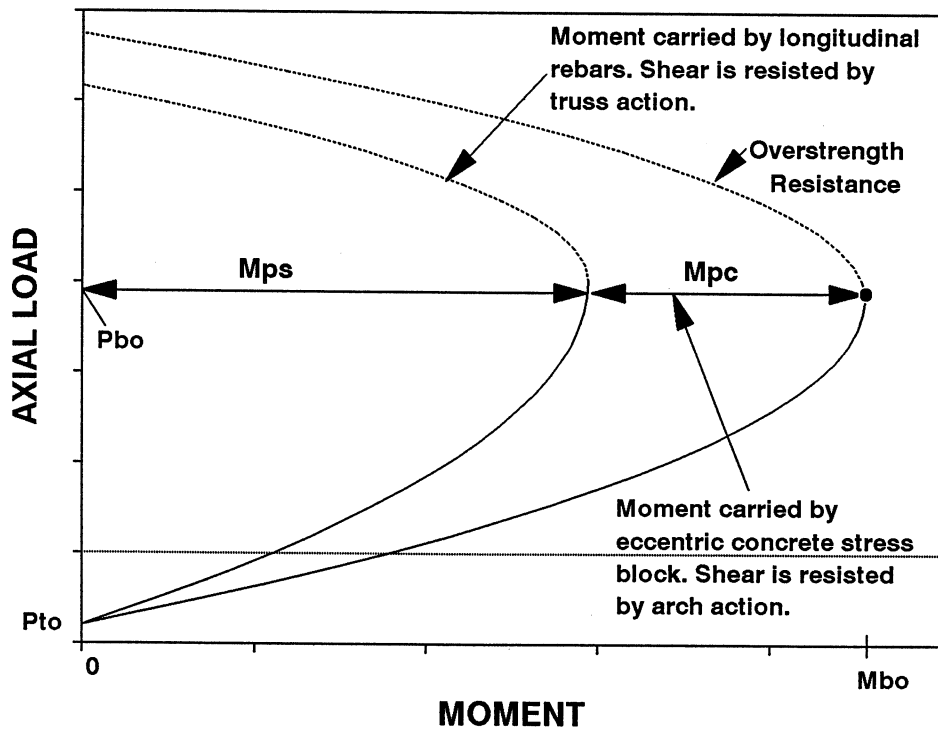
Figure 9-10 Interaction Diagram Approach to Shear Design.
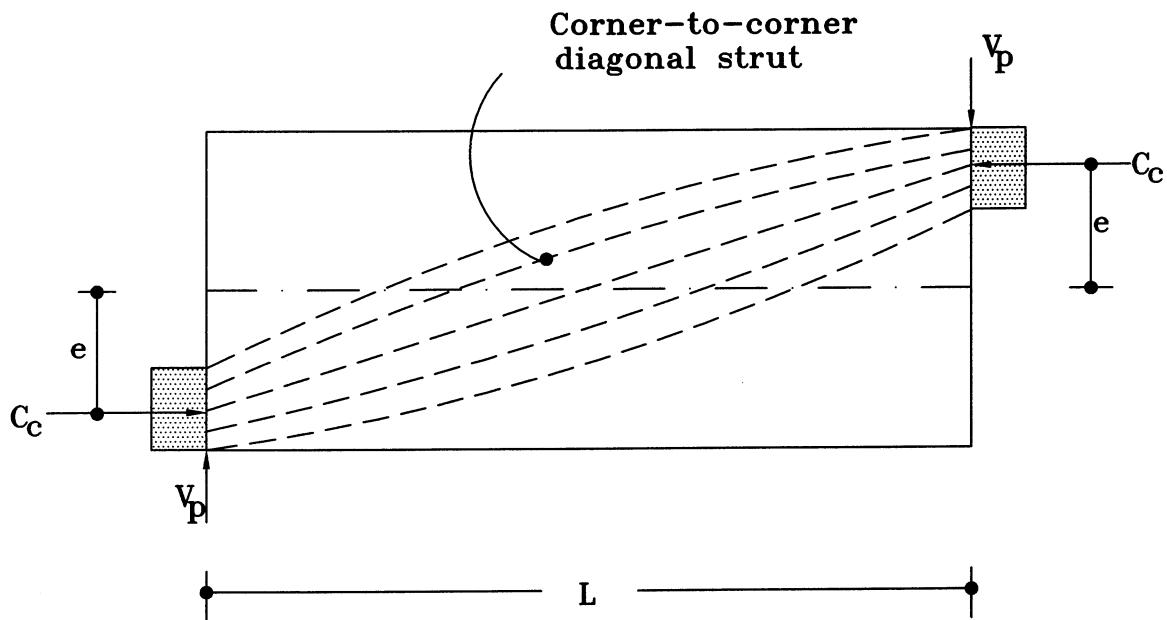
Figure 9-11 Shear Resistance of the Diagonal Strut.

161

where ϕ = undercapacity factor for shear customarily taken as 0.85, Λ = 1 or 2 depending on whether the column is fixed-pinned or fixed-fixed with L denoting the length of the column. By expanding both sides of the above equation it is possible to form simple design expressions for transverse reinforcement. Solutions are given for circular and square sections respectively.

Circular Sections

$$\phi A_v f_{yh} \frac{D''}{s} \cot\theta = 0.38\Lambda \, \rho_t f_{su} \frac{D'A_g}{L}\left(1 - \left(\frac{0.65 - P_e/\phi f_c' A_g}{0.65 + 1.2\,\rho_t f_{su}/f_c'}\right)^2\right) \qquad (9\text{-}58)$$

Assuming $A_v = \frac{\pi}{2}A_{bh}$ and noting that $\rho_s = 4A_{bh}/sD''$ and substituting into the above equation and solving for ρ_s gives

$$\rho_s^{circ} \geq 0.76\Lambda \, \frac{\rho_t}{\phi}\frac{f_{su}}{f_{yh}}\frac{A_g}{A_{cc}}\left(1 - \left(\frac{0.65 - P_e/\phi f_c' A_g}{0.65 + 1.2\,\rho_t f_{su}/f_c'}\right)^2\right)\tan\alpha \tan\theta \qquad (9\text{-}59)$$

with $\tan\theta \geq \tan\alpha$.

Square Sections

Following the same approach as for circular sections

$$\phi A_v f_{yh} \frac{D''}{s} \cot\theta = 0.45\Lambda \, \rho_t f_{su} \frac{D'A_g}{L}\left(1 - \left(\frac{0.65 - P_e/\phi f_c' A_g}{0.65 + 1.2\,\rho_t f_{su}/f_c'}\right)^2\right) \qquad (9\text{-}60)$$

Assuming $\rho_s^{square}/2 = A_v/sD''$ and substituting into the above equation and solving for ρ_s gives

$$\rho_v = \frac{\rho_s^{square}}{2} \geq \Lambda 0.45 \, \frac{\rho_t}{\phi}\frac{f_{su}}{f_{yh}}\frac{A_g}{A_{cc}}\left(1 - \left(\frac{0.65 - P_e/\phi f_c' A_g}{0.65 + 1.2\,\rho_t f_{su}/f_c'}\right)^2\right)\tan\alpha \tan\theta \qquad (9\text{-}61)$$

Above equation is also applicable to rectangular sections by replacing 0.45 with proper shape

162

factor. Note that in the equations (9-59) and (9-61) θ denotes the crack angle and is given by equation (9-51). Also in the same equations f_{su} = expected mean ultimate tensile strength and f_{yh} = specified yield strength. For Grade 60 reinforcement $f_{su} = 640\,MPa$ and $f_{yh} = 414\,MPa$. Since the expression for θ contains the term ρ_v which is equal to $\rho_s/2$ for symmetric cross sections, a few degree of iteration may be required before the solution converges. The algorithm for shear design may be stated as follows:

__Step 1__ Assume a value of the tangent of the crack angle. To start with assume $\theta = 30°$.

__Step 2__ Use either equation (9-59) or (9-61) to solve for the volumetric ratio of transverse steel.

__Step 3__ Check whether the value of ρ_s used in step 1 is within tolerable limits of the value obtained from step 2. If it is within limits then the solution can be considered to have converged. Otherwise, recalculate the crack angle using the updated ρ_s from equation (9-51) and return to step 2.

9.4.6 Effect of Member Slenderness

Schlaich et al. (1987) have defined beam-column and connection regions in terms of whether the stress field is disturbed due to end effects (D regions), or other regions away from the end disturbed regions where beam action is prevalent (B regions). The extent of these so-called D and B regions depends on the slenderness of the members; the more slender the member, the greater the B region and vise-versa.

In the seismic design of column members, for good flexural performance it is desirable that performance in the high moment regions (D regions) be not adversely affected by diagonal shear cracking. If the principles of capacity design are adhered to, that is the dependable shear capacity exceeds the flexural overstrength at all times, then the undisturbed regions (B regions) are easily identified as those zones in the low moment zone beyond the principal crack plane. Figure 9-12 shows the geometry of the D and B regions of flexure-shear interactions. The
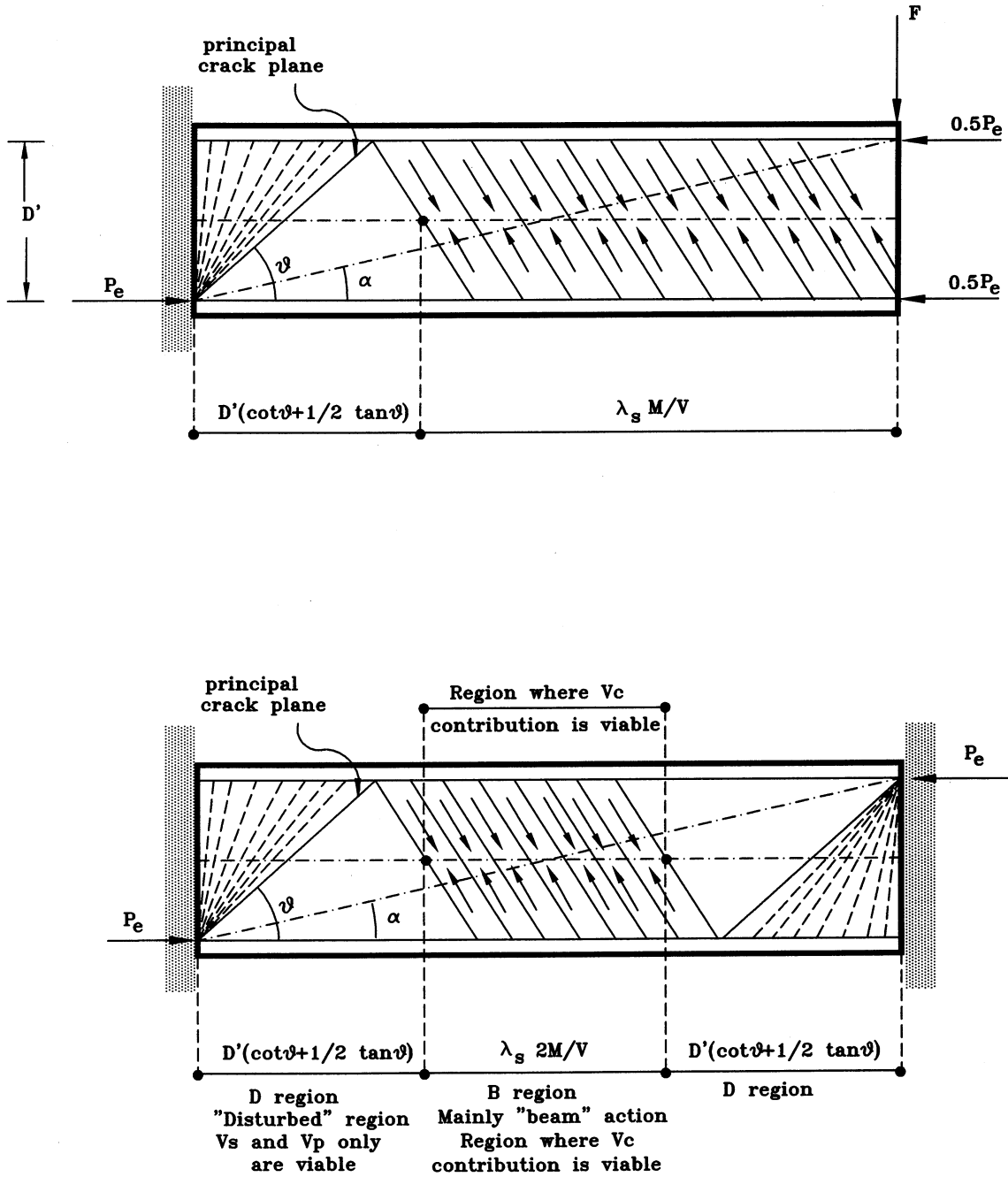
Figure 9-12 B and D Regions in a Cracked Reinforced Concrete Column Element

proportional length of the undisturbed *B* region can be calculated from the lesser of the following:

$$\lambda_s = \Lambda \tan \alpha \left[\frac{M}{VD} - \cot \theta - \frac{1}{2} \tan \theta \right] \qquad (9\text{-}62)$$

and

$$\lambda_f = \frac{M_y}{M_{po}} - \Lambda \frac{1}{2} \tan \alpha \tan \theta \qquad (9\text{-}63)$$

thus

$$\lambda = \min \left[\lambda_s, \lambda_f \right] \geq 0 \qquad (9\text{-}64)$$

where λ_s and λ_f are proportionality factors respectively governed by the extent of diagonal shear cracking and flexural yielding. All other terms in the above equations have been defined previously.

Over the low moment region of length $\lambda \frac{M}{V}$ measured from the inflection point, it may be assumed that the member is capable of sustaining some diagonal (shear) tension strength in the concrete, i.e., $V_c \neq 0$. This presents the opportunity to reduce the transverse steel quantity in slender members.

Note that from equation (9-62) above, shear carried by the concrete will only occur when

$$\frac{M}{VD} > \cot \theta + \frac{1}{2} \tan \theta \qquad (9\text{-}65)$$

As θ is expected to be in the range of 30° to 35°, it is recommended that for design, V_c be neglected unless $\frac{M}{VD} > 2$. For members where $\frac{M}{VD} < 2$, these should be defined as squat and potentially shear-critical. For slender members, the full shear design equation can be adopted:

$$V_u = V_s + V_p + V_c \qquad (9\text{-}66)$$

where V_c = shear carried by concrete and conservatively taken as

$$V_c = v_c A_v = v_c 0.8 A_g \qquad \text{(9-67)}$$

with

$$v_c = 0.167 \sqrt{f_c'} \ MPa = 2 \sqrt{f_c'} \ psi \qquad \text{(9-68)}$$

Using the above as a basis for designing the transverse reinforcement in the low moment central region of a column, the following approach can be used for determining the amount of transverse reinforcement:

Shear Capacity in End Region = Shear Capacity in Low Moment Region

Thus, $\qquad V_u = V_s + V_p = V_s^* + V_p + V_c$

Simplifying in terms of the steel provided in the end region

$$\frac{V_s^*}{V_s} = 1 - \frac{V_c}{V_s} \qquad \text{(9-69)}$$

where $V_s^* =$ shear carried by the transverse reinforcement in the low moment region, V_c is defined above, and $V_s = 0.5 \, \rho_s f_{yh} \cot\theta$. Since the shear carried by the transverse reinforcement is proportional to ρ_s, the above equation can be written in the form

$$\frac{\rho_s^*}{\rho_s} = 1 - \frac{0.33 \sqrt{f_c'}}{\rho_s f_{yh} \cot\theta} \qquad \text{(9-70)}$$

As an example of typical material properties, assume $\tan\theta = 2/3$, $f_c' = 30 \, MPa$ and $f_{yh} = 414 \, MPa$. Then, the above equation can also be expressed as

$$\rho_s^* = \rho_s - 0.0032 \qquad \text{(9-71)}$$

For columns with high axial load levels and longitudinal steel volumes, the proportional reduction of transverse reinforcement in the low moment zone of the column is not significant. Therefore, steel congestion will continue to prevail. Clearly, it is desirable to use low volumes

166

of longitudinal reinforcement to minimize not only congestion of that reinforcement, but also the placement of the transverse reinforcement.

9.5 SUMMARY AND CONCLUSIONS

The shear resistance of reinforced concrete members is still a contentious issue amongst many researchers and code writing bodies. Although it is generally agreed that such resistance comes from two major sources viz. concrete arch action and a steel truss mechanism, there is a wide variation in opinion as to how the concrete diagonal tension component should be treated. This results in markedly different shear design/analysis paradigms and little has been done to amalgamate these differences.

The transverse reinforcement contributes to the resistance by carrying a portion of the shear acting across a diagonally cracked shear plane. Since the inclination of the shear plane depends on the reinforcement characteristics of the beam column itself, this also is a source of inconsistency especially with respect to the proportioning of the transverse reinforcement for design purposes. However, this problem has recently been resolved by the research efforts of Kim and Mander (1998) who used an energy minimization technique to compute the inclination of the steepest crack angle in a diagonally cracked reinforced concrete beam-column element.

There is a consensus amongst various researchers that concrete resistance to shear decays progressively with increasing ductility. However based on their research findings, Kim and Mander (1998) concluded that at high level of plastification, this contribution is virtually nonexistent due to debonding between concrete and steel at the ends of the member and widening of tensile cracks within the central region of the member. Therefore, in the ultimate lateral load limit state the shear is mainly resisted by the transverse reinforcement in the form of truss action and by the concrete arch action due to the corner-to-corner diagonal strut. Using the research findings of Kim and Mander (1997), the basis of a new methodology for shear design was proposed in this section. This method, which is based on rational theory, overcomes the ambiguities inherent in most of the current empirical design approaches. Moreover it uses a

167

rigorous crack angle formulation and thereby gives a more sound prediction of lateral reinforcement requirements. Simple expressions are derived that capture the basic mechanics of shear resistance and at the same time are attractive for design office application as well. It should be emphasized that the proposed approach adheres to the tenets of the capacity design philosophy. Dependable shear resistance is designed for the ultimate flexural overstrength capacity, this being implicitly accounted for in the design formulation.

This work shows that oftentimes it is not permissible nor it is expedient to reduce the quantity of transverse reinforcement outside the so-called plastic hinge zone in columns. For simplicity of detailing and construction, it is recommended that differentiating between end regions and the low moment regions be ignored. It is also evident from the design methodology proposed herein, that if good performance is to be expected for a column with a large volume of longitudinal reinforcement, then that column must also possess substantial transverse reinforcement, principally to fulfill antibuckling and shear requirements. Such columns are difficult to construct due to overall congestion of reinforcement. It is therefore recommended that wherever possible the column dimensions be increased, and the longitudinal steel volume reduced.

It is conceded, however, that keeping the longitudinal steel volume low (ideally near 1%) is not always possible. Ways of overcoming longitudinal and transverse steel congestion will be suggested in the following section.

SECTION 10
SEISMIC DESIGN AND PERFORMANCE EVALUATION RECOMMENDATIONS

10.1 INTRODUCTION

In the foregoing sections of this report the three principal modes of failure of reinforced concrete elements were investigated in depth. After extensive theoretical development from a fundamental point of view, design equations were proposed for transverse reinforcement requirements in terms of: confinement of concrete to avoid transverse hoop fracture; confinement of the longitudinal steel to inhibit buckling of that steel (this is referred to as antibuckling); and to avoid shear failure both within and outside the zone of plastification.

These requirements are now gathered together in one location and a comparative study is made to assess under what circumstances certain potential failure modes become critical. In an inverse form to design, the transverse reinforcement provided for a given column can be assessed in terms of its low cycle fatigue resistance. This is important for defining displacement (plastic rotation) limit states for a performance based seismic evaluation of a given column design.

10.2 DESIGN RECOMMENDATIONS

It is recommended that the following language be adopted by code writers for the design of transverse reinforcement in a beam-column element.

10.2.1 Notations

A_{bh} = area of cross section of a single leg of transverse reinforcement.

A_{cc} = core area of concrete section measured to the center of transverse reinforcement.

A_g = gross area of concrete section.

169

A_v = total area of transverse reinforcement perpendicular to the axis of bending or along the direction of applied shear.

A_v' = total area of transverse reinforcement along the axis of bending or perpendicular to the direction of applied shear.

B' = width of section measured center to center of outermost longitudinal bars along the axis of bending or perpendicular to the direction of applied shear.

B'' = core sectional dimension of column measured center to center of outer legs of the hoops or spirals along the axis of bending or perpendicular to the direction of applied shear.

D = diameter of a circular column or outer dimension of a rectangular column along the direction of applied shear.

D' = width of section measured center to center of outermost longitudinal bars perpendicular to the axis of bending or along the direction of applied shear.

D'' = core sectional dimension of column measured center to center of outer legs of the hoops or spirals perpendicular to the axis of bending or along the direction of applied shear.

f_c' = unconfined compression strength of concrete.

f_{su} = ultimate strength of the longitudinal reinforcement.

f_y = yield strength of the longitudinal reinforcement.

f_{yh} = <u>specified</u> yield strength of the lateral reinforcement.

L = total length of the column.

$P_e / f_c' A_g$ = axial load ratio.

s = spacing of the lateral steel.

U_{sf} = strain energy capacity of transverse steel $= 110 \text{ MJ}/\text{m}^3$.

$\tan \alpha = D'/L$.

Λ = a constant = 2 for fixed-fixed and = 1 for fixed-pinned columns.

ϕ = under capacity factor.

ρ_s = volumetric ratio of transverse steel.

ρ_t = longitudinal steel volume.

θ = crack angle.

10.2.2 Recommendations

Transverse reinforcement shall be provided in flexural elements to satisfy the following requirements:

1. Confinement of Concrete

for circular sections

$$\rho_s = 0.008 \frac{f_c'}{U_{sf}} \left[12 \left(\frac{P_e}{f_c' A_g} + \rho_t \frac{f_y}{f_c'} \right)^2 \left(\frac{A_g}{A_{cc}} \right)^2 - 1 \right] \qquad \text{(CC-1)}$$

for rectangular sections

$$\frac{A_v}{s B''} + \frac{A_v'}{s D''} = 0.008 \frac{f_c'}{U_{sf}} \left[15 \left(\frac{P_e}{f_c' A_g} + \rho_t \frac{f_y}{f_c'} \right)^2 \left(\frac{A_g}{A_{cc}} \right)^2 - 1 \right] \qquad \text{(CC-2)}$$

2. Antibuckling

for circular sections

(a) for low to moderate seismic zones and/or "other" bridges (Seismic Performance categories SPC B and C)

$$\rho_s = 0.02 \frac{D}{s} \frac{s}{d_b} \rho_t \frac{f_y}{f_{yh}} \qquad \text{(AB-1)}$$

(b) for high seismic zones and critical bridges (Sesmic Performance Categories SPC D)

$$\rho_s = 0.025 \frac{D}{s} \frac{s}{d_b} \rho_t \frac{f_y}{f_{yh}} \qquad \text{(AB-2)}$$

for rectangular sections

(a) for low to moderate seismic zones and/or "other" bridges (Seismic Performance categories SPC B and C)

$$A_{bh} = \frac{1}{10} \frac{A_b f_y}{f_{yh}} \qquad \text{(AB-3)}$$

(b) for high seismic zones and critical bridges (Sesmic Performance Categories SPC D)

$$A_{bh} = \frac{1}{4} \frac{A_b f_y}{f_{yh}} \qquad \text{(AB-4)}$$

3. Shear

for circular sections

$$\rho_s^{circ} \geq \Lambda\, 0.76 \frac{\rho_t}{\phi} \frac{f_{su}}{f_{yh}} \frac{A_g}{A_{cc}} \left(1 - \left(\frac{0.65 - P_e / \phi f_c' A_g}{0.65 + 1.2\, \rho_t f_{su}/f_c'} \right)^2 \right) \tan\alpha \tan\theta \qquad \text{(SH-1)}$$

and for rectangular sections

$$A_v = 1.2 \Lambda s B'' \left[\frac{B'/D' + 0.5}{2(B'/D' + 1)} \right] \frac{\rho_t}{\phi} \frac{f_{su}}{f_{yh}} \frac{A_g}{A_{cc}} \left(1 - \left(\frac{0.65 - P_e / \phi f_c' A_g}{0.65 + 1.2\, \rho_t f_{su}/f_c'} \right)^2 \right) \tan\alpha \tan\theta \qquad \text{(SH-2)}$$

10.3 WHAT IS CRITICAL: CONFINEMENT, ANTIBUCKLING OR SHEAR?

At a glance it is not possible to ascertain which of the above recommended provisions will be critical in design. To give some insight into the sensitivity of each of the design equations, graphs (which may be considered as preliminary design charts) have been prepared for typical bridge columns. The following four parameters are significant:

* Axial load intensity $(P_e/f_c' A_g)$
* Aspect ratio (L/D)
* End fixity condition (fixed-fixed, or fixed-free)
* Longitudinal reinforcement ratio (ρ_t)
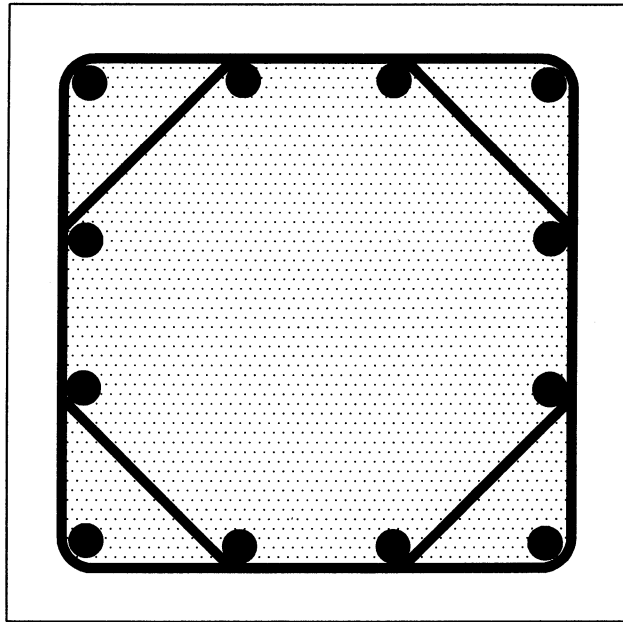
Figure 10-1 Square Section Used in the Illustrative Design Charts

173

Figures 10-2 and 10-3 present design charts for circular and square column sections, respectively. In preparing these graphs the following assumptions were made"

- Grade 60 reinforcement ($f_y = f_{yh} = 414$ MPa) was used for both longitudinal and transverse reinforcement. Hence $f_{su} = 700$ MPa was assumed as an expected value.
- Concrete with an unconfined confined strength ($f_c' = 30$ MPa) has been used all through.
- For antibuckling $D/s = 5.5$ and $s/d_b = 6$ was adopted.
- Undercapacity factor $\phi = 0.85$ and $A_{cc}/A_g = 0.8$ was used.

The square section used in the study is shown in figure 10-1. It consists of 12 bars held together by octagonal hoops. The lateral steel volume for such as configuration is given by

$$\rho_s = 2\rho_v = \frac{2 \times (2 + \sqrt{2})A_{bh}}{sD''} \tag{10-1}$$

where A_{bh} = area of a single leg of a hoop with the other symbols as explained previously. The longitudinal steel ratio is given by

$$\rho_t = \frac{12A_b}{D^2} \tag{10-2}$$

where A_b = area of a single longitudinal bar. If the buckling criteria of

$$A_{bh} \geq \frac{A_b}{10} \frac{f_y}{f_{yh}} \tag{10-3}$$

is chosen, then it is possible to relate the lateral steel volume to the longitudinal steel volume as

$$\rho_s = 0.064 \left(\frac{D}{s}\right) \frac{f_y}{f_{yh}} \rho_t \tag{10-4}$$

with $D/D' \approx 1.11$.

174
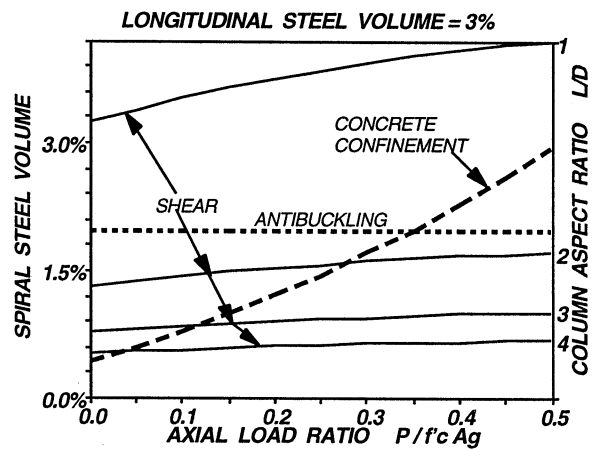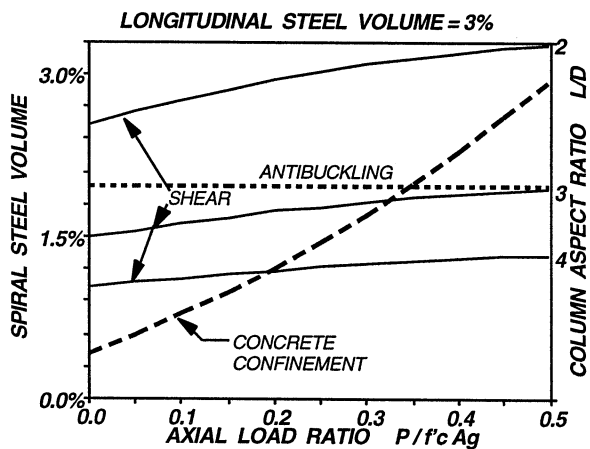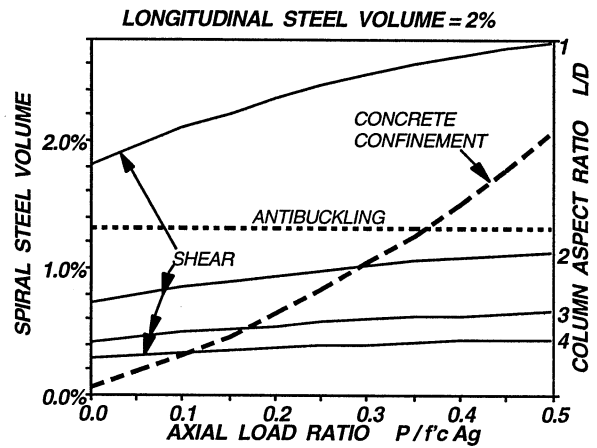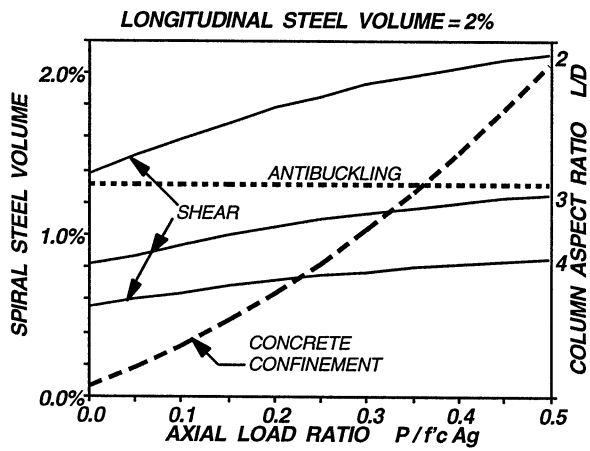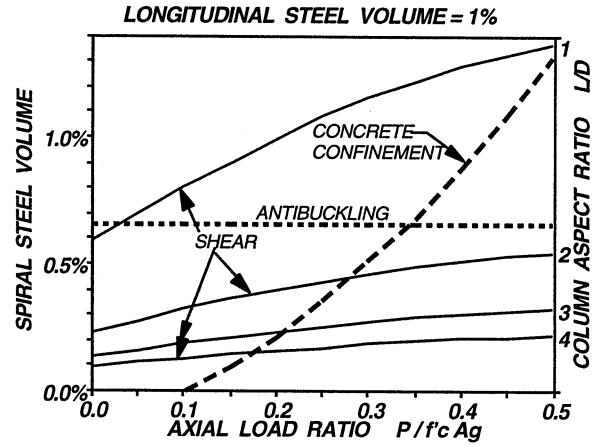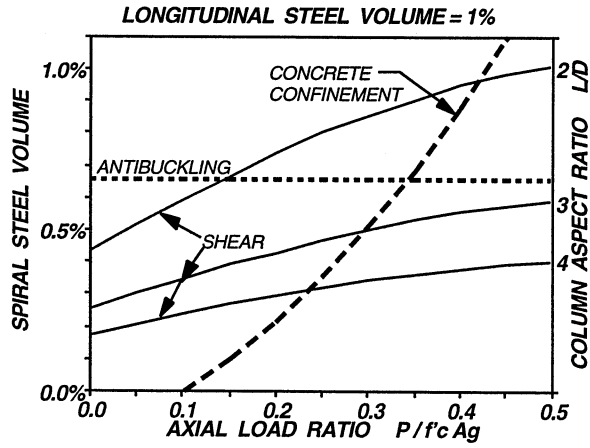
Figure 10-2 Design Charts for Circular Sections.

175
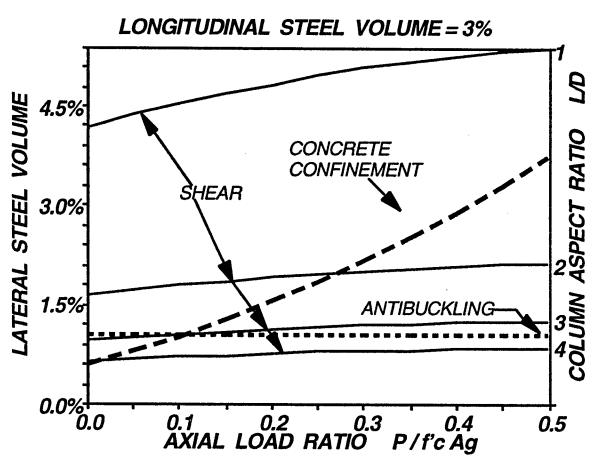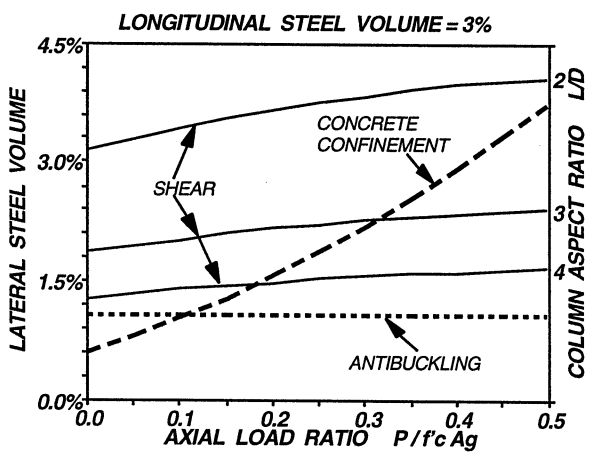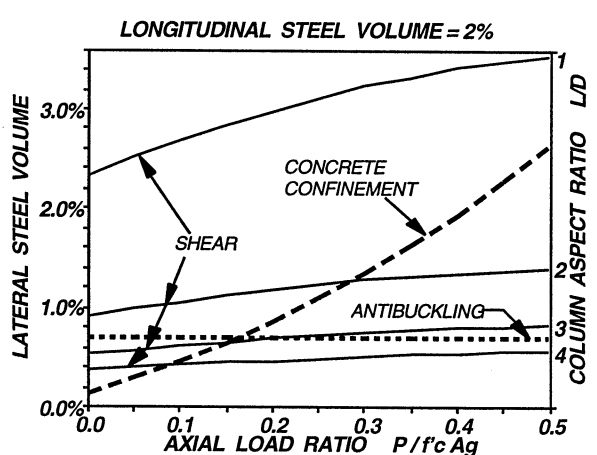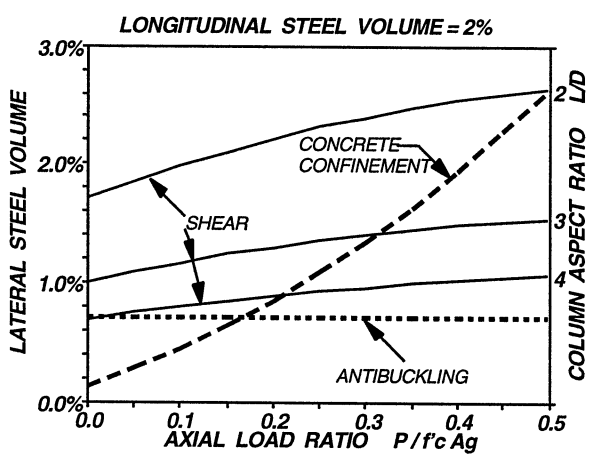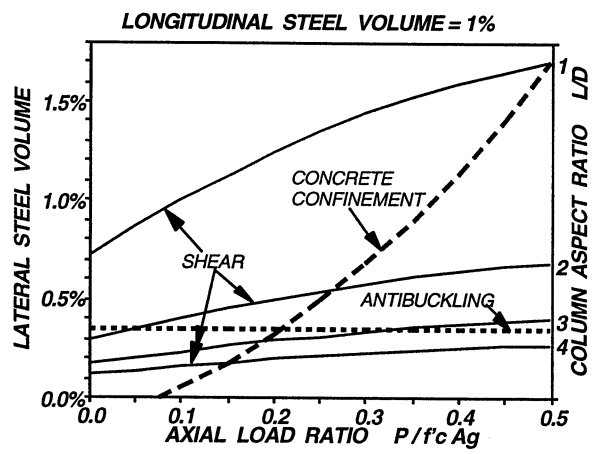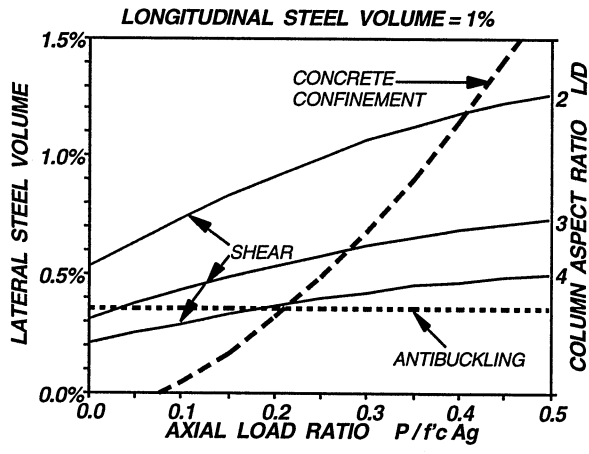
Figure 10-3 Design Charts for Square Sections.

176

10.4 COMMENTARY ON APPLICABILITY

From the design charts in figure 10-2, it can be seen that for fixed-fixed circular columns, concrete confinement is critical only at high axial load ratios $(P/f_c'A_g > 0.35)$. Shear reinforcement is more critical for members with high volumetric ratio of longitudinal steel. This is because for high ρ_t, the crack angle (θ) becomes smaller. However, since the volumetric ratio of lateral steel ρ_s is directly proportional to ρ_t, the net effect is higher ρ_s spread over a longer height. This is definitely an incentive to use slender members with low volumetric ratios of longitudinal steel. For cantilever members, anti-buckling reinforcement is almost always critical except at high axial loads when concrete confinement starts to govern.

The same conclusions are also true for fixed-fixed square columns. However, the effect of longitudinal steel ratio (ρ_t) is more pronounced on the shear reinforcement due to higher shape factor ($k_{shape}^{circ} = 0.318$ and $k_{shape}^{square} = 0.375$). Moreover, antibuckling restraint is more efficient for square (and/or rectangular) sections since the full capacity of the lateral reinforcement ($A_{sh}f_{yh}$) is utilized rather than a component ($2\pi/N$) for circular sections. This is reflected in fixed columns where buckling is only critical for very slender members over the range of longitudinal steel volume. Unlike fixed-fixed columns, however, concrete confinement in a cantilever starts to govern from low axial load ratios ($P_e/f_c'A_g > 0.2$) in case of square columns.

10.5 THE PROBLEM OF STEEL CONGESTION

It is evident from figures 10-2 and 10-3 that difficulty with reinforcement placement is likely when:

(a) the axial load level is high ($P_e > 0.3 f_c'A_g$)
(b) high amount of longitudinal reinforcement is present ($\rho_t > 0.015$)
(c) the members are squat ($L < 3D$)

177

For the above three cases transverse reinforcement is governed by confinement, antibuckling and shear, respectively. The most generally applicable way of overcoming the problem of congestion is to reduce the longitudinal steel volume (striving to keep it near the permitted minimum), and if a higher flexural strength is necessary, then use larger column. Stronger concrete may help, but not appreciably.

In the circumstances where high longitudinal steel volumes are unavoidable, a double ring of longitudinal reinforcement may reduce congestion. Consider for example, the case where $\rho_t = 0.03$ in figure 10-4. As can be seen from figure 10-4a, for the conventional placement of longitudinal reinforcement, the antibuckling reinforcement is critical at about 2%. This might lead to congestion of reinforcement especially at the potential plastic hinges at the column end zones. The way to circumvent the problem is suggested in figure 10-4b. The column longitudinal reinforcement is arranged in two distinct circular patterns each containing exactly half the amount required from flexural analysis. Since the antibuckling reinforcement is proportional to the longitudinal reinforcement ratio, the requirements for the outer ring now decreases by exactly one-half the amount that was previously required. This is shown in figure 10-4b. The inner ring can rely on the surrounding concrete for antibuckling restraint. Transverse steel is only provided to account for the difference between the shear requirement and the provided antibuckling reinforcement to ensure protection against shear failure. Although it might be agreed that such differential arrangement of longitudinal steel might reduce the flexural capacity, it was shown by Priestley et al. (1996) that such an effect is minimal. Hence by using simple techniques like this it is possible to design reinforced concrete columns that can have superior performance in the event of strong ground shaking.
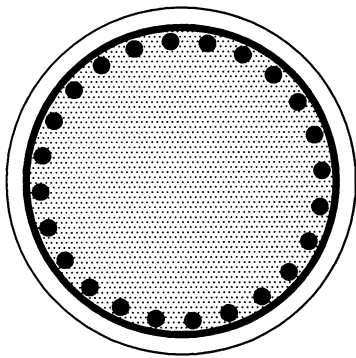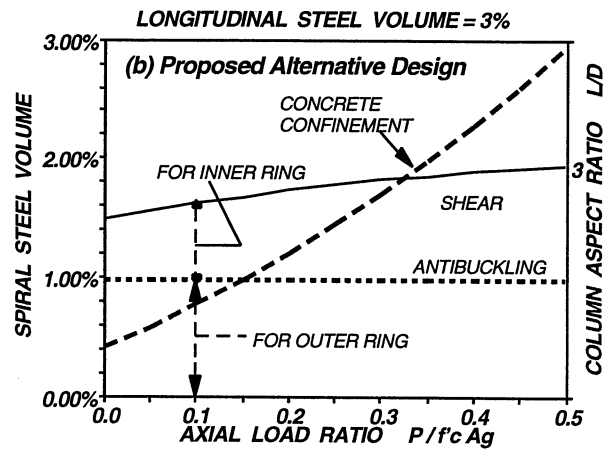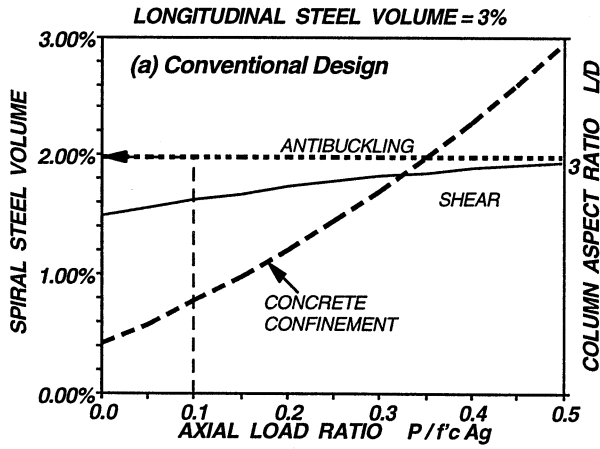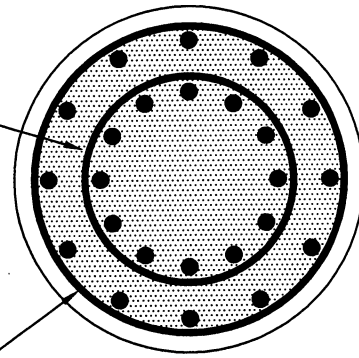
Figure 10-4   Showing alternative Techniques to tackle the Problem of Reinforcement Congestion.

10.6 Design Algorithm for Column Transverse Reinforcement

The following is a step-by-step algorithm that may be convenient for the systematic design of transverse reinforcement in columns.

Step 0.   **Design the Longitudinal Reinforcement**

Once the longitudinal steel volume (ρ_t) has been chosen other design actions that may come from a computer analysis should be <u>ignored</u>. Demands are based on the <u>provided</u> overstrength capacity of longitudinal steel.

Step 1.   **Design Anti-buckling Reinforcement**

If the bridge is in high seismic zone, then for circular sections use

$$\rho_{sbuc} \geq 0.025 \, \frac{D}{s} \, \frac{s}{d_b} \, \rho_t \, \frac{f_y}{f_{yh}} \tag{AB-1}$$

and for rectangular sections, use equation (8-46)

$$A_{bh} \geq \frac{A_b}{4} \, \frac{f_y}{f_{yh}} \tag{AB-2}$$

If the bridge is in low to moderate seismic zone, then for circular sections use

$$\rho_{sbuc} \geq 0.2 \frac{D}{s} \frac{s}{s_b} \rho_t \frac{f_y}{f_{yh}} \tag{AB-3}$$

and for rectangular sections

$$A_{bh} \geq \frac{A_b}{10} \frac{f_y}{f_{yh}} \tag{AB-4}$$

with the stipulation $D/s \geq 5$ and $s/d_b \leq 6$

Step 2.   **Design for Concrete Confinement**

For circular sections, use equation (7-7)

$$\rho_{scon} = 0.008 \frac{f_c'}{U_{sf}} \left[12 \left(\frac{P_e}{f_c' A_g} + \rho_t \frac{f_y}{f_c'} \right)^2 \left(\frac{A_g}{A_c} \right)^2 - 1 \right] \tag{CC-1}$$

and for rectangular sections use equation (7-7)

$$\rho_{scon} = 0.008 \frac{f_c'}{U_{sf}} \left[15 \left(\frac{P_e}{f_c' A_g} + \rho_t \frac{f_y}{f_c'} \right)^2 \left(\frac{A_g}{A_c} \right)^2 - 1 \right] \tag{CC-2}$$

Step 3.   **Design for Shear**

     (a)   With the maximum ρ_s from steps 1 and 2, find the crack angle from equation (9-51).

181

$$\theta = \tan^{-1}\left(\dfrac{\rho_v n + \zeta\,\dfrac{\rho_v}{\rho_t}\dfrac{A_v}{A_g}}{1 + \rho_v n}\right)^{1/4} > \alpha \qquad \text{(SH-1)}$$

(b) Find the shear reinforcement. For circular sections use equation (9-59).

$$\rho_{ssh} \geq \Lambda\,0.76\,\frac{\rho_t}{\phi}\,\frac{f_{su}}{f_{yh}}\,\frac{A_g}{A_{cc}}\left[1 - \left(\frac{0.65 - P_e/\phi f_c' A_g}{0.65 + \rho_t f_{su}/f_c'}\right)^2\right]\tan\alpha\,\tan\theta \qquad \text{(SH-2)}$$

and for rectangular sections, use equation (9-61)

$$\rho_{ssh} \geq 1.2\Lambda\,k_{shape}\,\frac{\rho_t}{\phi}\,\frac{f_{su}}{f_{yh}}\,\frac{A_g}{A_{cc}}\left[1 - \left(\frac{0.65 - P_e/\phi f_c' A_g}{0.65 + 1.2\rho_t f_{su}/f_c'}\right)^2\right]\tan\alpha\,\tan\theta \qquad \text{(SH-3)}$$

(c) If the shear reinforcement obtained from Step 3(b) is more than obtained at the end of Step 2, go back to Step 3(a) and recalculate θ with $\rho_v = 0.5\,\rho_{ssh}$ till convergence. Else, if $\rho_{ssh} < \max(\rho_{sbuc}, \rho_{scon})$, proceed to next step.

Step 4. Reinforcement Distribution

(a) Calculate the concrete confinement parameter K
For circular sections use equation (4-32)

$$K = 1 + 2.1\,\rho_s\,\frac{f_{yh}}{f_c'} \qquad \text{(RD-1)}$$

182

for rectangular sections use equation (4-19)

$$K = 1 + 2.7 \, \rho_s \frac{f_{yh}}{f_c'} \qquad \text{(RD-2)}$$

(b) Calculate the overstrength moment M_{po} using moment curvature analysis. Alteratively, the method suggested by Mander et al. (1997) may also be used. Calculate the maximum overstrength shear

$$K = 1 + 2.7 \, \rho_s \frac{f_{yh}}{f_c'} V_{po} = \frac{\Delta M_{po}}{L} \qquad \text{(RD-3)}$$

(c) Calculate the proportionality factor of B region using equations (9-62) and (9-63)

$$\lambda_s = \Lambda \tan \alpha \left[\frac{M}{VD} - \cot \theta - \frac{1}{2} \tan \theta \right] \qquad \text{(RD-4)}$$

$$\lambda_f = \frac{M_y}{M_{po}} - \Lambda \frac{1}{2} \tan \alpha \tan \theta \qquad \text{(RD-5)}$$

Use θ obtained at the end of Step 3. For the yield moment, one can conservatively assume $M_y = 0.75 M_n$. (Note: M_n = nominal moment capacity). Calculate

$$\lambda = minimum \ (\lambda_s, \lambda_f) \qquad \text{(RD-6)}$$

(d) Provide the maximum reinforcement obtained at the end of Step 3 over the length $(1 - \lambda)L$ distributed evenly over the two fixed ends for a fixed-fixed column and only at the fixed end for a cantilever

183

column. If either λ_s or $\lambda_f < 0$, then extend the maximum reinforcement over the entire height of the column.

(e)   For $\min(\lambda_s, \lambda_f) > 0$, calculate V_c form equation (9-70) and (9-71)

$$V_c = v_c \, 0.8 A_g = 0.167\sqrt{f_c' \, (MPa)} \, 0.8 A_g \tag{RD-7}$$

and from equation (9-30)

$$V_p = 0.85 \, P \tan \alpha \tag{RD-8}$$

Calculate shear to be carried by reinforcement

$$V_s = \frac{V_{po}}{\phi} - V_c - V_p \tag{RD-9}$$

Find the required spacing of shear reinforcement. For circular section using equation (9-28)

$$s = \frac{\pi}{2} \, \frac{A_{bh} f_{yh} D''}{V_s} \cot \theta \tag{RD-10}$$

and for rectangular section using equation (9-29)

$$s = \frac{A_v f_{yh} D''}{V_s} \cot \theta \tag{RD-11}$$

with an initial estimate of $\theta = 30°$

(f)   With the s obtained at the end of Step 4(e), calculate the reduced volumetric ratio of

184

lateral steel. For circular sections

$$\rho_{sred} = \frac{4A_{bh}}{sD''}$$ (RD-12)

and for rectangular sections

$$\rho_{vred} = \frac{A_v}{sD''}$$ (RD-13)

(g) Calculate the crack angle form equation (SH-1) with ρ_{sred} or ρ_{vred}. If $\theta \approx 30°$, move onto the next Step or else recalculate s from equations (RD-10) or (RD-11) using updated θ till convergence.

(h) Provide ρ_{sred} or ρ_{vred} over the length of λL of the column.

Step 5. Performance Evaluation

(a) Calculate c''/D'' ratio. For circular sections, use equation (4-27).

$$\frac{c''}{D''} = \left[\frac{\dfrac{P_e}{f_c' A_g} + 0.5\,\rho_t\,\dfrac{f_y}{f_c'}\left(\dfrac{1 - 2c''/D''}{1 - 2d''/D''}\right)}{0.9\,(1 + \rho_s f_{yh}/f_c')\,(1 + 2.7\,\rho_s f_{yh}/f_c')\,\dfrac{A_{cc}}{A_g}} \right]^{0.725}$$ (PE-1)

and for rectangular sections use equation (4-17)

185

$$\frac{c''}{D''} = \frac{\dfrac{P_e}{f_c' A_g} + \dfrac{\gamma_r \rho_t f_y / f_c'}{1 - 2d''/D''}}{0.625\,(1 + \rho_s f_{yh}/f_c')\,(1 + 2.1\,\rho_s f_{yh}/f_c')\dfrac{A_{cc}}{A_g} + \dfrac{2\gamma_r \rho_t f_y / f_c'}{1 - 2d''/D''}}$$ (PE-2)

(b)   Calculate Θ_{con} for circular sections using equation (4-28)

$$\Theta_{con} = \frac{4\left(0.008 + \rho_s \dfrac{U_{sf}}{f_c'}\right)}{\dfrac{\rho_t f_y}{f_c'}\left(0.5 + \dfrac{c''}{D''}\right)\dfrac{c''}{D''}\dfrac{D}{D''} + 0.67(1 + \rho_s f_{yh}/f_c')(1 + 2.7\,\rho_s f_{yh}/f_c')\left(\dfrac{c''}{D''}\right)^{2.38}\dfrac{D''}{D}}$$ (PE-3)

and for rectangular sections using equation (4-11)

$$\Theta_{con} = \frac{4\left(0.008 + \rho_s \dfrac{U_{sf}}{f_c'}\right)}{\dfrac{\rho_t f_y}{f_c'}\left((1 - \gamma_r) + 2\gamma_r \dfrac{c''}{D''}\right)\dfrac{c''}{D''} \cdot \dfrac{D''}{D} \cdot \dfrac{A_g}{A_{cc}} + 0.625(1 + \rho_s f_{yh}/f_c')(1 + 2.1\,\rho_s f_{yh}/f_c')\left(\dfrac{c''}{D''}\right)^2 \dfrac{D''}{D}}$$ (PE-4)

Use maximum ρ_s at the end of Step 3.

Plot the equation

$$\phi_p D = \Theta_{con} * (2N_c)^{-1}$$ (PE-5)

(c)   Calculate Θ_{lcf} as per equation (7-4)

$$\Theta_{lcf} = \frac{0.113}{1 - 2d'/D}$$ (PE-6)

Plot the equation

$$\phi_p D = \Theta_{lcf} * (N_c)^{-0.5}$$ (PE-7)

(d)   With ρ_s provided at the end of Step 3, calculate the

186

minimum crippling stress. Use equation (8-56)

$$\frac{f_{cr}}{f_{su}} = \frac{0.3\,(N_h + 1)(s/d_b)}{\left(\left|f_{su}/f_{cr}\right|^2 - 1\right)} \left[0.033\,(N_h + 1)\left(\frac{s}{d_b}\right)\left(1 - 0.4\left|\frac{f_{cr}}{f_{su}}\right|^2\right) - \frac{N_h}{\kappa}\frac{f_{su}}{f_{cr}}\frac{F_{yh}}{F_{su}}\right] \qquad \textbf{(PE-8)}$$

(e)   Calculate the ultimate strain using equation (8-60)

$$\varepsilon_{su}^- = \varepsilon_{su}^+ + \left(\varepsilon_{su}^+ - \varepsilon_{sh}^+\right)\left[\frac{1 - \left|f_{cr}/f_{su}^+\right|}{1 - f_y^+/f_{su}^+}\right]^{1/p} \qquad \textbf{(PE-9)}$$

(f)   Calculate Θ_{buc} form equation (8-63)

$$\Theta_{buc} = \frac{\varepsilon_y^- - \varepsilon_{su}^-}{c''/D'' - d''/D''} \cdot \frac{D}{D''} \qquad \textbf{(PE-10)}$$

(g)   Plot Θ_{buc} as a horizontal line in $\phi_p D$ vs N_c plot.

10.7 NUMERICAL EXAMPLE

In this section two numerical examples are presented to illustrate the procedure of design of transverse reinforcement for columns. The first example is that of a shear dominated fixed-fixed column . Such a large squat column may be typically found on an approach ramp bridge in California. The column is presumed to be $1400\,mm$ in diameter, reinforced with 24 - D40 bars having a specified yield strength of $414\,MPa$. The column has a clear height of $2800\,mm$ thereby giving an aspect ratio of 2. Concrete used in the column is presumed to have an unconfined compression strength of $30\,MPa$.

The second example is that of a flexure dominated column having an outside diameter of $900\,mm$. The column is reinforced with 20 - $20\,mm$ bars having a specified yield strength of $414\,MPa$ and a clear height of $6000\,mm$. Such a tall slender is commonly found in multi-column pier bents of bridges in the eastern and central United States. Concrete is as before presumed to have an unconfined compression strength of $30\,MPa$.

As per the tenets of capacity design, failure due to fracture and fatigue of the longitudinal bars is the final and unavoidable mode of failure. Hence a satisfactory design should be such that the performance of the structural member is not beset by any other form of failure but low cycle fatigue of the longitudinal reinforcement. The purpose of these examples is to show how such an objective can be achieved through design procedures developed as part of this research project. A performance based evaluation is also performed at the end of each example to show that the design objective has been attained.

Preliminary calculations for example #1

Clear height of the column $H_{cl} := 2800$ mm

Diameter of the section $D := 1400$ mm

Number of longitudinal bars $N := 24$

Diameter of longitudinal bar $d_b := 40$ mm

Properties of longitudinal bars : $f_y := 414$ MPa $E_s := 200000$ MPa

$\varepsilon_{sut} := 0.12$; $\varepsilon_{sht} := 0.0089$; $E_{sht} := 8000$ Mpa $f_{su} := 640$ MPa

Assume diameter of horizontal reinforcement $d_{bh} := 20$ mm

Specified yield strength of horizontal reinforcement $f_{yh} := 414$ MPa

Unconfined compression strength of concrete $f_c := 30$ MPa

Assume clear cover in the column $cov := 50$ mm

$A_{bh} := \frac{\pi}{4} \cdot d_{bh}^2$ $A_{bh} = 314.1593$ mm^2

$D_{core} := D - 2 \cdot (cov + 0.5 \cdot d_{bh})$; $D_{core} = 1.28 \cdot 10^3$ mm

$D_{pitch} := D - 2 \cdot (cov + d_{bh} + 0.5 \cdot d_b)$; $D_{pitch} = 1.22 \cdot 10^3$ mm

$d_{core} := 0.5 \cdot (d_b + d_{bh})$; $d_{core} = 30$ mm

Let A_g/A_{cc} be represented by A_{rat}

$A_{rat} := \left(\frac{D}{D_{core}}\right)^2$ $A_{rat} = 1.1963$;

189

$$\rho_t = \frac{N \cdot d_b{}^2}{D^2} \qquad ; \qquad \rho_t = 0.0196 \qquad ; \qquad A_g := \frac{\pi}{4} \cdot D^2 \qquad A_g = 1.5394 \cdot 10^6 \qquad mm^2$$

Step 1: Antibuckling Steel

$$\rho_{sbuc} := 0.02 \cdot \frac{D}{d_b} \cdot \frac{f_y}{f_{yh}} \cdot \rho_t \qquad\qquad ; \qquad\qquad \rho_{sbuc} = 0.0137$$

$$s_{buc} := 4 \cdot \frac{A_{bh}}{\rho_{sbuc} \cdot D_{core}} \qquad\qquad ; \qquad s_{buc} = 71.5858 \qquad mm$$

Step 2: Confinement reinforcement

Since bridge columns are usually lightly loaded assume $P_e = 0.1275 f_c A_g$

$$P_e = 0.1275 \cdot f_c \cdot A_g \qquad ; \qquad P_e = 5.8881 \cdot 10^6 \qquad N$$

Also   assume $U_{sf} = 110 \qquad MJ/m^3$

$$\rho_{scon} := 0.008 \cdot \frac{f_c}{U_{sf}} \cdot \left[12 \cdot A_{rat}{}^2 \cdot \left(\frac{P_e}{f_c \cdot A_g} + \rho_t \cdot \frac{f_y}{f_c} \right)^2 - 1 \right]$$

$$\rho_{scon} = 0.0037 \qquad ; \qquad s_{con} := 4 \cdot \frac{A_{bh}}{\rho_{scon} \cdot D_{core}} \qquad ==> s_{con} = 261.8367 \qquad mm$$

<u>Step 3: Shear Reinforcement</u>

(a) Potential plastic hinge end regions governed by buckling or confinement

To start with assume that $\rho_{ssh} = \max(\rho_{sbuc}, \rho_{scon})$

$$\rho_{ssh} = 0.0137 \qquad ; \qquad \rho_v = 0.5 \cdot \rho_{ssh} \qquad ; \qquad \rho_v = 0.0069$$

Modulus of elasticity of concrete

$$E_c = 4700 \cdot \sqrt{f_c} \qquad\qquad E_c = 2.5743 \cdot 10^4 \qquad\qquad MPa$$

$$n = \frac{E_s}{E_c} \qquad\qquad n = 7.7691 \qquad\qquad \text{Also,} \qquad A_v = 0.8 \cdot A_g$$

$$\tan\alpha = \frac{D_{pitch}}{H_{cl}} \qquad\qquad \tan\alpha = 0.4357$$

Since the column is fixed-fixed assume $\qquad \zeta = .5704 \qquad$ and $\quad \Lambda = 2$

Tangent of the crack angle given by:

$$\tan\theta = \left(\frac{\rho_v \cdot n + \zeta \cdot \rho_v \cdot \dfrac{A_v}{A_g \cdot \rho_t}}{1 + \rho_v \cdot n} \right)^{0.25} \qquad\qquad \tan\theta = 0.6704 \qquad > \tan\alpha \ \ (O.K.)$$

Undercapacity factor for shear $\qquad \phi = 0.85$

Therefore, the required volumetric ratio of transverse steel from shear considerations is given by:

191

$$\rho_{ssh} = \Lambda \cdot \frac{2.4}{\pi} \cdot \frac{\rho_t}{\phi} \cdot \frac{f_{su}}{f_{yh}} \cdot A_{rat} \cdot \left[1 - \left[\frac{0.65 - \dfrac{P_e}{\phi \cdot f_c \cdot A_g}}{0.65 + 1.2 \cdot \rho_t \cdot \dfrac{f_{su}}{f_c}} \right]^2 \right] \cdot \tan\alpha \cdot \tan\theta$$

$$\rho_{ssh} = 0.0154$$

Therefore the shear reinforcement governs. It is neccessary to recalculate the crack angle with this new reinforcement ratio. After the second iteration the solution converges for $\rho_{sh} = 0.016$. The calculations are shown below.

$$\rho_{ssh} = 0.016 \qquad\qquad \rho_v = 0.5 \cdot \rho_{ssh} \qquad\qquad \rho_v = 0.008$$

$$\tan\theta = \left(\frac{\rho_v \cdot n + \zeta \cdot \rho_v \cdot \dfrac{A_v}{A_g \cdot \rho_t}}{1 + \rho_v \cdot n} \right)^{0.25} \qquad\qquad \tan\theta = 0.6955 \qquad > \tan\alpha \ \ (O.K.)$$

$$\rho_{ssh} = \Lambda \cdot \frac{2.4}{\pi} \cdot \frac{\rho_t}{\phi} \cdot \frac{f_{su}}{f_{yh}} \cdot A_{rat} \cdot \left[1 - \left[\frac{0.65 - \dfrac{P_e}{\phi \cdot f_c \cdot A_g}}{0.65 + 1.2 \cdot \rho_t \cdot \dfrac{f_{su}}{f_c}} \right]^2 \right] \cdot \tan\alpha \cdot \tan\theta$$

$$\rho_{ssh} = 0.016$$

$$s_{sh} = 4 \cdot \frac{A_{bh}}{\rho_{ssh} \cdot D_{core}} \qquad\qquad s_{sh} = 61.3032 \qquad\qquad mm$$

<u>Provide double D-20 @ 120 mm c/c.</u> Thus the provided ρ_s is

$s = 120$ mm $\qquad \rho_s := 4 \cdot \dfrac{2 \cdot A_{bh}}{s \cdot D_{core}}$ $\qquad$ ====> $\qquad \rho_s = 0.0164$

Step 4: Reinforcement Distribution

Since this is a shear dominated fixed-fixed column,

$$\lambda_s = \tan\alpha \cdot \left(\frac{1}{\tan\alpha} - \frac{2}{\tan\theta} - \tan\theta \right) \qquad . \qquad \lambda_s = -0.556$$

Since this term is negative it is neccessary to extend the same reinforcement over the entire height of the column.

Step 5: Performance Evaluation

Confinement coefficient $\qquad K := 1 + 2.7 \cdot \rho_s \cdot \dfrac{f_{yh}}{f_c}$ $\qquad$ ==> $\qquad K = 1.6097$

(a) Evaluation of Neutral Axis Depth

Let the c"/D" ratio be denoted by c_{rat}. As an initial value of this quadratic assume

$$c_{rat} := 0.2$$

Also the confined stress block parameter

$$\alpha_c = 0.667 \cdot \left(1 + \rho_s \cdot \frac{f_{yh}}{f_c} \right) \qquad\qquad \alpha_c = 0.8176$$

193

$$cD_{rat} = \text{root}\left[\left[\frac{\dfrac{P_e}{f_c \cdot A_g} + 0.5 \cdot \rho_t \cdot \dfrac{f_y}{f_c} \cdot \dfrac{1 - 2 \cdot c_{rat}}{1 - 2 \cdot \dfrac{d_{core}}{D_{core}}}}{1.32 \cdot \alpha_c \cdot \dfrac{K}{A_{rat}}}\right]^{0.725} - c_{rat}, c_{rat}\right]$$

$cD_{rat} = 0.239$ ---------------->This is the solution of the polynomial.

(b) Cofinement Envelope

$$\Theta_{con} = 4 \cdot \frac{0.008 + \rho_s \cdot \dfrac{U_{sf}}{f_c}}{\left[\rho_t \cdot \dfrac{f_y}{f_c} \cdot \left(0.5 + cD_{rat}\right) \cdot cD_{rat} \cdot \dfrac{D}{D_{core}} + \alpha_c \cdot K \cdot cD_{rat}^{2.38} \cdot \dfrac{D_{core}}{D}\right]}$$

$\Theta_{con} = 2.953$

(c) Low Cycle Fatigue Envelope

$$\Theta_{lcf} = \frac{0.113}{1 - 2 \cdot \dfrac{d_{core}}{D_{core}}} \cdot \frac{D}{D_{core}} \qquad\qquad \Theta_{lcf} = 0.1297$$

(d) Buckling Envelope

For evaluating the maximum sustainable stress, upper bound value of ultimate stress must be considered. Thus

194

$$f_{suup} = 1.2 \cdot f_{su} \qquad \text{---->} \qquad f_{suup} = 768 \qquad MPa$$

Equation (8-56) is plotted in figure 10-5. From it the maximum stress = $0.945 f_{suup}$

$$p := E_{sht} \cdot \left(\frac{\varepsilon_{sut} - \varepsilon_{sht}}{f_{suup} - f_y} \right) \qquad\qquad p = 2.5107$$

(e) Ultimate strain

$$f_{cr} := 0.945 \cdot f_{suup} \qquad\qquad \varepsilon_{suc} := \varepsilon_{sut} + \left(\varepsilon_{sht} - \varepsilon_{sut} \right) \cdot \left[\frac{1 - \dfrac{f_{cr}}{f_{suup}}}{1 - \dfrac{f_y}{f_{suup}}} \right]^{\frac{1}{p}}$$

$$\varepsilon_{suc} = 0.0724 \qquad\qquad \Theta_{buc} := \frac{\left(\varepsilon_{suc} - \dfrac{f_y}{E_s} \right) \cdot D}{cD_{rat} \cdot D_{core}}$$

$$\Theta_{buc} = 0.3217$$

Comments on the design:

It can be seen from the performance envelope plotted in figure 10-6, that the minimum plastic curvature corresponding to any given cycle correspond to that determined by low-cycle fatigue of the longitudinal reinforcement. Hence the performance criteria is satisfied.

195
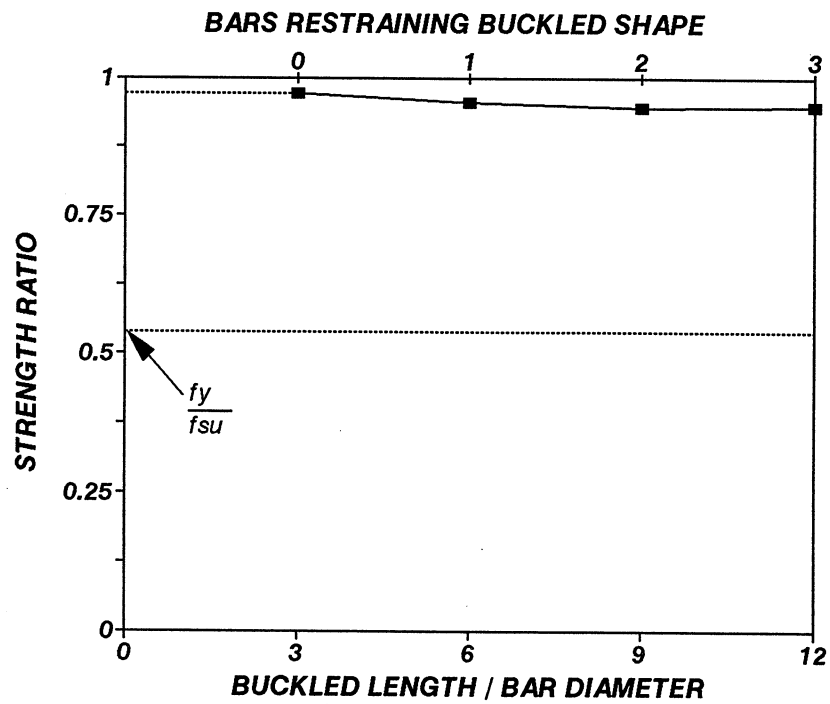
Figure 10-5 Buckling Performance.
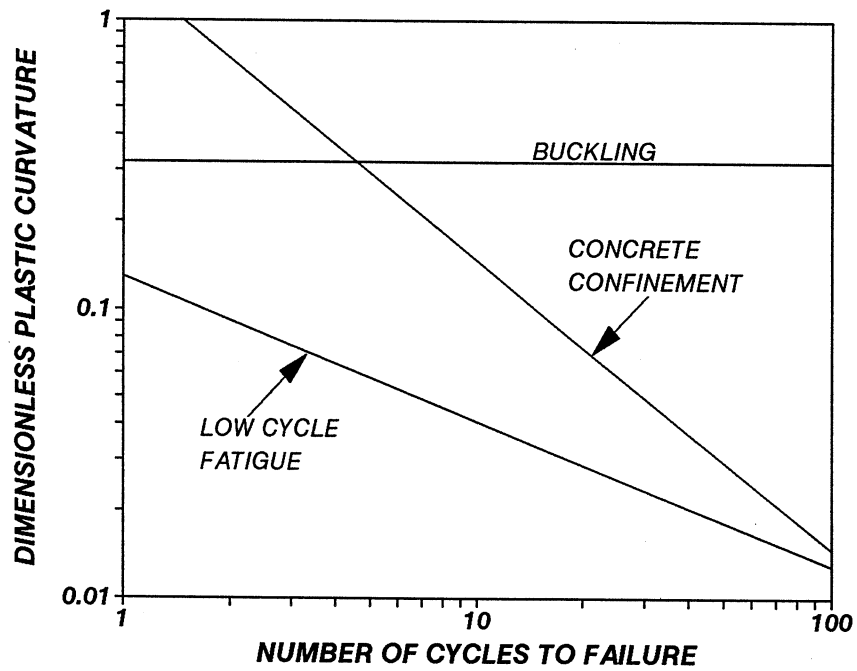
Figure 10-6 Fatigue Performance of the Desiged Column.

196

Preliminary calculations for example # 2

Clear height of the column $H_{cl} := 6000$ mm

Diameter of the section $D := 900$ mm

Number of longitudinal bars $N := 20$

Diameter of longitudinal bar $d_b := 28.6$ mm

Properties of longitudinal bars : $f_y := 414$ MPa $E_s := 200000$ MPa

$\varepsilon_{sut} := 0.12$; $\varepsilon_{sht} := 0.0089$; $E_{sht} := 8000$ Mpa $f_{su} := 640$ MPa

Assume diameter of horizontal reinforcement $d_{bh} := 16$ mm

Specified yield strength of horizontal reinforcement $f_{yh} := 414$ MPa

Unconfined compression strength of concrete $f_c := 30$ MPa

Assume clear cover in the column $cov := 50$ mm

$A_{bh} := \frac{\pi}{4} \cdot d_{bh}^2$ $A_{bh} = 201.0619$ mm^2

$D_{core} := D - 2 \cdot (cov + 0.5 \cdot d_{bh})$; $D_{core} = 784$ mm

$D_{pitch} := D - 2 \cdot (cov + d_{bh} + 0.5 \cdot d_b)$; $D_{pitch} = 739.4$ mm

$d_{core} := 0.5 \cdot (d_b + d_{bh})$; $d_{core} = 22.3$ mm

Let A_g / A_{cc} be represented by A_{rat}

$A_{rat} := \left(\frac{D}{D_{core}} \right)^2$ $A_{rat} = 1.3178$;

197

$$\rho_t := \frac{N \cdot d_b^2}{D^2} \qquad ; \qquad \rho_t = 0.0202 \qquad ; \qquad A_g := \frac{\pi}{4} \cdot D^2 \qquad A_g = 6.3617 \cdot 10^5 \qquad mm^2$$

Step 1: Antibuckling Steel

$$\rho_{sbuc} := 0.02 \cdot \frac{D}{d_b} \cdot \frac{f_y}{f_{yh}} \cdot \rho_t \qquad ; \qquad \rho_{sbuc} = 0.0127$$

$$s_{buc} := 4 \cdot \frac{A_{bh}}{\rho_{sbuc} \cdot D_{core}} \qquad ; \qquad s_{buc} = 80.7031 \qquad mm$$

Step 2: Confinement reinforcement

Since bridge columns are usually lightly loaded assume $P = 0.11 f_c A_g$

$$P := 0.11 \cdot f_c \cdot A_g \qquad ; \qquad P = 2.0994 \cdot 10^6 \qquad N$$

Also assume $\qquad U_{sf} := 110 \qquad MJ/m^3$

$$\rho_{scon} := 0.008 \cdot \frac{f_c}{U_{sf}} \cdot \left[12 \cdot A_{rat}^2 \cdot \left(\frac{P}{f_c \cdot A_g} + \rho_t \cdot \frac{f_y}{f_c} \right)^2 - 1 \right]$$

$$\rho_{scon} = 0.0047$$

$$s_{con} := 4 \cdot \frac{A_{bh}}{\rho_{scon} \cdot D_{core}} \qquad s_{con} = 218.8071 \qquad mm$$

198

Step 3: Shear Reinforcement

(a) Potential plastic hinge end regions governed by buckling or confinement

To start with assume that $\rho_{ssh} = \max(\rho_{sbuc}, \rho_{scon})$

$$\rho_{ssh} := \begin{vmatrix} \rho_{sbuc} & \text{if} & \rho_{sbuc} \geq \rho_{scon} \\ \rho_{scon} & \text{otherwise} \end{vmatrix}$$

$\rho_{ssh} = 0.0127$

$\rho_v := 0.5 \cdot \rho_{ssh}$ $\qquad \rho_v = 0.0064$

$E_c := 4700 \cdot \sqrt{f_c}$ $\qquad E_c = 2.5743 \cdot 10^4$ $\qquad$ MPa

$n := \dfrac{E_s}{E_c}$ $\qquad n = 7.7691$ $\qquad$ Also, $\quad A_v := 0.8 \cdot A_g$

$\tan\alpha := \dfrac{D_{pitch}}{H_{cl}}$ $\qquad \tan\alpha = 0.1232$

Since the column is fixed-fixed assume $\qquad \zeta := .5704 \qquad$ and $\quad \Lambda := 2$

$$\tan\theta := \left(\dfrac{\rho_v \cdot n + \zeta \cdot \rho_v \cdot \dfrac{A_v}{A_g \cdot \rho_t}}{1 + \rho_v \cdot n} \right)^{0.25} \qquad \tan\theta = 0.6549 \qquad > \tan\alpha \ (O.K.)$$

199

Undercapacity factor for shear $\phi := 0.85$

$$\rho_{ssh} := \Lambda \cdot \frac{2.4}{\pi} \cdot \frac{\rho_t}{\phi} \cdot \frac{f_{su}}{f_{yh}} \cdot A_{rat} \cdot \left[1 - \left[\frac{0.65 - \dfrac{P}{\phi \cdot f_c \cdot A_g}}{0.65 + 1.2 \cdot \rho_t \cdot \dfrac{f_{su}}{f_c}} \right]^2 \right] \cdot \tan\alpha \cdot \tan\theta$$

$\rho_{ssh} = 0.0048$

Thus this is a flexure dominated column in which antibuckling reinforcement governs. _Provide double D-16 @ 150 mm c/c._ Thus the provided ρ_s is

$s := 150$ mm $\rho_s := 4 \cdot \dfrac{2 \cdot A_{bh}}{s \cdot D_{core}}$ ====> $\rho_s = 0.0137$

Since the provided lateral reinforcement is even greater than the required buckling reinforcement, crack angle is not recalculated using $\rho_{ssh}=0.0137$

Step 4: Reinforcement Distribution

It is necessary to calculate the nominal moment and the overstrength factor at this point. Although a detailed moment curvature analysis can yield the overstrength factor, in lieu of such detailed calculation, an alternative method proposed by Mander et al. (1997) can be used. Readers can refer to the respective literature and only relevant results are used here.

The nominal moment, $M_n := 1924$ kN-m

The overstrength moment $M_{po} := 2690$ kN-m.

200

The overstrength factor $\qquad \lambda_{mo} := \dfrac{M_{po}}{M_n} \qquad\qquad \lambda_{mo} = 1.3981$

Assuming the yield moment My is approximately 75% of the nominal moment,

$$M_y := 0.75 \cdot M_n$$

$$\lambda_{sf} := \left(\frac{M_y}{M_{po}} - \tan\alpha \cdot \tan\theta \right) \qquad\qquad \lambda_{sf} = 0.4557$$

Also,

$$\lambda_{ssh} := \tan\alpha \cdot \left(\frac{1}{\tan\alpha} - \frac{2}{\tan\theta} - \tan\theta \right) \qquad\qquad \lambda_{ssh} = 0.5429$$

$$\lambda_s := \begin{vmatrix} \lambda_{sf} & \text{if } \lambda_{ssh} \geq \lambda_{sf} \\ \lambda_{ssh} & \text{otherwise} \end{vmatrix} \qquad\qquad \lambda_s = 0.4557$$

Maximum overstrength shear

$$V_{po} = \frac{2 \cdot M_{po} \cdot 1000}{H_{cl}} \qquad\qquad V_{po} = 896.6667 \qquad\qquad kN.$$

Outside the plastic hinge zone concrete contribution will be accounted for.
Thus, $V_{po} = V_c + V_p + V_s$ where

$$V_p := \frac{0.85 \cdot P \cdot \tan\alpha}{1000} \qquad\qquad V_p = 219.9054 \qquad\qquad kN.$$

201

$$v_c = 0.167 \cdot \sqrt{f_c} \qquad\qquad v_c = 0.9147 \qquad\qquad MPa$$

$$V_c := \frac{v_c \cdot A_v}{1000} \qquad\qquad V_c = 465.5239 \qquad\qquad kN.$$

$$V_s := \frac{V_{po}}{\phi} - V_c - V_p \qquad\qquad V_s = 369.4726 \qquad\qquad kN.$$

Assume an initial crack angle of 30 degrees. Thus the required lateral reinforcement spacing,

$$\theta := 30 \qquad\qquad tand(\theta) := tan(\theta \cdot deg)$$

$$s_{out} := \frac{\pi}{2} \cdot \frac{A_{bh} \cdot f_{yh} \cdot D_{core}}{V_s \cdot 1000 \cdot tand(\theta)} \qquad\qquad s_{out} = 480.5565 \qquad\qquad mm$$

But the maximum allowable spacing is s = 6*db. <u>Therefore outside the plastic hinge zone provide single D-16 @150 mm c/c.</u>

$$\rho_{sout} := \frac{4 \cdot A_{bh}}{150 \cdot D_{core}} \qquad\qquad \rho_{sout} = 0.0068$$

$$\rho_{vout} := 0.5 \cdot \rho_{sout} \qquad\qquad \rho_{vout} = 0.0034$$

Recalculate the crack angle using the provided ρ_s

$$tan\theta := \left(\frac{\rho_{vout} \cdot n + \zeta \cdot \rho_{vout} \cdot \dfrac{A_v}{A_g \cdot \rho_t}}{1 + \rho_{vout} \cdot n} \right)^{0.25}$$

$$tan\theta = 0.5639 \qquad (=29.5\ deg)$$

Note this is very close to the assumed 30 deg. Hence no change is required.

Summary of lateral reinforcement:

For the top and bottom 1650 mm, provide double D-16 @ 150 mm c/c. Rest provide single D-16 @ 150 mm c/c.

Step 5: Performance Evaluation

Confinement coefficient $\qquad K := 1 + 2.7 \cdot \rho_s \cdot \dfrac{f_{yh}}{f_c} \qquad ; \qquad K = 1.5096$

(a) Evaluation of Neutral Axis Depth

Let the c"/D" ratio be denoted by c_{rat}. As an initial value of this quadratic assume

$$c_{rat} := 0.2$$

Also the confined stress block parameter

$$\alpha_c := 0.667 \cdot \left(1 + \rho_s \cdot \dfrac{f_{yh}}{f_c} \right) \qquad \alpha_c = 0.7929$$

203

$$cD_{rat} := \text{root}\left[\left[\frac{\dfrac{P}{f_c \cdot A_g} + 0.5 \cdot \rho_t \cdot \dfrac{f_y}{f_c} \cdot \dfrac{1 - 2 \cdot c_{rat}}{1 - 2 \cdot \dfrac{d_{core}}{D_{core}}}}{1.32 \cdot \alpha_c \cdot \dfrac{K}{A_{rat}}}\right]^{0.725} - c_{rat}, c_{rat}\right]$$

$cD_{rat} = 0.2554$ ---------------->This is the solution of the polynomial.

(b) Cofinement Envelope

$$\Theta_{con} := 4 \cdot \frac{0.008 + \rho_s \cdot \dfrac{U_{sf}}{f_c}}{\left[\rho_t \cdot \dfrac{f_y}{f_c} \cdot (0.5 + cD_{rat}) \cdot cD_{rat} \cdot \dfrac{D}{D_{core}} + \alpha_c \cdot K \cdot cD_{rat}^{2.38} \cdot \dfrac{D_{core}}{D}\right]}$$

$\Theta_{con} = 2.2755$

(c) Low Cycle Fatigue Envelope

$$\Theta_{lcf} := \frac{0.113}{1 - 2 \cdot \dfrac{d_{core}}{D_{core}}} \cdot \frac{D}{D_{core}}$$
        $\Theta_{lcf} = 0.1375$

(d) Buckling Envelope

For evaluating the maximum sustainable stress, upper bound value of ultimate stress should be considered. Thus,

$$f_{suup} := 1.2 \cdot f_{su} \qquad \text{----->} \qquad f_{suup} = 768 \qquad MPa$$

Equation (8-56) is plotted in figure 10-7. From it the maximum stress = $0.7 \, f_{suup}$

$$p = E_{sht} \cdot \left(\frac{\varepsilon_{sut} - \varepsilon_{sht}}{f_{suup} - f_y} \right) \qquad\qquad p = 2.5107$$

(e) Ultimate Strain

$$f_{cr} := 0.7 \cdot f_{suup} \qquad\qquad \varepsilon_{suc} := \varepsilon_{sut} + \left(\varepsilon_{sht} - \varepsilon_{sut} \right) \cdot \left[\frac{1 - \dfrac{f_{cr}}{f_{suup}}}{1 - \dfrac{f_y}{f_{suup}}} \right]^{\frac{1}{p}}$$

$$\varepsilon_{suc} = 0.0264 \qquad\qquad \Theta_{buc} := \frac{\left(\varepsilon_{suc} - \dfrac{f_y}{E_s} \right) \cdot D}{cD_{rat} \cdot D_{core}}$$

$$\Theta_{buc} = 0.1092$$

Comments on the design:

It can be seen from the performance envelope plotted in figure 10-8, that the minimum plastic curvature corresponding to any given cycle > 2 correspond to that determined by low-cycle fatigue of the longitudinal reinforcement. However it is realized that for cycles < 2 the cover concrete will still be effective in restraining buckling. A a result a little latitude can be exercised in the design of transverse reinforcement for antibuckling. Hence the performance criteria can be conidered to have been satisfied.
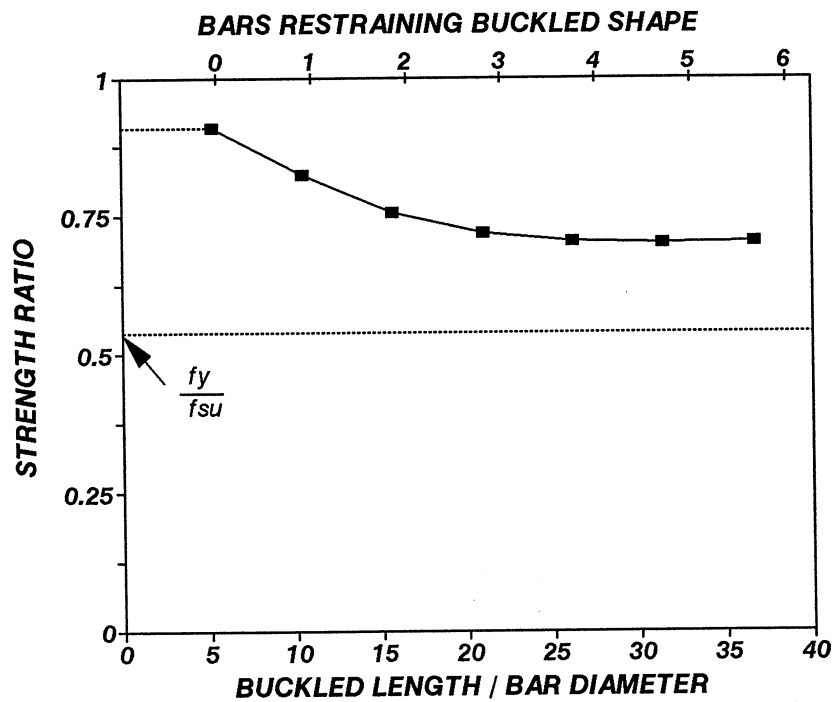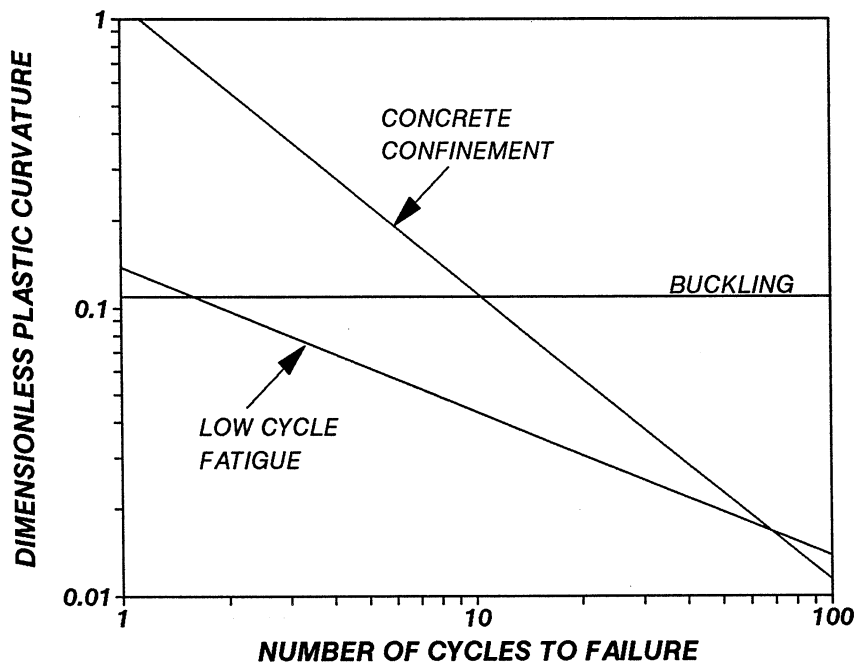
Figure 10-7 Buckling Performance.

Figure 10-8 Fatigue Performance of the Desiged Column.

206

SECTION 11

EPILOGUE

11.1 EXECUTIVE SUMMARY

When using the capacity design philosophy for designing earthquake resistant structures, the designer chooses a hierarchy of failure mechanisms. Inelastic (plastic) modes of deformation which provide ductility are preferred; this generally means flexural plastic hinging through ductile detailing. All other undesirable brittle failure mechanisms such as shear, bond and anchorage, compression failure (of both bars and concrete) are inhibited. Brittle regions are protected by ensuring their strength exceeds the demands originating from the maximum overstrength that can be generated at potential plastic hinge zones.

Using the above-mentioned principles of capacity design, it has been found that the last and unavoidable mode of failure in a reinforced concrete beam-column is the fatigue and fracture of the longitudinal reinforcement. Thus a designer's main objective should be to prolong this particular mode of failure as long as practicable and ensure that it is preceded by no other modes that might debilitate the structure. It has been observed experimentally, and theoretically, that such an objective can be attained by providing adequate hoop reinforcement the function of which is threefold: to confine the core concrete, to restrain longitudinal bars from buckling and to provide shear resistance. Each of these issues need to be considered if a designer is to detail a structural concrete element and expect satisfactory performance in a seismic event. Since this research is primarily concerned with ductile detailing of reinforced concrete sections, an in-depth study of each of these issues was made. Theoretical models capable of predicting the behavior of concrete elements were developed and validated against experimental observations. Specific design problems were also tackled and simplified expressions were derived that will impede all the possibilities of brittle failure when used in new construction.

207

11.2 PERFORMANCE EVALUATION

As for the requirements of the emerging Performance Based Design philosophy, a designer is required to evaluate the performance of the designed member. This includes the evaluation of the fatigue performance that yields the maximum plastic curvature obtainable from a section corresponding to a particular number of cycles. This is explained with reference to figure 11-1 which shows the pattern in which the ultimate fatigue capacity is related to the number of cycles. It can be seen that failures governed by concrete decay (i.e. hoop fracture) and longitudinal steel fatigue is dependant on the level of plastic straining and hence on the number of cycles. However, failure governed by buckling is essentially dependant on the level of plastic straining under monotonic loading. Following the principles of capacity design where the designer is expected to eliminate all undesirable modes of failure, a desirable design is such that the maximum plastic curvature capacity should correspond to the curvature demand imposed by low cycle fatigue of the longitudinal reinforcement. This will ensure ductile performance and proper hierarchy of failure mechanisms in accordance with the capacity design philosophy. A rational way to achieve this objective was shown in this research. Through a systematic analysis of the various failure mechanisms it was demonstrated how superior performance can be achieved from a concrete column if provisions are made for adequate transverse reinforcement leaving low cycle fatigue as the only failure mode which is essentially unavoidable.

11.3 FINAL CONCLUSIONS

Specific conclusions derived from this study are as follows:

(i)   Ductility of a reinforced concrete section depends almost entirely on the availability of adequate confining reinforcement. Since in capacity design philosophy the most desirable mode of failure is through low cycle fatigue of the longitudinal reinforcement, adequate transverse reinforcement needs to be provided so that proper hierarchy of failure modes is maintained.

208

(ii)   In a well designed reinforced concrete element, the ultimate curvature can be set to the limit state of horizontal bar fracture. Using the energy based methodology proposed in this research, such failure state can be dependably forecast.

(iii)   Longitudinal bar buckling in a reinforced concrete element can be detrimental from performance considerations. Present code provisions which are based on simple compression tests assume rigid end restraint in a bar segment which is not the case in a plastic hinge zone. This results in deficient design criteria, as has been portrayed repeatedly in simulated seismic load tests. A more rational approach is to allow limited buckling, taking into account yielding of hoops, and to expect the longitudinal steel to sustain a desired level of stress.

(iv)   Brittle shear failure of concrete members can also be extremely debilitating especially under seismic conditions. However, there is a tremendous inconsistency amongst the design approaches currently in use. Furthermore, most of the empirical methods are modified to be overconservative thereby undermining the spirit of limit based design. The proposed method overcomes these ambiguities and presents a more logical approach to the concept of shear design.

11.4 DIRECTIONS FOR FUTURE RESEARCH

This research was principally aimed at validating the energy based evaluation methodology for confined concrete sections. Experimental results of various researchers were used to verify the authenticity of the developed expressions. The principal assumption in the theoretical development was that the various failure modes are unrelated and the outcome of one particular mode has little effect on the other. However, in an actual scenario this may strictly not be the case. Moreover, all the test results were obtained from published literature where there is not always (due to space restrictions) an adequately detailed description of the failure progression. Notwithstanding this impediment, every effort was made to isolate test results and use only those that truly conform to a particular mode of failure. Unfortunately, failure modes like buckling and hoop fracture are oftentimes very closely related. Thus an experimental result

that showed hoop fracture, might actually be brought about while restraining the longitudinal bar from global buckling. In light of this it is realized that carefully detailed tests are required whereby it will be possible to identify and isolate all the possible failure types. This will greatly help in identifying the limitations of the energy based expressions, if any, and suggest improvements in the future.
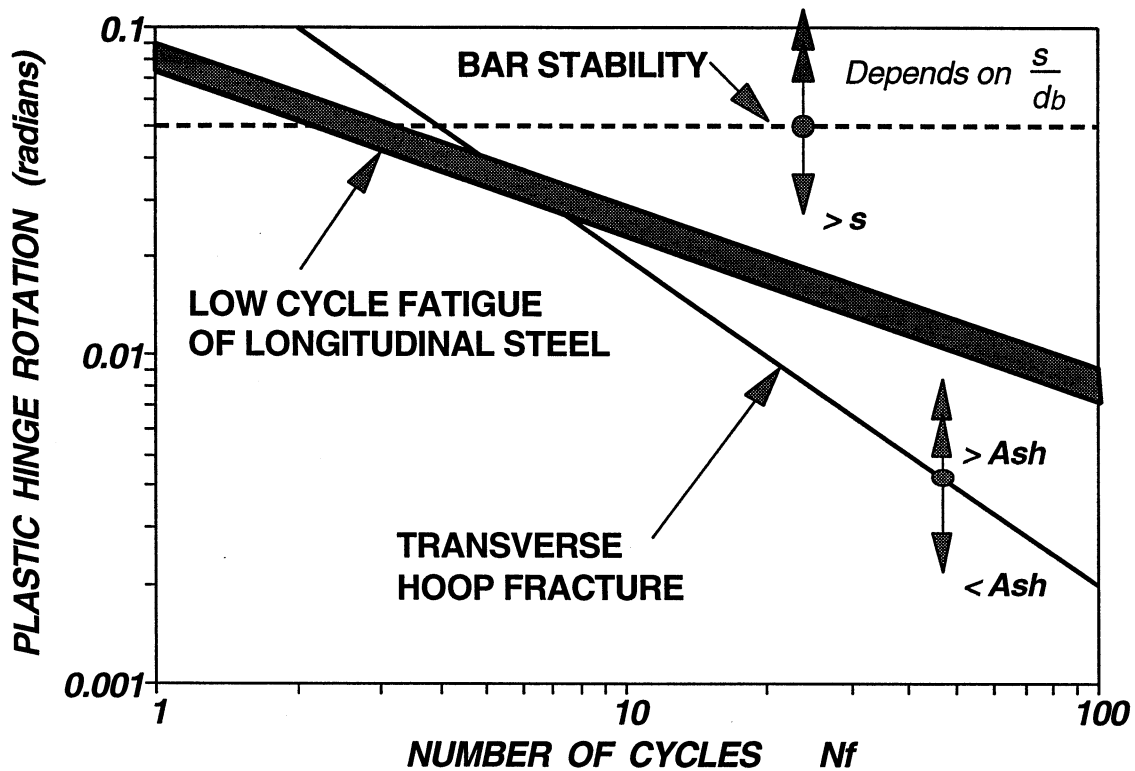

Figure 11-1 General Fatigue Theory for Confined Concrete Sections.

SECTION 12
REFERENCES

AASHTO (1996), *AASHTO Standard Specification for Highway Bridges*, 16th. ed.,American Association of State Highway and Transportation Officials, Washington, D.C.

AASHTO (1994), *AASHTO LRFD Bridge Design Specifications*, 1st ed., American Association of State Highway and Transportation Officials, Washington, D.C.

American Concrete Institute, (1995), *Building Code Requirements for Reinforced Concrete*, ACI-318-95, Detroit, Michigan.

Ang Beng Ghee, Priestley, M.J.N. and Paulay, T., (1989), "Seismic Shear Strength of Circular Reinforced Concrete Columns", ACI Structural Journal, Vol. 86, No.1, pp. 45-59.

Aschheim, M. (1997), "Seismic Vulnerability, Evaluation, Retrofit, and New Design of California Bridges-an Overview", *Proceedings* of the U.S.-Italian Workshop on Seismic Evaluation and Retrofit, Technical Report NCEER-97-0003, National Center for Earthquake Engineering Research, State University of New York at Buffalo.

Aschheim, M. and Moehle, J.P., (1992), *Shear Strength and Deformability of RC Bridge Columns Subjected to Inelastic Cyclic Displacement*, Report No. UCB/EERC 92/04, Earthquake Engineering Research Center, University of California at Berkeley, March-92.

ATC-32, (1996), *Improved Seismic Design Criteria for California Bridges: Provisional Recommendations*, Applied Technology Council, Redwood City, California.

Bresler, B. and Gilbert, P.H., (1961), "Tie Requirements for Reinforced Concrete Columns", ACI Journal, Vol.58, No.26, pp.555-570.

CDP 810/A, (1975), *Ductility of Bridges with Reinforced Concrete Piers*, Civil Division Publication, Ministry of Works and Development, Wellington.

CDP 701/D, (1978), *Highway Bridge Design Brief*, Civil Division Publication, Ministry of Works and Development, Wellington.

Chang, G.A. and Mander, J.B., (1994a), *Seismic Energy Based Fatigue Damage Analysis of Bridge Columns: Part I - Evaluation of Seismic Capacity*, Technical Report NCEER-94-0006, National Center for Earthquake Engineering Research, State University of New York at Buffalo.

Chang, G.A. and Mander, J.B.,(1994b), *Seismic Energy Based Fatigue Damage Analysis of Bridge Columns: Part II - Evaluation of Seismic Demand*, Technical Report NCEER-94-0013, National Center for Earthquake Engineering Research, State University of New York at Buffalo.

Chapra, S.C. and Canale, R.P.,(1995), *Numerical Methods for Engineers*, McGraw Hill Publishing Co., New York.

Cheng, C.T., (1997), *New Paradigms for the Seismic Design and Retrofit of Bridges*, Ph.D. Dissertation, Department of Civil Engineering, State University of New York at Buffalo, Buffalo, New York.

Coffin, L.F. Jr. (1954), "A Study of the Effects of Cyclic Thermal Stresses on a Ductile Metal", Transactions, American Society of Mechanical Engineers, New York, N.Y., vol. 76, pp. 931-950.

Collins, M.P. and Mitchell, D., (1991), *Prestressed Concrete Structures*, Prentice-Hall, Inc.

Dutta, A., (1995), *Fatigue Analysis of Non-Ductile Concrete Columns*, M.S. Thesis, Department of Civil Engineering, State University of New York at Buffalo, Buffalo, New York.

Engesser, F.Z., (1898), *Ver. deut. Ingr.*, vol-42, pp.927.

Goel, P. (1996), *On the Analysis of Flexural Overstrength in Capacity Design of Reinforced Concrete Structures*, M.S. Thesis, Department of Civil Engineering, State University of New York at Buffalo, Buffalo, New York.

Gomes, A. and Appleton, J., (1997), "Nonlinear Cyclic Stress-Strain Relationship of Reinforcing Bars including Buckling", Engineering Structures, Vol.19, No.10, pp.822-826.

Housner, G.W., (1956), "Limit Design of Structures to Resist Earthquake," *Proceedings* of 1st World Conference on Earthquake Engineering, Berkeley, California.

Ingham, J.M., Priestley, M.J.N. and Seible, F., (1997), "Seismic Response of Bridge Knee Joints Having Columns with Interlocking Spirals", Bulletin of the New New Zealand National Society for Earthquake Engineering, Vol.30, No.2, June-97, pp.114-132.

Kent, D.C. and Park, R.,(1971), "Flexural Members with Confined Concrete", Journal of the Structural Division, ASCE, Vol.97, No. ST7, Jul-71, pp.1969-1990.

Kim, J.H., (1996), *Seismic Evaluation of Shear-Critical Reinforced Concrete Columns and their Connections*, Ph.D. Dissertation, Department of Civil Engineering, State University of New York at Buffalo, Buffalo, New York.

Kim, J.H. and Mander, J.B., (1998), *Fundamental Shear-Flexure Interaction Theory for Strength and Deformation Analysis of Structural Concrete Elements*, Technical Report MCEER-97-00XX (to be published), Multidiciplinary Center for Earthquake Engineering Research, State University of New York at Buffalo.

Koh, S.K., Stephen, R.I., (1991), "Mean Stress Effects on Low-Cycle Fatigue for a High Strength Steel," Fatigue Fracture of Engineering Materials and Structure, Vol.14, No.4, pp.413-428.

Mander, J.B., Dutta, A. and Goel, P., (1998), *Capacity Design of Bridge Piers and the Analysis of Overstrength*, Technical Report MCEER-98-0003, Multidiciplinary Center for Earthquake Engineering Research, State University of New York at Buffalo.

Mander, J.B., Panthaki, F.D., and Kasalanati, A., (1994), "Low Cycle Fatigue Behavior of Reinforcing Steel," Journal of Materials in Civil Engineering, ASCE, Vol.6, No.4, pp.453-467.

Mander, J.B., Pekcan, G., and Chen, S.S., (1995a), "Low-Cycle Variable Amplitude Fatigue Modeling of Top-and-Seat Angle Connections," Engineering Journal, AISC, Vol.32, No.2.

Mander, J.B., Priestley, M.J.N. and Park, R.,(1988a), "Theoretical Stress-Strain Model for Confined Concrete", Journal of Structural Engineering, Vol.114, No.8, Aug-88, pp.1804-1826.

Mander, J.B., Priestley, M.J.N. and Park, R.,(1988b), "Observed Stress-Strain Behavior of Confined Concrete", Journal of Structural Engineering, Vol.114, No.8, Aug-88, pp.1827-1849.

Mander, J.B., Priestley, M.J.N. and Park, R., (1984), *Seismic Design of Bridge Piers*, Department of Civil Engineering, University of Canterbury, Report 84-2, Feb-84, 483 pp.

Mander, J.B., Priestley, M.J.N. and Park, R.,(1983), "Behavior of Ductile Hollow Reinforced Concrete Columns", Bulletin of the New Zealand National Society for Earthquake Engineering, Vol.16, No.4, Dec-83, pp.273-290.

Mander, J.B., and Cheng, C.T., (1995), "Renewable Hinge Detailing for Bridge Columns", Pacific Conference on Earthquake Engineering, Australia, pp.197-206.

Manson, S.S, (1953), "Behavior of Materials under Conditions of Thermal Stress," Heat Transfer Symposium, University of Michigan Engineering Research Institute.

Monti, G. and Nuti, C. (1992), "Nonlinear Cyclic Behavior of Reinforcing Bars Including Buckling", Journal of Structural Engineering, Vol.118, No.12, Dec-92, pp.3268-3284.

Osgood, W.R., (1935), "The Double Modulus Theory of Column Action"' Civil Engineering, Vol.5, No. 3, May-35, pp.173-175.

Papia, M., Russo,G. and Zingone, (1988), "Instability of Longitudinal Bars in RC Columns", Journal of Structural Engineering, Vol.114, No.2, pp.445-461.

Park, R. and Paulay, T.,(1975), *Reinforced Concrete Structures*, John Wiley, New York, 1975.

Park, R., Priestley, M.J.N., Park, R. and Gill, W.D., (1992), "Ductility of Square-Confined Concrete Columns", *Proceedings* ASCE, Structural Division, Vol. 108, No. ST4, April-82, pp. 929-950.

Paulay, T. and Priestley, M.J.N., (1992), *Seismic Design of Reinforced Concrete and Masonry Structures*, John Wiley and Sons, Inc., New York.

Popovics, S.,(1970), "A Review of Stress-Strain Relationship for Concrete", Journal of the American Concrete Institute, Vol.67, No.3, Mar-70, pp.243-248.

Priestley, M.J.N., Park, R. and Potangaroa, R.T., (1981), "Ductility of Spirally-Confined Concrete Columns", *Proceedings* ASCE, Structural Division, Vol. 107, No. ST1, January-81, pp. 181-202.

Priestley, M.J.N, Seible, F. and Calvi, G. M., (1996), *Seismic Design and Retrofit of Bridges*, John Wiley and Sons, Inc., New York.

Priestley, M.J.N., Seible, F., Xiao, Y., and Verma, R., (1994a), "Steel Jacketed Retrofitting of Reinforced Concrete Bridge Columns for Enhanced Shear Strength-Part 1 : Theoretical Considerations and Test Design," ACI Structural Journal, Vol. 91, No.4, pp.394-405.

Priestley, M.J.N., Seible, F., Xiao, Y., and Verma, R., (1994b), "Steel Jacketed Retrofitting of Reinforced Concrete Bridge Columns for Enhanced Shear Strength-Part 2 : Test Results and Comparison with Theory," ACI Structural Journal, 1994, Vol.91, No.5, pp.537-551.

Priestley, M.J.N., Verma, R., and Xiao, Y., (1994c), "Seismic Shear Strength of Reinforced Concrete Columns", Journal of Structural Engineering, ASCE, Vol.120, No.8, pp.2310-2329.

Richart, F.E., Brandtzaeg, A. and Brown, R.L., "The Failure of Plain and Spirally Reinforced Concrete in Compression", University of Illinois Engineering Experimental Station, Bulletin No. 190, 1929, pp. 74.

Schlaich, J., Schaeffer, K. and Jennewein, M., (1987), "Toward a Consistent Design of Structural Concrete", PCI Journal, Vol.32, No.3, May-June, pp.74-150.

Scribner, C.F., (1986), "Reinforcement Buckling in Reinforced Concrete Flexural Members", ACI Journal, Vol.83, No.85, pp.966-973.

Shahawy, M.A., and deV Batchelor, B., (1996), "Shear Behavior of Full-Scale Prestressed Concrete Girder: Comparison Between AASHTO Specifications and LRFD Code", PCI Journal, Vol.41, No.3, May-June-96, pp.48-62.

Shahawy, M.A., and dev Batchelor, B., (1996), "Shear Behavior of Full-Scale Prestressed Concrete Girder: Comparison Between AASHTO Specifications and LRFD Code", *Reader Comments*, PCI Journal, Vol.42, No.3, May-June-97, pp.72-93.

Shanley, F.R., (1947), "Inelastic Column Theory", Journal of the Aeronautical Sciences, Vol.14, No.5, pp. 261-268.

Standards New Zealand (1995), *New Zealand Code of Practice for the Design of Concrete Structures*, NZS 3101:1995 Part 1 and 2, Standards Association of New Zealand, Wellington.

Tsai, W.T., (1988), "Uniaxial Compressional Stress-Strain Relations of Concrete", Journal of Structural Engineering, ASCE, Vol.114, No.8, Sep-88, pp.2133-2136.

Uang, C.M., and Bertero, V.V., (1990), "Evaluation of Seismic Energy in Structures", Earthquake Engineering and Structural Dynamics, Vol.19.

Vecchio, F.J. and Collins, M.P., (1986), "The Modified Compression-Field Theory for Reinforced Concrete Elements Subjected to Shear", ACI Journal, Vol.83, No.2, pp.219-231.

Von Karman, Th., (1909), "Untersuchungen Uber Knic Festigkeit", Mitt. U. Forschungsarb. d.V.D.I., Heft 81, Berlin.

Watson, S., (1986), *Limited Ductility Design of Reinforced Concrete Columns*, Department of Civil Engineering, University of Canterbury, Report 86-10, March-86, 209 pp.

Watson, S., Zahn, F.A. and Park, R., (1994), "Confining Reinforcement for Concrete Columns", Journal of Structural Engineering, Vol.120, No.6, June-94, pp.1798-1824.

Yuk Lung Wong, (1990), *Squat Circular Bridge Piers Under Multi-Directional Seismic Attack*, Ph.D. Thesis, Department of Civil Engineering, University of Canterbury, Christchurch, New Zealand.

Zahn, F.A., (1986), *Design of Reinforced Concrete Bridge Columns for Strength and Ductility*, Research Report 86-7, Department of Civil Engineering, University of Canterbury, Christchurch, New Zealand.

APPENDIX A
STRESS-STRAIN EQUATIONS AND STRESS BLOCK PARAMETERS FOR UNCONFINED AND CONFINED CONCRETE

A-1 EQUATION FOR UNCONFINED CONCRETE

The equation to describe the monotonic compressive stress-strain curve for unconfined concrete is based on Tsai's (1988) equation:

$$y = \frac{nx}{1 + \left(n - \frac{r}{r-1}\right)x + \frac{x^r}{r-1}} \tag{A-1}$$

where $x = \varepsilon_{co}/\varepsilon_c'$, $y = f_{co}/f_c'$ with f_c' and ε_c' being the peak ordinate and the corresponding abscissae, and n,r are parameters to control the shape of the curve.

The equation parameter n is defined by the initial modulus of elasticity, the concrete strength and the corresponding strain. In S.I. units, the initial modulus of elasticity and strain at peak stress are given by

$$E_c = 8200 f_c'^{3/8}$$
$$\varepsilon_c' = \frac{f_c'^{1/4}}{1153} \tag{A-2}$$

Thus the parameter n is defined as:

$$n = \frac{E_c \varepsilon_c'}{f_c'} = \frac{E_c}{E_{sec}} = \frac{7.2}{f_c'^{3/8}} \quad MPa \tag{A-3}$$

and the parameter r as:

$$r = \frac{f_c'}{5.2} - 1.9 \quad MPa \tag{A-4}$$

However, to adequately reflect the behavior of unconfined cover concrete, a modification as suggested by Mander et al. (1988a) was adopted. It was decided that the cover concrete beyond a strain of $2\varepsilon_c'$ would be made to decay to zero linearly up to a strain ratio of x_{max} according to where $y_{2\varepsilon_c'}$ = normalized stress at $x = 2$ and $\tan\alpha = 1/|dy/dx|_{2\varepsilon_c'}$, with

217

$$y = y_{2\varepsilon_c'} - \frac{x-2}{\tan\alpha} \tag{A-5}$$

$$\left(\frac{dy}{dx}\right)_{2\varepsilon_c'} = \frac{n\left(1-2^r\right)}{\left[1+2\left(n-\frac{r}{r-1}\right)+\frac{2^r}{r-1}\right]^2} \tag{A-6}$$

and

$$x_{max} = 2 + y_{2\varepsilon_c'}\tan\alpha \tag{A-7}$$

A-2 Equation for Confined Concrete

The same equation A-1 can be used to describe the behavior of confined concrete. The peak strength enhancement due to ductility can be obtained using the procedure suggested by Mander et al. (1984, 1988a) and described in detail in subsections A-2.1 and A-2.2. Thus in equation A-1, the parameters can be redefined for confined concrete as $x = \varepsilon_{cc}/\varepsilon_{cc}'$ and $y = f_{cc}/f_{cc}'$ where f_{cc}' and ε_{cc}' are the confined concrete peak ordinate $(= Kf_c')$ and the corresponding abscissae given by Richart et al.(1929) as

$$\varepsilon_{cc}' = \varepsilon_c'(1+5(K-1)) \tag{A-8}$$

However, in order to have better control on the falling branch of the confined concrete, Mander et al. (1988b) based on experimental observations added a point on the falling branch. The following empirical relationship was proposed

$$\varepsilon_f = 3\,\varepsilon_{cc}'$$
$$f_f = f_{cc}' - \Delta f_{cc} \tag{A-9}$$
$$\Delta f_{cc} = K\,\Delta f_c\left(\frac{0.8}{K^5}+0.2\right)$$

where $\Delta f_{cc} = $ stress drop of the confined concrete at a strain of $3\,\varepsilon_{cc}'$, and $\Delta f_c = $ stress drop of the unconfined concrete at a strain of $3\,\varepsilon_c'$. Thus using $n = E_c/E_{sec}$ for confined concrete, the parameter r can be solved algebraically which will give a more realistic stress decay in the falling branch. Thus a complete stress-strain history of confined concrete can be obtained.

218

A-2.1 Confinement Coefficient for Circular Sections

Using the model proposed by Mander et al. (1988a), the effective lateral pressure for circular sections is given by

$$f_l = \frac{1}{2} k_e \rho_s f_s \qquad \text{(A-10)}$$

with k_e as the confinement effectiveness coefficient given by

$$k_e = \frac{A_e}{A_{cc}} \qquad \text{(A-11)}$$

The confining bars are assumed to yield by the time the maximum stress in the concrete is reached in which case $f_s = f_y$.

The effectively confined area shown in figure A-1a is calculated as

$$A_e = \frac{\pi D''^2}{4} \left(1 - 0.5 \frac{s'}{D''} \right) \qquad \text{(A-12)}$$

where D'' = diameter of the core concrete and s' = clear longitudinal spacing between spirals in which arching action of concrete develops. For sections with circular hoops, the coefficient 0.5 in the above equation should be replaced by 1.0.

The concrete core area is calculated as

$$A_{cc} = \left(1 - \rho_{cc} \right) \frac{\pi D''^2}{4} \qquad \text{(A-13)}$$

where ρ_s is the volumetric ratio of the transverse reinforcement to the confining core given by:

$$\rho_s = \frac{4 A_{sh}}{s D''} \qquad \text{(A-14)}$$

with A_{sh} = cross sectional area of the lateral steel and ρ_{cc} = volumetric ratio of the longitudinal steel in the confined core given by:

219

$$\rho_{cc} = \frac{4 A_{st}}{\pi D''^2} \tag{A-15}$$

where A_{st} = total area of the longitudinal reinforcement. With the maximum lateral pressure thus obtained, the peak confinement strength ratio can be obtained from

$$K = \frac{f'_{cc}}{f'_c} = -1.254 + 2.254 \sqrt{1 + 7.94 \frac{f_l}{f'_c} - 2 \frac{f_l}{f'_c}} \tag{A-16}$$

However, it was observed that for circular sections confined by spirals, the confinement coefficient can be very accurately represented by a linear equation obtained through regression analysis as

$$K = 1 + 2.7 \rho_s \frac{f_{yh}}{f'_c} \tag{A-17}$$

where all the symbols are easily identifiable.

A-2.2 Confinement Coefficient for Rectangular Sections

The effectively confined area for rectangular sections shown in figure A-1b is given by

$$A_e = \left(b'' D'' - \sum_{i=1}^{n} \frac{\omega_i'^2}{6} \right) \left(1 - 0.5 \frac{s'}{b''} \right) \left(1 - 0.5 \frac{s'}{D''} \right) \tag{A-18}$$

The concrete core area is given by

$$A_{cc} = b'' D'' - A_{st} \tag{A-19}$$

The lateral confinement pressure for rectangular sections can have different values in each direction. In this case a general three dimensional state of stress is obtained. The lateral pressure for each direction (x and y) is calculated as:

$$f_{l_y} = k_e \rho_y f_{yh} \tag{A-20}$$

$$f_{l_x} = k_e \rho_x f_{yh} \tag{A-21}$$

in which

220

$$\rho_x = \frac{A_{sx}}{sD''}$$

$$\rho_y = \frac{A_{sy}}{sb''}$$

(A-22)

with A_{sx}, A_{sy} = total area of transverse reinforcement parallel to the x and y axis respectively. With the maximum value of f_l/f_c' (i.e. either f_{l_x}/f_c' or f_{l_y}/f_c'), the confined strength ratio can be obtained from figure A-2. However, it was observed that for square sections confined by lateral ties, the confinement coefficient can be very accurately represented by a linear equation obtained through regression analysis as

$$K = 1 + 2.1 \rho_s \frac{f_{yh}}{f_c'}$$

(A-23)

where all the symbols are easily identifiable.

A-3 STRESS BLOCK ANALYSIS FOR CONFINED CONCRETE

Stress block analysis is a very efficient hand method of analysis by which the distribution of concrete stress over the compressed part of the section can be replaced by a constant stress block having the same magnitude and location as the original variable stress distribution. As was observed from the preceding discussion, the effect of confinement is to increase the ductility level of the concrete by increasing the level of maximum attainable stress and the corresponding strain. Stress block parameters which can capture the effect of confinement is thus necessary to accurately model the behavior of confined concrete. Such stress block parameters can be obtained from first principles as illustrated below.

A-3.1 General Stress Block Theory

Stress block parameters that are stress-strain curve dependent can be obtained from stress block theory. The distribution of concrete stress over the compressed part of the section may be found from the strain diagram and the stress-strain curve for concrete. This complex stress distribution can be replaced by an equivalent one of simpler rectangular outline such that it results in the same total compression force C_c applied at the same location as in the actual member. The average concrete stress ratio α and the stress block depth factor β of this equivalent rectangular stress block distribution can be determined as:

(i) <u>Effective Average Concrete Stress Ratio</u>, α: The area (A_c) under the stress-strain curve is

$$A_c = \int_0^{\varepsilon_{cm}} f_c \, d\varepsilon = \alpha \beta f_c' \varepsilon_{cm} \qquad \text{(A-24)}$$

Thus,

$$\alpha \beta = \frac{\int_0^{\varepsilon_{cm}} f_c \, d\varepsilon}{f_c' \varepsilon_{cm}} \qquad \text{(A-25)}$$

(ii) <u>Effective Stress Block Depth Factor</u>, β: The first moment of area (M_c) about the origin of area under the stress-strain curve is

$$M_c = \int_0^{\varepsilon_{cm}} f_c \varepsilon_c \, d\varepsilon = \left(1 - \frac{\beta}{2}\right) \varepsilon_{cm} \int_0^{\varepsilon_{cm}} f_c \, d\varepsilon \qquad \text{(A-26)}$$

Rearranging,

$$\beta = 2 - 2 \frac{\int_0^{\varepsilon_{cm}} f_c \varepsilon_c \, d\varepsilon}{\varepsilon_{cm} \int_0^{\varepsilon_{cm}} f_c \, d\varepsilon} \qquad \text{(A-27)}$$

For circular sections, studies conducted have shown that the compressive force C_c can be approximated to act at a distance of $0.6\beta c$ from the extreme compression fiber. Hence, the expression of $\alpha \beta$ will remain same as in rectangular sections. For stress block depth factor β, first moment of area under stress-strain can be expressed as:

$$M_c = \int_0^{\varepsilon_{cm}} f_c \varepsilon_c \, d\varepsilon = (1 - 0.6 \beta) \varepsilon_{cm} \int_0^{\varepsilon_{cm}} f_c \, d\varepsilon \qquad \text{(A-28)}$$

Rearranging,

$$\beta = \frac{1}{0.6}\left(1 - \frac{\int_0^{\varepsilon_{cm}} f_c \varepsilon_c \, d\varepsilon}{\varepsilon_{cm} \int_0^{\varepsilon_{cm}} f_c \, d\varepsilon}\right) \qquad \text{(4-8)}$$

222

A-3.2 Proposed Equation for Stress Block Analysis

In the present study attributes from the original models of Chang and Mander (1994), Mander et al. (1988a) and Kent and Park (1971) have been combined to propose a series of piece-wise stress-strain relationships applicable to both confined and unconfined concrete that can be easily integrated to give explicit closed form solutions for the stress block parameters. Equations for the proposed stress-strain model are as follows:

(i) Ascending Branch: A power curve (figure A-3) is assumed to describe the ascending branch of the stress-strain relation:

$$f_c = f_c' \left[1 - \left(\frac{\varepsilon_c}{\varepsilon_c'} - 1 \right)^n \right] \tag{A-30}$$

in which

$$n = \frac{E_c \varepsilon_c'}{f_c'} \tag{A-31}$$

where $\varepsilon_c =$ the strain at any stress of concrete f_c, and $E_c =$ modulus of elasticity of concrete $= 8200 f_c'^{3/8}$.

(ii) Descending Branch: The curve for the descending branch is assumed as a straight line:

$$f_c = f_c' \left(1 - E_f (\varepsilon_c - \varepsilon_c') \right) \tag{A-32}$$

where $E_f =$ modulus of the falling branch. Based on series of experiments performed by Mander et al. (1988b), the following empirical relationship for the modulus of the falling branch is proposed:

$$E_f = 0.3 E_c K^{-6} \tag{A-33}$$

where $K =$ confinement ratio of confined concrete. For equation A-32 f_c should not be less than $0.2 f_c'$ as shown in figure A-3.

A-3.2.1 Explicit Stress Block Parameters

The proposed piece-wise equations were integrated as in equations A-25 and A-27 to obtain explicit closed form analytical expressions for the stress block parameters that are function of the concrete strength, level of confinement and maximum strain. Since piecewise stress-strain model consists of three parts (figure A-3), three expressions were derived for the concrete stress ratio, $\alpha\beta$ and for stress block depth factor, β corresponding to the maximum strain of concrete and are presented below. In the following equations the normalized slope of the stress-strain curve is given by $z = E_f / K f_c'$ and $x_{20\%} = 0.8 / z\,\varepsilon_{cc}' + 1$.

(i) Equations for concrete stress ratio, $\alpha\beta$: The following equations were obtained for concrete stress ratio, $\alpha\beta$:

(a) For $\varepsilon_c < \varepsilon_c'$, i.e. $x < 1$

$$\alpha\beta = \left[1 - \frac{(1-x)^{n+1}}{(n+1)x} - \frac{1}{(n+1)x} \right] \qquad \text{(A-34)}$$

(b) For $\varepsilon_c' \le \varepsilon_c \le \left(\varepsilon_c' + \dfrac{0.8}{z} \right)$, i.e. $1 \le x \le \left(1 + \dfrac{0.8}{z\varepsilon_c'} \right)$

$$\alpha\beta = \left(\frac{n}{(n+1)x} \right) + \left(1 - \frac{1}{x} \right)(1 - 0.5z\varepsilon_{cc}(x-1)) \qquad \text{(A-35)}$$

(c) For $\varepsilon \ge \left(\dfrac{0.8}{z} + \varepsilon_c' \right)$, i.e $x \ge x_{20\%}$

$$\alpha\beta = \left(\frac{n}{(n+1)x} \right) + \frac{0.48}{z\varepsilon_{cc}x} + 0.2\left(1 - \frac{x_{20\%}}{x} \right) \qquad \text{(A-36)}$$

(ii) Equations for stress block depth factor, β : The following equations were obtained for stress block depth factor, β :

(a) For $\varepsilon_c < \varepsilon_c'$, i.e. $x < 1$

$$\beta = 2\left\{ 1 - \frac{\left(\dfrac{x^2}{2} - \dfrac{(1-x)^{n+2}}{n+2} + \dfrac{(1-x)^{n+1}}{n+1} - \dfrac{1}{(n+1)(n+2)} \right)}{x^2\,\alpha\beta} \right\} \qquad \text{(A-37)}$$

(b) For $\varepsilon_c' \le \varepsilon_c \le \left(\varepsilon_c' + \dfrac{0.8}{z} \right)$ i.e. $1 \le x \le \left(1 + \dfrac{0.8}{z\varepsilon_c'} \right)$

$$\beta = 2 - \frac{\left[(x^2 - 1) - \frac{z\varepsilon_{cc}}{3}(2x^3 - 3x^2 + 1) + \frac{n(n+3)}{(n+1)(n+2)}\right]}{x^2 \alpha \beta} \qquad \text{(A-38)}$$

(c) For $\varepsilon \geq \left(\frac{0.8}{z} + \varepsilon'_{cc}\right)$ i.e $x \geq x_{20\%}$

$$\beta = 2 - \frac{\left[((x_{20\%}^2 - 1) - \frac{z\varepsilon_{cc}}{3}(2x_{20\%}^3 - 3x_{20\%}^2 + 1) + \frac{n(n+3)}{(n+1)(n+2)} + 0.2(x^2 - x_{20\%}^2)\right]}{x^2 \alpha \beta} \qquad \text{(A-39)}$$

The stress block parameters for confined concrete can easily be derived using equivalent notations. Figure A-4 shows the plot of equivalent rectangular stress-block parameters calculated using the proposed closed form analytical expressions of stress block parameters. It may be observed that at nominal ultimate strain of 0.003 the value of the stress block parameters proposed by ACI and those obtained from the analytical expressions have approximately the same value. In the same figure the explicit stress block parameters are also compared with the stress block parameters of Mander et al.(1984) and Chang and Mander (1994a). These exact rectangular stress block parameters may be derived by numerical integration of their expressions using the various models of stress-strain curve studied before. It can be seen that the stress block parameters from the closed form equations compare well with those from other stress-strain relations.

Maximization of Stress Block Parameters: The maximum concrete compressive moment occurs when $\alpha\beta$ is maximum. The value of strain $(\varepsilon_{\alpha\beta}^{max})$ where $\alpha\beta$ is maximum is given by

$$x_{\alpha\beta}^{max} = \frac{\varepsilon_{\alpha\beta}^{max}}{\varepsilon'_{cc}} = \sqrt{1 + \left(\frac{2}{(n+1)z\varepsilon_{cc}}\right)} \qquad \text{(A-40)}$$

It can be observed maximum value of $\alpha\beta$ will occur in the descending branch of stress-strain model of concrete. Hence substituting the above equation of strain in equation (A-35), the following expression for maximum $\alpha\beta$ was obtained

$$\alpha\beta^{max} = \left(\frac{n}{(n+1)x_{\alpha\beta}^{max}}\right) + 0.5\left(1 - \frac{1}{x_{\alpha\beta}^{max}}\right)\left(2 - z\varepsilon'_{cc}(x_{\alpha\beta}^{max} - 1)\right) \qquad \text{(A-41)}$$

## A-3.2.2 Simplified Stress Block Parameters

It was observed that although the stress block parameters are explicit, there evaluation is not straightforward. Keeping this is in mind an analysis was performed on a wide range of confinement values starting from unity. These confinement ratios (K) were in turn be related to $\rho_s f_{yh}/f_c'$ (Mander et al. 1984, 1988a,b) for both rectangular and circular sections. Corresponding to every $\rho_s f_{yh}/f_c'$, the minimum value was chosen when the strain ratio was 5 and the maximum value chosen corresponding to equation (A-40). Finally a regression analysis was performed on the maximum and minimum values and the following equations for the stress block factor were obtained

$$\alpha_c^{rect} = 0.625 \left(1 + \rho_s \frac{f_{yh}}{f_c'} \right)$$

$$\alpha_c^{circ} = 0.667 \left(1 + \rho_s \frac{f_{yh}}{f_c'} \right)$$

(A-42)

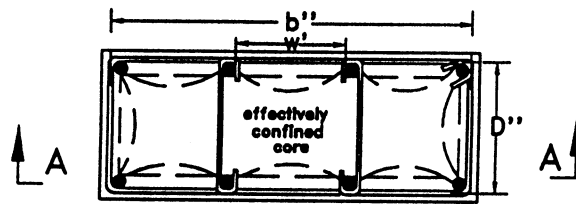Note that an upper bound value of 1.0 was assumed for the stress block depth factor β_c in these derivations.
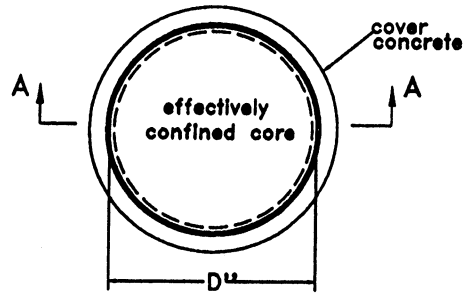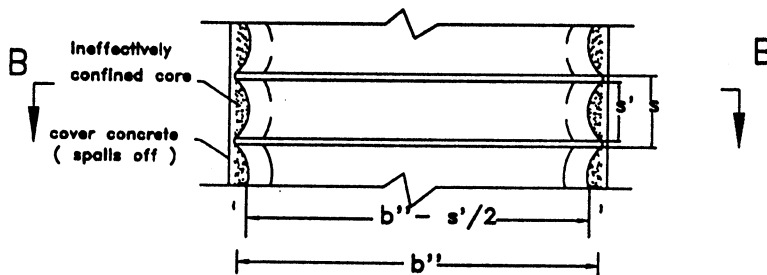
SECTION : B–B
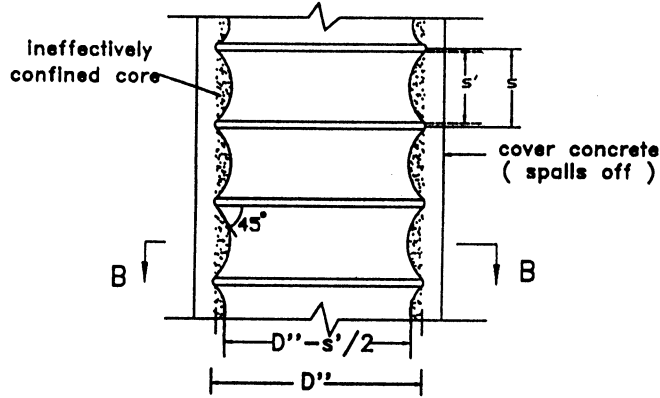
SECTION : A–A

(a) Circular Section

SECTION : B–B

SECTION : A–A

(b) Rectangular Section

Figure A-1 Showing Effectively Confined Core Areas for Circular and Rectangular Sections.
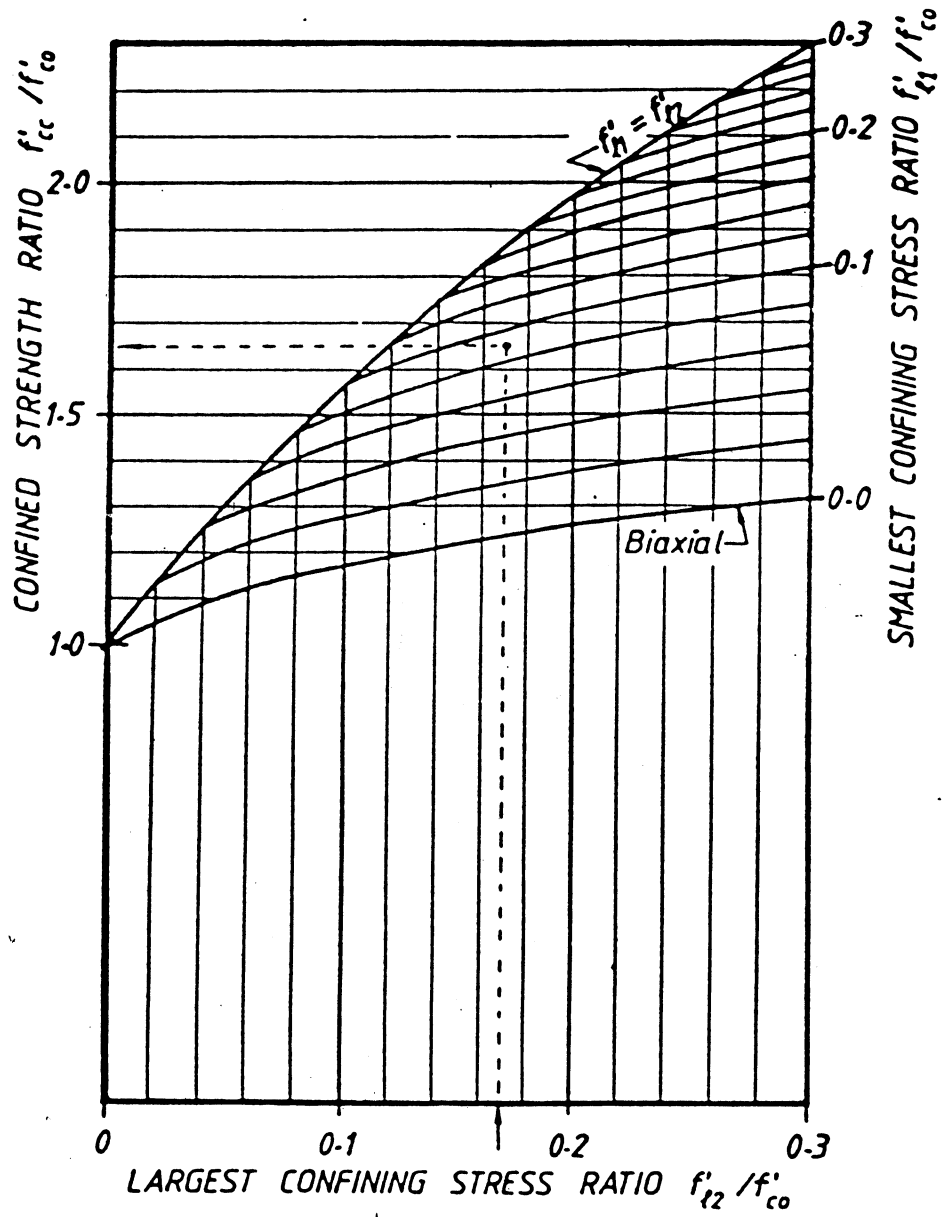
227

Figure A-2 Confined Concrete Strength Ratio based on the Multiaxial Confinement Model of Mander et al. (1988a).
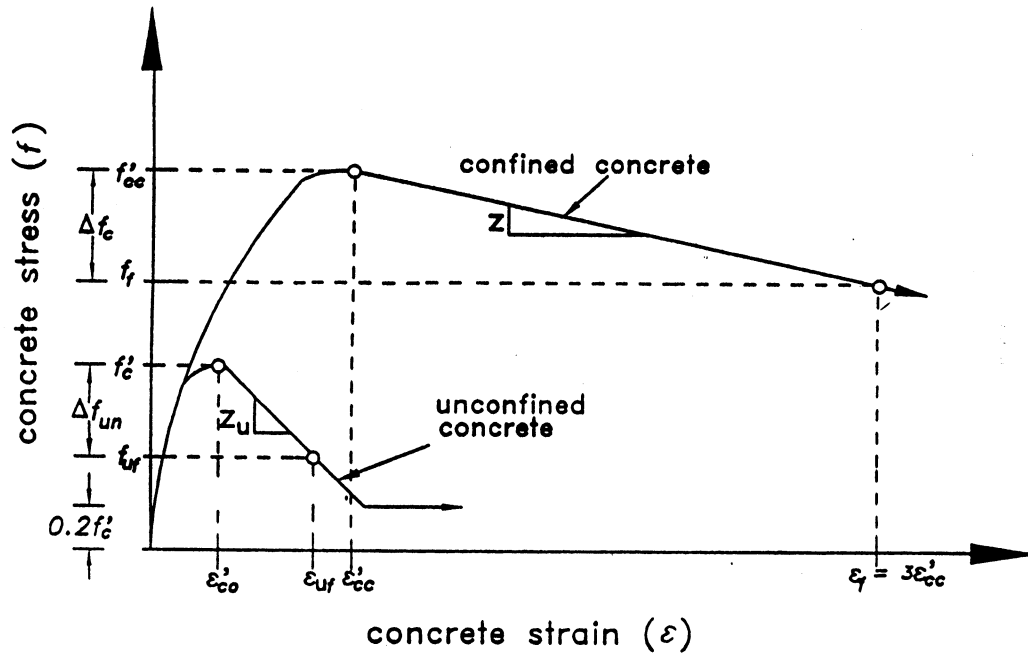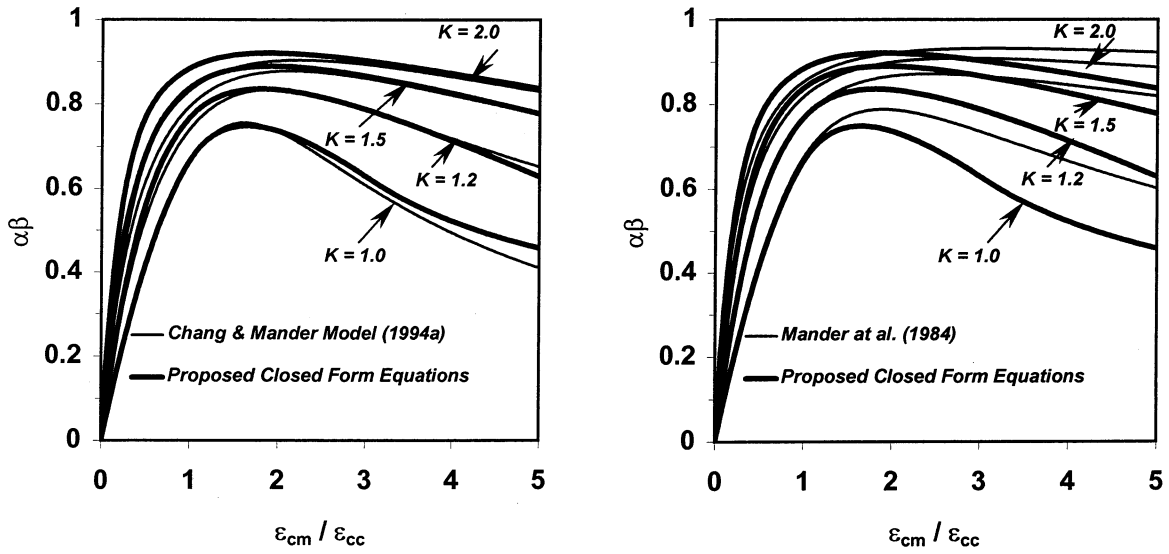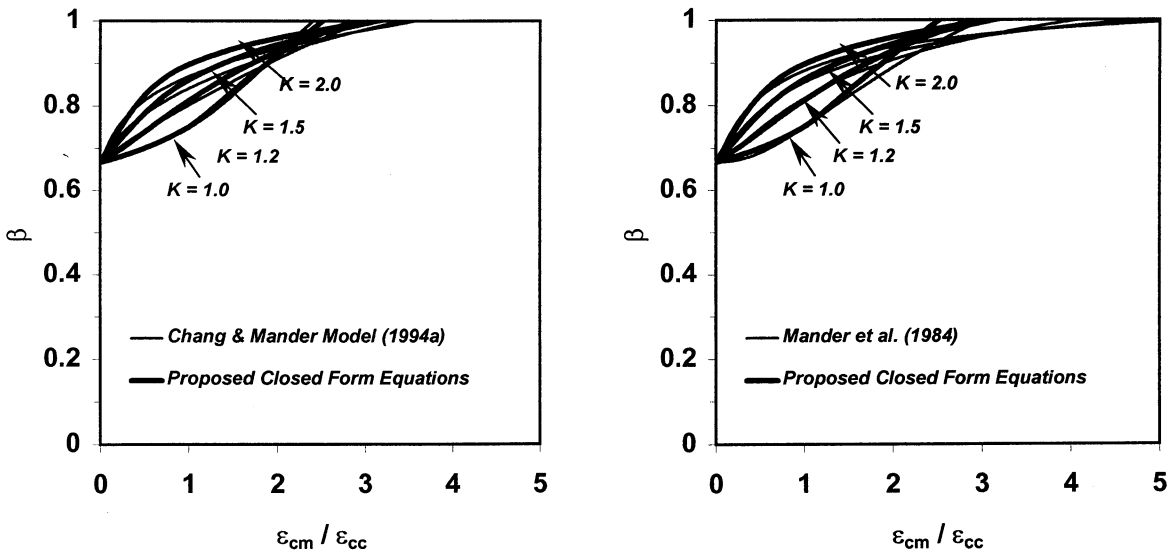
Figure A-3 Proposed Stress Strain Equation for Unconfined and Confined Concrete used in Stress-Block Analysis.

(a) alpha-beta parameter

(b) beta parameter

Figure A-4 Proposed Stress Block Parameters for f'$_c$ = 30 MPa.

APPENDIX B

WEIGHTING FACTORS FOR RECTANGULAR CONCRETE SECTIONS

B 1.1 INTRODUCTION

In a rectangular concrete section with one or two sets of overlapping transverse reinforcement, the external energy requirement of the concrete and the longitudinal steel in compression is not met uniformly by all the legs of the lateral steel. It is therefore important to identify the critical hoop that will fracture under the transverse straining. Mander et al.(1984) introduced weighting factors W_s and W_{cc} relating the proportion of the total work done on the longitudinal steel and core concrete respectively. The weighting factors are defined as

$$W_s = \frac{\textit{Effective number of bars restrained by the critical cross tie}}{\textit{Total number of longitudinal bars}} \qquad \text{(B-1)}$$

Similarly for concrete

$$W_{cc} = \frac{\textit{Length of the critical cross tie}}{\textit{Total length of the bar in one hoop set}} \qquad \text{(B-2)}$$

The effective number of bars restrained by the critical cross tie is defined as those bars that would buckle outward after the cover concrete has spalled. It is worth noting that the critical cross tie that will fracture first is identified as the tie which will give the largest W_s / W_{cc} ratio. This is illustrated with an example in the following.

B 1.2 EXAMPLE

Consider an 8 bar and a 12 bar square column. Let "a" denote the center to center distance between two adjacent bars. The critical ties to fracture are either the diagonal tie or the straight perimeter tie. The weighting factors for both are evaluated and the critical tie identified. Relevant information are given in Table B-1.

231

Table B-1 Comparative Analysis of the Weighting Factors

Type	Diagonal Leg			Straight Leg		
	W_s	W_{cc}	$\dfrac{W_s}{W_{cc}}$	W_s	W_{cc}	$\dfrac{W_s}{W_{cc}}$
8 bar	$1/8 = 0.125^1$	$\dfrac{\sqrt{2}a}{4\sqrt{2}a+8a}=0.104$	1.2	$1/8 = 0.125^3$	$\dfrac{2a}{4\sqrt{2}a+8a}=0.146$	0.86
12 bar	$2/12 = 0.167^2$	$\dfrac{\sqrt{2}a}{4\sqrt{2}a+16a}=0.065$	2.57	$1/12 = 0.083^4$	$\dfrac{3a}{4\sqrt{2}a+16a}=0.139$	0.6

1,3   For the 8 bar column the number of bars restrained from outward buckling by the interior and the perimeter hoop is 4. So the number of bars restrained by <u>one</u> diagonal or perimeter tie is 1.

2,4   For the 12 bar column the number of bars restrained from outward buckling by the diagonal leg of the interior hoop is 8. The number of bars restrained by the perimeter hoop is 4. So the number of bars restrained by <u>one</u> diagonal or perimeter tie are 2 and 1 respectively.

It is obvious from Table B-1 that the diagonal ties are more critical for both the type of columns since they give the highest W_s/W_{cc} ratio.
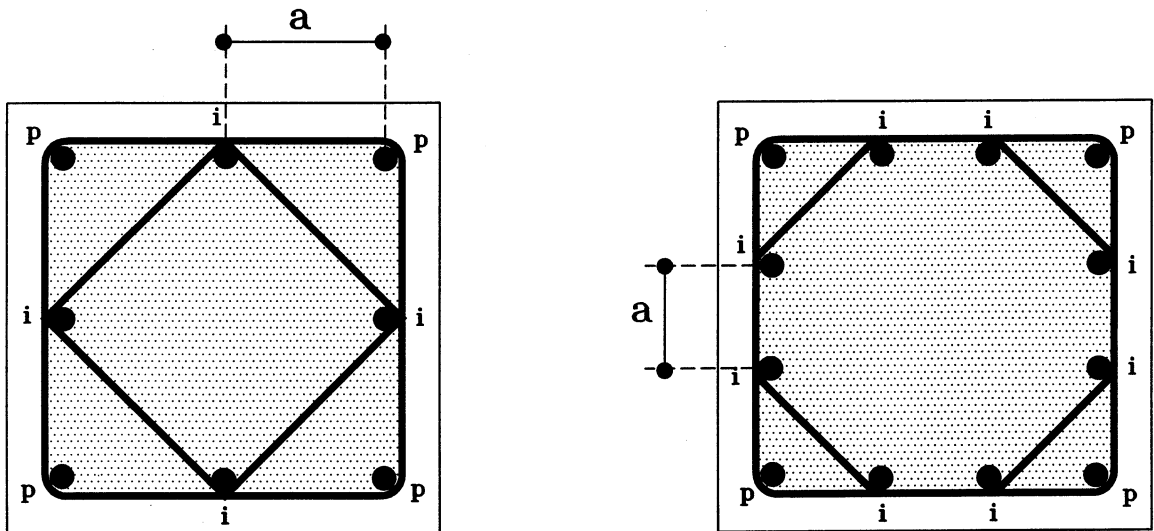
p = bars restrined by perimter ties.

i = bars resrianed by interior ties.

Figure B-1 Showing the 8 Bar and 12 Bar Column Sections.

APPENDIX C

SELECTED RESULTS OF STABILITY ANALYSIS

C-1 REDUCED MODULUS THEORY FOR CIRCULAR SECTIONS

A reduced Modulus Theory for a circular section shape is based on the same basic principles of Double Modulus Theory proposed by Von Karman. Fundamental assumptions in the theory are as follows: (i) the column is perfectly straight and has uniform cross-section; (ii) the relation between longitudinal stress and longitudinal strain in any individual fiber is the same as that indicated by the compressive stress-strain diagram of the material; and (iii) plane sections remain plane before and after bending.

Consider a circular column uniformly compressed by a force $P = A\sigma$, σ being average stress and then slightly deflected. As for the Double Modulus Theory (Secant Modification) the stresses on one side of the axis of average stress continue to rise in proportion to the Tangent Modulus (E_t) whereas on the other side the stresses are decreased in proportion to the Modulus of Elasticity since the deformations on that side are still elastic. The strains are decided as follows: The strain at the axis of average stress by ε_0; the strain at any point of the cross section at a distance of z from the axis of average stress by ε, where z is measured positive toward the concave side of the column; the strain in the least compressed fiber by ε_1 and the strain in the most compressed fiber by ε_2.

At any cross-section, the moment of the stress diagram about the centroidal axis equals the externally applied moment. This condition may be expressed by:

$$\int_{A_1} E_s(\varepsilon - \varepsilon_0)\,zdA + \int_{A_2} E_t(\varepsilon - \varepsilon_0)\,zdA = P.y \qquad \text{(C-1)}$$

in which A_1 and A_2 are the areas on either side of the axis over average stress subjected to increase or decrease of stress. The curvature as can be seen from figure C-1 is given by
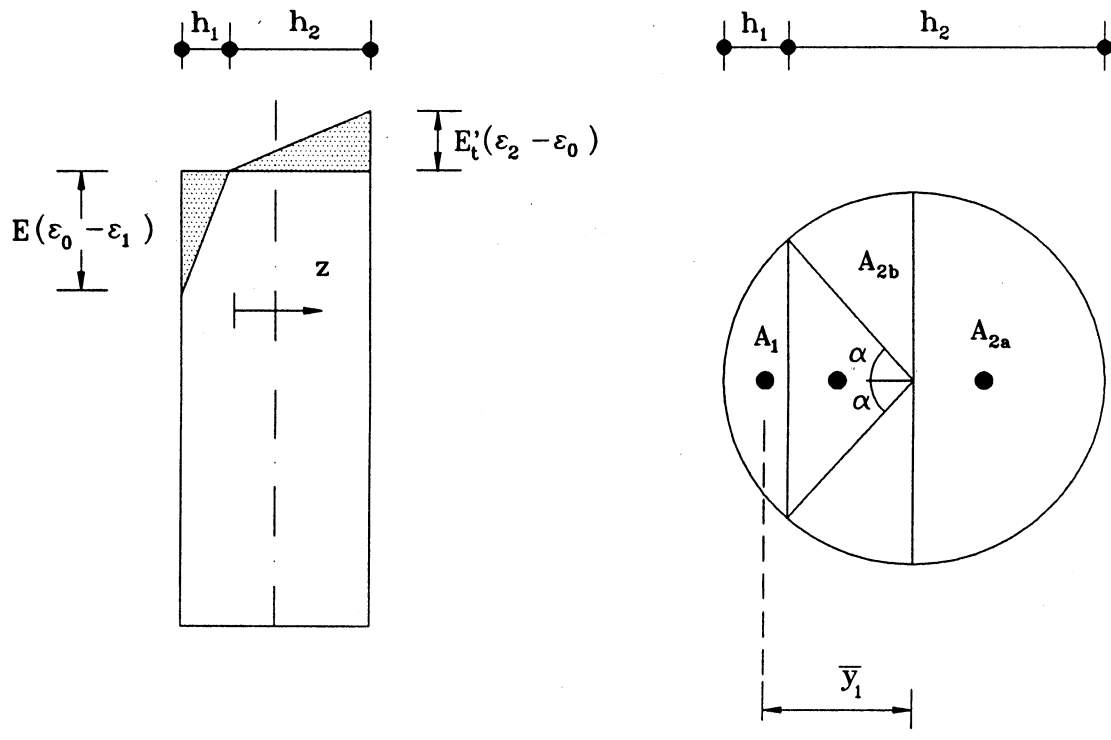
Figure C-1 Reduced Modulus Theory for Circular Sections.

234

$$\frac{d^2y}{dx^2} = -\frac{\varepsilon - \varepsilon_0}{z} \tag{C-2}$$

Substituting $\varepsilon - \varepsilon_0$ from equation (C-2) in equation (C-1) gives

$$E_s \frac{d^2y}{dx^2} \int_{A_1} z^2 \, dA + E_t \frac{d^2y}{dx^2} \int_{A_2} z^2 \, dA = -P \cdot y \tag{C-3}$$

where the integrals denote the moment of inertia of the areas A_1 and A_2 about the axis of average stress. Denoting these moments of inertia by I_1 and I_2, equation (C-3) becomes

$$(E_s I_1 + E_t I_2) \frac{d^2y}{dx^2} = -P \cdot y \tag{C-4}$$

or

$$E_r' \left(\frac{d^2y}{dz^2} \right) = -P \cdot y \tag{C-5}$$

where

$$\frac{E_r'}{E_s} = \frac{I_1 + \dfrac{E_t}{E_s} I_2}{I} \tag{C-6}$$

In order to determine I_1 and I_2, it is important to determine the axis of average stress which may be done as follows: At any cross-section the resultant of the distribution of stress must equal the applied load. Since σ is the average stress, this condition may be expressed as

$$\int_{A_1} E_s(\varepsilon - \varepsilon_o) \, dA + \int_{A_2} E_t(\varepsilon - \varepsilon_o) \, dA = 0 \tag{C-7}$$

Substituting $\varepsilon - \varepsilon_o$ from equation (C-1) yields

$$E_s \frac{d^2y}{dx^2} \int_{A_1} z \, dA + E_t \frac{d^2y}{dx^2} \int_{A_2} z \, dA = 0 \tag{C-8}$$

The two integrals in equation (C-8) are respectively the negative of the statical moment of A_1 and the statical moment of A_2 with respect to the axis of average stress. Denoting them by S_1

235

and S_2 one finally obtains

$$\frac{E_t}{E_s} = \frac{S_1}{S_2} \tag{C-9}$$

From figure C-1 it can be seen that the area in compression A_2 has been separated into a semicircular area A_{2a} given by $\pi d^2 / 4$ and an area A_{2b} given by

$$A_{2b} = A_{2a} - A_1 \tag{C-10}$$

where A_1 is the area in tension $= d^2 / 4$ $(\alpha - \sin \alpha \cos \alpha)$ and α is as shown in figure C-1. Moment of inertia of the area A_1 about the centroidal axis X-X and the center of gravity distance from the same can be obtained from strength of materials solution as

$$I_{xx} = \frac{d^4}{64} (\alpha - \sin \alpha \cos \alpha + 2 \sin^3 \alpha \cos \alpha) \tag{C-11}$$

and

$$\overline{y}_1 = \frac{d}{3} \left(\frac{\sin^3 \alpha}{\alpha - \sin \alpha \cos \alpha} \right) \tag{C-12}$$

Similarly, for the semicircular area A_{2a}, the moment of inertia and centroidal distance from the X-X axis are as $6.863 \times 10^{-3} d^4$ and $2d / 3\pi$, respectively. Equation (C-3) can therefore be plotted on a logarithmic scale against various values of E_t / E_s obtained from equation (C-9). Figure C-2 shows such a plot for $E_s = 200,000$ MPa.

This is also compared with the closed form solution for a rectangular section given by

$$\frac{E_s}{E_r} = \left[0.5 \left(\frac{E_s}{E_t} \right)^{1/2} + 0.5 \right]^2 \tag{C-13}$$

Using the above numerical relationship is unwieldy, therefore a regression analysis was performed on the results and a much simpler expression derived connecting E_s / E_r and E_s / E_t as
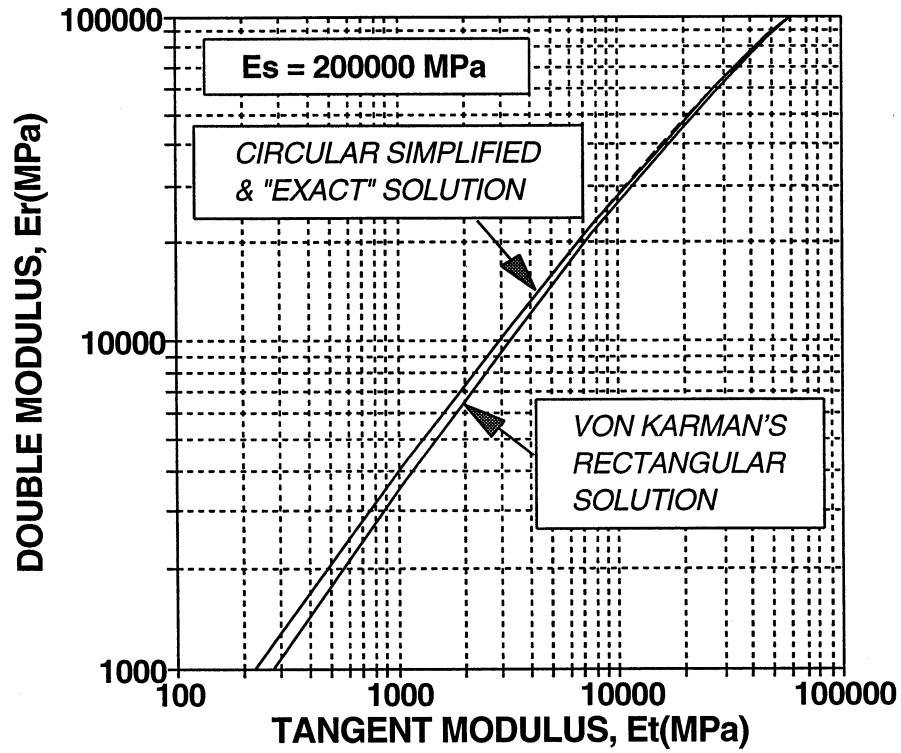
236

Figure C-2 Relationship between Double and Tangent Modulus.

$$\frac{E_s}{E_r} = \left[0.5 \left(\frac{E_s}{E_t} \right)^{\frac{1}{2.3}} + 0.5 \right]^{2.3} \tag{C-14}$$

When plotted on figure C-2, the result overlaps the ("exact") numerical solution with no discernable difference.

C-2 MOMENT CURVATURE ANALYSIS OF STEEL REINFORCEMENT

Moment curvature analysis of steel reinforcement can be performed in the same manner as was done for a complete concrete section. For a given strain in the geometric centroid of the section ε_c and section curvature ϕ, strain at any fiber can be found from

$$\varepsilon_i = \varepsilon_c + \phi y_i \tag{C-15}$$

where y_i denotes the distance of the i-th fiber from the centroid of the section. The stress corresponding to the strain ε_i can be found from the equation suggested by Chang and Mander (1994a):

$$f_i = \frac{E_s \varepsilon_i}{\left\{ 1 + \left| \frac{E_s \varepsilon_i}{f_y} \right|^{20} \right\}^{0.05}} + \left(\frac{1 + sign(\varepsilon_i - \varepsilon_{sh})}{2} \right) (f_{su} - f_y) \left[1 - \left| \frac{\varepsilon_{su} - \varepsilon_i}{\varepsilon_{su} - \varepsilon_{sh}} \right|^p \right] \tag{C-16}$$

in which, $\varepsilon_{su}=$ strain hardening strain, $f_{su}=$ ultimate stress, $E_{sh}=$ strain hardening modulus, $\varepsilon_{su}=$ ultimate strain of reinforcement and the power p is given by

$$p = E_{sh} \frac{\varepsilon_{su} - \varepsilon_{sh}}{f_{su} - f_y} \tag{C-17}$$

The stresses can be integrated over the entire section by using any numerical schemes like fiber element or gauss quadrature. If gauss quadrature is used then the equilibrium equation can be written as

238

$$d_b \sum_{i=1}^{n} w_i (b_i f_i) = P_{cr} \qquad\qquad \text{(C-18)}$$

where $n =$ order of gauss quadrature, $w_i =$ weighting factor corresponding to the i-th point having a width of b_i and stress f_i with d_b being the diameter of the section. Similarly the moments can be calculated as

$$M = d_b \sum_{i=1}^{n} w_i (b_i f_i y_i) \qquad\qquad \text{(C-19)}$$

The equilibrium equation (C-17) needs to be satisfied at every curvature. This requires the evaluation of the correct centroidal strain ε_c. A few degree of iterations may be required for this purpose. The Newton-Rhapson technique discussed in Section 3 may be used and is not repeated here for obvious reasons.

The results of a moment-curvature analysis for a typical Grade 60 ($f_y = 450\ MPa$ is assumed) is presented in figure C-3. These results, although they are theoretically "exact", are difficult to utilize for buckling analysis. Therefore, an appropriate direct approach is given below.

C-2.1 Approximate Moment Curvature Relationship

As discussed in the previous subsection, it is possible to obtain an exact moment-curvature relationship for circular steel sections using a Gauss quadrature numerical integration technique. Although such techniques are very exact, the computation involved does not make them viable for spreadsheet type analysis. Alternately, it was found that for grade 60 reinforcement, in the stress range $0.7 \leq f_{cr}/f_{su} \leq 1$, moment curvature relationship can be effectively expressed by a cubic formula as
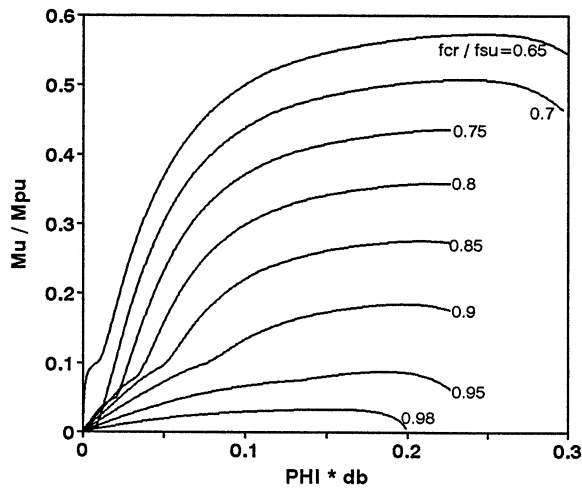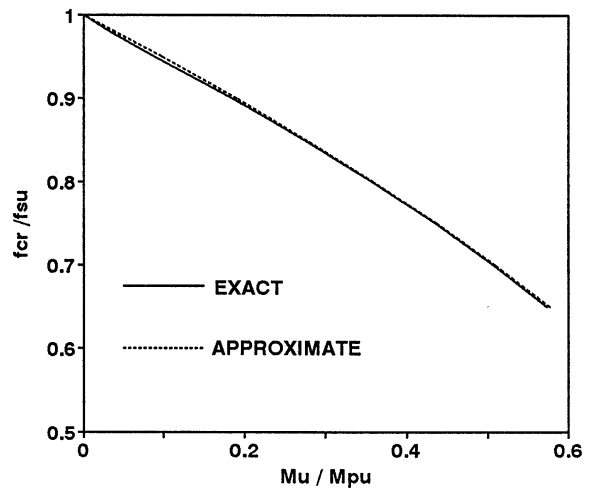
(a) Moment-Curvature
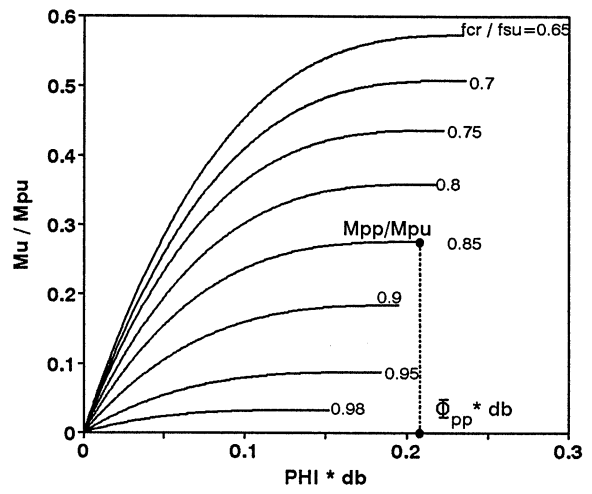
(b) Approximate Moment-Curvature
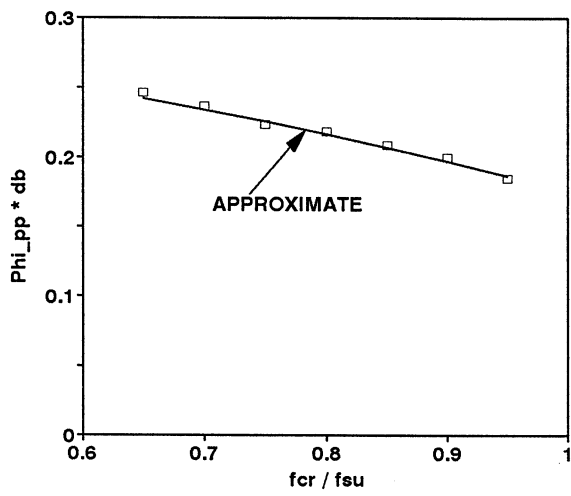
(c) Curvature and Critical Stress

(d) Interaction Diagram

Figure C-3 Moment/Curvature-Axial Load Interaction for Grade 60 Reinforcement.

240

$$M_p = M_{pp}\left[1 - \left(1 - \frac{\Phi_p}{\Phi_{pp}}\right)^3\right]$$ (C-20)

or

$$\Phi_p d_b = \Phi_{pp} d_b\left[1 - \left(1 - \frac{M_p}{M_{pp}}\right)^{1/3}\right]$$ (C-21)

where M_{pp} is the maximum plastic moment with Φ_{pp} being the corresponding curvature. These parameters are plotted in figure C-3. The maximum plastic moment M_{pp} corresponding to any stress f_{cr} may also be expressed in the form of the well-known parabolic relationship for axial load-moment interaction:

$$\frac{M_{pp}}{M_{pu}} = \left[1 - \left(\frac{f_{cr}}{f_{su}}\right)^2\right]$$ (C-22)

where M_{pu} = maximum plastic moment at zero axial load = $f_{su} d_b^3/6$. The corresponding curvature Φ_{pp} was obtained using a regression analysis as

$$\Phi_{pp} d_b = 0.175 + 0.115\frac{M_{pp}}{M_{pu}} = 0.29 + 0.115\left|\frac{f_{cr}}{f_{su}}\right|^2$$ (C-23)

The steel stress-strain parameters used for grade 60 reinforcement are given in table C-1.

Table C-1 Stress-Strain Parameters for grade 60 Reinforcement

f_y (MPa)	E_s (GPa)	ε_{sh}	E_{sh} (MPa)	ε_{su}	f_{su} (MPa)
450	200	0.0089	8000	0.12	640

C-2.2 Curvature Distribution

In a stability analysis it is essential that the correct distribution of curvatures are obtained over the height of the column. This important because the various components such as moments, curvatures and deflections are all inter-related as shown in figure C-4. Since a reinforcing bar is never perfectly straight, there is always an initial (accidental) eccentricity that gives rise to a moment at the base (note a cantilever has been used representing a quarter length of the bar between successive hoops). This in turn produces a curvature distribution that has to conform to the initial deflected shape. To obtain a complete force-lateral deformation relationship, such equilibrium needs to be satisfied at every point on the curve.

In an ultimate load analysis where it was shown that the critical buckling load occurs when the moment at the base of the column equals the maximum plastic moment M_{pp}, the corresponding curvature distribution is found to obey a power law given by

$$\frac{\Phi_p}{\Phi_{pp}} = 1 - \left(1 - \frac{x}{L}\right)^{\frac{1}{n}} \tag{C-24}$$

which has a zero slope at $x = L$ where $L =$ length of the cantilever column. For typical grade 60 reinforcement (table C-1), with the moment curvature relationship defined by a cubic curve, a non-linear least square analysis showed that the power n approximately equals 2.

The plastic rotation which is obtained by integrating the plastic curvature diagram is thus given by

$$\theta_p = \chi L \phi_p \tag{C-25}$$

where

$$\chi = \int_0^1 \frac{x}{L}\left(1 - \left(1 - \frac{x}{L}\right)^{1/n}\right) d\left(\frac{x}{L}\right) \tag{C-26}$$
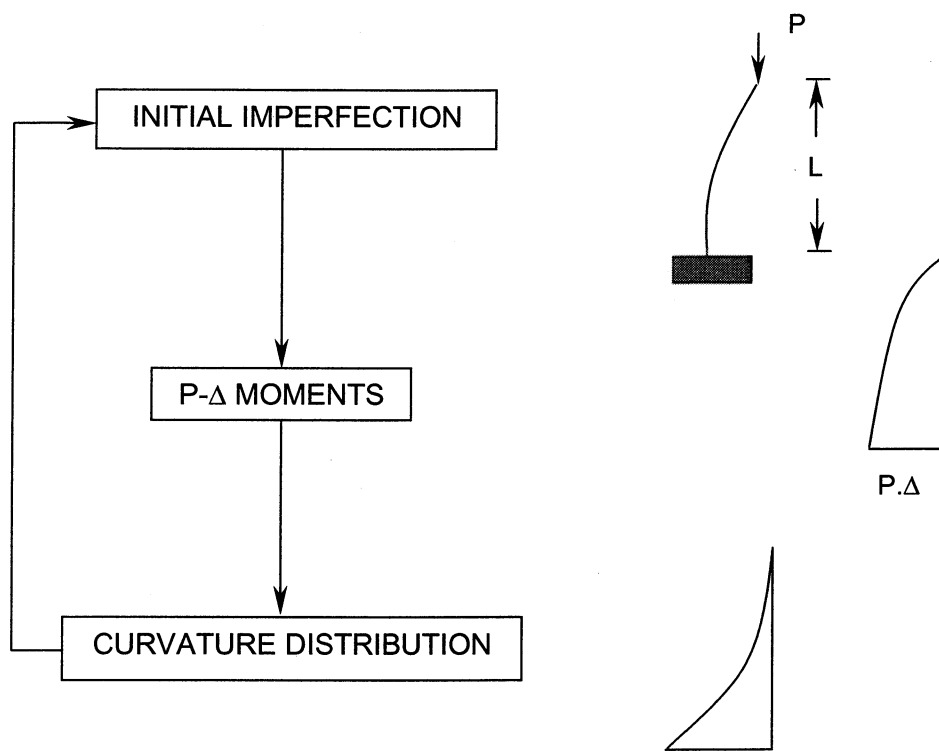
which for $n = 2$ equals 0.2333.

Figure C-4 Inter-relationship between various Components in a Stability Analysis.